

**ANALYSIS OF BIO-DERIVED PLATFORM CHEMICALS IN IONIC LIQUID
MEDIA BY DESORPTION/IONIZATION MASS SPECTROMETRY**

by

© Valerie H. Parsons

A thesis submitted to the

School of Graduate Studies

in partial fulfillment of the requirements for the degree of

Master of Science

Department of Chemistry

Faculty of Science

Memorial University of Newfoundland

December 2015

St. John's

Newfoundland and Labrador

Abstract

In this work, desorption/ionization mass spectrometry was employed for the analysis of sugars and small platform chemicals that are common intermediates in biomass transformation reactions. Specifically, matrix-assisted laser desorption/ionization (MALDI) and desorption electrospray ionization (DESI) mass spectrometric techniques were employed as alternatives to traditional chromatographic methods.

Ionic liquid matrices (ILMs) were designed based on traditional solid MALDI matrices (2,5-dihydroxybenzoic acid (DHB) and α -cyano-4-hydroxycinnamic acid (CHCA)) and 1,3-dialkylimidazolium ionic liquids ([BMIM]Cl, [EMIM]Cl, and [EMIM]OAc) that have been employed as reaction media for biomass transformation reactions such as the conversion of carbohydrates to valuable platform chemicals. Although two new ILMs were synthesized ([EMIM][DHB] and [EMIM][CHCA] from [EMIM]OAc), chloride-containing ILs did not react with matrices and resulted in mixtures of IL and matrix in solution. Compared to the parent solid matrices, much less matrix interference was observed in the low mass region of the mass spectrum (< 500 Da) using each of the IL-matrices. Furthermore, the formation of a true ILM (i.e. a new ion pair) does not appear to be necessary for analyte ionization.

MALDI sample preparation techniques were optimized based on the compatibility with analyte, IL and matrix. ILMs and IL-matrix mixtures of DHB allowed for qualitative analysis of glucose, fructose, sucrose and *N*-acetyl-D-glucosamine. Analogous CHCA-containing ILMs did not result in appreciable analyte signals under similar conditions. Small platform compounds such as 5-hydroxymethylfurfural (HMF) and levulinic acid

were not detected by direct analysis using MALDI-MS. Furthermore, sugar analyte signals were only detected at relatively high matrix:IL:analyte ratios (1:1:1) due to significant matrix and analyte suppression by the IL ions. Therefore, chemical modification of analytes with glycidyltrimethylammonium chloride (GTMA) was employed to extend this method to quantitative applications. Derivatization was accomplished in aqueous IL solutions with fair reaction efficiencies (36.9 – 48.4 % glucose conversion). Calibration curves of derivatized glucose-GTMA yielded good linearity in all solvent systems tested, with decreased % RSDs of analyte ion signals in IL solutions as compared to purely aqueous systems (1.2 – 7.2 % and 4.2 – 8.7 %, respectively). Derivatization resulted in a substantial increase in sensitivity for MALDI-MS analyses: glucose was reliably detected at IL:analyte ratios of 100:1 (as compared to 1:1 prior to derivatization). Screening of all test analytes resulted in appreciable analyte signals in MALDI-MS spectra, including both HMF and levulinic acid.

Using appropriate internal standards, calibration curves were constructed and this method was employed for monitoring a model dehydration reaction of fructose to HMF in [BMIM]Cl. Calibration curves showed wide dynamic ranges (LOD – 100 ng fructose/ μ g [BMIM]Cl, LOD – 75 ng HMF/ μ g [BMIM]Cl) with correlation coefficients of 0.9973 (fructose) and 0.9931 (HMF). LODs were estimated from the calibration data to be 7.2 ng fructose/ μ g [BMIM]Cl and 7.5 ng HMF/ μ g [BMIM]Cl, however relatively high S/N ratios at these concentrations indicate that these values are likely overestimated. Application of this method allowed for the rapid acquisition of quantitative data without the need for prior separation of analyte and IL.

Finally, small molecule platform chemicals HMF and levulinic acid were qualitatively analyzed by DESI-MS. Both HMF and levulinic acid were easily ionized and the corresponding molecular ions were easily detected in the presence of 10 – 100 times IL, without the need for chemical modification prior to analysis. DESI-MS analysis of ILs in positive and negative ion modes resulted in few ions in the low mass region, showing great potential for the analysis of small molecules in IL media.

Acknowledgements

First and foremost, I would like to express my gratitude to my supervisors Drs. Christina Bottaro and Fran Kerton, who have provided continuous guidance and support throughout the course of my research. The many insightful comments, advice, and encouragement that I have received were integral to making my graduate research experience an unforgettable one. I am extremely fortunate to have had supervisors who granted me with the freedom of exploring research, while providing invaluable knowledge and expertise, which were fundamental in building my confidence and motivation as a student.

I would like to acknowledge the many people who have contributed to the completion of this research. To Linda Winsor, Julie Collins, Dr. Stefana Egli, Dr. David Grant, and Dr. Celine Schneider, thank you for providing training and assistance with instrumentation in C-CART. I would also like to thank Dr. Chris Kozak, the members of the Green Chemistry and Catalysis group, and the Bottaro research group for providing suggestions and motivation throughout my research and contributing to valuable discussions concerning my work.

Lastly, I wish to thank Tyler and my wonderful parents, who effortlessly provided inspiration and support (both emotionally and financially) as I continued my education in pursuit of a better future.

Table of Contents

Abstract	ii
Acknowledgements	v
Table of Contents	vi
List of Tables	xii
List of Figures	xiii
List of Abbreviations and Symbols	xx
List of Appendices	xxiii
Chapter 1 : Introduction and Literature Review	1
1.1 Alternative Energy from Biomass	1
1.1.1 Overview	1
1.1.2 Sustainable Energy from Biomass	2
1.1.3 Valorization of Waste Biomass	3
1.2 Renewable Carbohydrate Feedstocks	3
1.2.1 Overview	3
1.2.2 Cellulosic Feedstocks	4
1.2.3 Ocean-Sourced Feedstocks	5
1.2.4 Sugar Feedstocks	6
1.2.5 Value-Added Chemicals from Biomass	9
1.2.6 Bio-Processing of Carbohydrates	12
1.3 Ionic Liquid Solvents in Green Processes	13
1.3.1 Overview and Brief History	13
1.3.2 Properties of Ionic Liquids	14

1.3.3	Ionic Liquids in Biomass Processing	16
1.3.4	Conversion of Biomass in Ionic Liquids	18
1.3.5	Synthesis of Ionic Liquids	19
1.3.6	Purification of Ionic Liquids	21
1.3.7	Ionic Liquids in Analytical Chemistry	23
1.4	Analysis of Platform Chemicals in Ionic Liquid Media	24
1.5	Matrix-Assisted Laser Desorption/Ionization Time-of-Flight Mass Spectrometry	27
1.5.1	Overview of MALDI-TOF MS	27
1.5.2	MALDI-TOF MS Instrumentation and Process	28
1.5.3	Traditional MALDI Matrices	30
1.5.4	Ionic Liquid Matrices	33
1.5.5	Analysis of Small Neutral Carbohydrates by MALDI-MS	35
1.6	Desorption Electrospray Ionization Mass Spectrometry	36
1.6.1	Overview	36
1.6.2	Instrumentation and Process	37
1.6.3	Ionization Mechanisms	40
1.6.4	Applications of DESI-MS	41
1.7	Project Aims	42
	References	45
Chapter 2 : Preparation and Characterization of Imidazolium-Based Ionic Liquid Matrices		51
2.1	Introduction	51
2.2	Materials	54
2.3	Instrumentation	54

2.3.1	¹ H and ¹³ C NMR Spectroscopy	54
2.3.2	UV-Vis Spectroscopy	55
2.3.3	IR Spectroscopy	55
2.4	Methods	55
2.4.1	UV-Vis Solution Preparation	55
2.4.2	Preparation of ILM-Matrix Mixtures	56
2.4.3	Preparation of Sodium Salts of Matrices	59
2.5	Results and Discussion	62
2.5.1	Ionic Liquid-Matrix Crystals	62
2.5.2	Characterization by NMR	64
2.5.3	Characterization by UV-Vis Spectroscopy	72
2.5.4	Colored Solutions of Matrices and [EMIM]Cl	74
2.5.5	Characterization by IR Spectroscopy	80
	References	90
Chapter 3: Optimization of IL-Containing Matrices for the Qualitative Analysis of Bio-Derived Platform Chemicals		92
3.1	Introduction	92
3.2	Materials	95
3.3	Instrumentation	96
3.3.1	MALDI-TOF MS	96
3.3.2	Scanning Electron Microscopy	96
3.4	Methods	97
3.4.1	Matrix/Sample Preparation	97
3.5	Results and Discussion	97

3.5.1	MALDI-TOF MS Analysis of DHB and DHB-IL Matrices	98
3.5.2	MALDI-TOF MS Analysis of CHCA and CHCA-IL Matrices.....	101
3.5.3	Physical Appearance	104
3.5.4	Optimization of Sample Preparation for MALDI Analysis with DHB and CHCA	106
3.5.5	Cationization of Sugar Analytes	107
3.5.6	Laser Intensity.....	112
3.5.7	Solvent System.....	114
3.5.8	Sample Spotting Technique	116
3.5.9	Matrix/IL Spotting Concentration.....	117
3.6	Qualitative Sugar Analysis	118
3.6.1	Sugar Analysis using DHB-Based Ionic Liquid Matrices	119
3.6.2	Matrix Interference.....	128
3.6.3	Sugar Analysis using CHCA-Based Ionic Liquid Matrices.....	130
3.6.4	Sample Spot Homogeneity.....	133
3.6.5	Matrix:IL:Analyte Ratio.....	136
3.6.6	Matrix/Analyte Suppression.....	140
3.7	Conclusions.....	146
	References	148
Chapter 4: Derivatization of Bio-Derived Platform Chemicals in Ionic Liquids for Quantitative MALDI-TOF MS Analysis		
4.1	Introduction.....	150
4.2	Materials	151
4.3	Instrumentation	152
4.3.1	MALDI-TOF MS	152

4.3.2	^1H NMR Spectroscopy	153
4.4	Methods	153
4.4.1	MALDI-TOF MS Sample Preparation.....	153
4.4.2	Standard Preparation for Derivatization Studies	154
4.4.3	Derivatization of Analyte Standards	154
4.4.4	Reaction Conditions for Dehydration Reaction of Sugar to HMF	155
4.4.5	Derivatization of Reaction Aliquots	155
4.4.6	MALDI-MS Sample Preparation of Derivatized Samples	155
4.5	Results and Discussion	156
4.5.1	Sugar Quantitation by MALDI-TOF MS.....	156
4.5.2	Derivatization of Sugar Analytes	161
4.5.3	Derivatization of Sugar Analytes with GTMA	165
4.5.4	Selection of Appropriate Internal Standards for Quantitation	169
4.5.5	Quantitative Analysis of GTMA-Derivatized Analytes in ILs	174
4.5.6	Application of MALDI-MS for the Analysis of GTMA-Sugar Ethers in IL Systems	179
4.5.7	Conclusions and Future Work.....	189
	References	191
Chapter 5: Qualitative Analysis of Small Molecule Platform Chemicals in Ionic Liquids by Desorption Electrospray Ionization Mass Spectrometry		
5.1	Introduction.....	192
5.2	Materials	193
5.3	Instrumentation	193
5.3.1	DESI-MS.....	193
5.4	Methods	194

5.4.1	Standard Preparation	194
5.4.2	Sample Deposition	195
5.5	Results and Discussion	195
5.5.1	Sample Preparation	195
5.5.2	Instrument Parameters	196
5.5.3	Initial Analyte Screening by DESI-MS	197
5.5.4	DESI-MS of IL Media	198
5.5.5	Qualitative DESI-MS Analysis of HMF in IL Media	203
5.5.6	Qualitative DESI-MS Analysis of Levulinic Acid in IL Media	205
5.6	Conclusions	207
	References	208
	Chapter 6: Conclusions and Future Work	209

List of Tables

Table 1-1: Properties of Selected Sugars	9
Table 2-1: Chemical Shift of Imidazolium C(2)-H Proton in ILs and IL-Matrix Mixtures	69
Table 2-2: Carbonyl Stretching Frequency of ILMs and Standards	85
Table 3-1: Identified Adducts and Fragments of DHB and DHB-IL Matrices (in Positive Ion Mode).....	100
Table 3-2: Identified Adducts and Fragments of CHCA and CHCA-IL Matrices (in Positive Ion Mode).....	103
Table 3-3: Relative Masses of Cation Adducts of Sugar Analytes.....	108
Table 3-4: Relative Laser Intensity for Studied Matrices	113
Table 3-5: Masses of Analytes of Interest	119
Table 4-1: Calibration Data for Selected Sugar Analytes as Analyzed by MALDI-TOF MS using DHB Matrix.....	157
Table 4-2: Glucose Conversion by GTMA in Selected Ionic Liquids.....	165
Table 4-3: Calculated LODs and LOQs of Glucose-GTMA in Various Solvent Systems by MALDI-MS	175
Table 4-4: Absolute Intensity of Glucose-d ₇ in Water and IL Solvent Systems	178
Table 4-5: Concentration of Fructose and HMF as a Function of Reaction Time in the Non-Catalyzed Dehydration Reaction in [BMIM]Cl at 80 °C	184
Table 4-6: Concentration of Fructose and HMF as a Function of Reaction Time in the CrCl ₃ -Catalyzed Dehydration Reaction in [BMIM]Cl at 80 °C	184
Table A5-1: Regression Statistics for Sugar Calibration Curves Constructed using MALDI-TOF MS (DHB Matrix); n = 5; 4-point calibration.....	243
Table A5-2: Average Absolute Peak Heights for Glucose	243
Table A5-3: Average Peak Height Ratios of Glucose/Glucose-d ₇ used for Calibration	244
Table A5-4: Calculated Fructose Conversion and HMF Yield as a Function of Reaction Time	244

List of Figures

Figure 1-1: Structure of Cellulose.....	4
Figure 1-2: Extensive Hydrogen-Bonding Network within Chains of Cellulose (Reproduced with permission from Ref. 12)	5
Figure 1-3: Structures of Chitin and Chitosan Biopolymers	6
Figure 1-4: Cyclic Conformers of Common Bio-Derived Sugars	8
Figure 1-5: Potential routes to value-added chemicals from glucose (Ref. 19 - Reproduced with permission from The Royal Society of Chemistry)	10
Figure 1-6: Structures of Common Ionic Liquid Ions	15
Figure 1-7: General Routes of Ionic Liquid Metathesis (adapted from Ref. 48).....	20
Figure 1-8: Annual Growth of Publications Concerning Ionic Liquids and Ionic Liquids in Analytical Chemistry (Data received via SciFinder Aug. 2014)	23
Figure 1-9: MALDI-TOF MS Schematic	30
Figure 1-10: Co-crystallization of Matrix and Analyte	31
Figure 1-11: Structures of Common MALDI Matrices CHCA and DHB	32
Figure 1-12: DESI-MS Process	37
Figure 1-13: Tuneable Geometric Parameters in DESI-MS Source (adapted from Ref. 71)	38
Figure 1-14: Effect of Solvent and Gas Flow Rates of Sample Impact Area in a Typical DESI-MS Experiment (adapted from Ref. 74)	40
Figure 2-1: Matrices and Ionic Liquids Employed for Matrix Design	53
Figure 2-2: General Reaction Scheme for ILM Preparation from Imidazolium-Based ILs	56
Figure 2-3: Proton and Carbon Assignment of Imidazolium Cation and Matrix Acids	64
Figure 2-4: ¹ H NMR Spectra of DHB Aromatic Proton Chemical Shifts: (a) DHB; (b) NaDHB; (c) [BMIM]Cl/DHB; (d) [EMIM]Cl/DHB; (e) [EMIM]OAc/DHB	65
Figure 2-5: ¹ H NMR Spectra of CHCA Aromatic Proton Chemical Shifts: (a) CHCA; (b) NaCHCA; (c) [BMIM]Cl/CHCA; (d) [EMIM]Cl/CHCA; (e) [EMIM]OAc/CHCA	66

Figure 2-6: UV-Vis Spectra of DHB and DHB-Containing ILMs in ACN (75 μ M)	
Figure 2-7: UV-Vis Spectra of CHCA and CHCA-Containing ILMs in ACN (25 μ M)	72
Figure 2-8: UV-Vis Spectra of Colored Complexes of [EMIM]Cl and DHB Matrices (in MeOH)	76
Figure 2-9: UV-Vis Spectra of Varying Ratios of [EMIM]Cl:DHB (100 mM DHB in MeOH)	76
Figure 2-10: UV-Vis Spectra of [EMIM]Cl and CHCA in MeOH	78
Figure 2-11: IR Spectra of DHB and DHB-Containing ILMs	82
Figure 2-12: IR Spectra of CHCA and CHCA-Containing ILMs	83
Figure 2-13: IR Characterization of Imidazolium C(2)-H Stretch in Novel [EMIM] ⁺ -Containing ILMs	86
Figure 2-14: Schematic Representation of Formation of ILMs and IL-Matrix Mixtures ..	87
Figure 2-15: Structures of IL-Matrix Mixtures and Novel ILMs (shown in bold)	87
Figure 3-1: Representative Mass Spectra of (a) DHB, (b) [BMIM]Cl-DHB, (c) [EMIM]Cl-DHB, (d) [EMIM][DHB]	99
Figure 3-2: Representative Mass Spectra of (a) CHCA, (b) [BMIM]Cl-CHCA, (c) [EMIM]Cl-CHCA, (d) [EMIM][CHCA]	102
Figure 3-3: SEM Images of (a) DHB Matrix; (b) 1:1 DHB:[BMIM]Cl; (c) 1:1 DHB:[EMIM]Cl; (d) 1:1 DHB:[EMIM]OAc (all spots with 1 μ L 10 mM NaCl)	105
Figure 3-4: MALDI-MS Spectra of Glucose with DHB (1:1): (a) with 1 μ L 10 mM NaCl; (b) with 1 μ L 10 mM KCl	109
Figure 3-5: Effect of Cationization of Glucose with DHB and CHCA Matrices (1:1 Matrix:Glucose): (a) DHB matrix without additive; (b) DHB matrix with 1 μ L 10 mM NaCl dopant; (c) CHCA matrix without additive; (d) CHCA matrix with 1 μ L 10 mM NaCl dopant	110
Figure 3-6: Analysis of Sugar Analytes with DHB Matrix (1:1 M:A + NaCl cationization agent): (a) Glucose, (b) Fructose, (c) Sucrose, (d) NAG	121
Figure 3-7: Analysis of Sugar Analytes with [BMIM]Cl-DHB Matrix (1:1 M:A + NaCl cationization agent): (a) Glucose, (b) Fructose, (c) Sucrose, (d) NAG	123

Figure 3-8: Analysis of Sugar Analytes with [EMIM]Cl-DHB Matrix (1:1 M:A + NaCl cationization agent): (a) Glucose, (b) Fructose, (c) Sucrose, (d) NAG	124
Figure 3-9: Analysis of Sugar Analytes with [EMIM][DHB] Matrix (1:1 M:A + NaCl cationization agent): (a) Glucose, (b) Fructose, (c) Sucrose, (d) NAG	127
Figure 3-10: Isotopic Distribution Patterns of Glucose (lower) and Interfering [EMIM] ⁺ Ion/Adduct (upper).....	129
Figure 3-11: MALDI-MS Spectra of (a) CHCA + Glucose; (b) CHCA + Sucrose (1:1 M:A, + NaCl Dopant)	131
Figure 3-12: MALDI-MS Spectrum of [EMIM][CHCA]	132
Figure 3-13: Comparison of Spectra Acquired from the (a) Center and (b) Edge of MALDI Spot Containing 1:1:1 DHB:[BMIM]Cl:Glucose	134
Figure 3-14: Acquisition Patterns Employed in MALDI-MS Analysis: (a) Random and (b) Edge-Biased	136
Figure 3-15: Scatterplot of Glucose and [EMIM] ⁺ Signals with Varying [EMIM]Cl:DHB Ratio	138
Figure 3-16: Scatterplot of Fructose and [EMIM] ⁺ Signals with Varying [EMIM]Cl:DHB Ratio	138
Figure 3-17: Scatterplot of Sucrose and [EMIM] ⁺ Signals with Varying [EMIM]Cl:DHB Ratio	139
Figure 3-18: Scatterplot of NAG and [EMIM] ⁺ Signals with Varying [EMIM]Cl:DHB Ratio	139
Figure 3-19: Absolute Intensities of DHB, Glucose and [BMIM] ⁺ Ions with Increasing [BMIM]Cl Concentration	141
Figure 3-20: Absolute Intensities of DHB, Glucose and [EMIM] ⁺ Ions with Increasing [EMIM]Cl Concentration.....	141
Figure 3-21: Absolute Intensities of DHB, Glucose and [EMIM] ⁺ Ions with Increasing [EMIM]Cl Concentration.....	142
Figure 3-22: MALDI-MS Spectra of Varying DHB:Glucose:[EMIM]Cl Ratios (based on 50 mM DHB and 50 mM Glucose + NaCl Dopant): (a) 50,000:50,000:1; (b) 5000:5000:1; (c) 500:500:1; (d) 5:5:1; (e) 2:2:1; (f) 1:1:1	143

Figure 4-1: Calibration Curve of Selected Sugars Analyzed by MALDI-MS using DHB Matrix (Error bars represent standard deviation of the mean, n = 5).....	158
Figure 4-2: MALDI-MS Spectrum of Triethylammonium chloride and [EMIM]Cl with DHB Matrix (M:IL:A = 50:50:1).....	160
Figure 4-3: Structures of Cationic Derivatizing Reagents for Sugar Modification: (a) GTMA; (b) Girard's reagent T.....	162
Figure 4-4: Reaction Scheme of Derivatization of Glucose with GTMA	163
Figure 4-5: ¹ H NMR Spectra of Glucose-GTMA Derivatization Reaction in [BMIM]Cl: (a) at t = 0, (b) at t = 2 h.....	164
Figure 4-6: MALDI-MS Spectra of Sugar Analytes after Derivatization with GTMA in [EMIM]Cl, M:IL:A = 10:10:1: (a) Glucose-GTMA; (b) Fructose-GTMA; (c) Sucrose-GTMA; (d) NAG-GTMA	166
Figure 4-7: MALDI-MS Spectra of 10:1 [BMIM]Cl:Glucose with DHB Matrix (a) Before derivatization with GTMA; (b) After derivatization with GTMA.....	168
Figure 4-8: MALDI-MS Spectra of (a) HMF-GTMA; (b) Levulinic Acid-GTMA (ester) with DHB Matrix (reaction carried out in H ₂ O).....	168
Figure 4-9: Calibration Curve of HMF-GTMA/Glucose-d ₇ -GTMA in [EMIM]Cl; Error bars represent standard deviation of the mean, n = 5	171
Figure 4-10: Structural Similarity of Potential Internal Standards for the Quantitative Analysis of HMF	172
Figure 4-11: MALDI-MS Spectrum of HMF-GTMA and BnOH-GTMA in [BMIM]Cl using DHB Matrix.....	174
Figure 4-12: Glucose-GTMA/Glucose-d ₇ -GTMA Response by MALDI-MS using DHB Matrix in the Presence of ILs	176
Figure 4-13: Reaction Scheme of CrCl ₃ •6H ₂ O-catalyzed Dehydration of Fructose to HMF in [BMIM]Cl.....	179
Figure 4-14: Calibration Curve of Fructose-GTMA/Glucose-d ₇ -GTMA vs. Concentration; Error bars represent standard deviations of the mean response, n = 5	180
Figure 4-15: Calibration Curve of HMF-GTMA/BnOH-GTMA vs. Concentration; Error bars represent standard deviations of the mean response, n = 5	181

Figure 4-16: MALDI-TOF MS Spectra of the Catalyzed Dehydration Reaction of Fructose to HMF in [BMIM]Cl: (a) at t = 10 min, (b) at t = 190 min	186
Figure 4-17: Reaction Monitoring of the Dehydration of Fructose to HMF (without catalyst) in [BMIM]Cl as a Function of Reaction Time by MALDI-MS	187
Figure 4-18: Reaction Monitoring of the Dehydration of Fructose to HMF (catalyzed by CrCl ₃) in [BMIM]Cl as a Function of Reaction Time by MALDI-MS	187
Figure 4-19: Comparison of HMF Yield as a Function of Reaction Time with and without Catalyst.....	188
Figure 5-1: DESI-MS Spectra of Method Blanks in Positive Ion Mode: (a) 2:1 ACN:H ₂ O, (b) 10 nmol [BMIM]Cl, (c) 10 nmol [EMIM]Cl, (d) 10 nmol [EMIM]OAc	200
Figure 5-2: DESI-MS Spectra of Method Blanks in Negative Ion Mode: (a) 2:1 ACN:H ₂ O, (b) 10 nmol [BMIM]Cl, (c) 10 nmol [EMIM]Cl, (d) 10 nmol [EMIM]OAc	202
Figure 5-3: DESI-MS Spectra of 10:1 IL:HMF in Positive Ion Mode: (a) [BMIM]Cl, (b) [EMIM]Cl, (c) [EMIM]OAc	204
Figure 5-4: DESI-MS Spectra of 10:1 IL:LA in Negative Ion Mode: (a) [BMIM]Cl, (b) [EMIM]Cl, (c) [EMIM]OAc	206
Figure A2-1: ¹ H NMR Spectrum of 2,5-dihydroxybenzoic acid (DHB)	219
Figure A2-2: ¹ H NMR Spectrum of Sodium 2,5-dihydroxybenzoate	219
Figure A2-3: ¹ H NMR Spectrum of α-cyano-4-hydroxycinnamic acid (CHCA).....	220
Figure A2-4: ¹ H NMR Spectrum of Sodium α-cyano-4-hydroxycinnamate (NaCHCA)	220
Figure A2-5: ¹ H NMR Spectrum of 1-butyl-3-methylimidazolium chloride ([BMIM]Cl)	221
Figure A2-6: ¹ H NMR Spectrum of 1-ethyl-3-methylimidazolium chloride ([EMIM]Cl)	221
Figure A2-7: ¹ H NMR Spectrum of 1-ethyl-3-methylimidazolium acetate ([EMIM]OAc)	222
Figure A2-8: ¹ H NMR Spectrum of 1-butyl-3-methylimidazolium chloride/2,5-dihydroxybenzoic acid ([BMIM]Cl-DHB)	222
Figure A2-9: ¹ H NMR Spectrum of 1-ethyl-3-methylimidazolium chloride/2,5-dihydroxybenzoic acid ([EMIM]Cl-DHB)	223

Figure A2-10: ^1H NMR Spectrum of 1-ethyl-3-methylimidazolium 2,5-dihydroxybenzoate ([EMIM][DHB]).....	223
Figure A2-11: ^1H NMR Spectrum of 1-butyl-3-methylimidazolium chloride/ α -cyano-4-hydroxycinnamic acid ([BMIM]Cl-CHCA)	224
Figure A2-12: ^1H NMR Spectrum of 1-ethyl-3-methylimidazolium chloride/ α -cyano-4-hydroxycinnamic acid ([EMIM]Cl-CHCA)	224
Figure A2-13: ^1H NMR Spectrum of 1-ethyl-3-methylimidazolium α -cyano-4-hydroxycinnamate ([EMIM][CHCA])	225
Figure A3-1: ^{13}C NMR Spectrum of 2,5-dihydroxybenzoic acid (DHB).....	227
Figure A3-2: ^{13}C NMR Spectrum of Sodium 2,5-dihydroxybenzoate (NaDHB)	227
Figure A3-3: ^{13}C NMR Spectrum of α -cyano-4-hydroxycinnamic acid (CHCA).....	228
Figure A3-4: ^{13}C NMR Spectrum of Sodium α -cyano-4-hydroxycinnamate (NaCHCA)	228
Figure A3-5: ^{13}C NMR Spectrum of 1-butyl-3-methylimidazolium chloride ([BMIM]Cl)	229
Figure A3-6: ^{13}C NMR Spectrum of 1-ethyl-3-methylimidazolium chloride ([EMIM]Cl)	229
Figure A3-7: ^{13}C NMR Spectrum of 1-ethyl-3-methylimidazolium acetate ([EMIM]OAc)	230
Figure A3-8: ^{13}C NMR Spectrum of 1-butyl-3-methylimidazolium chloride/2,5-dihydroxybenzoic acid ([BMIM]Cl-DHB)	230
Figure A3-9: ^{13}C NMR Spectrum of 1-ethyl-3-methylimidazolium chloride/2,5-dihydroxybenzoic acid ([EMIM]Cl-DHB)	231
Figure A3-10: ^{13}C NMR Spectrum of 1-ethyl-3-methylimidazolium 2,5-dihydroxybenzoate ([EMIM][DHB]).....	231
Figure A3-11: ^{13}C NMR Spectrum of 1-butyl-3-methylimidazolium chloride/ α -cyano-4-hydroxycinnamic acid ([BMIM]Cl-CHCA)	232
Figure A3-12: ^{13}C NMR Spectrum of 1-ethyl-3-methylimidazolium chloride/ α -cyano-4-hydroxycinnamic acid ([EMIM]Cl-CHCA)	232

Figure A3-13: ^{13}C NMR Spectrum of 1-ethyl-3-methylimidazolium α -cyano-4-hydroxycinnamate ([EMIM][CHCA])	233
Figure A4-1: FT-IR Spectrum of Sodium 2,5-dihydroxybenzoic acid (DHB).....	235
Figure A4-2: FT-IR Spectrum Sodium of 2,5-dihydroxybenzoate (NaDHB)	235
Figure A4-3: FT-IR Spectrum of α -cyano-4-hydroxycinnamic acid (CHCA)	236
Figure A4-4: FT-IR Spectrum of Sodium α -cyano-4-hydroxycinnamate (NaCHCA)	236
Figure A4-5: FT-IR Spectrum of 1-butyl-3-methylimidazolium chloride ([BMIM]Cl) .	237
Figure A4-6: FT-IR Spectrum of 1-ethyl-3-methylimidazolium chloride ([EMIM]Cl)..	237
Figure A4-7: FT-IR Spectrum of 1-ethyl-3-methylimidazolium acetate ([EMIM]OAc)	238
Figure A4-8: FT-IR Spectrum of 1-butyl-3-methylimidazolium chloride/2,5-dihydroxybenzoic acid ([BMIM]Cl-DHB)	238
Figure A4-9: FT-IR Spectrum of 1-ethyl-3-methylimidazolium chloride/2,5-dihydroxybenzoic acid ([EMIM]Cl-DHB)	239
Figure A4-10: FT-IR Spectrum of 1-ethyl-3-methylimidazolium 2,5-dihydroxybenzoate ([EMIM][DHB])	239
Figure A4-11: FT-IR Spectrum of 1-butyl-3-methylimidazolium chloride/ α -cyano-4-hydroxycinnamic acid ([BMIM]Cl-CHCA)	240
Figure A4-12: FT-IR Spectrum of 1-ethyl-3-methylimidazolium chloride/ α -cyano-4-hydroxycinnamic acid ([EMIM]Cl-CHCA)	240
Figure A4-13: FT-IR Spectrum of 1-ethyl-3-methylimidazolium α -cyano-4-hydroxycinnamate ([EMIM][CHCA])	241

List of Abbreviations and Symbols

a.i. – absolute intensity

A.U. – arbitrary units

ACN – acetonitrile

ASE – analyte suppression effect

BMIM – 1-butyl-3-methylimidazolium

CHCA – α -cyano-4-hydroxycinnamic acid

Da – Dalton

DESI – desorption electrospray ionization

DHB – 2,5-dihydroxybenzoic acid

DMAc – dimethylacetamide

DNS – 3,5-dinitrosalicylic acid

EMIM – 1-ethyl-3-methylimidazolium

EPR – electron paramagnetic resonance

ESI – electrospray ionization

eV – electron volt

Fru – fructose

GC – gas chromatography

Glu – glucose

GTMA – glycidyltrimethylammonium (chloride)

HMF – 5-hydroxymethylfurfural

HPLC – high performance liquid chromatography

IL – ionic liquid

ILM – ionic liquid matrix

IR – infrared

IS – internal standard

LA – levulinic acid

LDI – laser desorption/ionization

LOD – limit of detection

LOQ – limit of quantitation

M^{+} – molecular ion

M:A – matrix-to-analyte ratio

m/z – mass-to-charge ratio

MALDI – matrix-assisted laser desorption/ionization

MS – mass spectrometry

MSE – matrix suppression effect

NAG – *N*-acetyl-D-glucosamine

NMMO – *N*-methylmorpholine *N*-oxide

NMR – nuclear magnetic resonance

O.D. – optical density

OAc – acetate

PEG – polyethylene glycol

QAS – quaternary ammonium salt

RSD – relative standard deviation

RTIL – room temperature ionic liquid

S/N – signal-to-noise ratio

SA – sinapinic acid

SEM – scanning electron microscopy

Suc – sucrose

TFA – trifluoroacetic acid

TOF – time-of-flight

UV – ultraviolet

VOC – volatile organic compound

List of Appendices

Appendix I: Preparation of Ionic Liquid Matrices	213
Appendix II: ^1H NMR Spectra	218
Appendix III: ^{13}C NMR Spectra	226
Appendix IV: FT-IR Spectra	234
Appendix V: Chapter 4 Supplementary Material	242
Appendix VI: Statistical Analysis	245

Chapter 1: : Introduction and Literature Review

1.1 Alternative Energy from Biomass

1.1.1 Overview

The world currently relies on fossil fuels as our primary source of energy and platform chemicals for the production of a huge array of consumer goods. In fact, over 80 % of the total global energy is sourced directly from coal, natural gas and petroleum feedstocks.¹ Fossil fuels have long provided us with heat, electricity and an abundance of consumer goods such as plastics, pharmaceuticals, and electronics. Unfortunately, the fossil carbon feedstocks that supply and provide these amenities are non-renewable, and consequently, are unsustainable.² Furthermore, the burning of fossil fuels has resulted in a significant impact on the environment; atmospheric levels of CO₂ and other greenhouse gases have increased substantially, leading to global climate change, among other environmental and health concerns.³ As the world's population continues to rise, it becomes inevitable that alternative sources of energy will be required to supply future global demands.

The development of sustainable strategies to reduce our current reliance on fossil fuels has accelerated in the past decade, with considerable progress in the field. Several alternative sources of energy including wind, solar, and hydro-powered processes are currently being implemented for the generation of heat and electricity.³ However, in the future, liquid fuels and chemicals will also be in high demand, especially in the air and sea transportation sectors. Presently, biomass serves as the only renewable resource that is capable of supplementing these needs.⁴ Therefore, significant efforts have been put forth

to develop sustainable technologies for processing biomass and subsequently upgrading to valuable chemicals. As of 2014, renewable energy sources provided 11 % of consumed global energy, 5.5 % of which was supplied by biomass sources.¹

1.1.2 Sustainable Energy from Biomass

Unlike fossil fuels, biomass is ubiquitous in nature, being produced on a billion-ton scale annually.⁵ As a renewable resource, biomass can easily be replenished.

Exploitation of energy from biomass is a greener alternative to petrochemicals, as it taps into the natural carbon cycle, with net life-cycle emissions substantially lower than that of fossil fuel utilization. Similar to fossil fuels, however, biomass can also be directly incinerated to generate heat and energy, or can alternatively be processed and refined to yield liquid fuels and a variety of co-products. Therefore, it is practical to develop technologies for the extraction and processing of biomass energy to alleviate demands on petrochemicals.

Biomass refers to any non-fossilized organic matter (living or recently living). The definition is generally used to describe vegetation, but is extended to include algae, and animal wastes. The stored energy that can be extracted from these renewable biological sources is referred to as biomass energy (or bio-energy). Despite a simple definition, biomass is quite complex, as its composition can vary immensely depending on the source from which it is derived.

1.1.3 Valorization of Waste Biomass

Biomass feedstocks are readily abundant, and can be sourced from both the land and the ocean. Attractively, biomass can alternatively be sourced from wastes. Canada's economy relies heavily on its resource sector; with agriculture, forestry, and fisheries amongst the key industries contributing to the country's economy.⁶ Waste biomass obtained from agricultural and forestry processes (e.g. straw and bark), as well as from the ocean industry (e.g. crab and shrimp shells) is produced in large quantities. For instance, approximately 39,000 tons of shellfish waste is generated in NL per year. Currently, this waste is dumped back into the ocean or in specified landfills.⁷ This is a great opportunity for provinces, such as NL, with strong ocean industries to valorize these "wastes" as raw feedstocks for the production of fuels, plastics, food and pharmaceuticals, as well as various industrial and commercial products.^{4,8} The valorization of waste biomass in general also alleviates pressure of land usage for energy crops that could alternatively be used for food crops. Furthermore, the utilization of waste biomass reduces overall waste accumulation, and is quickly becoming a widely acceptable technology for the sustainable production of energy and chemicals.⁹

1.2 Renewable Carbohydrate Feedstocks

1.2.1 Overview

The bio-refinery concept relies on nature's ability to harvest solar energy. Through photosynthetic processes, plants and algae convert energy from the sun into chemical energy by fixing atmospheric CO_2 in the form of carbohydrates, $\text{C}_n(\text{H}_2\text{O})_n$. Through a series of chemical processes, the energy that is stored in the chemical bonds of

carbohydrates can be harvested and processed to yield sugars and small platform chemicals.

The carbohydrate content of biomass generally represents about 75 % of the total biomass.¹⁰ Plant biomass typically consists of three main components: cellulose, hemicellulose and lignin. The carbohydrate fraction, however, is highly variable and depends on the source from which it is derived. These carbohydrates act as robust structural polymers, and are integral components of the cell walls of plants.

1.2.2 Cellulosic Feedstocks

Cellulose is the most abundant bio-polymer on Earth,¹¹ and represents the largest fraction of plant biomass (40 – 50 % by weight).² Cellulose is a linear-chained polysaccharide, derived from the condensation of hundreds to thousands of D-glucose subunits via $\beta(1\rightarrow4)$ glycosidic bonds (Figure 1-1).

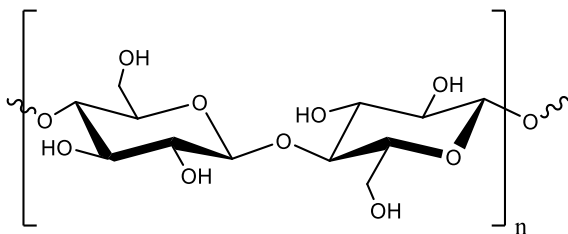


Figure 1-1: Structure of Cellulose

Cellulose is the major component of woody biomass, and can be abundantly sourced from the waste streams of agricultural and forestry processes, making it a readily renewable and available resource. Common sources of cellulosic feedstocks include wood, straw, bark, and food crop residues. Unlike other naturally occurring polymeric

species, such as starch and glycogen, cellulose lacks branching and coiling due to the equatorial conformation of its glucose subunits. The resulting structure of cellulose is therefore very rigid, and rod-like. The presence of hydroxyl substituents on integral glucose monomers leads to an extensive hydrogen-bonding network between polymer chains (Figure 1-2), which further strengthens the polymer.¹² The reinforcement of the polymer by hydrogen-bonding leads to poor dissolution in typical organic solvents; a limiting factor in the bio-processing of cellulose.¹²

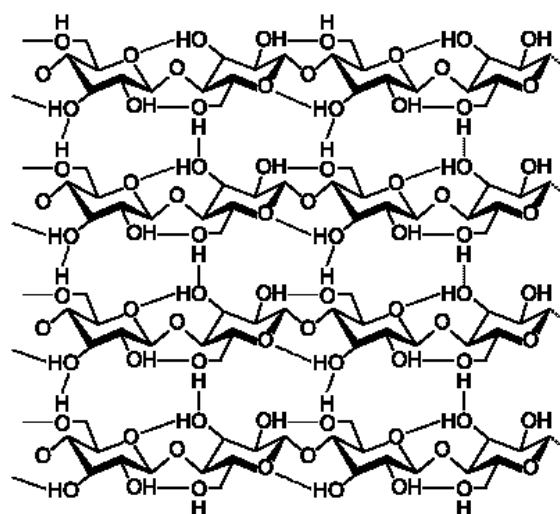


Figure 1-2: Extensive Hydrogen-Bonding Network within Chains of Cellulose
(Reproduced with permission from Ref. 12)

1.2.3 Ocean-Sourced Feedstocks

Although the primary source of biomass is plant-based organic matter, biomass can also be extracted from the ocean. The shells of crustaceans, for example, are sources of the carbohydrates chitin and its deacetylated product chitosan, with chitin being the second most abundant biopolymer after cellulose.¹³ The nitrogen-containing carbohydrate

chitin is analogous to cellulose, and functions as structural polymers in the exoskeletons of crustaceans.

Comparable to cellulose, chitin is also an abundant carbohydrate that can be sourced from wastes. Chitin occurs in the shells of crustaceans such as lobster, crab, and shrimp. The structure is similar to that of cellulose, exhibiting a crystalline, fibrous macrostructure due to the straight-chained linkage of monomer units. Rather than glucose, however, chitin is composed of *N*-acetyl-D-glucosamine (NAG) subunits linked in a $\beta(1\rightarrow4)$ fashion.

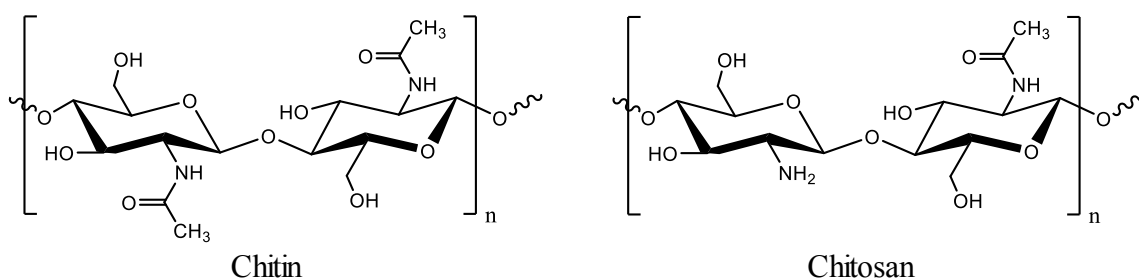


Figure 1-3: Structures of Chitin and Chitosan Biopolymers

Chitosan, which is normally produced from chitin, is composed of randomly distributed NAG and D-glucosamine subunits, and is often referred to as partially deacetylated chitin. Chitin and chitosan differ from cellulose in the fact that the monomeric units are nitrogen-containing, and can therefore serve as a viable renewable source of nitrogen-containing platform chemicals.¹⁴

1.2.4 Sugar Feedstocks

The sugars derived from larger biopolymers are valuable feedstocks for the production of platform chemicals. Other sugars can be derived from these monomers, or

can be extracted from specific types of biomass. Sugarcane, for example is an excellent source of the disaccharide sucrose, which can be hydrolyzed to yield glucose and fructose monomers. Fructose can be extracted from fruits and berries, or can alternatively be produced from the isomerization of glucose. Amino-sugars such as *N*-acetyl-D-glucosamine (NAG) and D-glucosamine are primarily derived from chitin and chitosan, respectively.

Monosaccharides are the smallest of the carbohydrates and generally consist of only C, H, and O, although derivatives containing nitrogen, sulfur and phosphorus are possible. Simple sugars (monosaccharides) are polyhydroxy-aldehydes or ketones (aldoses and ketoses, respectively). Glucose and NAG are examples of aldohexoses, whereas fructose is classified as a ketohexose. Intermolecular cyclization of sugars through a hydroxyl group and the carbonyl yield the hemiacetal or hemiketal form. This reaction results in a new stereocenter, referred to as the anomeric carbon (C-1; the carbonyl carbon in open-chained form). If a sugar contains an aldehyde (or hemiacetal) group, or can tautomerize to yield an aldehyde group, the sugar is classified as a reducing sugar. In nature, these sugars exist in both straight-chained and cyclic forms, with the cyclic form being the prevalent conformer in solution.

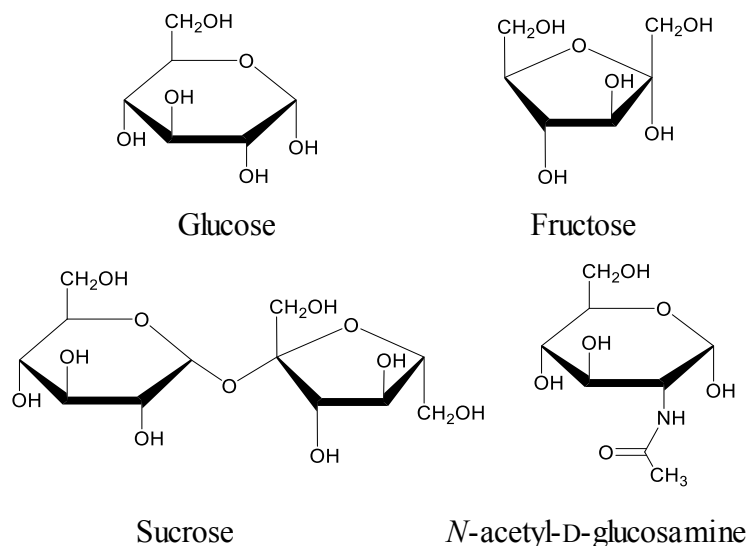


Figure 1-4: Cyclic Conformers of Common Bio-Derived Sugars

Cyclization yields further classification of sugars, based on the size of the ring. Six-membered rings are collectively referred to as pyranoses, while five-membered rings are termed furanoses. In cyclic form, glucose preferentially forms a six-membered ring, whereas fructose forms a five-membered ring. Sucrose is the product of the condensation reaction between glucose and fructose via an $\alpha(1 \rightarrow 2)$ glycosidic bond. Unlike its monomeric units, sucrose is a non-reducing sugar; that is, in solution, it contains neither hemiacetal nor aldehyde functional groups that can be oxidized.

Each of the aforementioned sugars are extremely water-soluble, crystalline solids. Due to the presence of many hydroxyl groups, these compounds have appreciable polarities, and have limited solubilities in many organic solvents. Since sugars are alcohols, they can be deprotonated in solution and have slightly acidic character (refer to Table 1-1).^{15,16} Typically, sugars are slightly more acidic than simple alcohols, and have relatively low proton affinities. Therefore, mass spectrometric analysis of sugars

generally requires the use of a cationization agent, such as sodium or potassium ions to promote ionization and allow detection of positively charged ions.

Table 1-1: Properties of Selected Sugars

Sugar	Molar Mass (g/mol)	Water Solubility at 25 °C (mg/mL)	p<i>K</i>_a (in water at 25 °C)^{15,16}
Glucose (C ₆ H ₁₂ O ₆)	180.16	909	12.28
Fructose (C ₆ H ₁₂ O ₆)	180.16	3750	12.03
Sucrose (C ₁₂ H ₂₂ O ₁₁)	342.30	2000	12.62
<i>N</i> -acetyl-D-glucosamine (C ₈ H ₁₅ NO ₆)	221.21	148	11.56

Reactions of sugars generally occur through the carbonyl functional group or via hydroxyl substituents. Common reactions of sugars include oxidation and reduction of the carbonyl, condensation of two or more sugars, and esterification and etherification of hydroxyl groups. Generally, the hydroxyl group of the anomeric carbon is the most reactive site,¹⁷ but this is obviously dependant on the nature of the reaction.

1.2.5 Value-Added Chemicals from Biomass

Chemical or enzymatic hydrolysis of cellulose and chitin yield glucose and NAG, respectively, which serve as sustainable precursors to a variety of compounds. The monomers are also valuable chemicals which can be directly used in the food and chemical industries. For instance, glucose and NAG are common products used in the food and pharmaceutical industries.¹⁸ These compounds can subsequently be chemically altered to yield a variety of useful compounds. The catalytic conversion of glucose has

received much attention as reactions can be tailored to selectively yield a number of value-added derivatives for fuels, plastics, etc.

The catalytic conversion of glucose has received much attention as reactions can be tailored to selectively yield a number of value-added derivatives for fuels, plastics, etc. Glucose can be readily converted to sugar alcohols (e.g. sorbitol, xylitol), acids (e.g. acetic acid, formic acid, and gluconic acid), etc. Glucose, as well as its isomer fructose, can also be used to produce valuable furan-containing compounds (Figure 1-5).

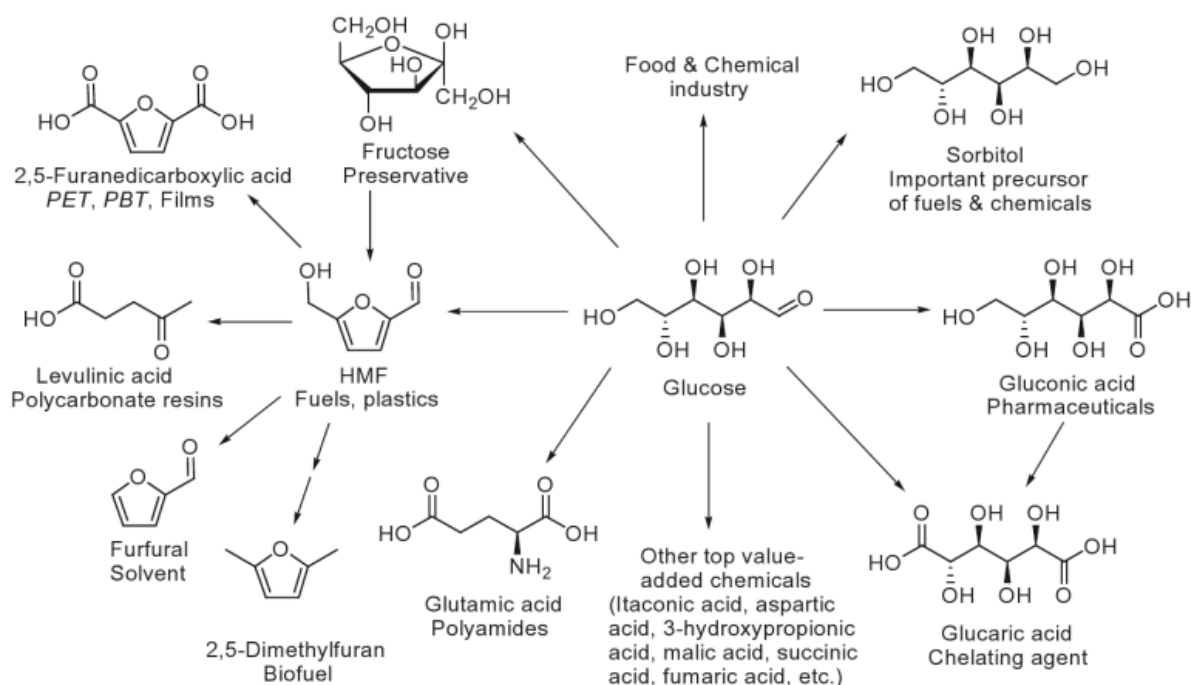


Figure 1-5: Potential routes to value-added chemicals from glucose (Ref. 19 - Reproduced with permission from The Royal Society of Chemistry)

In particular, the dehydration of glucose and fructose to 5-hydroxymethylfurfural (HMF) has received considerable attention as a valuable chemical building block.¹⁰ HMF is a precursor for the production of fuels, solvents and plastics, as well as a key intermediate in the production of liquid alkanes from glucose (or fructose).¹⁹ HMF can

also be further converted to a number of furan compounds that are useful in a variety of different applications. The dehydration of HMF can subsequently yield levulinic acid (LA), a valuable precursor for the manufacture of polymers and plastics, pharmaceuticals, food additives and biofuels, with wide industrial applications.²⁰ Furthermore, the disaccharide sucrose (commonly obtained from sugarcane biomass) can be hydrolyzed to yield its monomers glucose and fructose and subsequently processed to yield the same variety of platform chemicals.^{21,22}

Hydrolysis of chitin and chitosan yield nitrogen-containing sugars, NAG and D-glucosamine, which are also precursors for the production of platform chemicals HMF and LA.²³ More recently, NAG has also been dehydrated to form nitrogen-containing platform chemicals. For example, the production of a new renewable amide, 3-acetamido-5-acetylfuran (3A5AF) from NAG and chitin, has been reported.^{14,24,25} Unlike cellulosic sugars, which exclusively contain C, H and O, NAG and 3A5AF from chitin and chitosan can serve as renewable nitrogen-containing platform chemicals.

Several routes for the conversion of biomass to valuable chemicals have been investigated, including gasification, biological (i.e. fermentation) and chemical processing.¹⁹ These refining processes and technologies have allowed the extraction of valuable chemical products during biomass conversion processes using low-value and waste products as viable feedstocks. Energy-dense carbohydrates such as cellulose and chitin are examples of valuable compounds that can be extracted from biomass. The realization of the abundance of valuable chemicals that could be mass produced from such bio-feedstocks, aided in the foundation of the bio-refinery concept, whereby biomass

could be separated, processed, and converted into an array of products through catalytic or biochemical processes.^{2,4,20} The development of sustainable technologies to complement these processes for commercialization, however, are still underway.

1.2.6 Bio-Processing of Carbohydrates

Arguably the most challenging aspect of the utilization of biomass for fuels and chemicals is inherent in the difficulty of dissolving carbohydrate biopolymers in traditional solvents such as water and organic solvents.¹¹ To be competitive with the petrochemical industry, cheap, efficient technologies must be developed to allow economically-feasible biomass processing.¹⁰ Dissolution is often the first step to chemical processing, and is required to increase the rate of mass transfer, and hence reaction kinetics. In nature, both cellulose and chitin act as structural polymers that are innately resistant to changes in environment. Structural differences, in the degree of polymerization (i.e. the number of monomers per polymer), as well as the variations in size and polydispersity of the biopolymer, arise from the biomass from which it is sourced and how it is processed.^{12,26} Furthermore, the extensive hydrogen-bonded networks of polymer chains within cellulose and chitin lead to high cohesive energies, and therefore high solubility parameters.^{12,27,28} It follows, that the complex nature of these polysaccharides render them difficult to solubilize and further depolymerize in water and traditional organic solvents.

Dissolution is an equilibrium process driven by thermodynamics. To achieve dissolution of a large molecule, such as a biopolymer, there must be appreciable polymer-

solvent interactions that favor the process. Generally, dissolving crystalline polymers in solvents is an endothermic process, as polymer-solvent interactions are not as favorable as solvent-solvent or polymer-polymer interactions.^{29,30} Traditionally, cellulose and chitin have been solubilized in strong acids, aqueous solutions of mineral acids, *N,N*-dimethylacetamide/lithium chloride (DMAc/LiCl), and *N*-methylmorpholine oxide (NMMO).²⁹ Unfortunately, many of these traditional solvent systems are toxic or corrosive, require substantial heating for dissolution, and can be difficult to regenerate after the reaction,²⁷ which leads to energy-intensive processes with considerable safety hazards. Clearly, industrial scale-up is impractical under these conditions. An ideal solvent system must allow the dissolution of biopolymer, further transformation, and stabilization of products, while maintaining reasonable handling conditions.

1.3 Ionic Liquid Solvents in Green Processes

1.3.1 Overview and Brief History

Due to the growing concerns of the health and environmental effects caused by volatile organic solvents (VOCs), the use of alternative green solvents in chemical process design has grown tremendously.³¹ The use of solvent in industry, in particular, is of concern due to the large volumes of solvent used, and the difficulty in containing volatile species. Therefore, it is necessary to promote the use of greener, alternative solvents for use in such processes. In cases where a solvent cannot be omitted from a chemical process, several alternative solvents exist that may take the place of harmful VOCs and limit adverse chemical exposure, while providing a medium for heat and mass transfer, and solute dissolution while facilitating the reaction. Alternative solvents, such

as water, supercritical fluids and ionic liquids (ILs), are now taking the place of more harmful solvents in the manufacture of chemicals as well as consumer products such as paints, cosmetics and pharmaceuticals.³¹

Ionic liquids (formerly known as molten salts) are non-molecular compounds composed entirely of ions, which serve as alternative solvents for green chemistry. Ionic liquids differ from traditional inorganic salts in that they have relatively low melting points, existing in the liquid state at or below an arbitrary temperature – commonly below 100 °C or room-temperature. Although research into the use and applications of ionic liquids has only exploded throughout the last decade, ionic liquids have been known for some time. The credit for discovery of ionic liquids is a matter of debate, however, it is often attributed to Paul Wadden, who in 1914 synthesized ethylammonium nitrate ([EtNH₃][NO₃]) which has a melting point of 12 °C.³² Other materials that have since been classified as ionic liquids originated as late as the mid-19th century,³³ but the breakthrough in ionic liquid research followed the development of air- and moisture-stable imidazolium salts in 1992, which generated newfound interest in ionic liquid applications.³⁴

1.3.2 Properties of Ionic Liquids

Ionic liquids are generally composed of a bulky organic cation, with an organic or inorganic anion. Typical classes of ionic liquids are those based on imidazolium, pyridinium, and pyrrolidinium cations paired with a wide variety of anionic counterparts (Figure 1-6).

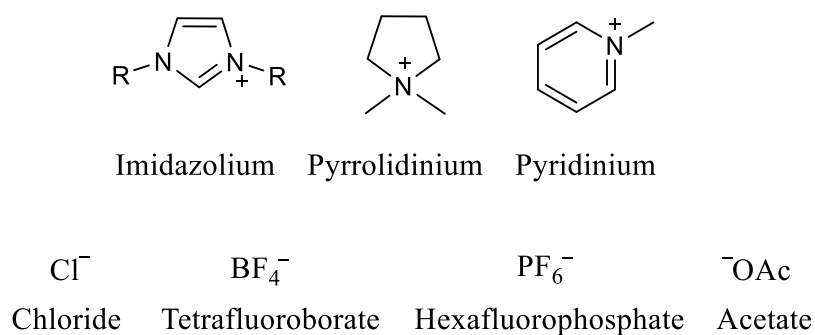


Figure 1-6: Structures of Common Ionic Liquid Ions

These ions have charge distribution over a much larger surface than typical salts such as NaCl, and form unstable lattices due to their bulky, unsymmetrical nature. The significantly lower symmetry of ionic liquids lead to their characteristic low melting points. Due to the vast number of possible cation-anion combinations, ionic liquids are often called “tuneable” solvents, as varying the nature of their two constituent ions can change their properties. These ionic compounds are attractive alternatives to VOCs, as they generally have no or negligible vapor pressures, low combustibility, and high thermal stabilities, meaning they are useful over a wide range of temperatures.³¹ The ionic nature of these solvents give rise to highly polar, non-coordinating solvents, which have also proven to be useful in catalytic processes.³² Those ionic liquids that are immiscible with water, can also act as part of a biphasic system, or as an extraction medium. Furthermore, ionic liquids exhibit powerful dissolution abilities, facilitating otherwise difficult reactions. These unique properties make ionic liquids attractive replacement solvents for processes that use VOCs. Nonetheless, it is important to note that toxicity data on many ionic liquids is scarce, and they must therefore be handled carefully. Studies

have attributed increasing toxicity of ionic liquids containing long cation alkyl chains and those that are composed of imidazolium and pyridinium cations.¹¹

The solubility of ionic liquids in water is an important property in determining their potential use in industry, as well as their possible cytotoxicity in the environment. Screening of ionic liquid properties is challenging due to the vast number of potential species. In saying that, many common ionic liquids have been experimentally tested for water solubility, and others have been predicted using computational methods.^{35,36} In general, the water solubility of a class of ionic liquids is strongly influenced by both the cation and anion hydrophobicities – that is, their hydrogen-bonding abilities. The cation can also be varied to influence the hydrophobicity of the resultant ionic liquid. For example, the alkyl chain lengths of the imidazolium and pyridinium cations can be tuned to promote water miscibility. In general, the hydrophobicity of the ionic liquid increases as alkyl chain increases.³⁶

1.3.3 Ionic Liquids in Biomass Processing

As charged species, ionic liquids exhibit appreciable polarity as solvents. Unlike most polar organic solvents, ionic liquids have the ability to dissolve both polar and non-polar species due to their strong solvation abilities.³⁷ The solvation ability of ionic liquids is attributed to various intermolecular solute-solvent interactions such as ionic interactions, dipole-dipole interactions, and hydrogen-bonding interactions. Due to their strong solvation ability, ionic liquids have been popular alternative solvents for biomass processing.^{26,28,38} As previously mentioned, one of the main challenges in cellulose processing is that the extensive hydrogen-bonding network within the polymer chains

inhibits dissolution by traditional organic solvents.^{11,28} Several ionic liquids, however, have shown superior dissolution of cellulose and other large biopolymers. In order to dissolve polymers such as cellulose and chitin, an ionic liquid must contain a cation or anion that is capable of disrupting the hydrogen-bonding network within the crystalline structure.³⁹ In fact, in a recent study by Andanson, Padua, and Gomes, the enthalpy of dissolution of cellulose in IL 1-ethyl-3-methylimidazolium acetate ([EMIM]OAc) was experimentally determined to be an exothermic process.³⁰ This implies that the interaction between cellulose and [EMIM]OAc solvent is energetically favorable, unlike most traditional solvents used for dissolution.

There are several properties of an ionic liquid that lead to dissolution of large carbohydrates, specifically, cellulose.^{12,28,39} This list of key attributes throughout the literature include:

- Solubility of cellulose increases with decreasing length of alkyl chains of 1-alkyl-3-methylimidazolium ionic liquids. Furthermore, 1-alkyl-3-methylimidazolium-based ionic liquids with even-numbered alkyl chains (ethyl, butyl) more readily dissolve cellulose than odd-numbered alkyl chains
- Within halide containing ionic liquids (e.g. [BMIM]Cl), Cl⁻ species dissolve cellulose better than the I⁻, and Br⁻ analogues, which is can be related to the stronger hydrogen-bond ability of Cl⁻
- Large non-coordinating anions lead to decreased solubility
- Cellulose dissolution decreases from CH₃COO⁻ > Cl⁻ > HCOO⁻ with a given cation

Overall, the most effective ionic liquids for cellulose dissolution were those with anions which are strong hydrogen-bond acceptors. This is not surprising, as such anions are required to disrupt intermolecular hydrogen-bonding between polymer chains. Although many ionic liquids have cellulose dissolution ability, the most commonly studied ionic liquids in cellulosic biomass processing include 1-butyl-3-methylimidazolium chloride ([BMIM]Cl), 1-ethyl-3-methylimidazolium chloride ([EMIM]Cl) and 1-ethyl-3-methylimidazolium acetate ([EMIM]OAc).

Ionic liquids have been employed for the dissolution of chitin and chitosan as well. Although the solubilities of both biopolymers are highly dependent on the degree of deacetylation, both generally dissolve more readily in [BMIM]OAc than [EMIM]OAc.²⁶ Furthermore, ionic liquids containing the Br⁻ anion have been reported to efficiently solubilize polyamines and polyamides. Chitin, for example, has been shown to have appreciable solubility in 1-allyl-3-methylimidazolium bromide ([AMIM]Br).³⁸

1.3.4 Conversion of Biomass in Ionic Liquids

Since gaining in popularity, ILs have been utilized for a wide range of organic reactions and catalytic processes.^{32,40,41} The discovery that alternative IL solvents exhibited powerful solvation ability towards biomass components has resulted in tremendous research towards establishing transformation reactions of biomass in ILs. Although many ILs have been used for the dissolution of large biopolymers such as cellulose and chitin, not all are well-suited for catalytic conversion reactions.¹² Hydrolysis of cellulose and chitin in water is generally accomplished using Brønsted acids. In ILs, however, these catalytic systems are less efficient. In IL media, on the other hand, these

reactions are particularly efficient using metal chloride catalysts.^{10,12,21} Upon depolymerization of cellulose (or chitin), sugars can be upgraded to platform chemicals, using a variety of catalysts, but most often using mineral acids or metal chlorides in 1,3-dialkylimidazolium chloride ILs. Examples include the CrCl₃-catalyzed dehydration of glucose, fructose, sucrose and cellulose to yield HMF,^{10,42,43} as well as the hydrolysis of chitin/chitosan to NAG and glucosamine using mineral acids H₂SO₄ or HCl in ILs such as [EMIM]Cl and [BMIM]Cl.⁴⁴ In some cases, the IL not only facilitates dissolution for mass transfer, but may also participate in the reaction. The ability of IL solvents to facilitate the deconstruction of large biopolymers and subsequently dehydrate the resulting sugar monomers has also led to the development of several one-pot reactions for the production of HMF.^{43,45-47}

1.3.5 Synthesis of Ionic Liquids

Ionic liquids have been tailor-made to suit a variety of chemical applications. The combinations of different cations and anions are nearly limitless. Generally, ionic liquids are synthesized by salt metathesis, via different routes (Figure 1-7) depending on the water solubility of the target ionic liquid product.⁴⁸

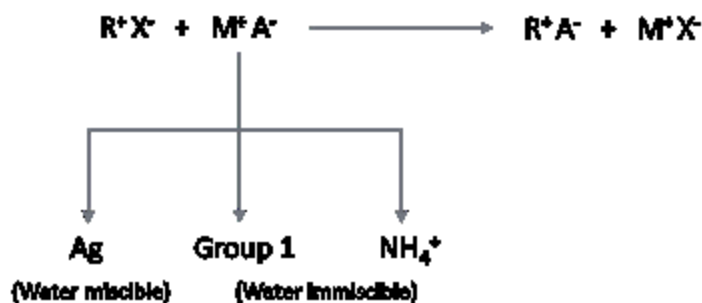


Figure 1-7: General Routes of Ionic Liquid Metathesis (adapted from Ref. 48)

The most common synthetic routes for the generation of water-immiscible ionic liquids utilize the corresponding halide salt of the desired cation with the free acid or Group I salt of the anion.⁴⁸ The simplicity of this reaction, and often ease of separation from the acid or salt by-product renders this the most favorable route. The reagents can be dissolved or suspended into minimal solvent, refluxed, and subsequently concentrated. The acid or salt by-product generated from the reaction with the free acid or salt of the anion, can often be easily washed away with water. Alternatively, the ionic liquid product can be extracted into CH₂Cl₂ (or other appropriate organic solvent), and isolated by evaporation of the solvent. However, this method is only useful for those ionic liquids that are not miscible with the aqueous phase, and have appreciable solubility in an organic phase, which may not always be the case.

Methods for the synthesis of water-miscible ionic liquids are also well explored, but are often more complex, due to the difficulties in removing by-products.⁴⁸ Several methods that currently exist involve the chloride or bromide salt of the desired cation, with the silver salt of the desired anion in order to precipitate the by-product silver halide salt. Although this method works well, silver-containing starting materials can be very

expensive, and the generation of silver halide waste is undesirable. Currently, several alternative avenues for the production of water-soluble ionic liquids have been developed, including the use of ion exchange materials, quaternization of cationic starting materials, and through the formation of *N*-heterocyclic carbene intermediates. The synthetic route of choice should consider both the relative water and organic solubility of the desired product, as well as the ease of isolation and purification.

Similarly, the synthesis of ionic liquid matrices (ILMs) for use in matrix-assisted laser desorption/ionization mass spectrometry (MALDI-MS) has been reported in several research papers (discussed in more detail in Section 1.5.4).⁴⁹⁻⁵¹ Most commonly, the free acid matrix is dissolved in minimal organic solvent, to which equimolar organic base (aniline, pyridine, etc.) is added, and the solution is often heated for 30 min to promote product stability. The solvent is then either removed and the product dried using a high vacuum line, or the solution is used as is to spot the MALDI plate. In the latter case, the resulting mixture of ionic liquid matrix and by-product is used as is without subsequent purification.⁵⁰ It is presumed that the additional acid by-product may be useful in the protonation of some analytes, and removal is deemed unnecessary.

1.3.6 Purification of Ionic Liquids

A major concern with the synthesis of ionic liquids is purification of the final product. Common ionic liquid impurities include adventitious water, organics (residual solvent and unreacted starting materials), halide by-products, and metals.⁴⁸ Water is the most common ionic liquid impurity, as many ionic liquids are extremely hygroscopic. It follows, that water is often a difficult impurity to remove during synthesis. Common

methods for the removal of residual solvent and water include evaporation under high vacuum. Unreacted volatile starting materials can also be removed this way, or similarly by washing with a low boiling organic solvent, which can then be readily removed by evaporation. Other methods of solvent and water removal include azeotropic distillation, molecular sieves, and drying agents. The method of purification chosen depends on the properties of the ionic liquid in question, and therefore should be used as appropriate. Acid and salt by-products of metathesis reactions are also often difficult to remove and their presence can greatly alter the properties of the ionic liquid. In the case of hydrophobic ionic liquids, these impurities can generally be easily removed through subsequent washings with water. Water-miscible ionic liquids, however, are much more difficult to purify this way. In such cases, the ionic liquid can be dissolved in a water-immiscible organic solvent, and extracted using water, but this results in significant loss of product. Precipitation of by-product alkali salts can also be attempted using an appropriate organic solvent, however, the smallest traces of water can greatly influence the dissolution behaviour of the ionic liquid.⁴⁸ Alternatively, alkali salts can be removed by passing an organic solution of the ionic liquid and impurity through a short silica column. Generally, the purification process will greatly depend on the ionic liquid in question, and therefore should be tailored to maximize yield and efficiency.

1.3.7 Ionic Liquids in Analytical Chemistry

Within the past couple of decades, research into the use of ionic liquids as alternative solvents has grown substantially (Figure 1-8). Following suit, the use of ionic liquids in analytical chemistry has been increasingly investigated.

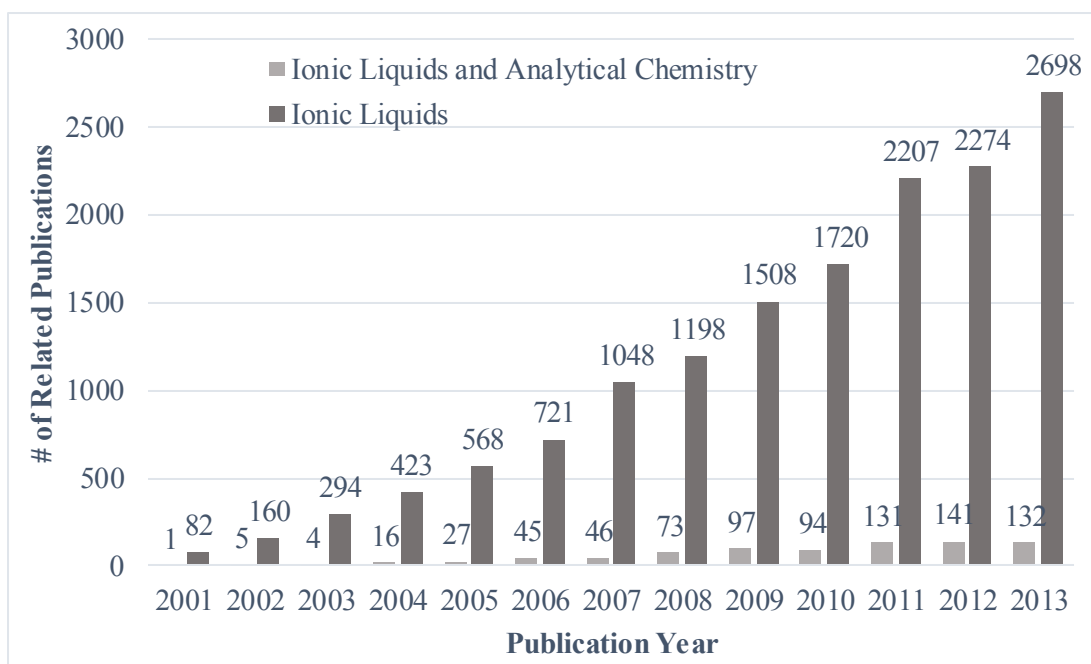


Figure 1-8: Annual Growth of Publications Concerning Ionic Liquids and Ionic Liquids in Analytical Chemistry (Data received via SciFinder Aug. 2014)

The unique, tuneable properties of ionic liquids make them useful media for many analytical applications. In recent literature, ionic liquids have been designed and used as extraction media, as gas and liquid chromatographic stationary phases and mobile phase additives, as capillary electrophoresis buffers, as complexing agents for mass spectrometric detection, and finally, as MALDI matrices, amongst others.³⁴ However, the link between biomass processing in ionic liquids, and the applicability of existing analytical methods, has not yet been well established.

1.4 Analysis of Platform Chemicals in Ionic Liquid Media

Unfortunately, the adoption of greener technologies in industry has been slowed by the inevitable costs of replacing existing technologies with facilities that are compatible with green processes. Furthermore, there are few analytical techniques that are used for the detection and analysis of biomass transformation products.⁵² Those that presently exist, are primarily chromatographic methods that suffer from extensive sample preparation, long analysis times, and must be carefully tailored for both analyte class and source. For example, the analysis of sugars generally require derivatization prior to GC or LC analyses. In an industrial setting, such methods are limited by low sample throughput and cost, resulting in a growing demand for cost-effective analytical techniques to accompany such analyses. The recent movement to use of environmentally-friendly ionic liquids as alternative solvents in synthesis and processing, introduces new complications into analysis, such as tedious extraction steps, and potential incompatibilities with traditional methods of analytical separation and detection. Therefore, typical reactions in ILs require the separation of the analyte(s) from the IL solvent, prior to analysis. This can be particularly difficult, as separation of the analytes may require extraction, precipitation and/or filtration, followed by purification. For example, the IL-mediated transformation of glucose to HMF typically requires solvent extraction of HMF from the IL using organic solvents (e.g. ethyl acetate), evaporation, and reconstitution in an appropriate solvent for GC or LC analyses. The untransformed carbohydrate (and possibly by-products) are often left behind. In the case of imidazolium-ILs (which are commonly employed for such reactions) the common polarities of the solvent and carbohydrate (i.e.

glucose) result in difficulties in separation. Use of anti-solvents (to promote precipitation),⁵³ as well as complexing agents⁵⁴ have been employed to separate these, however, these additional steps render these processes uneconomical and time consuming.

The high viscosities and ionic character of typical ILs also lead to incompatibilities with typical means of chemical monitoring. Specifically, NMR analyses of IL-containing systems often suffer due to high viscosities and interference of radio frequency pulses, which lead to poor resolution.⁵⁵ Furthermore, depending on the structure of the IL, overlapping solvent peaks arise, leading to difficulties in analyte structure elucidation and subsequent quantification. Furthermore, free sugars are generally difficult to accurately analyze by NMR, as these compounds rapidly interconvert between straight-chain and cyclic forms in solution. Although the cyclic form predominates in aqueous solutions, the presence of ILs and other reaction components can have unpredictable effects on this equilibrium.

Other methods for analysis of IL-containing systems include spectroscopic techniques such as UV-Vis and IR. HMF can be directly analyzed by UV-Vis (284 nm), and derivatization of reducing sugars such as glucose with 3,5-dinitrosalicylic acid (DNS) allows for detection by UV-Vis at 498 nm.⁴⁷ However, spectra acquired using these methods can quickly become convoluted with substrate, catalyst and side-product peaks. Furthermore, colored impurities (which are often difficult to remove from ILs) can cause interference in the visible region of the spectrum.

A more recent investigation into the use of direct infusion-ESI analysis for monitoring chemical systems (specifically glucose conversion to HMF) in ILs has been proposed.⁵⁶ This method offers much faster analysis times than traditional chromatography and allows simultaneous detection of reaction intermediates, but requires careful instrument tuning to avoid hardware damage and source contamination from abundant IL species. For reaction conditions whereby the IL is the major component (as is the case when it serves as the solvent), typical ESI-MS spectra suffer from dominant IL ions, and analyte ion suppression. Furthermore, at relatively higher concentrations of IL, carry-over between analyses is a potential problem. By tuning the ion gate to selectively acquire spectra in the range of the analyte (i.e. via tandem MS), detection of these ions can be avoided. Filtration of these interfering ions resulted in enhanced sensitivities for compounds of interest (e.g. glucose and HMF).

It is clearly advantageous to develop novel, advanced analytical methods for the analysis of bio-derived compounds in IL media. Ideally, the methods will allow the simultaneous detection of starting materials and products (as well as by-products), without the need for prior separation from the IL, to be superior to current applications. Furthermore, the methods should have appreciable tolerance to impurities and other reaction components. Desorption/ionization mass spectrometric techniques have the potential to replace existing methods, offering high sample throughput, little to no sample preparation, and ease of data analysis.

1.5 Matrix-Assisted Laser Desorption/Ionization Time-of-Flight Mass Spectrometry

1.5.1 Overview of MALDI-TOF MS

Matrix-assisted laser desorption/ionization (MALDI) is a soft ionization method, which was developed from laser desorption/ionization (LDI) methods. The term MALDI, was first coined in 1985, by Franz Hillenkamp and Michael Karas, after showing enhanced ion yield of alanine (a non-absorbing amino acid) when mixed with the UV-active amino acid, tryptophan.⁵⁷ Following these findings, in 1987, Koichi Tanaka and co-workers combined cobalt nanoparticles in glycerol, for ionization with a nitrogen laser.⁵⁸ This breakthrough method allowed the ionization of biomolecules with molecular weights greater than 30,000 Da. The introduction of an absorbing “matrix” into laser desorption mass spectrometry to promote ionization of high molecular weight analytes, regardless of individual absorption characteristics, offered new insight into the fields of proteomics, polymer chemistry and microbiology.

The relatively simple sample preparation and low sample consumption that is required for MALDI-MS analysis, lead to its sudden popularity in analytical chemistry, as many samples could be analyzed over a short period of time. As a soft ionization technique, MALDI-MS is also known for the ease of spectral analysis, as generally the only ions observed are singly charged analyte ion peaks and adducts. MALDI-MS is, however, limited by the difficulties in achieving quantitative information. Spot inhomogeneity is the primary cause of increased sample analysis times and difficulty in attaining quantitative results, by contributing to poor reproducibility. Additionally, the

choice of MALDI matrix for a particular set of analytes is often not straightforward, and requires an extensive trial and error approach.

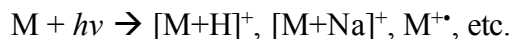
Although MALDI-MS techniques were primarily used for the analysis of high molecular weight proteins, and synthetic polymers, recent advances in MALDI-MS have allowed the analysis of small molecules (<500 Da).⁵⁹ Originally, MALDI analysis of small molecules was avoided, due to the inherent interference from low molecular weight matrix fragments and adducts. However, studies involving matrix suppression, and the use of novel matrices such as ionic liquid matrices, have made small molecule analysis by MALDI-MS much more achievable.⁵⁹

1.5.2 MALDI-TOF MS Instrumentation and Process

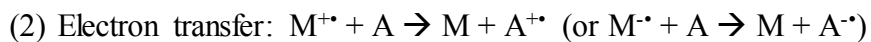
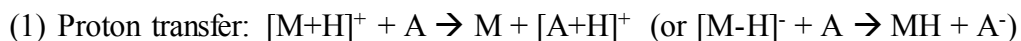
In MALDI analysis, the analyte is first co-crystallized with a UV-absorbing matrix on a sample plate. Upon introduction to the instrument, the plate is placed under vacuum ($10^{-6} - 10^{-7}$ torr) and the sample is irradiated by a pulsed laser, promoting desorption and ionization. The matrix serves to absorb incoming laser energy, and encourage ablation of the sample, while protecting the analytes from decomposition. Ionization and ion transfer in the hot plume due to this process results in the ionization of both matrix and analyte which are then accelerated into a mass analyzer.

Several mechanisms of ion formation in MALDI exist, but a single mechanism cannot explain all of the ions that are observed in a typical MALDI spectrum.⁶⁰ It is important, however, to consider the different ion formation mechanisms, as they apply to a group of analytes to improve ion abundance, and control fragmentation. Several

possible ion formation mechanisms exist, which can generally be divided into two main categories: primary and secondary ionization. Primary ionization refers to the initial ionization of neutral molecules in the sample, which are often the matrix species (M), as a result of interaction with incoming photons:



Secondary ionization includes the ionization of molecules in the MALDI plume, including ionization of the analyte (A), and generally occurs by one of three reactions:



The ions that are observed in the resulting mass spectrum are highly dependent on the matrix used, dopant (if present), and the intrinsic properties of the analyte class.

MALDI-MS instruments are commonly equipped with linear or reflector time-of-flight (TOF) mass spectrometers, the latter which offers high resolution with (theoretically) no mass limitation. A TOF mass analyzer separates and detects ions based on differences in travel time to the detector which is inversely proportional to the mass-to-charge (m/z) ratio. All ions are accelerated using the same potential, which imparts all ions with the same kinetic energy when reaching the flight tube. Therefore, smaller ions travel at higher velocities through the flight tube and reach the detector before larger ions. The detector calculates the m/z ratio based upon the time of ion flight, resulting in a mass spectrum corresponding to the abundance of ions at particular time intervals. Often, TOF

analyzers are equipped with an ion mirror (reflectron) which reflects ions via an electric field (Figure 1-9). This essentially doubles the ion path distance, and compensates for small differences in kinetic energy, leading to increased resolution. The use of an ion mirror is particularly useful for the analysis of small molecular weight molecules.

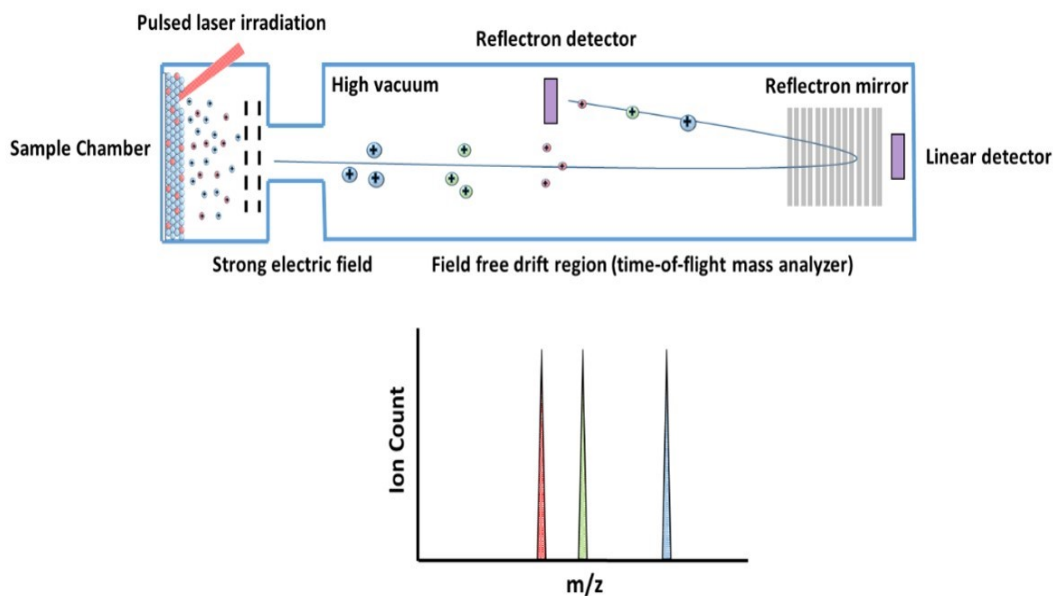


Figure 1-9: MALDI-TOF MS Schematic

1.5.3 Traditional MALDI Matrices

The key to designing an effective MALDI-MS experiment, is often the choice of matrix used to co-crystallize with the analyte of interest. Generally, MALDI matrices serve two primary purposes: to absorb incoming laser irradiation so that the matrix can promote ionization and prevent decomposition of the analyte, and to isolate analyte molecules from one another to prevent analyte-analyte association.⁶¹ In saying that, the matrix is often selected by its ability to embed and isolate the analyte, having similar solubility in compatible MALDI preparation solvents, and to promote desorption and

ionization of the analyte of interest. Furthermore, the matrix must be compatible with MALDI instrumentation, in that it must be able to absorb the wavelength of laser irradiation, be resistant to thermal degradation, and have appreciable vacuum stability (depicted in Figure 1-10).⁵⁰

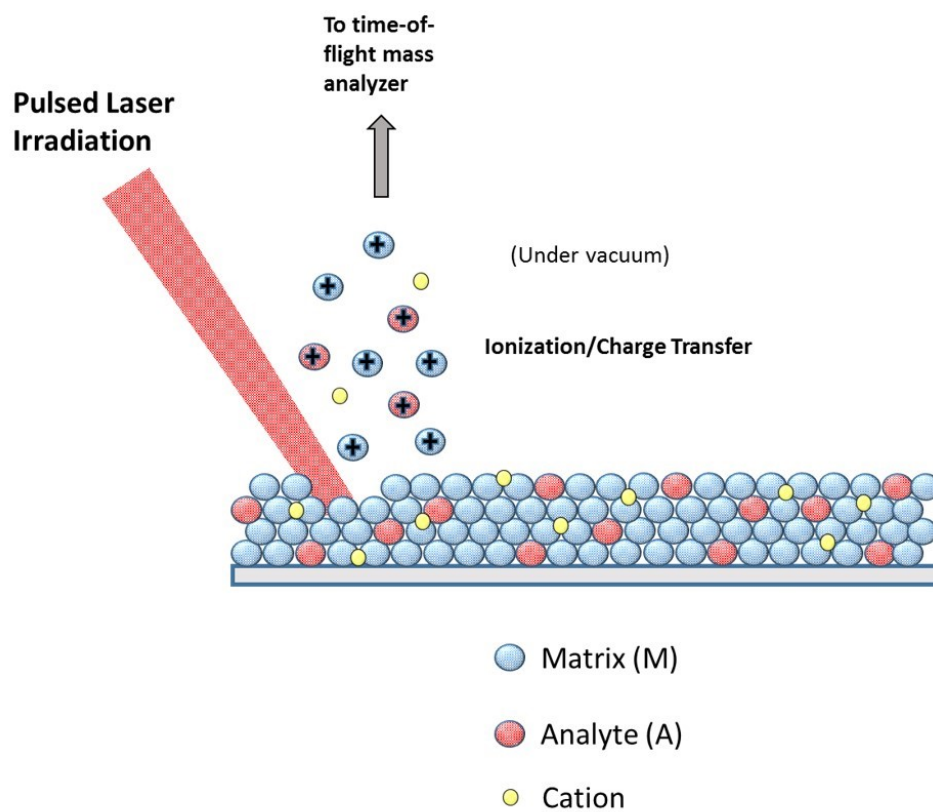


Figure 1-10: Co-crystallization of Matrix and Analyte

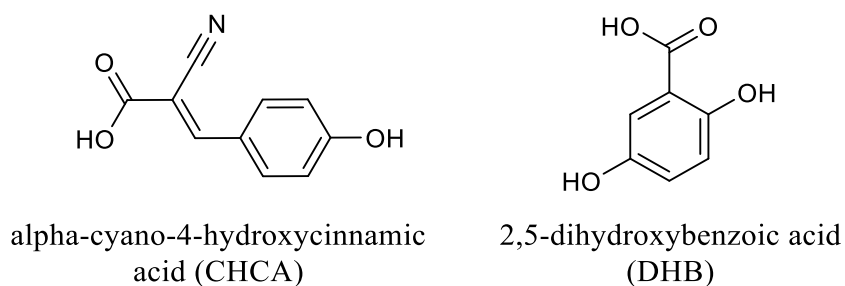


Figure 1-11: Structures of Common MALDI Matrices CHCA and DHB

Typically, MALDI matrices are substituted aromatic organic compounds. The most commonly employed commercially available MALDI matrices are carboxylic acids: sinapinic acid (SA), 2,5-dihydroxybenzoic acid (DHB), and α -cyano-4-hydroxycinnamic acid (CHCA) (Figure 1-11). Carboxylic acid matrices work particularly well when operating the MS in positive mode, as the labile acidic protons readily protonate neutral analyte species.⁵⁰ For analytes that require a more acidic environment, a strong acid additive such as trifluoroacetic acid (TFA) is often used along with the matrix, to ensure protonation. In cases where acidic conditions are unfavorable (such as in the analysis of neutral carbohydrates), a cationization agent may be used to promote adduct formation.⁶² The choice of matrix for the analysis of a particular analyte can be quite intricate, as matrices that work well for a group of compounds may not necessarily be suitable for others. Therefore, selecting an appropriate matrix is often accomplished through trial and error. The major setback with most of these commonly employed MALDI matrices is that they are solids. The difficulty in controlling the crystallization and segregation of analyte molecules throughout the spot leads to both poor shot-to-shot and spot-to-spot homogeneity, and thus poor reproducibility which is a major limitation for quantitative analysis.

1.5.4 Ionic Liquid Matrices

Ionic liquid matrices (ILMs) were first introduced to MALDI-MS analyses by Armstrong *et al.* in 2001,⁴⁹ as potential replacement matrices for solid matrices.

Traditional solid matrices such as DHB and CHCA rely on co-crystallization of matrix and analyte, which can lead to sample spot heterogeneity and poor reproducibility in MALDI-MS analyses. Furthermore, use of such matrices can cause longer analysis times, through searching for “hot spots” where the analyte is most concentrated. Although liquid matrices (which are characteristically more homogeneous) are available to account for spot heterogeneity, many of these matrices suffer due to excessive volatilities, and often do not have desirable UV chromophores. Armstrong proposed that by incorporating common solid UV-active matrix anions into ionic liquids, novel matrices with negligible volatilities could be designed to enhance spot-to-spot and shot-to-shot reproducibility.

Armstrong *et al.* synthesized several UV-active ILMs from cinnamic acid derivatives and common organic bases such as alkylamines and substituted imidazoles and pyridines. The resulting ILMs were tested for their solubilizing ability of test analytes and subsequently used in MALDI-MS for the analysis of peptides and proteins.⁴⁹ Several of the novel ILMs were successful in promoting ionization of test analytes such as bradykinin (high molecular weight peptide) and PEG-2000 (polyether), with substantially better reproducibility than traditional MALDI matrices. For example, the ILM 1-methylimidazolium CHCA, outperformed solid CHCA, having relative standard deviations (RSDs) of 16 %, as compared to 150 %. Furthermore, for many of the ILMs tested, analyte signal intensities were slightly better than those obtained using the

analogous solid matrix. Other observations of this study, included the conclusion that solid matrices that preferentially ionize a particular class of analytes retain this property as an ILM. Armstrong *et al.* also concluded that ILMs designed from room temperature ionic liquids (RTILs) such as 1,3-dialkylimidazolium ILs (e.g. [BMIM][CHCA]) were deemed unsuitable as matrices, likely due to poor laser absorption and lack of transferable protons. In a follow-up study by Crank and Armstrong, the effect of the ILM cation was further investigated with a series of CHCA derivatives. Several cationic amines were tested, and those that performed well as matrices generally had pK_a values ≥ 11 and gas phase proton affinities ≥ 930 kJ/mol.⁵¹

After their introduction to MALDI-MS, ILMs have been designed for many classes of analytes, including small molecules (< 500 Da). The use of ILMs for small molecule analysis also had particular advantages over using traditional solid matrices, beyond increased sample homogeneity. Matrix signals were often suppressed, and less fragmentation of both matrix and analyte was observed.⁶³ This translates to less matrix interference in the low-mass region, as well as ease in spectra interpretation.

The discovery that ILMs could not only increase reproducibility of MALDI analyses, with similar or lower detection limits than traditional matrices, but also be tailored to a particular class of analytes, prompted further investigation by other researchers into the potential of ionic liquid matrices in MALDI-MS. Although a number of UV-active ILs have been designed for these purposes, these novel matrices have not been investigated for their ability to monitor chemical reactions in ILs.

1.5.5 Analysis of Small Neutral Carbohydrates by MALDI-MS

Upon the expansion of MALDI-MS analyses to small molecule classes, there was renewed interest in the rapid analysis of smaller biologically relevant oligo- and mono-saccharides. Through matrix screening, DHB was found to be superior to most commonly used organic acid matrices for the analysis of small neutral carbohydrates.⁶⁴ However, it was determined that smaller sugars were rarely protonated in the process, and $[M+H]^+$ ions were seldom observed. Rather, sugars such as glucose and sucrose, primarily form alkali metal adducts. This observation is consistent with the lack of basic sites within sugars that would bind protons. Therefore, the analysis of sugars by MALDI-MS is generally performed with the use of a cationization agent, often sodium- or potassium-based, but still suffers from low binding efficiency.⁶⁵ Despite these conditions, glucose and sucrose analysis by MALDI-MS has been reported using a variety of supporting materials in matrices including DHB,⁶⁶ carbon nanotubes,⁶⁵ wood charcoal,⁶² and DHB-pyridine ionic liquids⁶⁷ with LODs in the pmol range.

Due to the inherently low ionization efficiency of sugars, derivatization of the analytes is often desirable. This may be deemed unnecessary when analyzing systems with relatively high sugar concentrations,⁶⁶ but for those systems with wide, or low concentration ranges, derivatization by introduction of a more “ionizable” functional group should overcome sensitivity problems.⁶⁸ A variety of derivatizing agents for sugars have been employed for this purpose, including reductive amination, silylation, as well as introduction of quaternary ammonium centers. Introducing functional groups that are more readily ionized have been reported to give increases of sensitivity over several

orders of magnitude. Other limitations of MALDI-MS analyses of sugars, include spot inhomogeneity, which can limit quantitative analyses. The choice of matrix, use of an internal standard, and a greater number of replicate analyses, however, can significantly improve reproducibility.

1.6 Desorption Electrospray Ionization Mass Spectrometry

1.6.1 Overview

Amongst the most recent advances in mass spectrometry, desorption electrospray ionization (DESI) has become a popular tool in analytical chemistry. DESI-MS was developed in 2004 by Professor R. Graham Cooks' research group from Purdue University.⁶⁹ DESI is applicable to a variety of analyte classes with high sensitivities, and rapid analysis times. Since its commercialization, DESI has become a popular, versatile instrument for chemical analysis under ambient conditions in chemistry, biology and forensics.⁶⁹⁻⁷²

DESI couples desorption ionization with traditional electrospray ionization (ESI) methods. Unlike ESI, DESI allows ionization to be accomplished at ambient temperature and pressure, rather than under vacuum or within an enclosed source.⁶⁹ Ionization is achieved by first spraying electrically charged droplets at the sample surface. Interaction between charged spray droplets and the analyte results in ion transfer, while the pneumatic pressure of the incoming spray causes projection of secondary analyte ions into the gas phase. The secondary analyte ions travel a short distance through air into the mass spectrometer via an atmospheric ion-transfer line (Figure 1-12).⁷¹

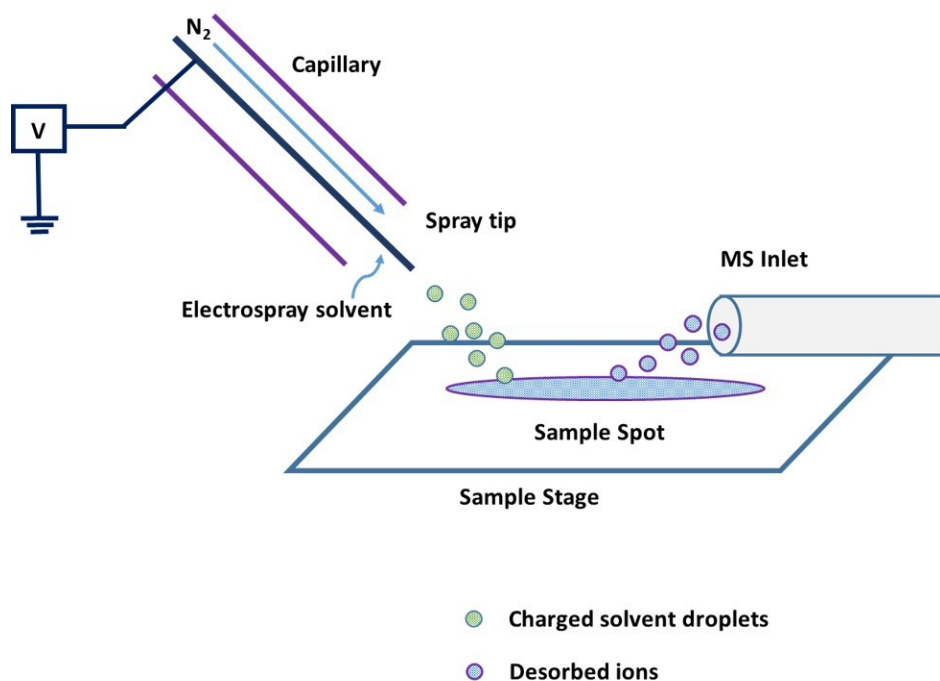


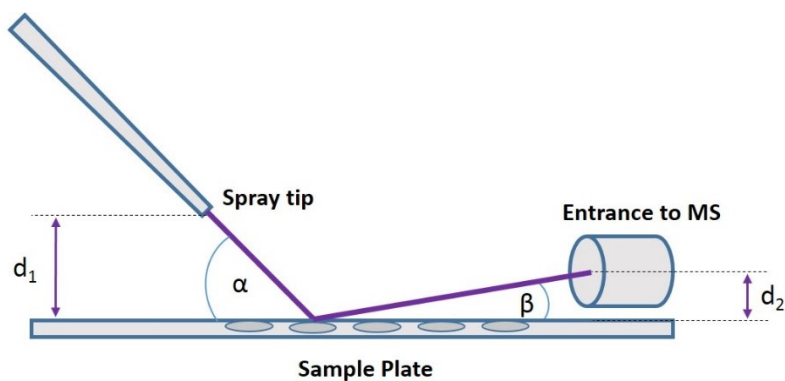
Figure 1-12: DESI-MS Process

1.6.2 Instrumentation and Process

The DESI source consists of a moveable pneumatic electrospray source and sample stage, which can be mounted to interface any atmospheric pressure mass spectrometer. The sprayer is mounted on a vertical stage which can then be mounted to a 3D movable sample stage. The flexibility of the source components allow for tuning sprayer-to-MS and sprayer-to-surface distances, which is critical in achieving a high ion signal. The sample chamber contains a coated aluminum block which contains a heater that can withstand temperatures between room temperature and 300 °C.⁷¹

Preparation for DESI-MS analysis consists of very little to no sample pretreatment. Many samples can be analyzed directly under the spray, and others are simply spotted as is onto a DESI sample plate and inserted into the sample chamber. Like

MALDI-MS, DESI-MS requires very little sample, and can achieve qualitative results with only 5 – 10 μL of sample within approximately 5 seconds.⁷¹ A major advantage of DESI-MS over MALDI-MS is that no matrix is required to promote analyte ionization, and samples can often be directly analyzed in their native form.



α	Incident angle	0 - 90°
β	Collection angle	5 - 10°
d_1	Tip to surface distance	1 – 10 mm
d_2	MS inlet from surface distance	0 – 2 mm

Figure 1-13: Tuneable Geometric Parameters in DESI-MS Source (adapted from Ref. 71)

The most influential geometric parameters of the DESI (Figure 1-13) include the incident angle of solvent spray (α), the collection angle (β), the spray-to-tip distance (d_1), the surface-to-inlet distance (d_2), the solvent composition and flow rate, gas flow rate and applied potential.⁷¹ These parameters can be sequentially tested in preliminary work to determine optimal signal intensity for a particular set of analytes. Parameters α and d_1 directly affect the ionization process, while β and d_2 affect collection efficiency. The optimal settings for each of the aforementioned parameters can be determined and

tailored to suit a particular class of analytes for optimal signal-to-noise or signal intensity.⁷¹

The spray solvent of choice can also be optimized for DESI-MS. Typically, spray solvents are aqueous solutions containing organic solvent fractions of desired polarity. Ideal spray solvents will dissolve the analytes of interest upon impact, resulting in selective desorption of the target compounds. Additives such as acids or bases to promote protonation or deprotonation are also commonly added to the spray solvent. Similarly, cationization agents (e.g. NaCl, KCl, etc.) can be used to increase sensitivity of neutral compounds such as sugars, and other analytes with poor ionizability, which prefer adduction. The spray solvent can also be altered to contain complexing agents, or reagents that selectively react with the analyte of interest upon impact. This technique is collectively referred to as reactive DESI-MS. Doping the spray solvent allows for a range of reaction types such as redox reactions, metal complexation, and functional group modification, which enhance the selectivity of the method towards particular analyte classes.⁷⁰ For example, reactive DESI has been employed for the analysis of glucose with the addition of benzenboronate anions to the DESI spray solvent. This allows the formation of glucose phenylboronate complexes which selectively react with cis-diol compounds.⁷³ Applications such as this allow for selective ionization of glucose with less background noise and higher sensitivity.

The spray flow and gas flow rates are also important parameters in a DESI experiment, as these control the size of incoming droplets and the overall area of the sample which is impacted. Solvent flow rates typically vary from 1 – 5 $\mu\text{L}/\text{min}$. The flow

rate influences the fluctuation of incoming droplets, as well as the size of the impact area (Figure 1-14).⁷⁴

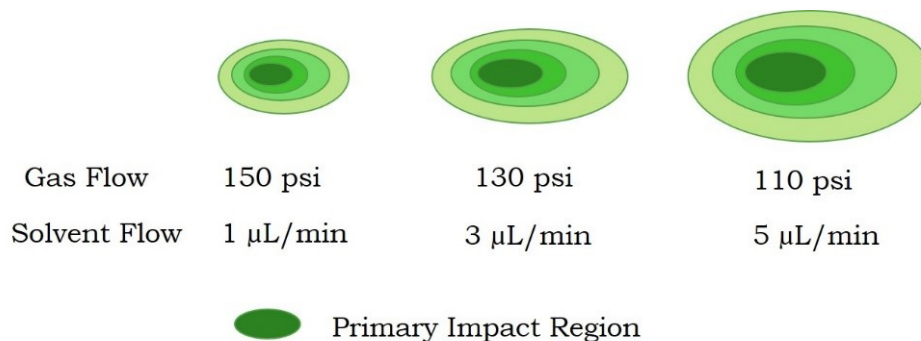


Figure 1-14: Effect of Solvent and Gas Flow Rates of Sample Impact Area in a Typical DESI-MS Experiment (adapted from Ref. 74)

High solvent flow rates lead to increased sample impact area, but excessive flow can lead to sample dilution, or redistribution of the analyte within the sample. Similarly, the gas flow (typically 100 – 150 psi) affects solvent droplet formation. Lower pressures lead to larger incoming solvent droplets, which may also lead to analyte dilution. Optimization and validation of these parameters should be determined before quantitative analysis is attempted as other parameters such as solvent composition and flow rate, gas flow rate and potential can alter signal intensity.

1.6.3 Ionization Mechanisms

Mechanistic studies of the DESI ionization process suggest that a droplet-pick-up process is occurring.⁷² Upon spraying the sample, wetting of the sample surface likely results in a pooled solvent layer into which analyte may partition or collect. With

subsequent spraying, newly arriving droplets transfer momentum to this layer, and secondary droplets are expelled from the sample surface.

Ionization by DESI occurs by two mechanisms depending on the relative mass of the analyte.⁷¹ For low molecular weight molecules, ionization occurs via charge transfer by an electron or a proton, resulting in primary ion formation. Charge transfer can occur between a solvent ion and an analyte molecule on the sample surface, or in the gas phase (at high vapor pressure). Additionally, when the spray to surface distance is large, charge transfer can occur between a gas phase solvent ion and an analyte molecule on the surface.

Mass spectra of high molecular weight analytes, such as proteins, show multiply charged ions, which suggests desorption of the analyte followed by multiple charge transfer from the solvent. The now ionized and solvated analyte (charged droplet) enters the mass analyzer inlet, and is subsequently desolvated. DESI-MS spectra are analogous to ESI-MS spectra, featuring multiply charged ions, alkali metal adducts, and ions of noncovalent complexes. DESI is therefore a useful technique for the analysis of peptides and proteins. Furthermore, the DESI source is superior for ionizing nonpolar compounds, which are not easily ionized by ESI.

1.6.4 Applications of DESI-MS

Since its introduction, DESI-MS has been employed for numerous applications in chemistry, biology and forensics. The applications range from biological sampling of plant and animal tissues, explosive detection, and environmental analysis. The number of

applications for DESI-MS is continuously growing, as more and more analytes can be detected under mild DESI conditions.

Neutral carbohydrates, including glucose, have also been previously analyzed using DESI-MS.^{73,75-77} Much like the ESI spectra of these compounds, salt adducts were the primary ions observed (most often sodium adducts in positive ion mode). Apart from the biological applications for analyzing glucose, and other small sugars, DESI-MS has been used to monitor cellulose degradation in paper.⁷⁶ In reported cases, glucose could be detected at as low as 25 pmol. Similar desorption methods exist for the analysis of HMF, including differential mobility DESI-MS,⁷⁸ and direct analysis in real-time (DART)-MS⁷⁹ for the analysis of HMF in foods (i.e. honey, caramel, etc.), and interestingly, extractive electrospray ionization (EESI) for qualitative monitoring of HMF production from fructose in [EMIM]Cl ionic liquid.⁸⁰ In the latter case, quantitation was not attempted, and fructose detection was not reported, however increasing HMF intensities were monitored as the reaction progressed. It follows that there is significant research to be conducted for the analysis of platform chemicals in ILs, an application that may be well suited for DESI-MS.

1.7 Project Aims

The aim of this research is to develop novel analytical methods for the rapid, qualitative/quantitative analysis of bio-derived platform chemicals and to monitor chemical transformation reactions of bio-derived sugars in ionic liquid media. By incorporating previous research in the fields of analytical chemistry and carbohydrate

processing, novel methods for the *in situ* analysis of small platform chemicals have been proposed, using desorption/ionization mass spectrometric techniques. The use of these MS techniques is complementary to industrial processes: there is little to no sample preparation necessary, sample analyses are rapid (seconds) leading to high sample throughput, and data analysis is very straightforward.

Selected bio-derived sugars and platform chemicals have been chosen as target analytes for this study: glucose, fructose, sucrose, *N*-acetyl-D-glucosamine, 5-hydroxymethylfurfural and levulinic acid. These compounds will be analyzed in ILs that are commonly used for catalytic biomass transformation, specifically, 1-butyl-3-methylimidazolium chloride ([BMIM]Cl), 1-ethyl-3-methylimidazolium chloride ([EMIM]Cl) and 1-ethyl-3-methylimidazolium acetate ([EMIM]OAc). The goal of this work is to be able to remove an aliquot of a reaction mixture (containing both analyte and ionic liquid), and analyze directly using MALDI-TOF MS and/or DESI-MS.

For MALDI-TOF MS analyses, the applicability of selected MALDI matrices and ILs will be investigated for their ability to promote ionization of the analytes of interest. Studies will be conducted to optimize sample preparation procedures, as well as operating parameters to afford the highest sensitivity and selectivity. Finally, properties of the IL-matrix mixtures will be investigated to aid in rational experimental design. DESI-MS will be similarly conducted to analyze mixtures of analytes in ILs under ambient ionization conditions. Operating parameters will be optimized to develop an efficient means of chemical monitoring. The proposed methods will be applied to monitor chemical transformation reactions in ILs, and compared to existing methods. Finally, figures of

merit will be determined to define applicability and limitations of the methods towards the systems of interest.

References

1. U.S. Energy Information Administration: Primary Energy Overview - March 2015. http://www.eia.gov/totalenergy/data/monthly/pdf/sec1_3.pdf (accessed April 10, 2015).
2. Alonso, D. M.; Bond, J. Q.; Dumesic, J. A. *Green Chem.* **2010**, *12*, 1493-1513.
3. Lee, S.; Speight, J. G.; Loyalka, S. K., Eds. *Handbook of Alternative Fuel Technologies*; CRC: Boca Raton, FL, 2007.
4. Klass, D. L. *Biomass for Renewable Energy and Fuels*; Academic Press: San Diego, CA, 1998.
5. Perlack, R. D.; Wright, L. L.; Turhollow, A. F.; Graham, R. L. *Biomass as Feedstock for a Bioenergy and Bioproducts Industry: The Technical Feasibility of a Billion-Ton Annual Supply*. Oak Ridge National Lab TN, 2005.
6. Environment Canada - Planning for a Sustainable Future: A Federal Sustainable Development Strategy for Canada. <https://www.ec.gc.ca/dd-sd/default.asp?lang=En&n=16AF9508-1> (accessed March 5, 2015).
7. Kerton, F. M.; Liu, Y.; Omari, K. W.; Hawboldt, K. *Green Chem.* **2013**, *15*, 860-871.
8. Iakovau, E.; Karagiannidis, A.; Vlachos, D.; Toka, A.; Malamakis, A. *Waste Manage.* **2010**, *30*, 1860-1870.
9. Pfaltzgraff, L. A.; De bruyn, M.; Cooper, E. C.; Budarin, V.; Clark, J. H. *Green Chem.* **2013**, *15*, 307-314.
10. Zakrzewska, M. E.; Bogel-Lukasik, E.; Bogel-Lukasik, R. *Chem. Rev.* **2011**, *111*, 397-417.
11. Zakrzewska, M. E.; Bogel-Lukasik, E.; Bogel-Lukasik, R. *Energy Fuels* **2010**, *24*, 737-745.
12. Zhang, Z. C. *WIREs Energy Environ.* [Online] **2013**, doi: 10.1002/wene.67

13. Dutta, P. K.; Dutta, J.; Tripathi, V. S. *J. Sci. Ind. Res.* **2004**, *63*, 20-31.
14. Drover, M. W.; Omari, K. W.; Murphy, J. N.; Kerton, F. M. *RSC Adv.* **2012**, *2*, 4642-4644.
15. Feng, S.; Bagia, C.; Mpourmpakis, G. *J. Phys. Chem. A.* **2013**, *117*, 5211-5219.
16. Bhattacharyya, L. Ion Chromatography - Principles and Applications. In *Applications of Ion Chromatography for Pharmaceutical and Biological Products*; Bhattacharyya, L.; Rohrer, J., S., Eds.; John Wiley & Sons, Inc.: Hoboken, New Jersey, 2012, pp 3-21.
17. El Khadem, H. *Carbohydrate Chemistry: Monosaccharides and their Oligomers*; Academic Press: London, 1988.
18. Clark, J. H.; Deswarte, F. *Introduction to Chemicals from Biomass*. John Wiley and Sons: West Sussex, UK, 2008.
19. Crocker, M. *Thermochemical Conversion of Biomass to Liquid Fuels and Chemicals*; RSC: Cambridge, UK, 2010.
20. Song, J.; Fan, H.; Ma, J.; Han, B. *Green Chem.* **2013**, *15*, 2619-2635.
21. Stahlberg, T.; Fu, W.; Woodley, J. M.; Riisager, A. *ChemSusChem.* **2011**, *4*, 451-458.
22. Wang, Z.; Keshwani, D. R. Biomass Resources. In *Biomass to Renewable Energy Processes*, Cheng, J., Ed.; CRC: Boca Raton, FL, 2010, pp 41-70.
23. Omari, K. W.; Besaw, J. E.; Kerton, F. M. *Green Chem.* **2012**, *14*, 1480-1487.
24. Chen, X.; Chew, S. L.; Kerton, F. M.; Yan, N. *Green Chem.* **2014**, *16*, 2204-2212.
25. Omari, K. W.; Dodot, L.; Kerton, F. M. *ChemSusChem.* **2012**, *5*, 1767-1772.
26. Bochek, A. M.; Murav'ev, A. A.; Novoselov, N. P.; Zaborski, M.; Zabivalova, N. M.; Petrova, V. A.; Vlasova, E. N.; Volchek, B. Z.; Lavrent'ev, V. K. *Russ. J. Appl. Chem.* **2012**, *85*, 1718-1725.
27. Pillai, C. K. S.; Paul, W.; Sharma, C. P. *Prog. Polym. Sci.* **2009**, *34*, 641-678.

28. Swatloski, R. P.; Spear, S. K.; Holbrey, J. D.; Rogers, R. D. *J. Am. Chem. Soc.* **2002**, *124*, 4974-4975.
29. Wang, H.; Gurau, G.; Rogers, R. D. *Chem. Soc. Rev.* **2012**, *41*, 1519-1537.
30. Andanson, J. M.; Padua, A. A.; Costa Gomes, M. F. *Chem. Commun.* **2015**, *21*, 4485-4487.
31. Kerton, F. M.; Marriott, R. *Alternative Solvents for Green Chemistry*, 2nd ed. RSC Publishing: Cambridge, UK, 2013.
32. Welton, T. *Chem. Rev.* **1999**, *99*, 2071-2083.
33. Wilkes, J. S. *Green Chem.* **2002**, *4*, 73-80.
34. Sun, P.; Armstrong, D. W. *Anal. Chim. Acta.* **2010**, *661*, 1-16.
35. Ranke, J.; Othman, A.; Fan, P.; Muller, A. *Int. J. Mol. Sci.* **2009**, *10*, 1271-1289.
36. Freire, M. G.; Santos, L.; Fernandes, A. M.; Coutinho, J. A. P.; Marrucho, I. M. *Fluid Phase Equilib.* **2007**, *261*, 449-454.
37. Freemantle, M. *An Introduction to Ionic Liquids*; RSC Publishing: Cambridge, UK, 2010.
38. Kadokawa, J. *Green Sustainable Chem.* **2013**, *3*, 19-25.
39. Tan, S.; MacFarlane, D. R. Ionic Liquids in Biomass Processing. In *Ionic Liquids*; Kirchner, B., Ed.; Springer: Berlin Heidelberg, 2010, pp 311-339.
40. Jain, N.; Kumar, A.; Chauhan, S.; Chauhan, S. M. S. *Tetrahedron* **2005**, *61*, 1015-1060.
41. Tadesse, H.; Luque, R. *Energy Environ. Sci.* **2011**, *4*, 3913-3929.
42. Zhao, H.; Holladay, J. E.; Brown, H.; Zhang, Z. C. *Science* **2007**, *316*, 1597-1600.
43. Li, C.; Zhang, Z.; Zhao, Z. K. *Tetrahedron Lett.* **2009**, *50*, 5403-5405.
44. Zhang, Z.; Li, C.; Wang, Q.; Zhao, Z. *Carb. Polym.* **2009**, *78*, 685-689.

45. Liu, B.; Zhang, Z.; Zhau, Z. K. *Chem. Eng. J.* **2013**, *15*, 517-521.
46. Su, Y.; Brown, H. M.; Huang, X.; Zhou, X.; Amonette, J. E.; Zhang, Z. C. *App. Catal. A.* **2009**, *361*, 117-122.
47. Zhou, L.; Liang, R.; Ma, Z.; Wu, T.; Wu, Y. *Bioresour. Technol.* **2013**, *129*, 450-455.
48. Clare, B.; Sirwardana, A.; Macfarlane, D. R. *Top. Curr. Chem.* **2010**, *290*, 1-40.
49. Armstrong, D. W.; Zhang, L.; He, L.; Gross, M. L. *Anal. Chem.* **2001**, *73*, 3679-3686.
50. Tholey, A.; Heinze, E. *Anal. Bioanal. Chem.* **2006**, *386*, 24-37.
51. Crank, J. A.; Armstrong, D. W. *J. Am. Soc. Mass Spectrom.* **2009**, *20*, 1790-1800.
52. Murzin, D.; Holmbom, E. Analytical Approaches in Biomass Catalysis. In *Catalysis for the Conversion of Biomass and its Derivatives*; Behrens, M., Datye, A. K., Eds.; epubli: Germany, 2013, pp 183-212.
53. Hassan, E.; Mutelet, F.; Pontvianne, S.; Moise, J. *Environ. Sci. Technol.* **2013**, *47*, 2809-2816.
54. Brennan, T. C. R.; Datta, S.; Blanch, H. W.; Simmons, B. A.; Holmes, B. M. *Bioenerg. Res.* **2010**, *3*, 123-133.
55. Ananikov, V. P. *Chem. Rev.* **2011**, *111*, 418-454.
56. Khemchyan, L. L.; Khokhlova, E. A.; Seitkalieva, M. M.; Ananikov, V. P. *ChemistryOpen* **2013**, *2*, 208-214.
57. Karas, M.; Bachmann, D.; Hillenkamp, F. *Anal. Chem.* **1985**, *57*, 2935-2939.
58. Tanaka, K.; Waki, H.; Ido, Y.; Akita, S.; Yoshida, Y.; Yoshida, T. *Rapid Commun. Mass Spectrom.* **1988**, *2*, 151-153.
59. Cohen, L.; Go, E. P.; Siuzdak, G. Small Molecule Desorption/Ionization Mass Analysis. In *MALDI MS: A Practical Guide to Instrumentation, Methods and*

Applications; Hillencamp, F., Peter-Katalinic, J., Eds.; Wiley-VCH Verlag: Weinheim, 2007, pp 299-337.

60. Zenobi, R.; Knochenmuss, R. *Mass Spectrom. Rev.* **1998**, *17*, 337-366.

61. Hillencamp, F.; Peter-Katalinic, J. *MALDI MS: A Practical Guide to Instrumentation, Methods and Applications*. Wiley: Hoboken, 2013.

62. Lee, S. *Mass Spectrom. Lett.* **2010**, *1*, 33-36.

63. Zabet-Moghaddam, M.; Heinzle, E.; Tholey, A. *Rapid Commun. Mass Spectrom.* **2004**, *18*, 141-148.

64. Harvey, D. J. *Mass Spectrom. Rev.* **1999**, *18*, 349-451.

65. Ren, S. F.; Zhang, L.; Cheng, Z. H.; Guo, Y. L. *J. Am. Soc. Mass Spectrom.* **2005**, *16*, 333-339.

66. Grant, G. A.; Frison, S. L.; Yeung, J.; Vasanthan, T.; Sporns, P. *J. Agric. Food Chem.* **2003**, *51*, 6137-6144.

67. Yang, H.; Lee, A.; Lee, M.; Kim, W.; Kim, J. *Bull. Korean Chem. Soc.* **2010**, *31*, 35-40.

68. Harvey, D. J. *Mass Spectrom. Rev.* **2012**, *31*, 183-311.

69. Takats, Z.; Wiseman, J. M.; Gologan, B.; Cooks, R. G. *Science* **2004**, *306*, 471-473.

70. Cooks, R. G.; Ouyang, Z.; Takats, Z.; Wiseman, J. M. *Science* **2006**, *311*, 1566-1570.

71. Takats, Z.; Wiseman, J. M.; Cooks, R. G. *J. Mass Spectrom.* **2005**, *40*, 1261-1275.

72. Venter, A.; Nefliu, M.; Cooks, R. G. *Trends Anal. Chem.* **2008**, *27*, 284-290.

73. Chen, H.; Cotte-Rodriguez, I.; Cooks, R. G. *Chem. Commun.* **2006**, 597-599.

74. Desorption Electrospray Ionization - Technology Description.

<http://www.prosolia.com/desorption-electrospray-ionization> (accessed November 10, 2014).

75. Kauppila, T. J.; Talaty, N.; Jackson, A. U.; Kotiaho, T.; Kostianinen, R.; Cooks, R. G. *Chem. Commun.* **2008**, 2674-2676.
76. Stephens, C. H.; Shrestha, B.; Morris, H. R.; Bier, M. E.; Whitmore, P. M.; Vertes, A. *Analyst* **2010**, *135*, 2434-2444.
77. Zhang, Y.; Chen, H. *Int. J. Mass Spectrom.* **2010**, *289*, 98-107.
78. Galhena, A. S.; Harris, G. A.; Kwasnik, M.; Fernandez, F. M. *Anal. Chem.* **2010**, *82*, 9159-9163.
79. Rajchl, A.; Drgova, L.; Gregrova, A.; Cizkova, H.; Sevcik, R.; Voldrich, M. *Anal. Bioanal. Chem.* **2013**, *405*, 4737-4745.
80. Law, W. S.; Chen, H.; Ding, J.; Yang, S.; Zhu, L.; Gamez, G.; Chingin, K.; Ren, Y.; Zenobi, R. *Angew. Chem.* **2009**, *121*, 8427-8430.

Chapter 2: : Preparation and Characterization of Imidazolium-Based Ionic Liquid Matrices

2.1 Introduction

Matrix-assisted laser/desorption ionization mass spectrometry (MALDI-MS) is a versatile analytical tool for the analysis of a variety of molecule classes. The numerous matrix choices allow MALDI-MS methods to be developed that are specific to a particular class of analytes, and these methods can be tailored to enhance analyte selectivity and sensitivity.¹ MALDI-MS is an attractive analytical technique for industrial processes, as sample preparation is often minimal, and samples can be analyzed rapidly and efficiently. Matrices for MALDI-MS analyses are continually designed to optimize ionization efficiency, as well as to minimize sample inhomogeneity, a characteristic drawback of MALDI-MS analysis. More recently, ionic liquid matrices (ILMs) have been introduced, which incorporate UV-active MALDI matrices with bulky organic cations, forming liquid matrices with increased uniformity.² Since the introduction of ILMs, many classes of these liquid matrices have been developed for specific analyte classes, from large biomolecules to small analytes (< 500 Da).²⁻⁴

Ionic liquids (ILs) have not only found applications in analytical chemistry, but across almost all disciplines of chemistry.⁵ Specifically, green chemistry applications use ILs as alternative solvents, and there has been significant progress in using ILs for biomass transformations for the production of bio-derived platform chemicals, as well as for upgrading these bio-feedstocks to usable materials such as biofuels, plastics, and a

variety of other consumer goods.⁶⁻⁸ Although the prospects of such bio-based technologies are attractive, analytical methods to complement such progress are often a major limiting factor.^{9,10} Therefore, there is an ample opportunity to combine the recent progress in ILM development of MALDI-MS methods with IL-containing reaction systems, such as those employed for biomass conversion.

In this work, traditional MALDI matrices were incorporated with common ILs used in biomass processing with the intention of forming ionic liquid matrices (ILMs) for the analysis of common bio-derived platform chemicals. The goal of this work is to develop analytical methods which require minimal sample preparation and allow rapid analyses for the acquisition of qualitative and quantitative information. Although many methods exist for the synthesis of task-specific ILs,¹¹ including ILMs,^{2,3,12} simple combinations of matrix and IL were employed as a means of reducing the time required for sample preparation. It is hypothesized that for MALDI-TOF MS analyses, solutions of both matrix and IL (and analyte) could be mixed and directly spotted onto a MALDI substrate for analysis, without the need for solvent separation or further purification. For the purposes of characterization, however, the matrices were isolated in solid (or liquid) form to determine some of the physicochemical properties of the new matrices, and to determine whether a new ionic liquid matrix (ILM) is formed *in situ*.

The matrices of interest in this study are 2,5-dihydroxybenzoic acid (DHB) and α -cyano-4-hydroxycinnamic acid (CHCA), which are commonly employed matrices for carbohydrates and small molecule classes.^{1,13} ILs that are commonly used in biomass processing, specifically those used in carbohydrate dissolution and transformation^{7,8,14}

were employed as the IL-counterpart in these studies. Three representative imidazolium-based ILs were chosen to be included in this work: 1-butyl-3-methylimidazolium chloride ([BMIM]Cl), 1-ethyl-3-methylimidazolium chloride ([EMIM]Cl) and 1-ethyl-3-methylimidazolium acetate ([EMIM]OAc).

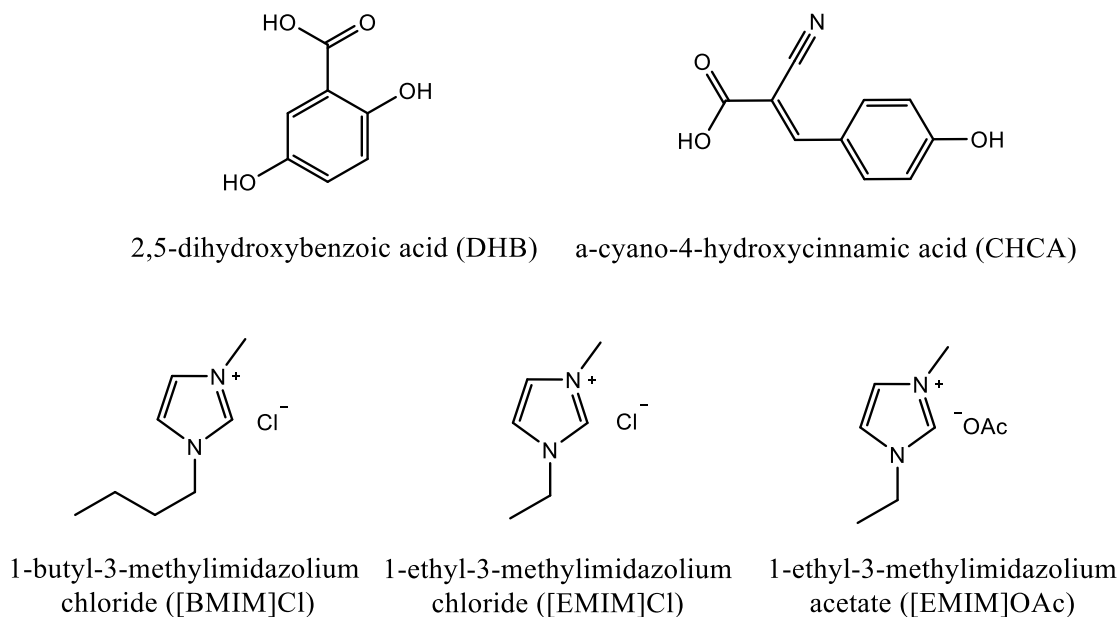


Figure 2-1: Matrices and Ionic Liquids Employed for Matrix Design

The resulting matrix systems were characterized using spectroscopic techniques to determine some physicochemical properties of the products and to aid in further experimental design. These methods allow differentiation between mixtures of parent acid and IL and newly formed ILMs which incorporate the conjugate base of the matrix species. As previously mentioned, the ideal sample preparation methods for the proposed work should be relatively quick and simple. Therefore, mixtures of matrix acid and IL were to be mixed in an appropriate solvent and spotted as is onto the MALDI plate. It is

important to note that a new IL ion pair is not necessarily formed in this manner. To establish whether or not the mixtures of matrix and IL formed a new ion pair, the products (or mixtures of products) were isolated and analyzed by NMR, UV-Vis and IR spectroscopies. The sodium salts of each matrix acid were prepared and used as standards for the formation of the matrix anion. In each case, the parent acid and anionic matrix were analyzed to serve as an indicator of reaction completion and the successful formation of a new ion pair (i.e. a new ILM).

2.2 Materials

2,5-Dihydroxybenzoic acid (DHB) (98 %), α -cyano-4-hydroxycinnamic acid (CHCA) (≥ 98 %), and 1-ethyl-3-methylimidazolium chloride ([EMIM]Cl) (98 %) were obtained from Sigma-Aldrich (St. Louis, MO). The 1-butyl-3-methylimidazolium chloride ([BMIM]Cl) (96 %) was purchased from Alfa Aesar (Ward Hill, MA), and 1-ethyl-3-methylimidazolium acetate ([EMIM]OAc) (> 95 %) was purchased from Io-Li-Tec (Tuscaloosa, AL). Deuterated dimethyl sulfoxide- d_6 (99.9 % + 0.05 % TMS v/v) and methanol- d_4 (99.8 %) were purchased from Cambridge Isotopes (Andover, MA). Water, methanol and acetonitrile (HPLC grade, 99.9 %) were obtained from Fisher Scientific (Fair Lawn, NJ). All chemicals were used without further purification.

2.3 Instrumentation

2.3.1 ^1H and ^{13}C NMR Spectroscopy

^1H NMR and ^{13}C NMR spectra were acquired at room temperature using a Bruker AVANCE III 300 MHz NMR spectrometer. Samples were dissolved in DMSO- d_6 or

MeOH-d₄ at concentrations of ~ 10 - 20 mg/mL. Chemical shifts are reported in parts per million (ppm) from TMS reference. Data was analyzed using MestreNova 9.0.1 (licenced software through Memorial University).

2.3.2 UV-Vis Spectroscopy

Solutions of varying concentrations were transferred to clean quartz cuvettes (1 cm path length), and inserted into a fiber-optic cell connected to an Ocean Optics DH-2000-BAL deuterium halogen lamp source and an Ocean Optics USB4000 UV-Vis spectrometer. The spectrometer was operated with an integration time of 5 ms, spectra were measured over a range of 200 – 800 nm and all acquired spectra were averaged over 50 scans. Raw data was exported to Microsoft Excel for processing.

2.3.3 IR Spectroscopy

IR spectra of solid samples were obtained using an ALPHA FT-IR Spectrometer (Bruker) equipped with an ALPHA Platinum ATR single reflection diamond ATR module. Spectra were recorded in the spectral range of 400 – 4000 cm⁻¹ with spectral resolution of 4 cm⁻¹. Data was exported to Microsoft Excel for processing.

2.4 Methods

2.4.1 UV-Vis Solution Preparation

Stock solutions of 2 mM ILMs and starting materials were prepared in acetonitrile for UV-Vis analysis. The stock solutions were diluted in the appropriate solvent to yield working standards of 25, 50, 75 and 100 µM. Acetonitrile was used as the method blank.

For those mixtures resulting in colored species, UV-Vis analysis was carried out using methanol as the solvent, at specified concentrations. In these cases, methanol was employed as the method blank.

2.4.2 Preparation of ILM-Matrix Mixtures

The ionic liquid matrices (ILMs) were prepared and used as is for MALDI analyses, without removal of solvents or by-products, and without further purification. However, for the purposes of characterization, products (or mixture of products) were isolated. All following procedures were carried out at 1-2 g scale. ILMs were synthesized by modified procedures of previously reported methods,² based on salt metathesis (Figure 2-2).

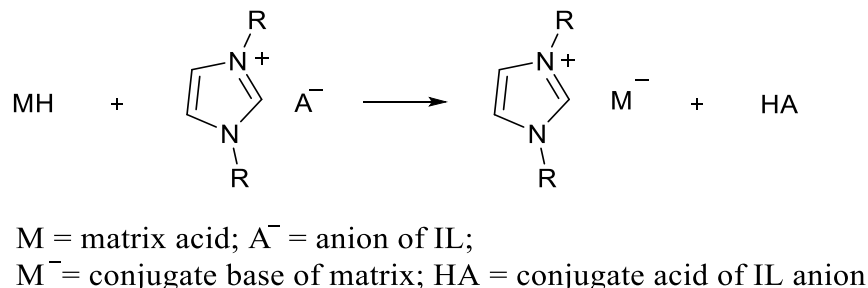


Figure 2-2: General Reaction Scheme for ILM Preparation from Imidazolium-Based ILs

Simply, equimolar amounts of organic solutions of both the free acid and a commercially available imidazolium ionic liquid (as a cation donor) were combined, and heated to promote dissolution. The following procedure represents the general methodology for the preparation (more detailed procedures specific to each product can

be found in Appendix I). Approximately 10 mmol of ionic liquid ([EMIM]Cl, [EMIM]OAc, or [BMIM]Cl) was weighed into a round bottom flask with a magnetic stir bar. An equivalent of matrix acid (DHB or CHCA) was dissolved in minimal organic solvent (MeOH or ACN) and quantitatively transferred to the reaction flask. The mixture was stirred (or sonicated if necessary) to fully dissolve the reagents, and heated over a hot water bath for 30 min. Upon cooling, the bulk of the solvent was removed by rotary evaporation, followed by evaporation under a gentle stream of N₂ gas for 30 min. All products were isolated in yields >100 %, indicating presence of impurities such as the by-product acid and residual solvent, which was difficult to remove. In the case of mixtures containing matrix and [EMIM]OAc which produced AcOH by-product, the AcOH was removed by multiple azeotropic distillations with toluene (as described in Section 2.4.4). All products were transferred to vials, purged with N₂ gas, tightly sealed and stored at room temperature. The products were used as MALDI matrices without further purification for preliminary screening of potential analytes (as described in Chapter 3). There was little emphasis placed on the purity of these matrices at this point, as the overall goal of this research is to simplify sample preparation as much as possible. If the matrices worked reasonably well while impure, it was hypothesized that a reaction mixture in ionic liquid media could then be mixed with an appropriate MALDI matrix acid to form the ILM *in situ*, and subsequently analyzed by MALDI-MS.

(1): 1-butyl-3-methylimidazolium chloride/2,5-dihydroxybenzoic acid [BMIM]Cl-DHB (mixture): Thick, clear brown liquid (104 %). ¹H NMR (300 MHz, DMSO, 298 K) δ 9.29 (s, 1H), 7.81 (dd, *J* = 1.8 Hz, 1H), 7.74 (dd, *J* = 1.8 Hz, 1H), 7.19 (d, *J* = 2.9 Hz, 1H), 6.99 (dd, *J* = 8.8, 3.1 Hz, 1H), 6.78 (d, *J* = 8.8 Hz, 1H), 4.18 (t, *J* = 7.2 Hz, 2H), 3.87

(s, 3H), 1.88 – 1.62 (m, 2H), 1.40 – 1.14 (m, 2H), 0.90 (t, J = 7.3 Hz, 3H); ^{13}C NMR (75 MHz, DMSO, 298 K) δ 171.7, 154.0, 149.5, 136.6, 123.7, 123.6, 122.2, 117.6, 114.6, 112.6, 48.4, 35.7, 31.3, 18.7, 13.2.

(2): 1-ethyl-3-methylimidazolium chloride/2,5-dihydroxybenzoic acid [EMIM]Cl-

DHB (mixture): Pale yellow crystalline solid (106 %). ^1H NMR (300 MHz, DMSO, 298 K) δ 9.31 (s, 1H), 7.83 (dd, J = 1.8 Hz, 1H), 7.74 (dd, J = 1.8 Hz, 1H), 7.19 (d, J = 3.0 Hz, 1H), 7.00 (dd, J = 8.9, 3.1 Hz, 1H), 6.78 (d, J = 8.9 Hz, 1H), 4.21 (q, J = 7.3 Hz, 2H), 3.87 (s, 3H), 1.42 (t, J = 7.3 Hz, 3H); ^{13}C NMR (75 MHz, DMSO, 298 K) δ 171.7, 154.0, 149.5, 136.3, 123.7, 123.5, 122.0, 117.6, 114.5, 112.6, 44.1, 35.7, 15.1.

(3): 1-ethyl-3-methylimidazolium 2,5-dihydroxybenzoate ([EMIM][DHB]): Thick, brown liquid with acetic acid by-product (121 %), brown waxy solid (purified, 101 %). ^1H NMR (300 MHz, DMSO, 298 K) δ 13.79 (s, 1H), 9.20 (s, 1H), 7.78 (dd, J = 1.8 Hz, 1H), 7.70 (dd, J = 1.8 Hz, 1H), 7.12 (d, J = 3.0 Hz, 1H), 6.59 (dd, J = 8.6, 3.2 Hz, 1H), 6.43 (d, J = 8.5 Hz, 1H), 4.19 (q, J = 7.3 Hz, 2H), 3.85 (d, J = 0.5 Hz, 3H), 1.41 (t, J = 7.3 Hz, 3H); ^{13}C NMR (75 MHz, DMSO, 298 K) δ 171.2, 155.0, 147.4, 136.3, 123.5, 121.9, 120.8, 118.6, 115.7, 115.5, 44.1, 35.6, 15.1. Presence of AcOH confirmed by ^1H NMR δ 1.90 (s, 3H); ^{13}C NMR δ 172.0, 21.2.

(4): 1-butyl-3-methylimidazolium chloride/ α -cyano-4-hydroxycinnamic acid

[BMIM]Cl-CHCA (mixture): Large yellow crystals (106 %). ^1H NMR (300 MHz, DMSO, 298 K) δ 10.99 (s, 1H), 9.25 (s, 1H), 8.18 (s, 1H), 7.97 (d, J = 8.8 Hz, 3H), 7.80 (dd, J = 1.8 Hz, 1H), 7.73 (dd, J = 1.8 Hz, 1H), 6.99 (d, J = 8.8 Hz, 2H), 4.18 (t, J = 7.2 Hz, 3H), 3.86 (s, 4H), 1.86 – 1.67 (m, 2H), 1.42 – 1.11 (m, 3H), 0.90 (t, J = 7.3 Hz, 4H);

^{13}C NMR (75 MHz, DMSO, 298 K) δ 164.0, 162.7, 154.1, 136.6, 133.6, 123.6, 122.5, 122.2, 116.9, 116.3, 98.2, 48.4, 35.7, 31.3, 18.8, 13.3.

(5): 1-ethyl-3-methylimidazolium chloride/ α -cyano-4-hydroxycinnamic acid

[EMIM]Cl-CHCA (mixture): Orange/tan crystalline solid (103 %). ^1H NMR (300 MHz, DMSO, 298 K) δ 10.82 (s, 1H), 9.16 (s, 1H), 8.18 (s, 1H), 7.97 (d, J = 8.8 Hz, 3H), 7.79 (dd, J = 1.7 Hz, 1H), 7.70 (dd, J = 1.7 Hz, 1H), 6.96 (d, J = 8.8 Hz, 3H), 4.19 (q, J = 7.3 Hz, 2H), 3.85 (s, 3H), 1.41 (t, J = 7.3 Hz, 3H); ^{13}C NMR (75 MHz, DMSO, 298 K) δ 162.8, 154.0, 136.3, 133.6, 123.5, 122.5, 122.0, 116.9, 116.4, 48.5, 44.1, 35.7, 15.1.

(6): 1-ethyl-3-methylimidazolium α -cyano-4-hydroxycinnamate [EMIM][CHCA]:

Thick viscous yellow liquid (116 %). ^1H NMR (300 MHz, DMSO, 298 K) δ 11.30 (s, 1H), 9.24 (s, 1H), 7.82 (s, 1H), 7.79 (dd, J = 1.8 Hz, 1H), 7.76 (d, 2H), 7.71 (dd, J = 1.8 Hz, 1H), 6.89 (d, 2H), 4.20 (q, J = 7.3 Hz, 2H), 3.85 (s, 3H), 1.41 (t, J = 7.3 Hz, 3H); ^{13}C NMR (75 MHz, DMSO, 298 K) δ 163.4, 160.5, 147.3, 136.4, 131.5, 123.9, 123.6, 122.0, 120.0, 115.9, 109.1, 44.1, 35.7, 15.1. Presence of AcOH confirmed by ^1H NMR δ 1.91 (s, 3H); ^{13}C NMR δ 172.2, 21.5.

2.4.3 Preparation of Sodium Salts of Matrices

The sodium salts of DHB and CHCA were prepared as controls for the characterization of matrices in the presence of IL. These salts were prepared by mild neutralization of the acid with equimolar amounts of aqueous NaHCO_3 . Approximately 5 mmol of NaHCO_3 was dissolved in ~ 20 mL of water to form a clear, colorless solution. An equimolar amount of DHB or CHCA was weighed into a round bottom flask.

Aqueous NaHCO_3 was added in small increments with swirling which liberated CO_2 gas, and formed a clear, light brown solution in the case of DHB, and a clear yellow solution in the case of CHCA (pH 7 by universal pH indicator). The solutions were gently refluxed in an oil bath at $\sim 130^\circ\text{C}$ for 30 min, followed by the removal of bulk water by simple distillation. Products were dried under a gentle stream of N_2 for 30 min, yielding solid products. The resulting salts were suspended in 10 mL of cold ethyl acetate, sonicated, and suction filtered to remove excess starting material. Upon drying, NaDHB was a pale off-white powder and NaCHCA was a yellow powder, both obtained in quantitative yield with traces of water present.

(7) Sodium 2,5-Dihydroxybenzoate (NaDHB): Beige solid (110 %). ^1H NMR (300 MHz, DMSO, 298 K): δ 14.93 (s, 1 H), 8.43 (s, 1H), 7.13 (d, $J = 3.1$ Hz, 1H), 6.59 (dd, $J = 8.6, 3.2$ Hz, 1H), 6.44 (d, $J = 8.6$ Hz, 1H); ^{13}C NMR (75 MHz, DMSO- d_6 , 298 K): δ 171.69, 154.90, 147.49, 120.62, 118.69, 115.72, 115.52.

(8) Sodium α -cyano-4-hydroxycinnamate (NaCHCA): Bright yellow solid (102 %). ^1H NMR (300 MHz, DMSO, 298 K): δ 7.81 (s, 1H), 7.75 (d, 2H), 6.84 (d, 2H); ^{13}C NMR (75 MHz, DMSO- d_6 , 298 K): δ 164.10, 162.00, 147.47, 131.58, 123.38, 120.11, 116.09, 108.35.

2.4.4 Purification of Acetic Acid-Containing Products

As previously mentioned, the ILMs in this study were used without further purification as MALDI matrices. It is evident, however, by the high yields and NMR data that the ILMs contain some impurities. Most notably, evidence for acetic acid was seen in

the [EMIM]-containing ILMs that were synthesized using [EMIM]OAc. To assess whether the presence of acetic acid has a considerable effect on the MALDI analysis (i.e. matrix interference) particularly of [EMIM][DHB], several attempts were made to purify the ILM.

Since these synthesized ILMs are water-miscible (at least the ILM-by-product mixture was water-miscible) it was expected that purification would be difficult. The apparent solubilities of these ILMs in various organic solvents (at room temperature) were screened to find potential solvents for washing and/or recrystallization. Several attempts were made to purify the acetic acid-containing [EMIM][DHB] by washing it with various immiscible organic solvents, but to no avail. Washing with water, and subsequent distillation and rotary evaporation did lead to acidic distillate, but very little acetic acid was removed according to ^1H NMR analysis. The difficulty in removing the acetic acid is due to its high boiling point (118.5 °C). Use of a Schlenk line (for 5 h) also did not remove significant amounts of the acid. Finally, a modified azeotropic distillation using toluene (boiling point: 110.6 °C) was employed. A 78% (by weight) mixture of toluene and acetic acid forms an azeotrope with a boiling point of 105 °C, which successfully removed 93 % of the acetic acid after seven consecutive washings and distillations. This method of washing and removing the solvent/acetic acid was also attempted using rotary evaporation, but this procedure only removed very small amounts of acid. This is due to the fact that the azeotrope of toluene/acetic acid is pressure-sensitive, so simple distillation was employed for all subsequent experiments. Although the use of toluene in purification is undesirable, the acidic distillate can be extracted with

water to remove the acid, and recycled throughout the process. Upon removal of the bulk of the acetic acid, [EMIM][DHB] solidified to form a light brown, waxy solid.

2.5 Results and Discussion

2.5.1 Ionic Liquid-Matrix Crystals

Upon preparation of the IL-matrix mixtures, it was noted that the chloride-containing ILs and each matrix form block crystals from saturated solutions of the starting materials. Upon separation and dissolution in DMSO- d_6 , it was determined that each type of crystal contained a stoichiometric 1:1 ratio of IL:acid. Although deprotonation of the matrix acid is not evident, it seems as though weaker interactions may be responsible for such crystallization. Imidazole and its derivatives have become popular in crystal engineering, for the formation of hydrogen-bonded synthons (co-crystals or molecular salts) for a variety of applications such as organic molecular switches and pharmaceuticals.^{15,16} Such interactions of heterocyclic compounds such as imidazole,¹⁷ theophylline,¹⁸ and caffeine¹⁹ are often paired with organic carboxylic acids, as the pair can be stabilized through a donor-acceptor relationship via hydrogen-bonding (i.e. $N\cdots H-O$). Proton transfer between imidazole and acid can also lead to $N-H\cdots O$ interactions with the carboxylate anion. Through extensive molecular arrangement, the solvent of crystallization can also be incorporated into the structure (specifically those solvents capable of hydrogen-bonding). The inclusion of protic solvents such as H_2O and MeOH can also serve as bridges for hydrogen-bonds.²⁰ In cases where the imidazolium IL of interest is disubstituted, the C(2)-H proton (as well as C(4,5)-H protons) are capable of

hydrogen-bonding. Inductive withdrawal of electrons by neighboring nitrogen atoms, allows the C(2)-H to act as an H donor with appreciable acidity.¹⁷

Previous studies indicate that this proton can hydrogen-bond to carboxylate oxygen, carbonyl oxygen, as well as hydroxyl groups.¹⁶ Given the structures of the acids used in this study, there is ample opportunity to form stable interactions through hydrogen-bonding. Other potential interactions of imidazolium cations and aromatic acids include π - π stacking and van der Waals interactions.

The formation of an ionic-neutral co-crystal should be evident by NMR and IR spectroscopies.¹⁶ However, NMR studies in this work were accomplished in solution, whereby the introduction of hydrogen-bonding solvents can lead to the formation of new hydrogen bonds and the weakening of existing hydrogen bonds between IL cation and anion. IR spectroscopy (in solid phase), however, may offer evidence of co-crystal formation. Since this work mainly focuses on the mass spectrometric applications of these materials, little focus was placed on solid characterization. Future work could include more in depth characterization of these compounds, including confirmation of co-crystal formation (by X-ray powder diffraction) and molecular structure analysis by single crystal X-ray crystallography. Such techniques could offer insight into the interactions between the IL moiety and the carboxylic acid, and the formation of crystalline materials.

2.5.2 Characterization by NMR

The ^1H and ^{13}C NMR spectra of both parent matrix acids DHB and CHCA, as well as the sodium salts, NaDHB and NaCHCA were acquired (Figures 2-4 (a), (b) and 2-5 (a), (b)).¹ The peaks were assigned to the appropriate protons (or carbon atoms) according to relative chemical shift, integrated area and splitting patterns (See Figure 2-3 for proton and carbon assignments, noting that matrix protons are assigned with prime (')). There are notable differences between each pair of compounds that are a result of deprotonation of the acidic $-\text{COOH}$ moiety. Specifically, the chemical shifts of the aromatic protons were distinct between the parent acid and analogous sodium salt.

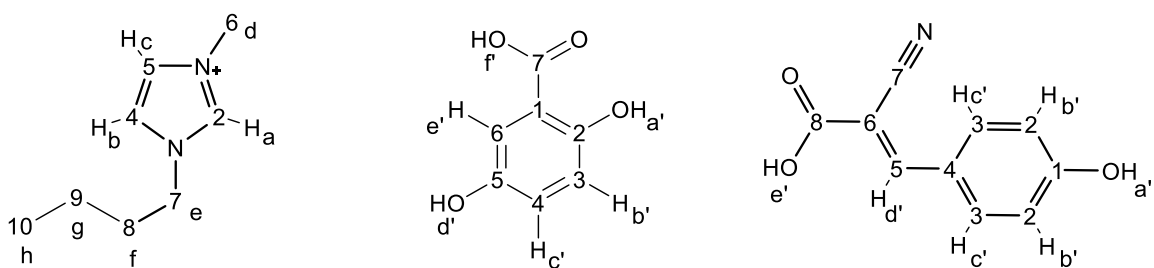


Figure 2-3: Proton and Carbon Assignment of Imidazolium Cation and Matrix Acids

The ^1H NMR spectra of DHB and NaDHB can easily be differentiated by examination of the aromatic proton region (6.5 – 7.5 ppm). In parent acid form, the aromatic region clearly shows three peaks, corresponding to each of the three aromatic protons. The peak at 7.16 ppm corresponds to $\text{H}_{\text{e}'}$, and appears as a doublet with relatively small J-coupling value, due to ortho-coupling to $\text{H}_{\text{c}'}$. Similarly, $\text{H}_{\text{c}'}$ (6.97 ppm) appears as a doublet of doublets due to neighboring $\text{H}_{\text{b}'}$ and ortho-coupling to $\text{H}_{\text{d}'}$. Finally, another

¹ Note that ^1H and ^{13}C NMR spectra for all starting materials and ILMs can be found in Appendices II and III.

doublet appears at 6.79 ppm corresponding to $H_{b'}$. The hydroxyl protons ($H_{d'}$ and $H_{a'}$) appear at 9.15 ppm and 10.82 ppm, respectively.

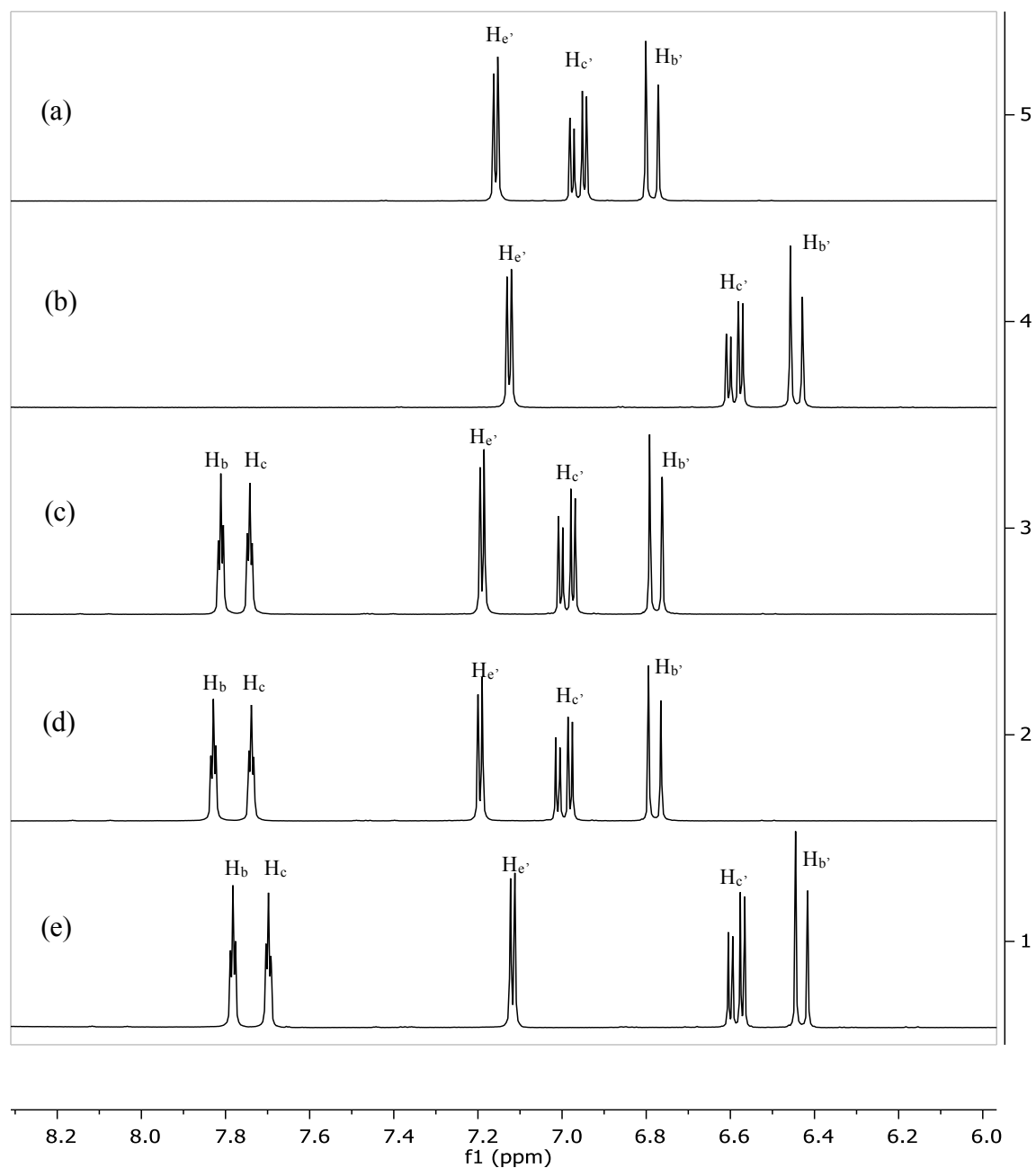


Figure 2-4: ^1H NMR Spectra of DHB Aromatic Proton Chemical Shifts: (a) DHB; (b) NaDHB; (c) [BMIM]Cl/DHB; (d) [EMIM]Cl/DHB; (e) [EMIM]OAc/DHB

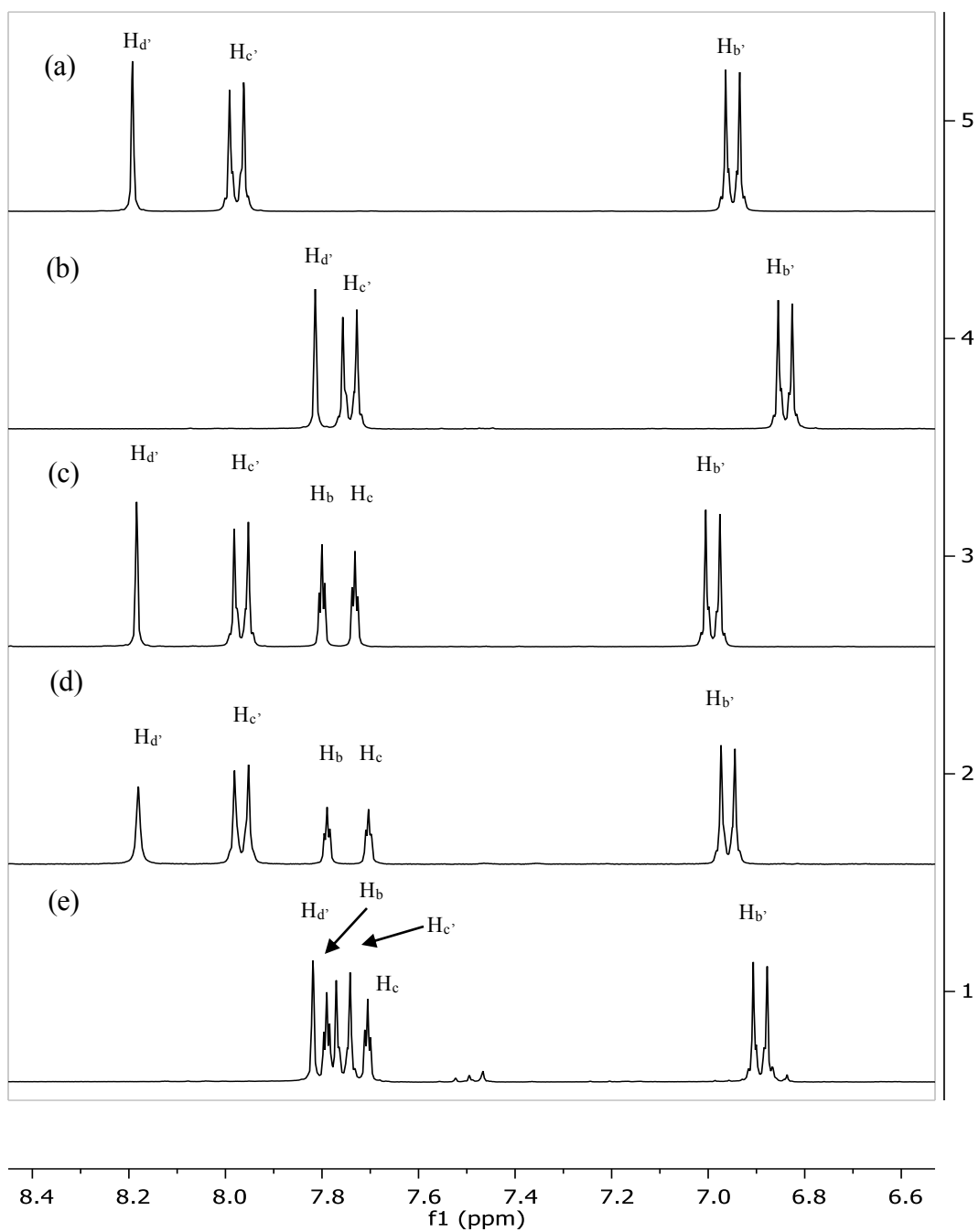


Figure 2-5: ^1H NMR Spectra of CHCA Aromatic Proton Chemical Shifts: (a) CHCA; (b) NaCHCA; (c) [BMIM]Cl/CHCA; (d) [EMIM]Cl/CHCA; (e) [EMIM]OAc/CHCA

Upon deprotonation of the acid to yield the sodium salt, NaDHB, the most obvious differences in the ^1H NMR spectrum are the chemical shifts of the aromatic protons. All three aromatic protons shift upfield (are more shielded) upon deprotonation. This can be explained by a combination of inductive effects from the hydroxyl and carboxylate groups. Other notable differences include the acidic carboxylic acid proton of DHB (H_r , 13.4 ppm, broad singlet), which is no longer visible in the spectrum of NaDHB, and noticeable shifts of hydroxyl protons (H_d and H_a) is evident. The upfield shift from 9.15 ppm to 8.43 ppm of H_a is the most prominent of these differences. Upon deprotonation, the electron withdrawing carboxylic acid group ($-\text{COOH}$) is effectively removed. Carboxylic acid groups ($-\text{COOH}$) are electron-withdrawing groups by resonance. This means that electrons in the aromatic ring are pulled towards the acid group, leaving partially positive charges on the ortho- and para- positions. Therefore, any protons residing at these carbon atoms are less shielded by magnetic field, and therefore will exhibit a downfield shift in NMR spectra. Unlike the $-\text{COOH}$ group, $-\text{COO}^-$ does not have appreciable resonance throughout the ring, due to the stabilization of electron density across two electronegative oxygen atoms. This delocalization of electrons effectively removes the electron-withdrawing by resonance effect. The $-\text{COO}^-$ group is however, a moderate electron-donor by induction. The donation of electrons into the ring produce small partially negative charges on the ortho- and para- positions. A combination of the resonance stabilized delocalization of electrons throughout the aromatic ring, along with existing inductive effects and electron contribution from $-\text{OH}$ substituents can explain these differences.

In the case of CHCA and NaCHCA (Figure 2-5 (a) and (b)), a similar observation can be made regarding the aromatic protons. The aromatic protons of CHCA ($H_{c'}$ and $H_{b'}$) appear at 7.98 ppm and 6.95 ppm, respectively. Deprotonation causes these peaks to shift to 7.75 ppm and 6.84 ppm. Again, this is a result of the resonance stabilization of the carboxylate ion. The formation of the electron donating carboxylate group inductively pushes electron density into the conjugated system. This is evident in the upfield shifts of aromatic protons $H_{c'}$ and $H_{b'}$, as well as $H_{d'}$, due to increased concentration of electron density due to the absence of resonance withdrawal by $-COOH$. Furthermore, the acidic carboxylic acid proton is no longer evident in NaCHCA, as expected. These findings are consistent with the ^{13}C NMR data, which shows a significant shielding effect of C_5 (from 155 to 147.5 ppm) and a deshielding effect of C_6 (from 98.5 to 108 ppm) upon deprotonation.

The distinct differences in NMR spectra between the protonated and deprotonated matrices can be used to indicate whether or not a reaction between the IL and matrix occurs. The deprotonation of the matrix implies the formation of a new ion pair between the IL cation and the anion of the matrix, resulting in a new ionic liquid matrix. Examination of the aromatic region of the NMR spectra of each proposed product indicates that not all of the mixtures result in the formation of a new ILM. Specifically, the mixtures of chloride-containing ILs ([BMIM]Cl and [EMIM]Cl) and each matrix exhibit NMR spectra that are most similar to the parent matrix (Figure 2-4 (a), (c), (d) and Figure 2-5 (a), (c), (d)). The mixtures of acetate-containing IL ([EMIM]OAc), however, are strikingly similar to the corresponding sodium salt of the matrix (i.e. the deprotonated

matrix) as shown in Figure 2-4 (b), (d) and Figure 2-5 (b), (d). This suggests that only two of the proposed products are true ILs resulting from the reaction of each corresponding matrix with [EMIM]OAc. Further evidence of this includes the shift of methyl protons of the acetate ion downfield upon formation of acetic acid, the by-product of the metathesis reaction (peak at ~1.9 ppm as shown in Figures A2-10 and A2-13 in Appendix II). Note that in both sets of spectra, the apparent triplets (actually doublet of doublets) at ~7.7 and 7.8 ppm arise from the imidazolium cation (H_b and H_c) in Figures 2-4 and 2-5 (c)-(e). All other peaks shown belong to the corresponding matrix.

Table 2-1: Chemical Shift of Imidazolium C(2)-H Proton in ILs and IL-Matrix Mixtures

Species/Mixture	Chemical Shift (ppm) of Imidazolium Proton	
	C(2)-H (H_a)	C(4,5)-H (H_b , H_c)
[BMIM]Cl	9.42	7.85, 7.78
[EMIM]Cl	9.45	7.87, 7.77
[EMIM]OAc	9.86	7.84, 7.75
[BMIM]Cl/DHB	9.29	7.81, 7.74
[EMIM]Cl/DHB	9.31	7.83, 7.74
[EMIM]OAc/DHB (deprotonated)	9.20	7.78, 7.70
[BMIM]Cl/CHCA	9.25	7.80, 7.73
[EMIM]Cl/CHCA	9.16	7.79, 7.70
[EMIM]OAc/CHCA	9.24	7.79, 7.71
(deprotonated)		

Also notable are the chemical shifts of the acidic C(2)-H proton of the imidazolium cation (H_a) (refer to Table 2-1). In all cases, the mixture of matrix and IL results in a chemical shift of this proton. In the native ILs, the chemical shift of the C(2)-H proton is more upfield in the case of chloride-containing ILs than the acetate-containing IL. In the literature, the chemical shift of this acidic proton has been correlated with the hydrogen-bond strength between cation and anion.²¹ Interaction of this proton with a stronger hydrogen-bond acceptor leads to deshielding of this proton and a subsequent downfield shift, as is observed with in the presence of the acetate ion in [EMIM]OAc (as compared to [EMIM]Cl). This is consistent with literature results, whereby the hydrogen-bond between acetate and imidazolium cations was shown to be significantly stronger than that of chloride.²¹

In this case, the presence of another compound (i.e. the matrix), regardless of the formation of a new ion-pair results in a shift of this proton. Therefore, for those mixtures that do not react (i.e. chloride-containing ILs), the C(2)-H proton shift was used as a standard. For [BMIM]Cl and [EMIM]Cl, the change in chemical shift of this proton from the pure IL to when DHB is added is 0.13 ppm and 0.14 ppm (upfield), respectively. The mixture of [EMIM]OAc and DHB, however, the difference in chemical shift is 0.66 ppm (shifted upfield) from [EMIM]OAc and ~ 0.1 ppm (shifted upfield) as compared to chloride-containing mixtures of DHB. This implies that the interaction between the imidazolium cation and the DHB anion is weaker than with the acetate ion. This is likely a result of steric effects, as DHB is significantly larger and bulkier than the acetate anion.

The relatively large chemical shift of this proton also implies that the interaction between the acetate anion and the imidazolium cation has been altered.

Similarly, the CHCA-containing mixtures show a larger C(2)-H chemical shift (0.62 ppm) between the [EMIM]OAc and the [EMIM]OAc-CHCA mixture, than that of either of the chloride-containing mixtures. Interestingly, the C(2)-H chemical shift of the imidazolium cation in the presence of either DHB or CHCA does not show a significant difference between the parent and deprotonated matrix (i.e. mixtures of [EMIM]Cl-matrix and [EMIM]OAc-matrix). In both cases, however, the shift is less than the observed shift for both acetate and chloride ions, indicating that the hydrogen-bond may be weakened. Furthermore, the presence of CHCA in both chloride-containing ILs results in a slightly more upfield shift of the acidic proton than DHB. However, it is important to note that since the C(2)-H proton is capable of hydrogen bonding, it may therefore shift due to changes in solvent polarity, as well as due to the presence of water (which is a common impurity in DMSO- d_6), which may solvate and/or stabilize the cation. Therefore, it is not conclusive that the presence of the matrix is directly affecting the chemical environment of the acidic imidazolium proton.

Overall, the chemical shifts of the aromatic protons of the matrix component of these IL-matrix mixtures are the best indicator of the formation of a new ion-pair. Of the mixtures that were studied in this work, only those containing the [EMIM]OAc IL reacted and formed a new ILM, which is evident in the similarities between the matrix component of the mixture and the sodium salts of the matrices. Therefore, it is appropriate to refer to those matrices that react as new ion pairs. Using IL nomenclature,

these ILMs will be further referred to as [EMIM][DHB] and [EMIM][CHCA], whereby the matrix component in parentheses actually refers to the conjugate base of the matrix.

2.5.3 Characterization by UV-Vis Spectroscopy

Deprotonation of the parent matrix can alternatively be determined using UV-Vis spectroscopy. Upon deprotonation of the carboxylic acid matrix, the extent of conjugation of the molecule is disrupted, due to the resonance stabilization of the -COO^- moiety. In polar (aprotic) solvents, this effect can be observed through a significant hypsochromic shift (decreased λ_{max}). The delocalization of electrons and resonance stabilization of the carboxylate group leads to a more stable ground state than the parent acid, disrupting the extent of conjugation throughout the molecule. This leads to an apparent hypsochromic (blue) shift of UV bands. (Conjugation of aromatic acids generally lead to red shifts). This apparent blue shift of carboxylate ions can therefore be used as an indicator of deprotonation. Again, as a control, NaDHB and NaCHCA were employed as standards for the carboxylate anion. It is important to note, however, that the synthesized matrices have not been purified before analysis. This can explain the slight variations in absorbance intensity in all matrices as compared to the corresponding parent matrix, as the molar fraction of matrix may be artificially high or low in solid/liquid ILMs and IL-matrix mixtures. These differences are more readily evident in the UV spectra of CHCA matrices, which have higher molar absorptivity than DHB matrices. Thus small changes in concentration result in apparently large discrepancies between absorbance intensities.

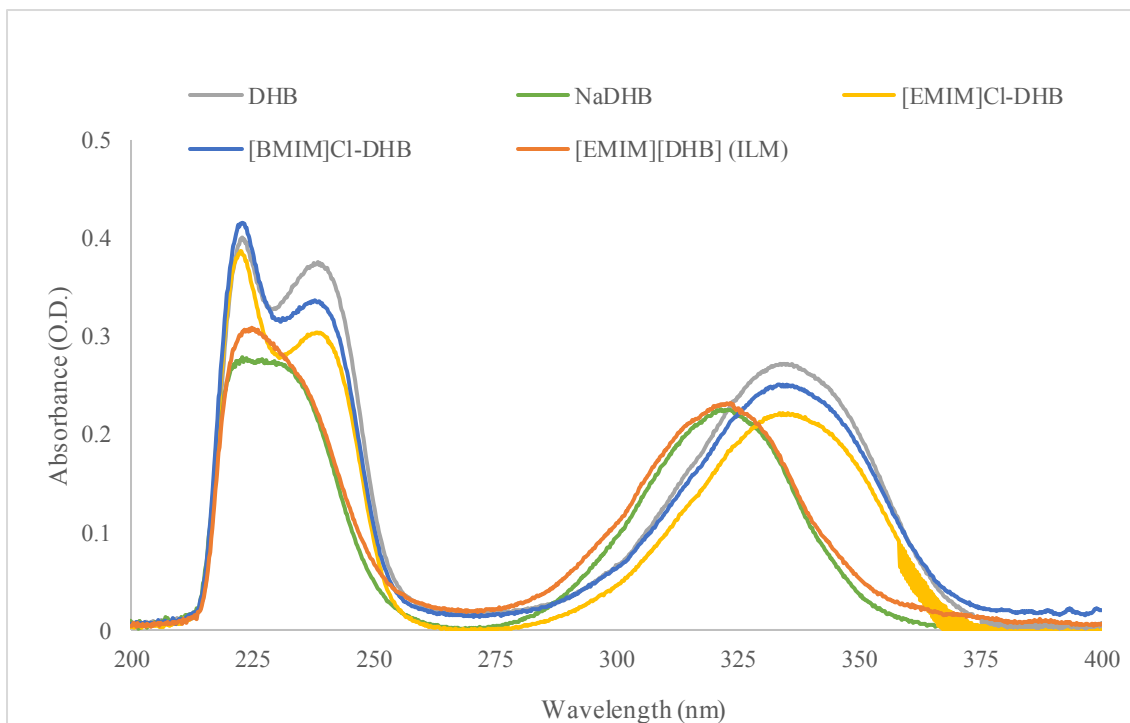


Figure 2-6: UV-Vis Spectra of DHB and DHB-Containing ILMs in ACN (75 μM)

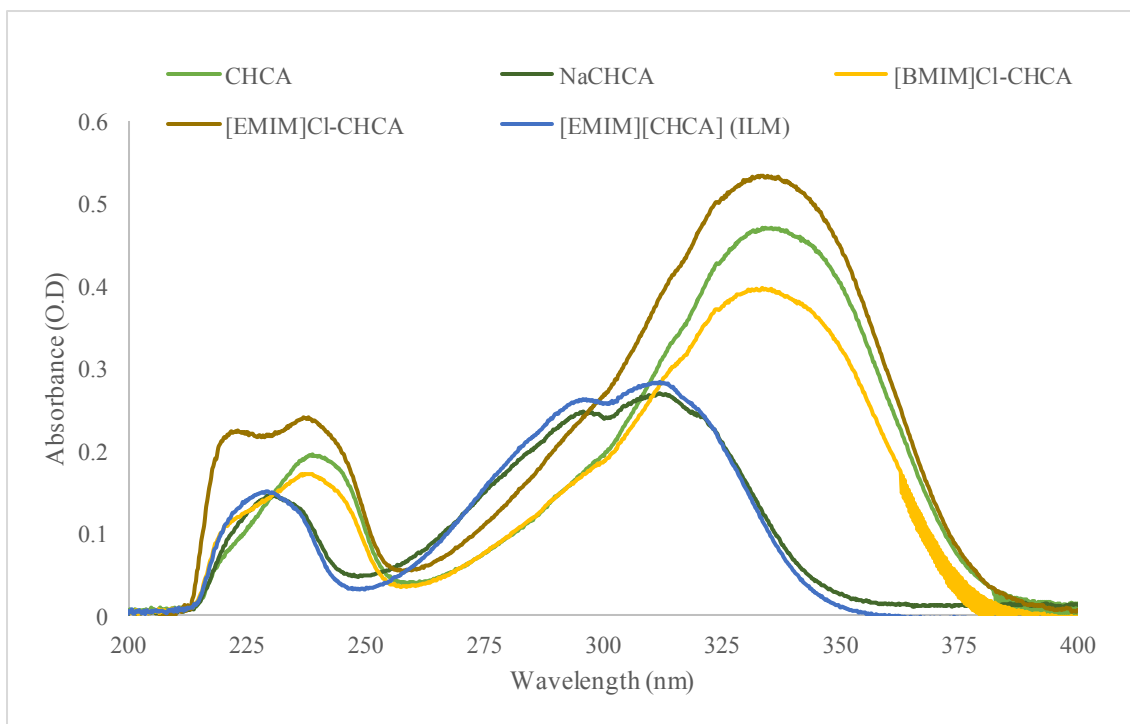


Figure 2-7: UV-Vis Spectra of CHCA and CHCA-Containing ILMs in ACN (25 μM)

As shown in Figures 2-6 and 2-7, there are significant hypsochromic shifts from the parent matrix acid to the analogous sodium carboxylate salt, (i.e. from DHB to NaDHB and CHCA to NaCHCA), as well as a slight hypochromic effect, evident through the decreased intensity of absorbance at the same molar concentration. This decrease in peak absorbance is indicative of the stabilization of non-bonding electrons, which occurs by delocalization of electrons across the carboxylate group. Also evident in the UV-vis spectra are the loss of fine structure of DHB, and now visible fine structure associated with CHCA upon deprotonation. Analysis of the acquired spectra show that the only IL-matrix mixture to exhibit similar characteristics to the sodium salt matrices (NaDHB and NaCHCA) are [EMIM][DHB] and [EMIM][CHCA], which result when the matrix is combined with [EMIM]OAc as the cation-donor. These findings are consistent with the NMR data, and indicate that of the proposed combinations of matrix and IL, only two true ILMs are formed.

2.5.4 Colored Solutions of Matrices and [EMIM]Cl

Initially, characterization of the matrix acids and corresponding solutions with ILs was carried out using acetonitrile as the solvent. When the solvent was switched to methanol, however, mixtures of [EMIM]Cl and the matrices resulted in unexpected color changes that were not observed in acetonitrile solutions. For example, when dissolved in methanol, [EMIM]Cl forms a light yellow/green solution, while DHB forms a clear, beige solution. When these are combined however, the resulting solution gives rise to a deep blue color. Similarly, methanolic solutions of [EMIM]Cl and NaDHB unexpectedly turn dark purple. Interestingly, solutions of [EMIM]Cl and CHCA (both clear, yellow

solutions) form a bright orange solution, but [EMIM]Cl and NaCHCA mixtures do not result in any unpredicted color change. To investigate these color changes, experiments were carried out using UV-Vis.

Despite the intense color changes, analysis by UV-Vis reveal that the absorbance band for each corresponding matrix-IL mixture is only present at relatively high concentrations. Typical concentrations of matrices in this work were 25 – 100 μ M, whereas the observed absorbance peaks in the visible region of [EMIM]Cl/DHB and [EMIM]Cl/NaDHB were 200 mM and 25 mM respectively (Figure 2-8), whereby corresponding matrix peaks are saturated (not shown). This indicates that the band is relatively weak (the chromophore has a low molar extinction value). Notably, methanolic solutions of [EMIM]Cl with DHB and NaDHB both result in well-defined bands, which are not present in either of the individual components.

As can be seen in Figure 2-8, the solution of [EMIM]Cl and DHB has a λ_{max} value of ~ 616 nm and that of [EMIM]Cl and NaDHB has a λ_{max} value of ~ 540 nm, corresponding to the complementary colors blue and purple, respectively. Furthermore, as the concentration of [EMIM]Cl increases, the intensity of each corresponding peak increases (Figure 2.9).

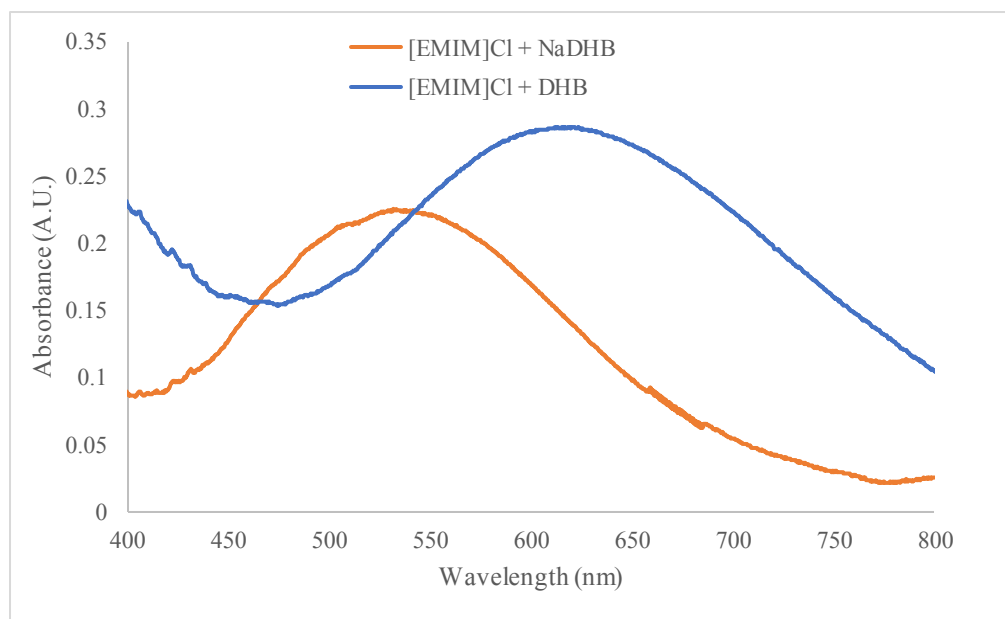


Figure 2-8: UV-Vis Spectra of Colored Complexes of [EMIM]Cl and DHB Matrices (in MeOH)

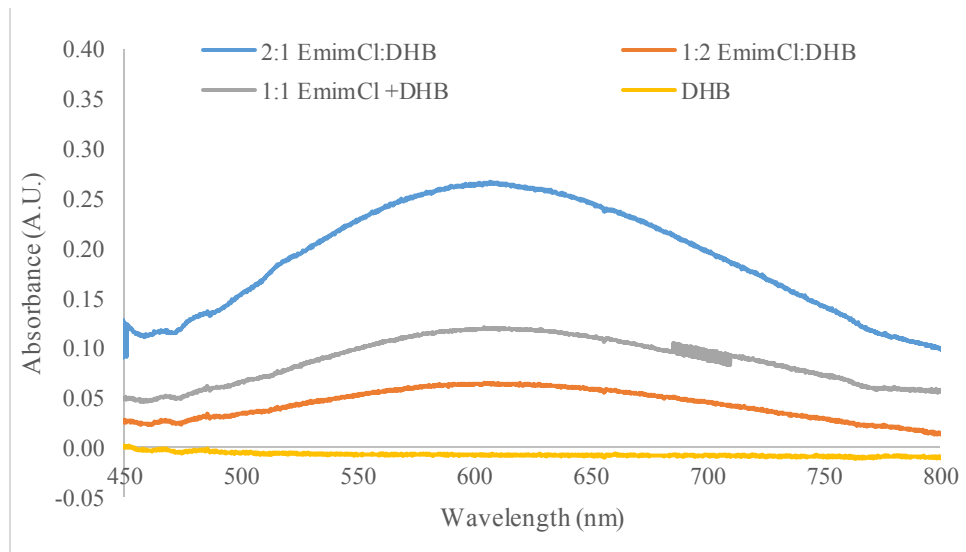


Figure 2-9: UV-Vis Spectra of Varying Ratios of [EMIM]Cl:DHB (100 mM DHB in MeOH)

Interestingly, the intensity of the peak is dependent on the species of the matrix present. The data shown in Figure 2-9 displays the spectra of each matrix with varying amounts of [EMIM]Cl. The concentration of DHB and NaDHB (~ 6 mM) is held constant, and though the peaks are relatively similar in intensity, there is eight times as much [EMIM]Cl in the DHB solution (~ 200 mM) than in the NaDHB solution (~25 mM). At such high concentrations, band broadening, light scattering and possible dimerization can occur in solution, which limit true quantitation of such solutions. Nonetheless, the solution of [EMIM]Cl and NaDHB produces a much more intense band in the visible region than that of [EMIM]Cl and DHB.

When the IL counterpart is replaced by [BMIM]Cl or [EMIM]OAc, no unexpected color changes are observed, so it appears that [EMIM]Cl is a major contributor to the apparent color change. Furthermore, even at high concentrations of [EMIM]Cl, no absorbance was observed between 500 – 800 nm. This suggests that the interaction between the IL and the matrix is responsible for a change in electronic properties. To confirm this, the same experiment was carried out using CHCA. Interestingly, [EMIM]Cl and CHCA (both clear yellow solutions) form a bright orange solution in methanol but [EMIM]Cl and NaCHCA solutions do not exhibit an apparent color change, but form a cloudy light brown suspension. The color change of [EMIM]Cl and CHCA, does not show obvious absorbance bands in the visible region of the spectrum, however (Figure 2-10).

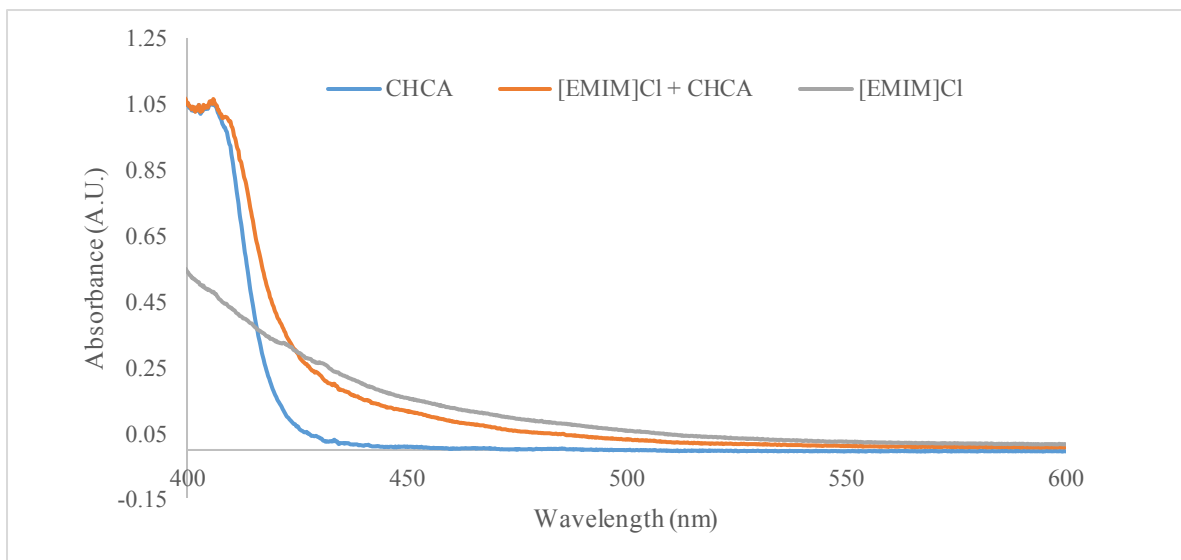


Figure 2-10: UV-Vis Spectra of [EMIM]Cl and CHCA in MeOH

This may be the result of spectrum saturation at the required concentrations to observe the newly formed bands. Peak broadening due to [EMIM]Cl appears to overlap and conceal new bands in the region where blue light is absorbed (and orange color is perceived). In fact, this band would be expected to appear at ~ 480 nm, where there is noticeable tailing of the [EMIM]Cl absorbance band.

Another interesting observation of these colored methanolic solutions, is that the blue color of [EMIM]Cl and DHB fades over time to clear, colorless, whereas the other colored solutions retain their color. Upon color loss, ^1H NMR spectra appear identical to that of the colored solution, which indicates that significant molecular structural changes (i.e. proton transfer, ion separation, etc.) are unlikely to blame for the color change. Furthermore, no significant differences were noted between isolated products from acetonitrile or from methanol.

The solvent in these cases is obviously a crucial parameter, as the color is dependent on the solvent properties. No color change was observed for IL-matrix mixtures in acetonitrile, or DMSO, but it was readily apparent in solution of methanol or water. This suggests that polar protic solvents are involved in the formation (or stabilization) of the chromophore. Solvents have a significant influence on the electronic properties of organic compounds. Specifically, hydrogen-bond formation in protic, polar solvents (e.g. methanol or water) can occur between the solvent and solute(s) and stabilize or destabilize the ground state or excited state molecular orbitals. This, however, typically results in shifts of existing absorbance peaks, rather than the formation of new absorbance bands.

Ratios of IL to each matrix (or salt) were varied from 1:2 to 1:1 to 2:1 in deuterated methanol and analyzed by ^1H NMR to examine whether or not differences in the chemical environments of imidazolium protons exist based on the relative amount of matrix. Very subtle differences were noticed, however. Slight shifts in the C(2)-H peak were noted, however the shifts seem to correlate with [EMIM]Cl concentration, rather than with the other species in solution. As the concentration of [EMIM]Cl increases in each solution from 50 mM to 100 mM to 200 mM, the acidic imidazolium proton shifts more downfield (by approximately 0.1 ppm increments). This is likely due to increased polarity of the solution and therefore, more significant hydrogen-bonding (deshielding). In each of the [EMIM]Cl:matrix mixtures that resulted in color change, there were no observed differences between the ^1H NMR of the mixtures and the corresponding individual components in the solvents tested (methanol- d_4 and DMSO- d_6).

Finally, electron paramagnetic resonance (EPR) experiments were attempted, to identify possible unpaired electron species. Unfortunately, after several attempts, no peaks were observed and therefore no spectra were collected. It appears that the colored species are not likely the result of radical species in solution.

Unfortunately, the cause of the color change of solutions of [EMIM]Cl and matrices was not determined. Spectroscopic evidence does not indicate any significant molecular changes in polar, protic solvents with the exception of the color change. It is possible that the color arises due to the presence of an impurity in the [EMIM]Cl starting material. Imidazolium ILs are most often colorless, but are subject to colored impurities throughout commercial production. In particular, the [EMIM]Cl used in this study was a green solid, however, other manufacturers supply the same IL as a brown solid. Furthermore, the relatively low absorptivity of the newly formed absorbance bands suggests that the species giving rise to the color may be quite dilute, compared to the matrix (assuming similar electronic transitions give rise to the bands), which may explain why impurities are not detected by ^1H NMR (i.e. they may be below the detection limit). Further characterization of these solutions would be required to conclusively determine whether or not an impurity is the cause of these observations.

2.5.5 Characterization by IR Spectroscopy

IR spectroscopy is another useful technique to obtain structural information about molecules. This technique can be readily used to identify deprotonation of a carboxylic acid by examining differences in C=O frequencies. Furthermore, IR studies of imidazolium-based ILs can yield information about the interactions between cation and

anion through hydrogen-bonding. Specifically, the stretching frequency of C(2)-H (the acidic site between ring nitrogen atoms) can offer insight into the strength of the hydrogen-bond between cation and anion (C(2)-H \cdots anion).²¹

The IR spectra were obtained by ATR FT-IR spectroscopy of the products in the solid state. IR spectra of parent acid matrices DHB and CHCA, along with the sodium salts of the two matrices were again used as standards for deprotonation.² The IR spectra are shown (staggered) in Figures 2-11 and 2-12. Identifiable peaks of DHB and NaDHB agree well with previously published literature.²²

Deprotonation of an aromatic acid can be identified in IR spectra by various characteristic vibrational stretching and bending modes. These include the shift of the carbonyl stretching frequency from -COOH to -COO⁻, the disappearance of -OH (-COOH) in plane bending mode, and the appearance of asymmetric bending of -COO⁻, amongst others.²² Upon addition of the IL-counterpart in these studies, however, the IR spectra can quickly become convoluted with many peaks corresponding to both matrix acid and imidazolium cation. Therefore, deprotonation was determined by the frequency of the carbonyl stretch.

² FT-IR spectra of all starting materials and ILMs can be found in Appendix IV

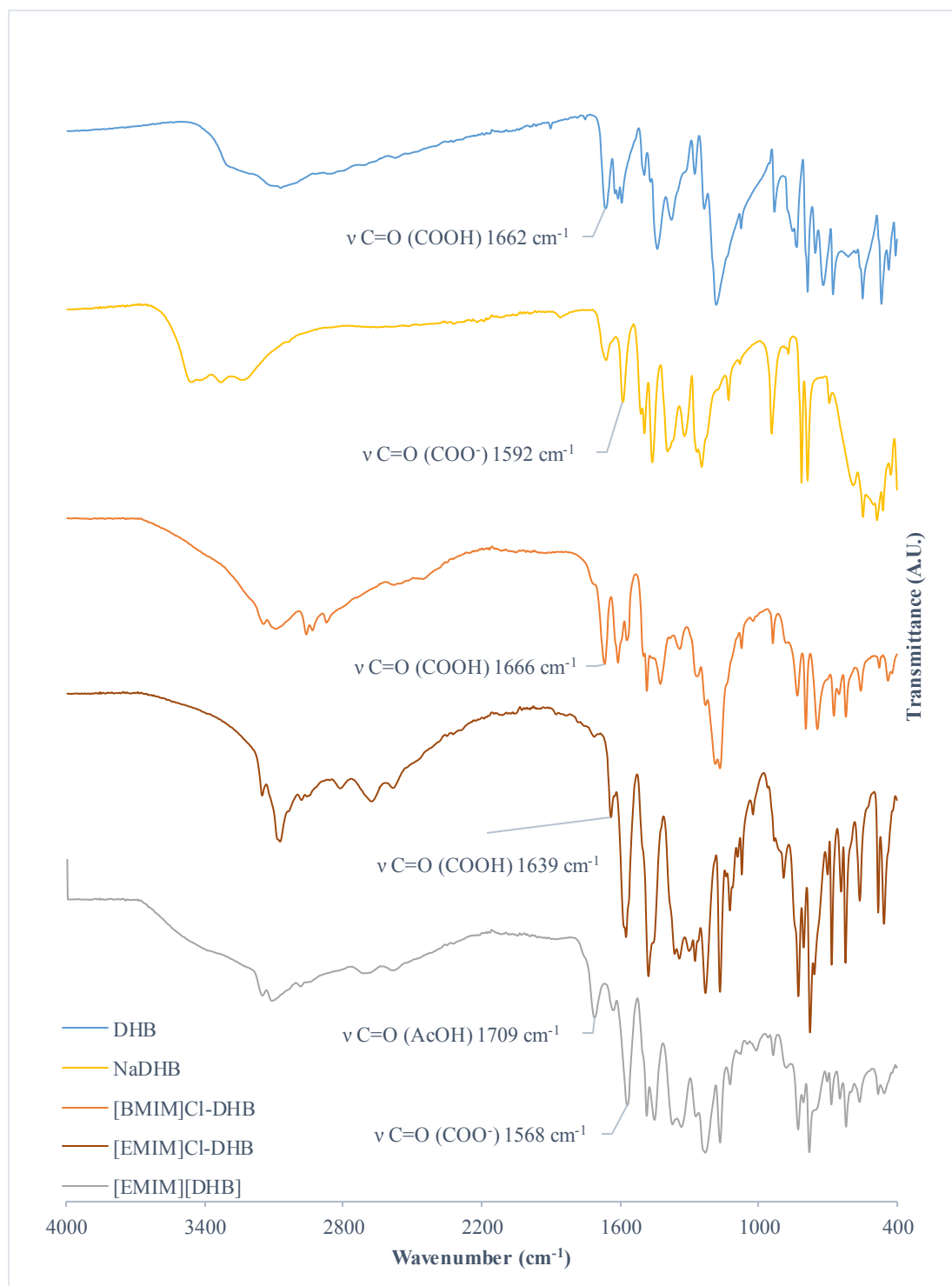


Figure 2-11: IR Spectra of DHB and DHB-Containing ILMs

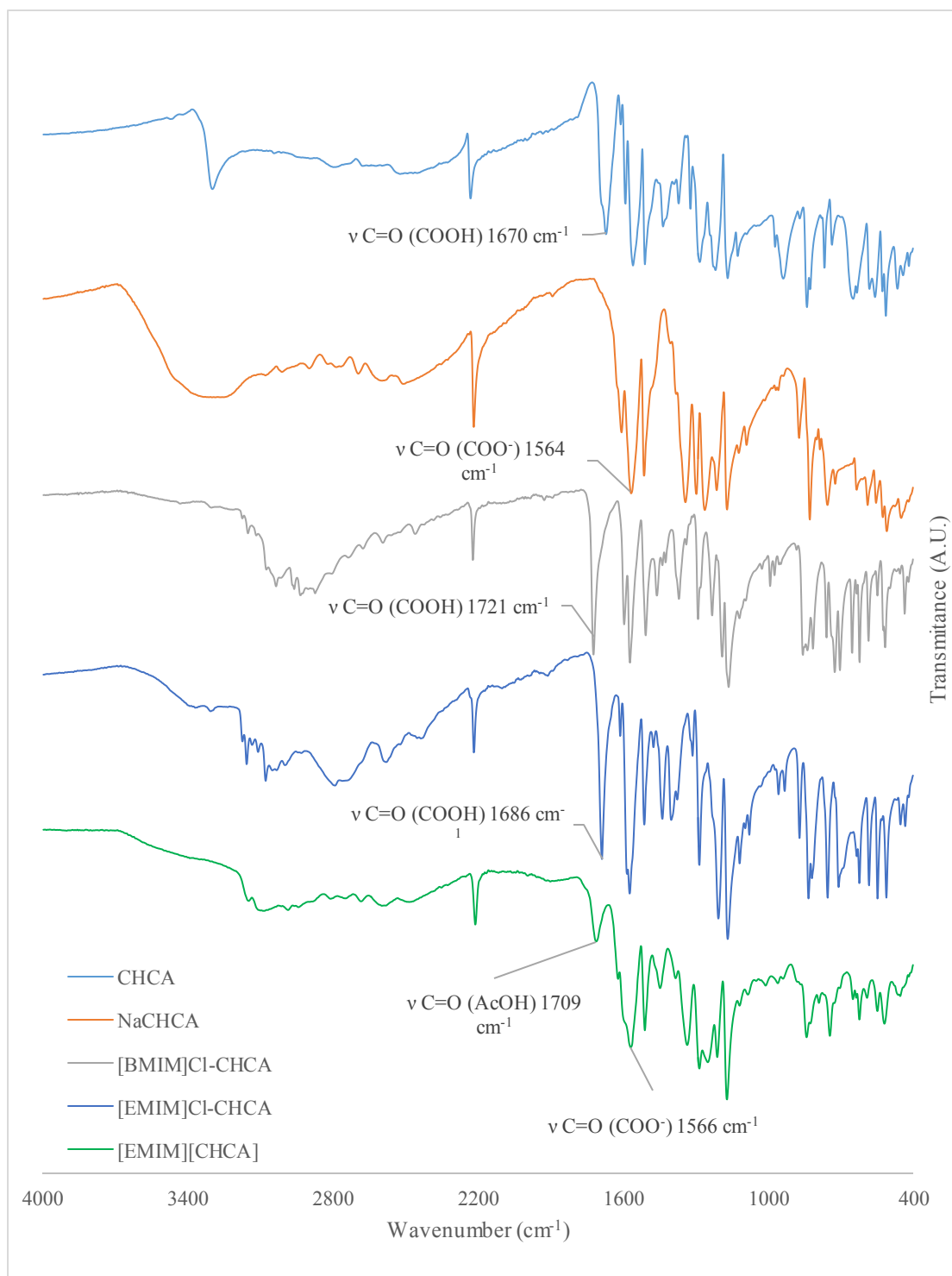


Figure 2-12: IR Spectra of CHCA and CHCA-Containing ILMs

The carbonyl C=O stretch of aromatic carboxylic acids can generally be found between 1690 – 1760 cm^{-1} (as labelled in Figures 2-11 and 2-12). Visual inspection of the acquired spectra of both DHB and CHCA reveal C=O stretches of 1662 and 1670 cm^{-1} , respectively. Upon deprotonation of the acid, and therefore delocalization of the non-bonding electrons across the -COO^- group, the C=O stretch lessens in energy (generally $< 1600 \text{ cm}^{-1}$). However, it should be noted that for those ILs that were produced from [EMIM]OAc (i.e. [EMIM][DHB] and [EMIM][CHCA]), the acetate anion will also produce a signal in the same region as the expected carboxylate ion of the matrix acid. Therefore, the formation of the IL can be inferred from the absence of the carboxylic acid $\text{C=O}_{(\text{COOH})}$ stretch ($> 1600 \text{ cm}^{-1}$), but not from the presence of the -COO^- carbonyl stretch, as this could refer to unreacted acetate. Furthermore, if these ILs are analyzed before purification, the presence of acetic acid C=O (which appears at a slightly higher frequency than aromatic carboxylic acids) can indicate that a reaction has occurred. For instance, the IR spectra of [EMIM][DHB] and [EMIM][CHCA] both show peaks at $\sim 1709 \text{ cm}^{-1}$, corresponding to the carbonyl stretch of acetic acid.

Due to the various stretching and bending modes of these compounds, as a result of their conjugated systems, it is difficult to assign the peaks with great certainty. It is evident, however, in all cases that the energy of the C=O stretch is changing upon deprotonation. It is important to note that peak identification was based on literature, as well as by comparison with the starting materials. [EMIM]Cl-DHB, for example, appears to have a significant C=O stretch at 1572 cm^{-1} which suggests deprotonation of the acid.

However, this peak appears in the IR spectrum of pure [EMIM]Cl. Therefore, it is important to carefully analyze the spectra.

As expected, the ILMs [EMIM][DHB] and [EMIM][CHCA] have C=O stretches similar to that of NaDHB and NaCHCA, respectively, and more notably, do not show aromatic C=O stretches above 1600 cm⁻¹ (Table 2-2). The IL-matrix mixtures also have expected carbonyl stretches, similar to that of the parent acid. One anomaly that should be noted, however, was that [BMIM]Cl-CHCA had a slightly higher carbonyl stretching frequency, the reason for which is unclear.

Table 2-2: Carbonyl Stretching Frequency of ILMs and Standards

Compound	ν C=O (cm ⁻¹)
DHB	1662
NaDHB	1592
[BMIM]Cl-DHB	1666
[EMIM]Cl-DHB	1639
[EMIM][DHB]	1568
CHCA	1670
NaCHCA	1564
[BMIM]Cl-CHCA	1721
[EMIM]Cl-CHCA	1686
[EMIM][CHCA]	1566
[EMIM]OAc	1562

The region between 3100 – 3200 cm^{-1} of [EMIM]-containing ILs (Figure 2-13) can be attributed to the C-H stretching modes involving ring C atoms.²³ The stretches of C(4,5)-H are expected at $\sim 3150 \text{ cm}^{-1}$ and the C(2)-H stretch is expected at $\sim 3105 \text{ cm}^{-1}$.²⁴ Specifically, the frequency of the C(2)-H (acidic) stretch has been correlated with hydrogen-bond strength to the anion. Red-shifted peaks suggest stronger hydrogen-bonding interactions. Therefore this region of the spectra of ILMs [EMIM][DHB] and [EMIM][CHCA] was analyzed.

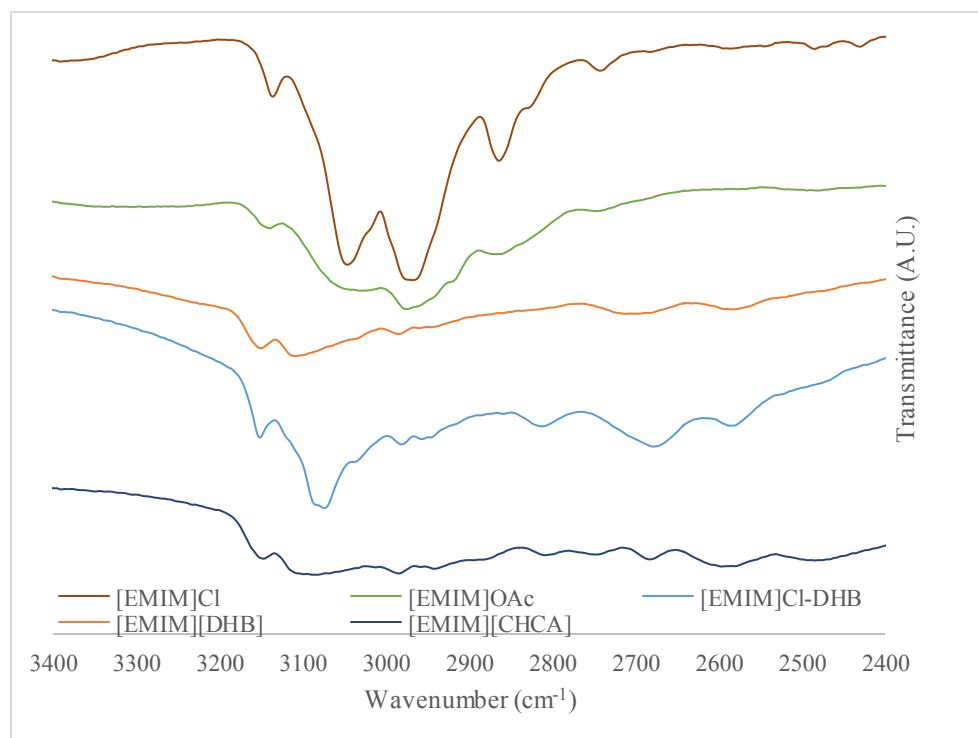


Figure 2-13: IR Characterization of Imidazolium C(2)-H Stretch in Novel [EMIM]⁺-Containing ILMs

The C(4,5)-H stretches are evident in each species between 3136 and 3150 cm^{-1} . Both $[\text{EMIM}]^+$ -containing ILMs have slightly higher frequency peaks. Poor resolution of the obtained IR spectra, as well as likely interference from the presence of water, however, limits the ability to assign the C(2)-H peak with certainty. Removal of water, and further studies to deconvolute these spectra would be required to make accurate conclusions. The C(4,5)-H peaks in each IL are much more evident, however, these peaks have not been correlated with specific cation-anion interactions.

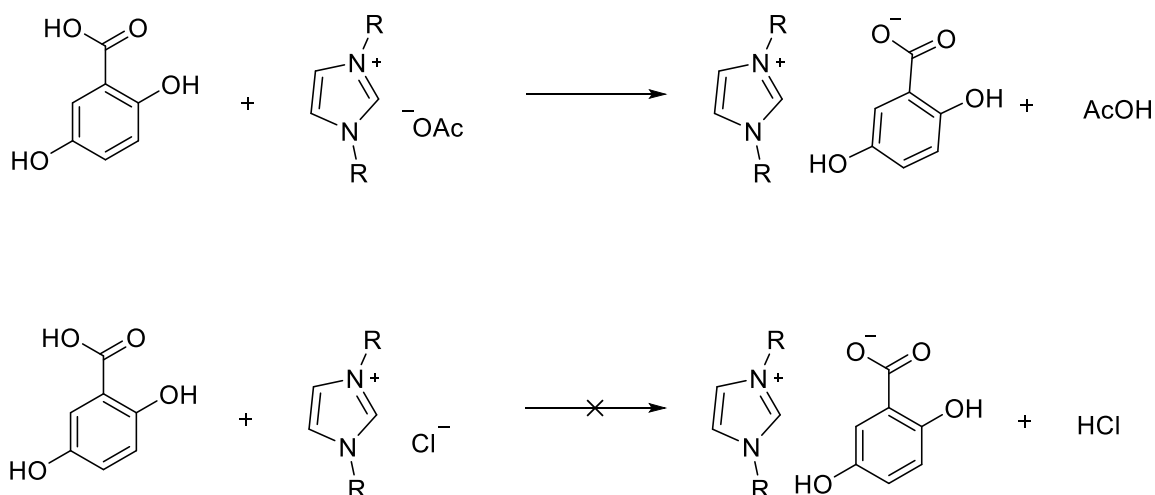


Figure 2-14: Schematic Representation of Formation of ILMs and IL-Matrix Mixtures

In general, ILMs refer to ion pairs of a cation and an anion of a traditional MALDI matrix. In this case, however, only two “true” ILMs were prepared *in situ* resulting from the reaction of each matrix acid with $[\text{EMIM}]\text{OAc}$. In the case of chloride-containing ionic liquids, $[\text{BMIM}]\text{Cl}$ and $[\text{EMIM}]\text{Cl}$, a new ion pair was not formed with either of the tested matrices, and the resulting solution consisted of dissolved ionic liquid and parent acid. These observations are as expected, since these metathesis reactions are

primarily driven by proton transfer (as the formation of a gas, water or precipitate are not likely). It follows that the weaker acid (and the more stable conjugate base) will be favored. In the case of chloride-containing ILs, the corresponding acid upon formation of a new ion pair would be HCl (pK_a -8), which is a much stronger acid than both DHB and CHCA (pK_a 2.95 and 1.17, respectively). Therefore, a mixture of parent acid and IL remains in solution. However, acetic acid (pK_a 4.75) is preferentially formed in solutions of [EMIM]OAc and matrix acid, as the conjugate bases of DHB and CHCA are significantly more stabilized by resonance than the acetate ion. Therefore, the “true” ILMs are herein denoted by conventional IL nomenclature: [EMIM][DHB] (**3**) and [EMIM][CHCA] (**6**), and those co-existing IL-matrix mixtures denoted as [BMIM]Cl-DHB, [BMIM]Cl-CHCA, etc. to differentiate.

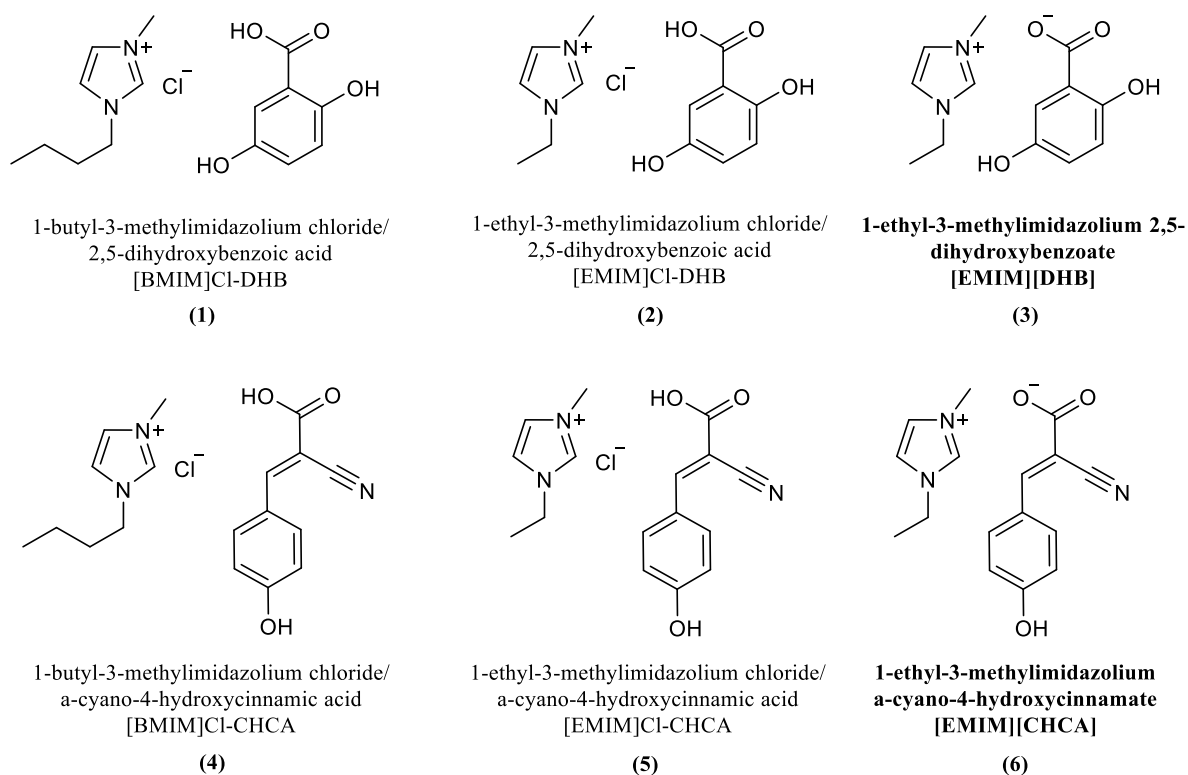


Figure 2-15: Structures of IL-Matrix Mixtures and Novel ILMs (shown in bold)

In conclusion, the evidence from the NMR, UV-vis and IR data suggest that the attempted metathesis reactions using [BMIM]Cl and [EMIM]Cl did not go to completion, and that the isolated products are most similar to their respective parent acids. The strength of the by-product acid is the factor that is hindering these reactions. [EMIM]OAc mixtures of each matrix, however, do show evidence of the formation of new ion-pair and therefore are true ILMs. Although methods exist to synthesize ILMs using chloride-containing IL starting materials, the formation of IL-matrix mixtures and analogous ILMs allows for comparison between the two with respect to their ability to ionize analytes of interest by MALDI-MS, which will be examined in following chapters.

References

1. Cohen, L.; Go, E. P.; Siuzdak, G. Small Molecule Desorption/Ionization Mass Analysis. In *MALDI MS: A Practical Guide to Instrumentation, Methods and Applications*; Hillencamp, F., Peter-Katalinic, J., Eds.; Wiley-VCH Verlag: Weinheim, 2007, pp 299-337.
2. Armstrong, D. W.; Zhang, L.; He, L.; Gross, M. L. *Anal. Chem.* **2001**, *73*, 3679-3686.
3. Crank, J. A.; Armstrong, D. W. *J. Am. Soc. Mass Spectrom.* **2009**, *20*, 1790-1800.
4. Li, Y. L.; Gross, M. L. *J. Am. Soc. Mass Spectrom.* **2004**, *15*, 1833-1837.
5. Kerton, F. M.; Marriott, R. *Alternative Solvents for Green Chemistry, 2nd ed.* RSC Publishing: Cambridge, UK, 2013.
6. Wang, H.; Gurau, G.; Rogers, R. D. *Chem. Soc. Rev.* **2012**, *41*, 1519-1537.
7. Swatloski, R. P.; Spear, S. K.; Holbrey, J. D.; Rogers, R. D. *J. Am. Chem. Soc.* **2002**, *124*, 4974-4975.
8. Tan, S.; MacFarlane, D. R. Ionic Liquids in Biomass Processing. In *Ionic Liquids*; Kirchner, B., Ed.; Springer: Berlin Heidelberg, 2010, pp 311-339.
9. Zakrzewska, M. E.; Bogel-Lukasik, E.; Bogel-Lukasik, R. *Chem. Rev.* **2011**, *111*, 397-417.
10. Murzin, D.; Holmbom, E. Analytical Approaches in Biomass Catalysis. In *Catalysis for the Conversion of Biomass and its Derivatives*; Behrens, M., Datye, A. K., Eds.; epubli: Germany, 2013, pp 183-212.
11. Clare, B.; Sirwardana, A.; Macfarlane, D. R. *Top. Curr. Chem.* **2010**, *290*, 1-40.
12. Tholey, A.; Heinzle, E. *Anal. Bioanal. Chem.* **2006**, *386*, 24-37.
13. Harvey, D. J. *Mass Spectrom. Rev.* **1999**, *18*, 349-451.

14. Bochek, A. M.; Murav'ev, A. A.; Novoselov, N. P.; Zaborski, M.; Zabivalova, N. M.; Petrova, V. A.; Vlasova, E. N.; Volchek, B. Z.; Lavrent'ev, V. K. *Russ. J. Appl. Chem.* **2012**, *85*, 1718-1725.
15. Wang, L.; Zhao, L.; Liu, M.; Chen, R.; Yang, Y.; Gu, Y. *Sci. China* **2012**, *55*, 2115-2122.
16. Kathalikkattil, A. C.; Damodaran, S.; Bisht, K. K.; Suresh, E. *J. Mol. Struct.* **2011**, *985*, 361-370.
17. MacDonald, J. C.; Dorrestein, P. C.; Pilley, M. M. *Cryst. Growth Des.* **2001**, *1*, 29-38.
18. Sarma, B.; Saikia, B. *Cryst. Eng. Comm.* **2014**, *16*, 4753-4765.
19. Bucar, D.; Henry, R. F.; Lou, X.; Duerst, R. W.; MacGillivray, L. R.; Zhang, G. G. Z. *Cryst. Growth Des.* **2009**, *9*, 1932-1943.
20. Utas, J. E.; Kritikos, M.; Sandstrom, D.; Akermark, B. *Biochimica et Biophysica Acta* **2006**, *1757*, 1592-1596.
21. Cha, S.; Ao, M.; Sung, W.; Moon, B.; Ahlstrom, B.; Johansson, P.; Ouchi, Y.; Kim, D. *Phys. Chem. Chem. Phys.* **2014**, *16*, 9561-9601.
22. Regulska, E.; Kalinowska, M.; Wojtulewski, S.; Korczak, A.; Sienkiewicz-Gromiuk, J.; Rzaczyńska, Z.; Swislocka, R.; Lewandowski, W. *Spectrochim. Acta. A* **2014**, *132*, 713-725.
23. Hoff, O.; Bahr, S.; Kempter, V. *Langmuir* **2008**, *24*, 11562-11566.
24. Zhang, Q.; Wang, N.; Yu, Z. *J. Phys. Chem. B.* **2010**, *114*, 4747-4754.

Chapter 3: Optimization of IL-Containing Matrices for the Qualitative Analysis of Bio-Derived Platform Chemicals

3.1 Introduction

Biomass energy is an attractive source of alternative energy for reducing our current reliance on non-renewable fossil fuels. Biomass can serve as a renewable feedstock for the generation of liquid fuels and chemicals to supplement fossil fuel use, and to supply future global demands.¹ Furthermore, the introduction of alternative ionic liquid (IL) solvents has allowed significant advances in the extraction and production of valuable chemicals from biomass.^{2,3}

ILs are non-molecular salts, generally consisting of a bulky organic cation with an organic or inorganic anion. ILs have attractive properties such as low/negligible vapor pressures, great dissolution abilities, and are both tuneable and recyclable.^{4,5} Specifically, 1,3-dialkylimidazolium ILs containing anions of appreciable hydrogen-bond basicities have been employed for the dissolution of large bio-derived carbohydrates.^{3,6,7} Further processing of carbohydrates in these ILs yield energy-dense sugars, which can then be transformed into other valuable platform chemicals. For example, the depolymerization of cellulose to yield glucose, can be followed by catalytic transformation of glucose to 5-hydroxymethylfurfural (HMF) in ILs.⁸⁻¹⁰ HMF is a versatile precursor for the development of fuels and plastics, or can be further transformed to yield other valuable compounds.

Currently, few analytical methods exist for the direct analysis of bio-derived compounds in IL media.¹¹ Those that do exist are primarily chromatographic and require tedious separation of the analytes from the IL media prior to analysis. Rather than separating the analyte from the IL, a method of analysis based on matrix-assisted laser desorption/ionization mass spectrometry (MALDI-MS) has been proposed, allowing the detection of analytes in IL reaction mixtures with the addition of a common MALDI matrix.

Matrix-assisted laser desorption/ionization mass spectrometry (MALDI-MS) was originally developed in the 1980s as an effective tool for the analysis of large non-volatile compounds such as proteins, carbohydrates, and polymers.^{12,13} Since its introduction, MALDI-MS has become a useful tool for the analysis of small molecule classes as well. As a soft ionization technique, with the ability to rapidly analyze samples, MALDI-MS is a desirable tool for analytical chemistry, biology, and forensics.

MALDI affords ionization through laser ablation of a substrate containing co-crystallized analyte and matrix. Subsequent vaporization of matrix and analyte molecules result in ionization of analytes through a variety of proposed mechanisms such as charge transfer, photoionization, or through desorption of preformed ions.¹⁴ The matrix also serves to embed and protect the analyte from incoming laser irradiation. A wide range of compounds have been employed as MALDI matrices which vary depending on the application. Common MALDI matrices are conjugated organic acids such as derivatives of cinnamic acids and substituted benzoic acids, which absorb UV energy at the energy of common MALDI lasers.¹⁵ The choice of matrix in a MALDI experiment is crucial, as the

matrix plays an important role in promoting ionization of the target analytes.^{16,17} The choice of matrix can have significant effects on the ability to obtain analyte signals, as some matrices are well-suited to particular analyte classes, and perform poorly for others. Further care must be taken when analyzing small molecule classes (< 500 Da), as interferences from matrix adduct peaks and fragments may mask analyte signals, and cause deterioration of the quality of acquired mass spectra.

Substituted benzoic acids are popular matrices for carbohydrate and sugar analyses, as they absorb energy at the wavelength of common MALDI lasers (as is required by any MALDI matrix), and promote cation or alkali metal adduct formation, which is often required for analyte detection. In fact, DHB is often the most popular matrix for carbohydrate analysis.¹⁷ Other organic acids such as CHCA have also been employed, but suffer from increased matrix interference in the low mass region. Due to their popularity in MALDI analyses, DHB and CHCA were chosen as model matrices for designing new matrices for carbohydrate analysis in ILs. Quantitative applications of MALDI-MS, however, are limited by the commonly used solid MALDI matrices, due to non-uniform crystallization which causes poor shot-to-shot and spot-to-spot reproducibility.^{16,18}

In 2001, Armstrong and coworkers introduced a new class of UV-active liquid matrices based on ionic liquids.¹⁸ These ionic liquid matrices (ILMs) were designed from amines and the anions of common matrices, α -cyano-4-hydroxycinnamic acid (CHCA) and sinapinic acid (SA). The resulting ILMs successfully enhanced reproducibility of analyte signals of test analytes, and their success prompted the design of many new ILMs

for the analysis of various molecule classes. Despite several attempts, few successful ILMs based on 1,3-alkylimidazolium ILs have been reported.

In this research, novel IL-containing matrices were designed using ILs that are commonly used in biomass transformation reactions. Of particular interest to this work is the analysis of sugars and small platform chemicals that can be produced using IL solvent systems. Specifically, test analytes were chosen as glucose and fructose (products and intermediates in cellulose processing), sucrose, *N*-acetyl-D-glucosamine (as produced from chitin/chitosan processing), and two valuable platform chemicals which can further be derived from the aforementioned sugars: 5-hydroxymethylfurfural and levulinic acid. Sample preparation techniques were optimized and the IL-containing matrices were screened for their use in the detection of bio-derived analytes by MALDI-MS.

3.2 Materials

D-(+)-Glucose ($\geq 99.5\%$), D-(-)-fructose ($\geq 99.9\%$), sucrose ($\geq 99.5\%$), 2,5-dihydroxybenzoic acid (DHB) (98 %), α -cyano-4-hydroxycinnamic acid (CHCA) ($\geq 98\%$), and 1-ethyl-3-methylimidazolium chloride ([EMIM]Cl) (98 %) were obtained from Sigma-Aldrich (St. Louis, MO). The 1-ethyl-3-methylimidazolium acetate ([EMIM]OAc) ($> 95\%$) was purchased from Io-Li-Tec (Tuscaloosa, AL). The 1-butyl-3-methylimidazolium chloride ([BMIM]Cl) (96 %), 5-hydroxymethylfurfural (HMF) (98 %) and *N*-acetyl-D-glucosamine (NAG) (98 %) were obtained from AK Scientific (Union City, CA), and levulinic acid (98 %) was purchased from Alfa Aesar. Deuterated dimethyl sulfoxide- d_6 (99.9 % + 0.05 % TMS v/v) was purchased from Cambridge

Isotopes (Andover, MA). Water, methanol and acetonitrile (HPLC grade, 99.9 %) were obtained from Fisher Scientific (Fair Lawn, NJ). All chemicals were used without further purification.

3.3 Instrumentation

3.3.1 MALDI-TOF MS

MALDI-MS analyses were carried out using an Applied Biosystems MDS SCIEX 4800 MALDI TOF/TOF mass spectrometer equipped with a 355-nm Nd:YAG laser (200 Hz). Ions were accelerated into the mass analyzer at a voltage of 1.796 kV. Spectra, acquired in positive reflectron ion mode, resulted from 16 sub-spectra from each from each laser shot for an average of 25 laser shots or a total of 400 sub-spectra. Laser intensity was varied per sample as appropriate. Data was exported to mMass (open source software) for processing.

3.3.2 Scanning Electron Microscopy

Scanning electron micrographs were obtained using a FEI MLA 650F scanning electron microscope equipped with a field emission gun (FEG). 1 μ L of solutions containing 50 mM matrix and 50 mM IL (1:1 ratio) in 2:1 methanol:water solution were spotted onto an aluminum substrate and allowed to dry. 1 μ L of 10 mM NaCl solution (in the same solvent system) was spotted on top, and the spots allowed to dry for approximately 20 min before introduction into the SEM chamber (no coating was necessary). The microscope was operated in secondary electron mode with an accelerating voltage of 15 kV.

3.4 Methods

3.4.1 Matrix/Sample Preparation

Solutions of 200 mM DHB or CHCA were prepared daily using 2:1 MeOH:H₂O (v:v) as the solvent (unless otherwise specified). Similarly, 200 mM solutions of ionic liquids [BMIM]Cl, [EMIM]Cl and [EMIM]OAc, and 10 mM solution of NaCl were similarly prepared using the same solvent system. Equal volumes of matrix and ionic liquid solutions were combined to yield 100 mM solutions with 1:1 molar ratio of matrix:ionic liquid. 200 mM stock solutions of glucose, fructose, sucrose, NAG, HMF and levulinic acid were prepared in 2:1 MeOH:H₂O (v:v). Stock solutions were serially diluted in the same solvent system to yield working standards of 100 mM, 10 mM, and 1 mM. Equal volumes (typically 100 μ L) of 100 mM matrix/ionic liquid solution and analyte solution were mixed in a small vial resulting in final solution concentrations of 50 mM matrix/IL. 1 μ L spots were deposited onto a stainless steel 384 well stainless steel Opti-TOF MALDI plate and allowed to air-dry (~ 15 min) before analysis.

3.5 Results and Discussion

The prepared matrices were screened by MALDI-TOF MS to assess relative matrix interferences in the low mass region (m/z 50 – 400), and compared to the parent matrix acid. The goal of using MALDI methods for small molecule analysis in ionic liquids is to be able to remove an aliquot of a reaction mixture, mix it with an appropriate MALDI matrix and analyze the sample directly. With this in mind, a solution containing

IL and analyte could be directly mixed with a solution of an appropriate matrix, spotted, and analyzed in a similar manner.

In this study, traditional MALDI matrices DHB and CHCA were compared to the prepared IL-containing matrices and screened for matrix ion peaks and relative fragmentation/adduct formation in the low mass region (m/z 50 – 400). All matrices were prepared as outlined in the Methods section of this chapter. All of the following MALDI mass spectra (unless otherwise specified) were subject to post-acquisition acceptance criteria for data analysis. Peaks exceeding S/N ratio of 3 and relative intensity threshold of 10 % were labelled. Labelled peaks represent the monoisotopic masses of each ion. No further deconvolution was required. Note that spectra shown represent a single analysis, which was selected based on signal intensity and the presence of analyte signal (where applicable).

3.5.1 MALDI-TOF MS Analysis of DHB and DHB-IL Matrices

DHB is the most popular MALDI matrix for the analysis of carbohydrates.¹⁷ Unfortunately, for low mass analytes, spectra acquired using DHB suffer from matrix peak interference resulting from fragmentation and adduct formation, and therefore analysis is often limited to qualitative analysis. To assess whether IL-containing systems could be alternatively used for such analysis, solutions of DHB and selected imidazolium-based ILs ([BMIM]Cl, [EMIM]Cl and [EMIM]OAc) were mixed, and analyzed by MALDI-TOF MS to evaluate relative matrix interferences. It is important to note that in the case of DHB-[EMIM]OAc mixtures, a new ILM is formed *in situ* ([EMIM][DHB]),

and is therefore differentiated from the other chloride-containing IL-mixtures, which do not form a new ion pair (as described in Chapter 2).

From the resulting mass spectrum of DHB (Figure 3-1 (a)), the difficulties in small molecule analysis in positive ion mode become clear, as there are considerable matrix peaks over the range of detected m/z values. Fortunately, there is no significant matrix interference between m/z 200-260, which is where cation adducts of glucose, fructose and NAG peaks are expected to appear. However, there are significant peaks in the $m/z > 300$ range, which may cause interferences with the analysis of larger sugars

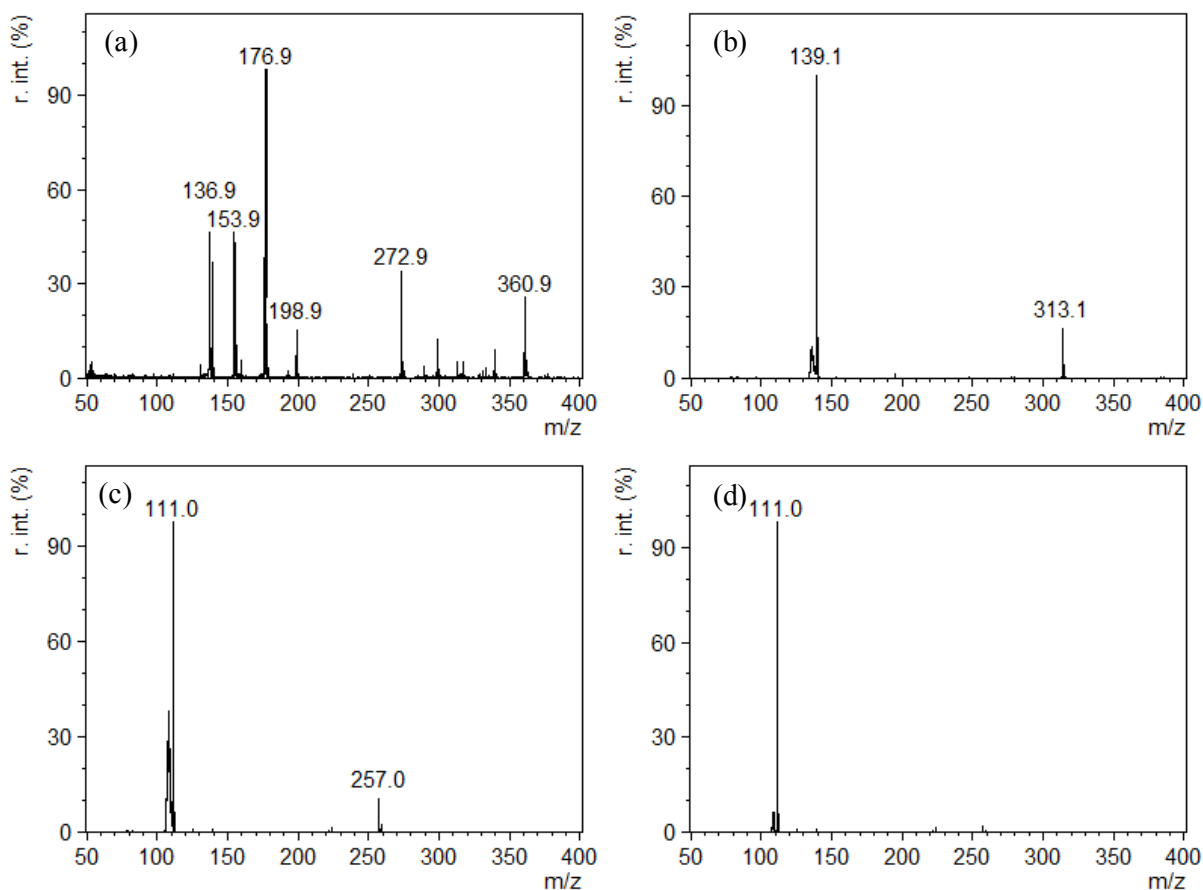


Figure 3-1: Representative Mass Spectra of (a) DHB, (b) [BMIM]Cl-DHB, (c) [EMIM]Cl-DHB, (d) [EMIM][DHB]

such as sucrose, as well as in the $m/z < 200$ range where small platform chemicals are expected to appear. Figure 3-1 displays a typical mass spectrum of each DHB and IL-containing DHB matrices. Several characteristic fragments and adduct peaks that are typical of DHB have been identified,¹⁹ as well as characteristic ions of each ILM according to their isotopic distribution patterns. As can be seen in Figure 3-1, the matrices containing IL have practically no matrix interference over the entire range of 50 - 400 Da. For matrices used with chloride-containing ILs (i.e. [BMIM]Cl-DHB and [EMIM]Cl-DHB), the spectra are dominated by two major ions: the ionic liquid cation, and a chloride-adduct of two cations (identified in Table 3-1), each of which were confirmed by isotopic distribution patterns.

Table 3-1: Identified Adducts and Fragments of DHB and DHB-IL Matrices (in Positive Ion Mode)

DHB		[BMIM]Cl-DHB		[EMIM]Cl-DHB		[EMIM][DHB]	
m/z	Ion	m/z	Ion	m/z	Ion	m/z	Ion
137	[DHB+H-H ₂ O] ⁺	139	[BMIM] ⁺	111	[EMIM] ⁺	111	[EMIM] ⁺
154	DHB ⁺	313	[BMIM ₂ Cl] ⁺	257	[EMIM ₂ Cl] ⁺		
155	[DHB+H] ⁺						
177	[DHB+Na] ⁺						
199	[DHB+2Na-H] ⁺						
273	[2DHB+H-2H ₂ O] ⁺						

Similarly, the ILM [EMIM][DHB] has only one characteristic [EMIM]⁺ ion. The presence of these ions is reasonable, as the IL counterpart in these cases is already ionized, and would likely be desorbed from the substrate surface. Interestingly, there are no significant ions of DHB adducts in the mass spectra of either IL-containing matrix, which may be a result of matrix peak suppression by the presence of the IL. Overall, the IL-containing matrices show very minimal matrix interference in the absence of analyte, which appears promising for small molecule analysis.

3.5.2 MALDI-TOF MS Analysis of CHCA and CHCA-IL Matrices

Similarly, the CHCA matrices with and without IL were compared as potential MALDI matrices for the sugar analytes of interest, and screened for potential matrix interferences before analysis. As seen in Figure 3-2, the fragment ion and adduct ion formation of CHCA is much different than that of each of the mixtures of IL and CHCA. The ionization of CHCA leads to few intense matrix peaks, most of which do not appear as if they will directly interfere with the analysis of the target analytes. [EMIM][CHCA], on the other hand, has an abundance of matrix ions formed, as well as significant noise along the baseline in the *m/z* range of 200 – 250. Although the peak corresponding to [EMIM]⁺ is evident, there are a number of unidentified peaks that arise (*m/z* 88, 125, 205, 221, 233). Remarkably, none of these peaks could be identified as common CHCA adducts or fragments. This is also strikingly different from the matrix spectrum of [EMIM][DHB] (Figure 3-1 (d)). The mixtures of [BMIM]Cl-CHCA and [EMIM]Cl-CHCA, however appear identical in nature to [BMIM]Cl-DHB and [EMIM]Cl-DHB,

showing the two matrix peaks corresponding to the $[\text{BMIM}]^+ / [\text{EMIM}]^+$ cations and corresponding chloride adducts, with no appreciable ions from the matrix acid.

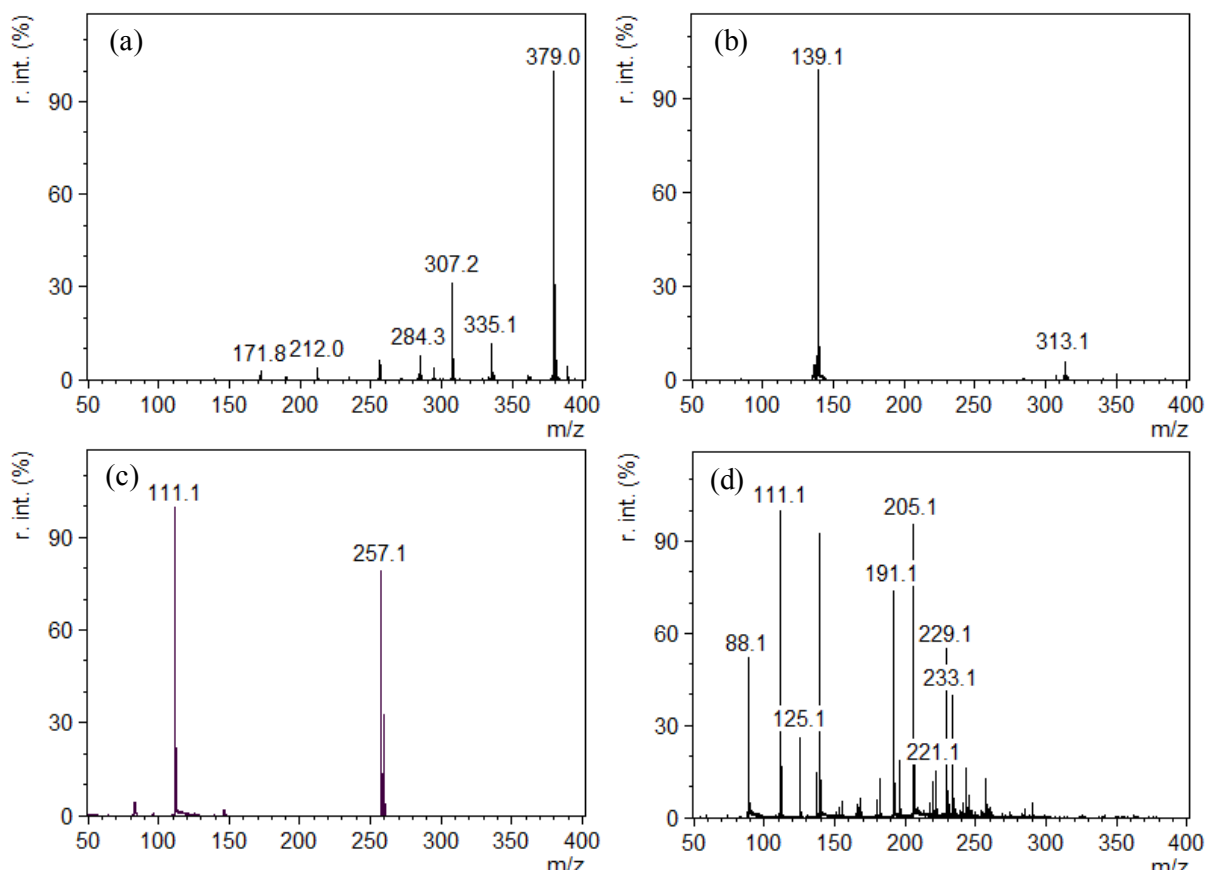


Figure 3-2: Representative Mass Spectra of (a) CHCA, (b) $[\text{BMIM}]\text{Cl-CHCA}$, (c) $[\text{EMIM}]\text{Cl-CHCA}$, (d) $[\text{EMIM}][\text{CHCA}]$

It was first unclear why the ILM $[\text{EMIM}][\text{CHCA}]$ exhibits a much more complex spectrum than $[\text{EMIM}][\text{DHB}]$. However, closer inspection of the spectra of each matrix, show some similarities. Although they appear at much lower intensities with respect to the base peak ($[\text{EMIM}]^+$), many of the unidentified matrix ions generated by $[\text{EMIM}][\text{CHCA}]$ are present in $[\text{EMIM}][\text{DHB}]$ as well. Specifically, m/z 88, 125, 139, 191, 205, 221 and 233 are common between the two upon enlarging the corresponding

spectra (not shown). Additionally, these peaks do not correspond with typical matrix peaks formed from the stainless steel plate, and also do not appear in the [BMIM]⁺-containing analogues. This implies that these peaks are likely a result of the [EMIM]⁺ cation. Furthermore, upon mixing [EMIM]OAc and each of the tested matrices, acetic acid is formed as a by-product. This may be a factor in generating some of these matrix ions, by adduct-formation or acidic decomposition. Notably, some of these ions exhibit peak differences of 14 amu, which suggests alkyl chains may be present (-CH₂-). (Note that the nitrogen-rule does not apply to many of these peaks, as the [EMIM]⁺ ion is charged prior to analysis). Despite several attempts, these ions have yet to be identified.

Table 3-2: Identified Adducts and Fragments of CHCA and CHCA-IL Matrices (in Positive Ion Mode)

CHCA		[BMIM]Cl-CHCA		[EMIM]Cl-CHCA		[EMIM][CHCA]	
<i>m/z</i>	Ion	<i>m/z</i>	Ion	<i>m/z</i>	Ion	<i>m/z</i>	Ion
172	[CHCA-H ₂ O+H] ⁺	139	[BMIM] ⁺	111	[EMIM] ⁺	111	[EMIM] ⁺
190	[CHCA+H] ⁺	313	[BMIM ₂ Cl] ⁺	257	[EMIM ₂ Cl] ⁺		
212	[CHCA+Na] ⁺						
234	[CHCA-H+2Na] ⁺						
335	[2CHCA-CO ₂ +H] ⁺						
379	[2CHCA+H] ⁺						

Overall, it was interesting to observe the suppression of matrix peaks in most of the IL-containing matrix spectra. If the DHB and CHCA peaks remain suppressed in the presence of analyte, the presence of the IL may lead to reduced matrix interference, and prove to be beneficial for small molecule analysis.

3.5.3 Physical Appearance

The major limiting factor of quantitative MALDI-MS analyses is due to the use of solid matrices which crystallize non-uniformly on the MALDI plate, and lead to poor shot-to-shot and spot-to-spot reproducibility. On the other hand, liquid matrices afford a more uniform sample spot, leading to increased spot homogeneity, and have been employed for quantitative MALDI applications. ILMs are often liquids, but may also crystallize upon spotting, depending on physicochemical characteristics such as melting point and hygroscopicity.¹⁸

Of the isolated IL-containing matrices in this study, those that were produced from chloride-containing IL starting materials were all isolated as solids which precipitated from solutions containing IL and matrix upon solvent evaporation. In the case of reactions of each matrix with [EMIM]OAc, however, the product ILMs were viscous solutions, containing acetic acid by-product (as confirmed by ¹H NMR). Purification of [EMIM][DHB] (by azeotropic distillation with toluene) yielded a brown, waxy solid (purification of [EMIM][CHCA] was not attempted). However, upon reconstitution in solvent and spotting on the MALDI plate, all IL-containing matrices appeared as glassy liquid spots, with the exception of mixtures of [BMIM]Cl and [EMIM]Cl with CHCA which crystallized upon solvent evaporation.

To further investigate the physical properties and homogeneity of the synthesized IL-matrix compounds, the DHB-containing IL mixtures were analyzed by scanning electron microscopy (SEM). Matrix solutions were prepared as outlined above, and 1 μ L volumes were spotted onto an aluminum substrate, allowed to dry, and then spotted with 1 μ L 10 mM NaCl solution. Magnification of the sample spots showed significant differences in spot topography upon addition of the IL.

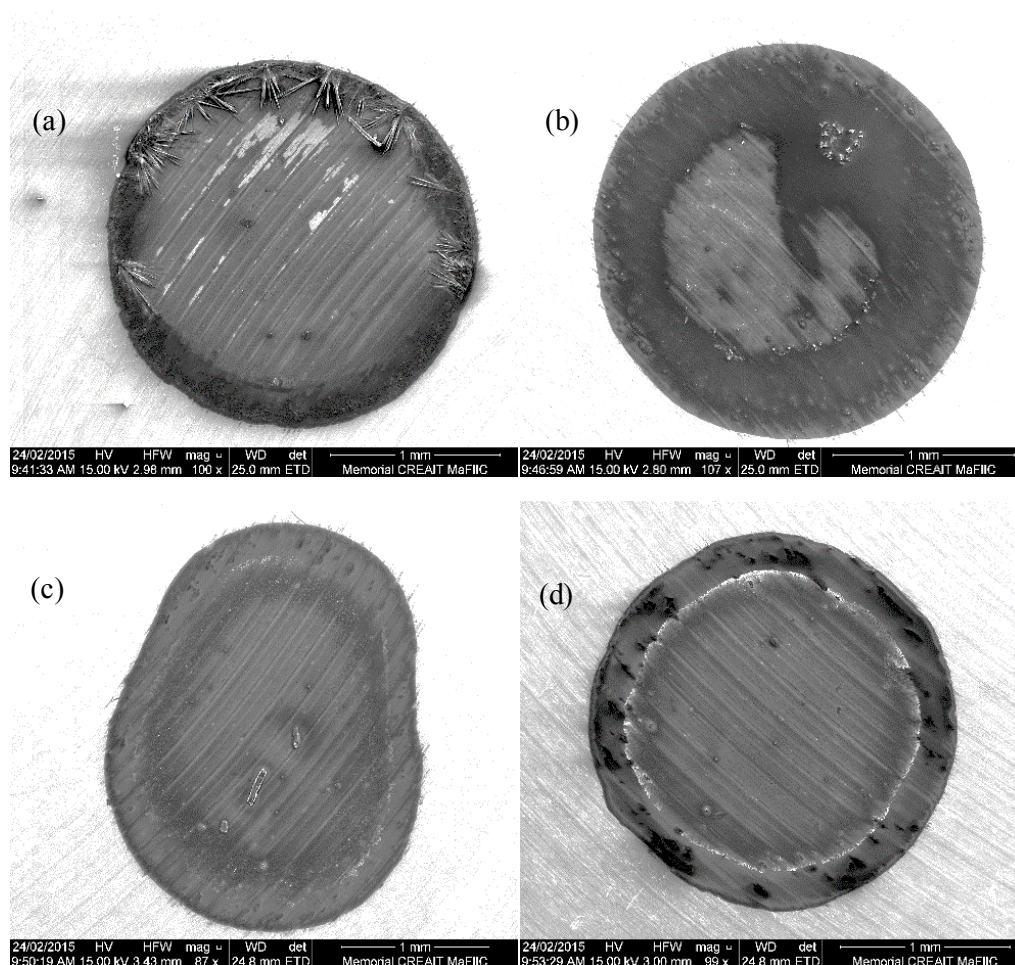


Figure 3-3: SEM Images of (a) DHB Matrix; (b) 1:1 DHB:[BMIM]Cl; (c) 1:1 DHB:[EMIM]Cl; (d) 1:1 DHB:[EMIM]OAc (all spots with 1 μ L 10 mM NaCl)

As can be seen in Figure 3-3 (a), upon drying DHB crystallizes forming “needles” at the edge of the sample spot. (Note that striations within sample spots correspond to imperfections in the aluminum substrate and that the absence of sample wells lead to imperfect circular spots). This crystallization behavior is responsible for the inconsistency in replicate analyses using this matrix. The IL-containing matrices, however, form glassy, liquid spots upon drying. There are identifiable solid aggregates in the IL-containing spots, however, overall, the consistency of the topography is significantly improved from that of DHB. In the case of each IL-matrix, a noticeable inner ring is observed, which may be a result of spotting NaCl on each spot after initial matrix/IL spotting.

3.5.4 Optimization of Sample Preparation for MALDI Analysis with DHB and CHCA

One of the aspects of MALDI-MS that lead to its popularity with small molecule classes is that sample preparation is relatively quick and easy. It is important to optimize sample preparation techniques to suit both matrix and analyte, and enhance analyte ionization. Such preparation techniques include the solvent system, additives, spotting technique, and acquisition mode (linear/reflectron). In the interest of quantitative work, spot homogeneity is also crucial, as mentioned previously. In the case of IL-containing samples, the critical parameters must also be tailored to be compatible with IL compounds which have high ionic character, viscosities, and hygroscopicities. In this work, several parameters including the use of additives, solvent systems and relative concentrations of sample components were optimized by systematic trial and error. The optimized conditions were based on compatibility with matrix, IL, and analyte, as well as overall analyte signal intensities and signal-to-noise.

3.5.5 Cationization of Sugar Analytes

Preliminary analysis by MALDI-MS using DHB and CHCA matrices (in the absence of IL) yielded no detectable protonated molecular ion ($[M+H]^+$) of the target analytes, even at relatively high analyte loading (M:A 1:1). Often, in the case where these protonated ions are desirable, small amounts of strong acids such as trifluoroacetic acid (TFA) are added to the MALDI matrix solution to promote analyte protonation. Addition of TFA, however, did not prove to be useful for the protonation of the sugar analytes in this study, as significant amounts of the protonated analyte signals were not detected.

The poor tendency of sugars to form protonated molecular ions in MALDI-MS can be attributed to their weak basicities. It follows that in the gas phase, these analytes have low proton affinities, as compared to more highly functionalized compounds. Sugars, however, are polyalcohols, and have a tendency to form adducts with small cations, such as sodium, potassium and ammonium ions.^{3,19} It is notable that in the absence of additives, the sodium and potassium adducts of each sugar analyte are often easily identifiable in the mass spectra. In the absence of additives, these adducts commonly result from adventitious ions in solvents, reagents, and from glassware leaching. To enhance the signal of these adducts and increase analyte sensitivity, it is common to add additional cations to the sample by using a cationization agent. In this study, NaOH, NaCl, KCl, and NH₄Cl (1 μ L of 10 mM solution, unless otherwise specified) were employed as potential cationization agents to increase analyte sensitivity.

Table 3-3: Relative Masses of Cation Adducts of Sugar Analytes

Sugar Analyte	m/z	Na ⁺ Adduct	K ⁺ Adduct	NH ₄ ⁺ Adduct
		m/z (+23 amu)	m/z (+ 39 amu)	m/z (+ 19 amu)
Glucose	180	203	219	199
Fructose	180	203	219	199
Sucrose	342	365	381	361
NAG	221	244	260	240

Addition of NaOH to the analyte did increase the abundance of [M+Na]⁺ ions of sugars when analyzed using DHB as the matrix. However, the overall intensities of the mass spectra were low, with increased baseline noise (data not shown). This may be a result of deprotonation of the matrix acid which may lead to shifts in the electronic behavior of the matrix (Chapter 2). Therefore, the use of NaOH as a cationization agent was avoided, due to its higher reactivity versus other dopants such as salts.

The use of salts as cationization agents was particularly useful when analyzing sugars with DHB. Addition of NaCl or KCl led to a significant increase of [M+Na]⁺ and [M+K]⁺ adducts of glucose, fructose, sucrose and NAG (corresponding m/z values of adducts shown in Table 3-3). In all cases, the addition of NaCl led to higher abundance of the sodium adduct and addition of KCl led to higher abundances of the potassium adduct (as demonstrated with glucose shown in Figure 3-4). The use of NH₄Cl as a cationization

agent did not result in any detectable amounts of ammonium-adducted sugars, but did resemble spectra obtained without the use of cationization agent (spectra not shown).

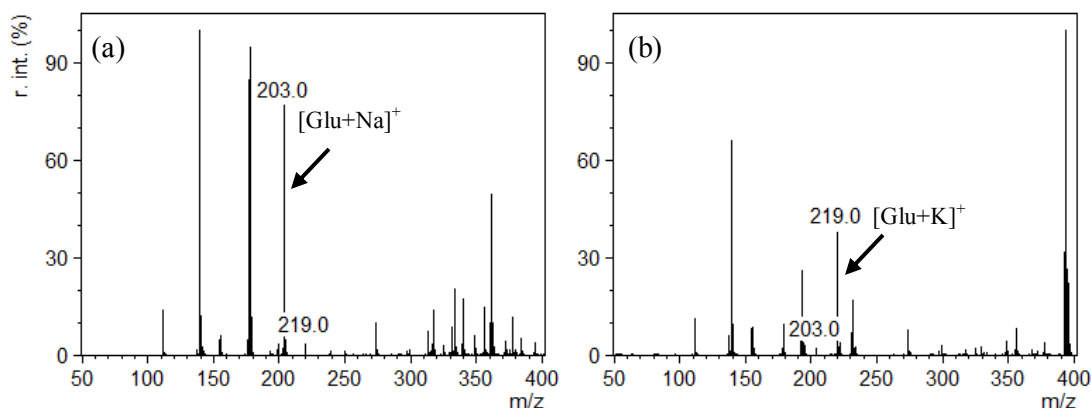


Figure 3-4: MALDI-MS Spectra of Glucose with DHB (1:1): (a) with 1 μ L 10 mM NaCl; (b) with 1 μ L 10 mM KCl

Adducts corresponding to HMF and levulinic acid were not detected using either of the tested cationization agents. Furthermore, the addition of the salt improved the overall quality of mass spectra. Specifically, many DHB-matrix peaks were suppressed upon addition of the salts (Figure 3-5). Similar analysis of CHCA, however, did not result in an apparent benefit. As shown in Figure 3-5, glucose peaks can be seen at m/z 203 (Na^+ adduct) and m/z 219 (K^+ adduct) in the absence of a cationization agent when analyzed with DHB (Figure 3-5 (a)), but is not apparent in the corresponding spectrum when the same analyte is analyzed using CHCA (Figure 3-5 (c)). Upon addition of NaCl dopant, the sodiated glucose peak is readily apparent with DHB (Figure 3-5 (b)) with an overall reduction in matrix peaks, with the exception of sodiated DHB adducts (m/z 177). The addition of NaCl to glucose when analyzed using CHCA, however do not give rise to appreciable sodiated glucose peaks.

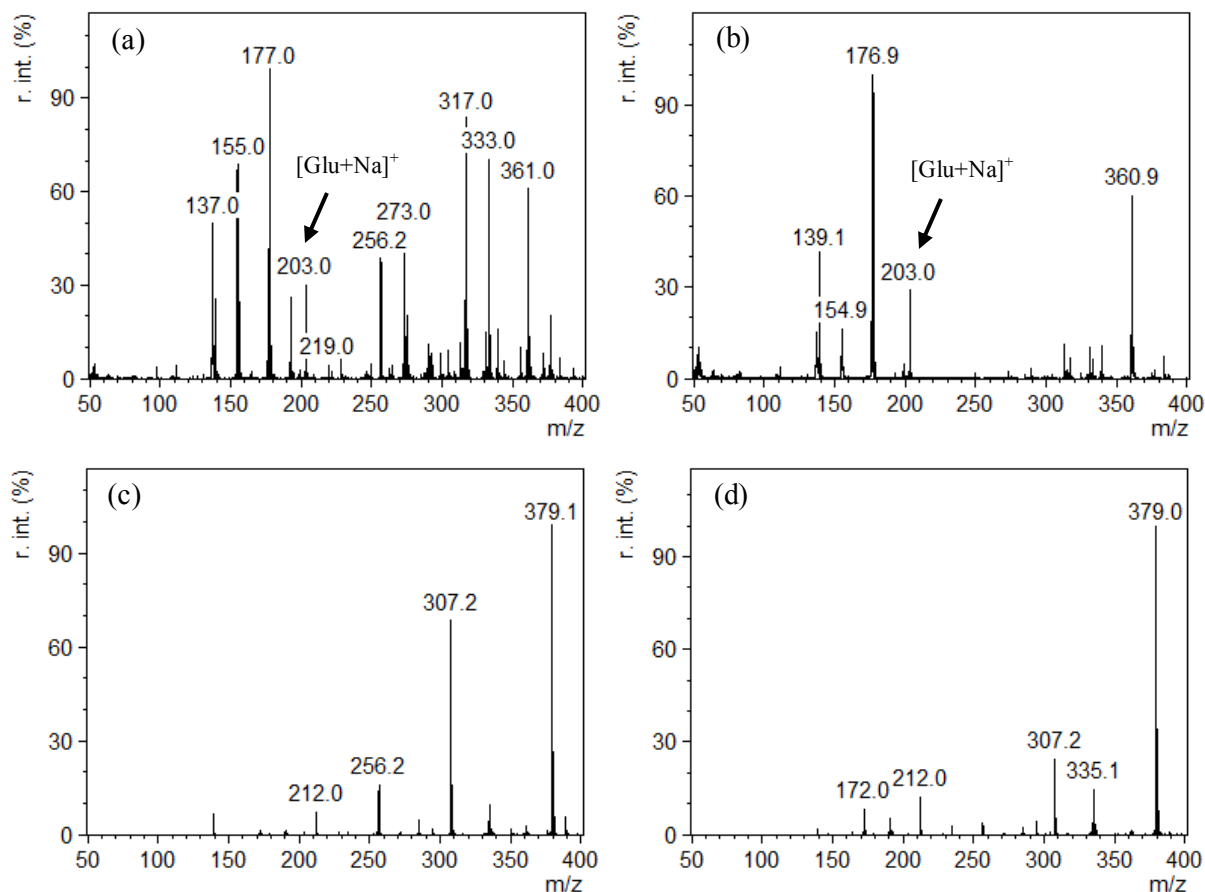


Figure 3-5: Effect of Cationization of Glucose with DHB and CHCA Matrices (1:1 Matrix:Glucose): (a) DHB matrix without additive; (b) DHB matrix with 1 μ L 10 mM NaCl dopant; (c) CHCA matrix without additive; (d) CHCA matrix with 1 μ L 10 mM NaCl dopant

The cationization agents NaCl, KCl and NH₄Cl were screened with each sugar analyte using each DHB and CHCA. Overall, the cationization agents employed in this study yielded very low intensity analyte adducts (< 1 % relative intensity) when analyzed with CHCA under the same conditions as those analyzed with DHB. Glucose and fructose were seldom detected at all, and HMF and levulinic acid were not detected. Sodium adducts of both sucrose and NAG (m/z 365 and 244, respectively) and potassium adducts of NAG (m/z 260) were generally easily identifiable. The potassium adduct of sucrose

(m/z 381) was also observed, but suffered from matrix interference from the isotopic abundances of the CHCA dimer (m/z 379). Similar to the observations of the DHB matrix with NH_4Cl dopant, no ammonium-adducted sugars were observed.

The formation of adducts (in positive ion) MALDI-MS depends on the affinity of the cation towards the analyte and the size of the cation. In the case of NH_4Cl , no ammonium adducts of either analyte were detected, whereas sodium and potassium adducts of the sugars were easily identified (especially when analyzed with DHB). Sodium is a smaller cation and can more easily associate within the hydroxyl groups of the sugars. Potassium adducts seem to be preferentially formed with larger sugars such as NAG and sucrose in the presence of CHCA. Finally, these results suggest that DHB is better suited for the analysis of sugars than CHCA, and tends to promote cationization, as adducts of all tested analytes were easily identifiable. Sodium and potassium cationization agents prove to be the most useful of those tested for enhancing analyte signal. The absence of signals for HMF and levulinic acid is likely attributable to their higher volatilities, which may allow evaporation from the plate upon entering the instrument and prevent detection. This may not be the case when the matrix is combined with IL, which will be discussed further.

Finally, these experiments were repeated in the presence of each IL. Interestingly, the formation of adducts is retained upon the addition of the IL. DHB-IL mixtures allowed detection of sodium and potassium adducts of sugar analytes, whereas CHCA-IL mixtures suffered from low analyte ion intensities and appreciable matrix interference. The relative abundances of the Na^+ and K^+ ions were not determined however, due to

high variability between spots. Regardless of the cationization agent used (i.e. NaCl vs. KCl), adducts of both sodium and potassium of each glucose, fructose, sucrose and NAG were identified, in varying amounts. Notably, potassium adducts of glucose and fructose (m/z 219) were often overlapping with an unidentified matrix peak in [EMIM]⁺-containing matrices. Therefore, NaCl was chosen as an appropriate cationization agent for further analysis.

Addition of equal molar amounts of NaCl (to the analyte) did not result in increased analyte signal in the case of either matrix and also lead to poor spot quality. It is speculated that the high concentration of salt may have had a salting out effect, and evaporation of the solvent led to inhomogeneous spots. Furthermore, cationization is known to have low efficiency, and an excess of Na⁺ appears to be unhelpful. Therefore, 1 μ L of 10 mM NaCl solution (5:1 matrix:salt molar ratio) was prepared in the same solvent system and spotted on top of the deposited matrix/analyte/IL solution before analysis.

3.5.6 Laser Intensity

By analyzing the matrices, it became evident that the ILMs required higher laser intensities than their analogous solid matrices. This finding has been previously described in ILM studies.³ To determine the relative laser intensity required for each matrix, the laser intensity that afforded a base peak ion count above 10000 (arbitrary units) was monitored. The laser intensity is given both as the absolute value (arbitrary units as shown on the mass spectrometer software), as well as a percentage of the maximum laser power. Note that this was the intensity needed to form appreciable matrix ions, and that

the presence of analyte meant that slightly higher laser power would be required.

Additionally, laser intensity was variable between analyses. Therefore, before analysis of a given sample set, the optimum laser intensity was determined, and recorded.

Table 3-4: Relative Laser Intensity for Studied Matrices

Matrix	Laser Intensity	Laser Intensity (%) (relative to the maximum)
DHB	5800	73 %
[BMIM]Cl-DHB	7200	91 %
[EMIM]Cl-DHB	6500	82 %
[EMIM][DHB]	7200	91 %
CHCA	4200	53 %
[BMIM]Cl-CHCA	6200	78 %
[EMIM]Cl-CHCA	6000	76 %
[EMIM][CHCA]	5800	73 %

Generally, all IL-containing matrices require significantly higher laser intensity to produce spectra of similar base peak intensities, and DHB-matrices require higher laser intensities than the corresponding CHCA-matrices. It is notable that both [BMIM]Cl-CHCA and [EMIM]Cl-CHCA crystallize on the MALDI plate. The slightly lower laser intensities required to promote ionization may be a result of easier ablation from the surface. In the case of these ILs in combination with DHB, the spots appear glassy, as the

IL seems to entirely cover/dissolve the matrix. Therefore, a higher laser intensity may be required to reach the UV-active matrix. Finally, [BMIM]⁺-containing matrices tend to require higher laser intensities to form similar ion abundances to [EMIM]⁺-containing matrices. This may be correlated with the size of the cation, as larger cations such as [BMIM]⁺ will likely require more energy to become desorbed from the surface. Further studies of a homologous series of imidazolium cations could be conducted in future work to confirm these findings.

Since the laser intensities required to produce good ion signals is very high, the laser intensity was adjusted to yield reasonable ion signal (i.e. > 1000 A.U.) to avoid detector saturation by the most abundant ions (IL cations). Upon addition of analytes, the laser intensity would require readjustment to achieve reasonable ion intensities. Although variable, notably higher laser intensities were recorded for analyses of NAG and sucrose containing samples than for those samples containing equal amounts of glucose and fructose. This may also be correlated to the size of the analyte or to the degree of cationization.

3.5.7 Solvent System

The role of the solvent system used for MALDI sample preparation is to dissolve both the matrix and analyte, so that upon solvent evaporation, the matrix and analyte will co-crystallize on the MALDI substrate. In choosing the solvent, the relative surface tension and viscosity should also be considered, as these properties can affect sample spot quality upon deposition. In this case, the optimal solvent should be compatible with the matrix and analyte, as well as the IL, and result in uniform sample spots upon drying.

Generally, aqueous solutions of organic solvents are used as solvent systems for MALDI analysis. The ratio of water to organic solvent can be tailored to allow the dissolution of matrix and analyte, as well as to control the rate of solvent evaporation.

Acetonitrile:water mixtures are commonly used to dissolve CHCA matrices, and methanol/ethanol:water solutions are employed for DHB matrices. Sugar analytes typically have low solubilities in ethanol, and so, methanol:water solutions were tested with DHB matrices. The ILs of interest are very water-soluble, and easily dissolve in aqueous solutions of both acetonitrile and methanol. Water, methanol and acetonitrile were chosen as potential solvents, and the solvent systems were first tested in different ratios, to determine the best spot integrity (i.e. how easily spots could be deposited onto the plate and held in the sample wells). Using only water as the solvent, the surface tension of spots was very high, forming beads on the stainless steel substrate. Drying times of these spots were very long, and resulting spots appeared much thicker than those spotted using organic solvents. This is likely due to the low volatility of water, in addition to the hygroscopic-nature of the ILs. Upon introduction into the mass spectrometer, much more time was needed to reach low pressures in the vacuum chamber when these thicker spots were present, due to high moisture levels. Using 100 % acetonitrile or methanol as the spotting solvent resulted in very poor sample spots, as the low surface tension and high volatilities resulted in smearing across many sample wells. Finally, 1:1 and 2:1 solutions of acetonitrile/methanol:water were tested. Each solvent system resulted in good quality spots which appeared uniform across the sample well, with no distinguishable differences. Ultimately a 2:1 ratio of organic solvent to water was selected, due to faster drying times.

The solvent system was also tested for compatibility with sample additives. In the case of the neutral sugar analytes, a cationization agent was required to promote ionization. Upon addition of NaCl to sugar solutions in ACN:H₂O, however, phase separation occurs. This phenomenon known as “sugaring-out” has been previously reported for aqueous acetonitrile solutions.²⁰ Since this was not the case for aqueous methanol solutions, this supports the choice of 2:1 MeOH:H₂O as the solvent system for further experimentation.

3.5.8 Sample Spotting Technique

There are several spotting techniques that can be used for MALDI analysis.^{21,22} Commonly, samples are deposited onto the plate via the dried-droplet method, which is the simplest preparation technique.¹³ This technique involves pre-mixing solutions of analyte and matrix, and pipetting onto the substrate. Other techniques include thin-layer spotting, and sandwich methods (matrix, analyte, matrix). Both the dried-droplet and sandwich methods were tested in this study, leading to no obvious differences in the resulting mass spectra. Since the goal of these analyses is to be able to remove an aliquot of a bio-transformation reaction in IL media, and mix it with a MALDI matrix before directly spotting the sample, the dried-droplet method was employed for subsequent analysis for simplicity. Furthermore, addition of a cationization agent after drying results in re-dissolution of the matrix and analyte.

3.5.9 Matrix/IL Spotting Concentration

The concentration of the matrix is an important parameter in any MALDI analysis, as it dictates how well the sample spot will deposit upon drying, and can affect ionization behavior, and the formation of adducts.^{3,15} Generally, solid MALDI matrices are used at a concentration of 10 – 20 mg/mL for sample spot volumes of 0.5 – 1 μ L. ILMs may also crystallize depending on the relative melting point and hygroscopicity of the substance, but are often observed as liquid or glassy spots.¹⁸ Therefore it is important to determine the optimal matrix concentration for ILMs that cover the entire sample well.

Throughout preliminary studies, it was observed that the amount of IL deposited per spot had a drastic effect on the resulting mass spectra. At relatively low amounts of IL, the IL (and dissolved matrix and analyte) form small concentrated spots at the edge of the sample well. Upon spectra acquisition, the amount of interference throughout the m/z 300 - 400 region was significantly increased. It is likely that this additional interference is a result of laser ablation of the stainless steel surface. In a previous study, similar interfering ions were identified as benzylalkylmethylammonium salts, which originate from the stainless steel MALDI substrate.²³ Since the MALDI process acquires many sub-spectra by multiple laser shots of a single spot to generate the average response, a much higher abundance of these stainless steel interference peaks arise when little sample covers the well. At relatively high IL loading (> 50 mM IL in the spotted solution or ~ 10 μ g/spot), samples resulted in thick, glassy liquids.

As previously mentioned, high water content in the sample spots can lead to instrumental problems when attempting to reach low pressures in the vacuum chamber.

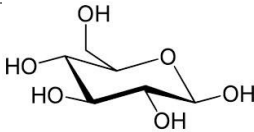
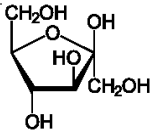
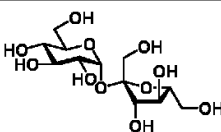
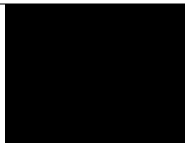
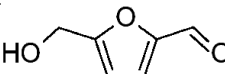
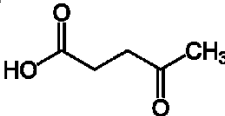
The thick sample spots, containing hygroscopic imidazolium ILs likely have high water contents, causing a similar effect. Therefore, the optimized amount of IL per spot (50 mM IL in spotting solution) was determined by the formation of thin, uniform spots that completely covered the sample well. Since the final concentration of the matrix when spotted is half that of the stock solution (upon mixing equal volumes of matrix solution and analyte solution), stock concentrations of 100 mM were selected as the optimal matrix concentration. The matrix was also spotted in 0.5- μ L or 1- μ L aliquots. For all spots containing 0.5 μ L of the matrix solution, fewer good quality spots were observed with poor reproducibility of spots. This is likely a result of difficulties in pipetting small volumes of viscous solutions. Therefore, all subsequent analyses used 1 μ L spotting volumes.

3.6 Qualitative Sugar Analysis

The synthesized ILMs were employed as MALDI matrices for the analysis of glucose, fructose, sucrose, NAG, HMF and levulinic acid. Optimized MALDI sample preparation and acquisition techniques were employed, using a matrix:IL:analyte ratio of 1:1:1 for qualitative screening purposes. Initial screening of the matrices was performed with all test analytes: glucose, fructose, sucrose, NAG, HMF and levulinic acid. It is important to emphasize that the following spectra each represent one analysis, and variations between spots and sets of samples were inevitable. In each case, the spectrum chosen is one from optimized analyses, and where the analyte signal is visible. Furthermore, comparison of matrix performance was done within a sample set (i.e. from the same sample plate and date of analysis). In all cases, the $[M+Na]^+$ peak was

monitored to determine the intensity of each analyte, and spectra were normalized with respect to the base peak.

Table 3-5: Masses of Analytes of Interest

Analyte	Chemical Formula	Monoisotopic Mass (amu)	Sodium Adduct (M+Na) ⁺ (amu)
 Glucose	C ₆ H ₁₂ O ₆	180.06	203.05
 Fructose	C ₆ H ₁₂ O ₆	180.06	203.05
 Sucrose	C ₁₂ H ₂₂ O ₁₁	342.12	365.11
 N-acetyl-D-glucosamine	C ₈ H ₁₅ NO ₆	221.09	244.08
 5-hydroxymethylfurfural	C ₆ H ₆ O ₃	126.03	149.02
 Levulinic Acid	C ₅ H ₈ O ₃	116.05	139.04

3.6.1 Sugar Analysis using DHB-Based Ionic Liquid Matrices

As suggested by the initial matrix screening, DHB and the DHB-IL matrices may be suitable matrices for small sugar analysis, as little matrix interference is observed in

the appropriate mass regions for the analytes of interest. To compare the novel ILMs to their parent solid matrix, all analytes were also tested with DHB (Figure 3-6). It appears that the addition of the analyte results in suppression of some DHB matrix peaks, and in all cases the sodiated analyte $(M+23)^+$ is readily apparent for all of the sugar analytes (glucose, fructose, sucrose and NAG).

Use of DHB as a matrix yielded good results for the analysis of glucose, fructose, sucrose and NAG. All peaks were readily identifiable (the sodiated peak is labelled on corresponding spectra) with no apparent matrix interferences, and in several cases, the analyte peak could be identified as the base peak. For both glucose and fructose analysis with DHB (m/z 203), the spectra show little matrix overlap in the analyte region, making DHB a feasible matrix for MALDI-MS analysis of these sugars. Additionally, DHB appears to be a suitable matrix for sucrose (m/z 365), as there is a significant suppression of matrix peaks. NAG was also identifiable as the sodium adduct at m/z 244. The presence of NAG, however, does not appear to have as much of a matrix suppression effect on DHB, as the signal compared to the matrix ions is much smaller than that of the other sugar analytes.

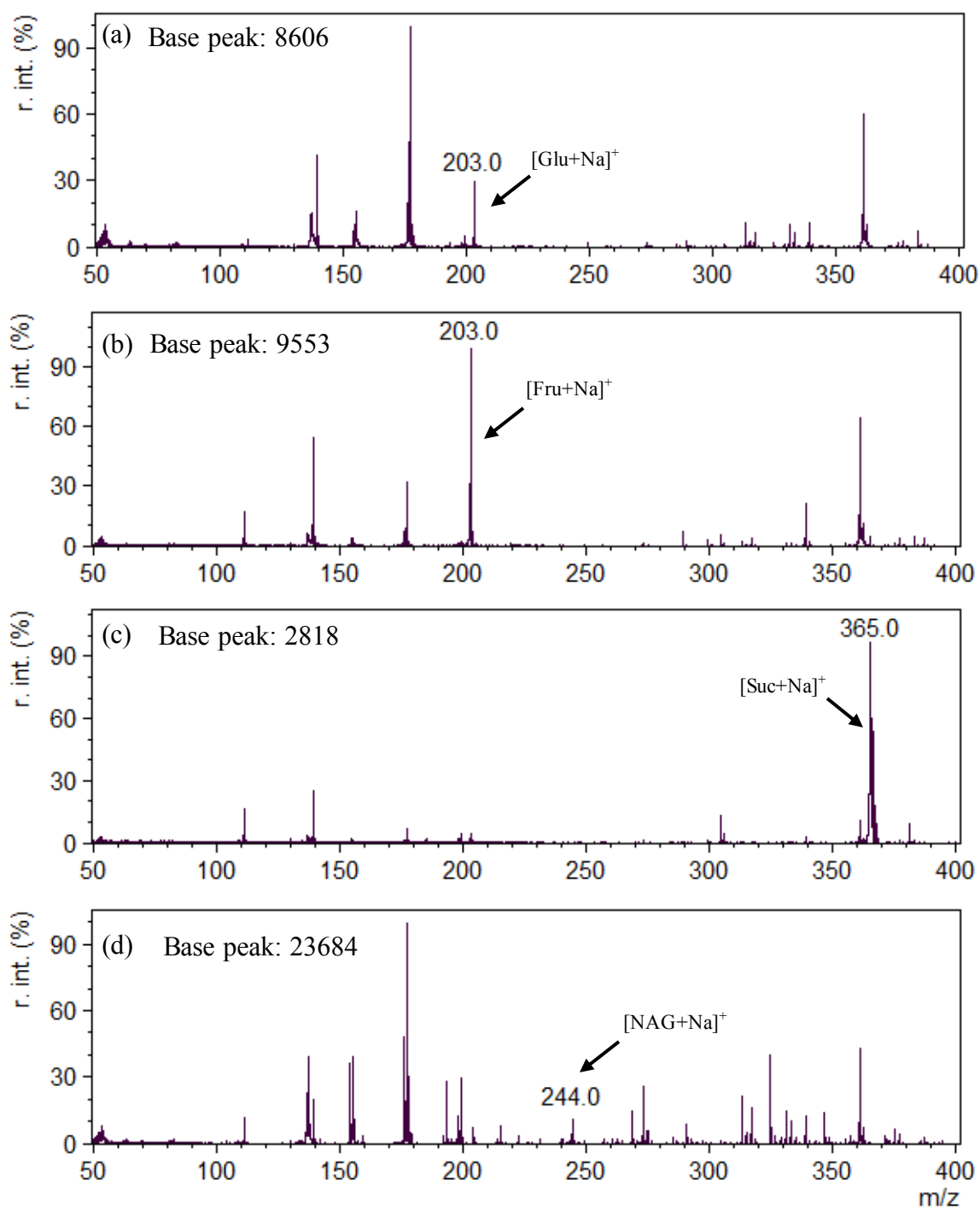


Figure 3-6: Analysis of Sugar Analytes with DHB Matrix (1:1 M:A + NaCl cationization agent): (a) Glucose, (b) Fructose, (c) Sucrose, (d) NAG

Since this matrix appeared to work well with the test analytes, HMF and levulinic acid were also tested to determine the applicability of these novel matrices for small, volatile platform chemicals. Unfortunately however, the two platform chemicals HMF and levulinic acid were not detected. It is speculated that the high volatilities of these compounds result in evaporation from the sample plate upon introduction into the low-pressure atmosphere of the instrument. Even relatively high concentrations of each of these analytes did not result in any identifiable ion signals.

Analysis of the same sugar analytes using the [BMIM]Cl-DHB matrix reveal much less matrix interference. Specifically, almost all of the ions and adducts formed by DHB are suppressed in the presence of the IL, yet the sodiated analyte peaks are still easily detected (Figure 3-7). The analytes were detected at varying abundances, and it was noted that reproducibility between shots (within a single spot) and between spots was poor. For the purposes of qualitative screening, however, the analytes could be identified with minimal interference from DHB. In some cases sodiated DHB (m/z 177) is visible, and in all cases the base peak of the spectra is [BMIM]⁺ (m/z 139). Glucose, fructose, sucrose and NAG were all detected using this matrix, but again HMF and levulinic acid were not detected.

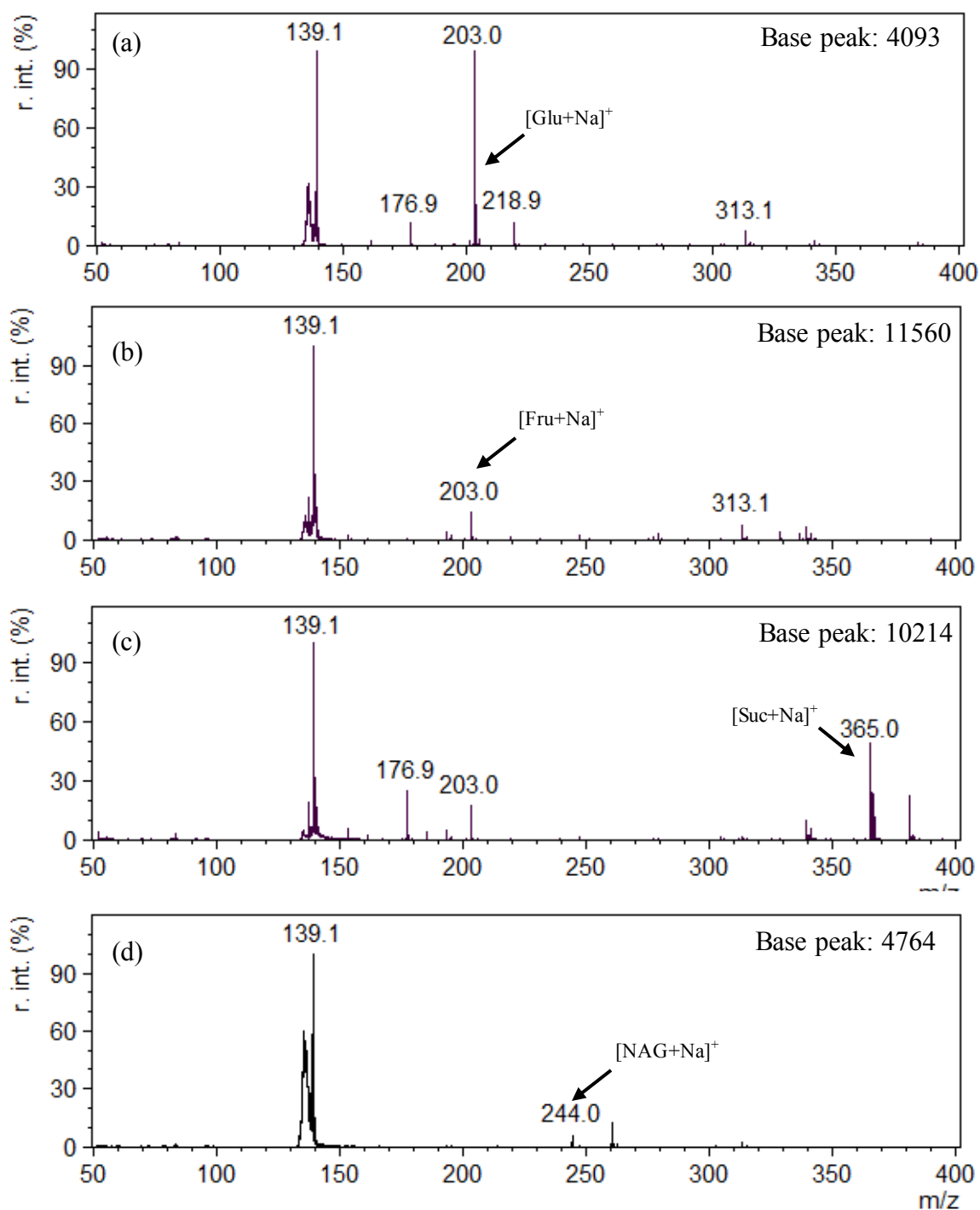


Figure 3-7: Analysis of Sugar Analytes with [BMIM]Cl-DHB Matrix (1:1 M:A + NaCl cationization agent): (a) Glucose, (b) Fructose, (c) Sucrose, (d) NAG

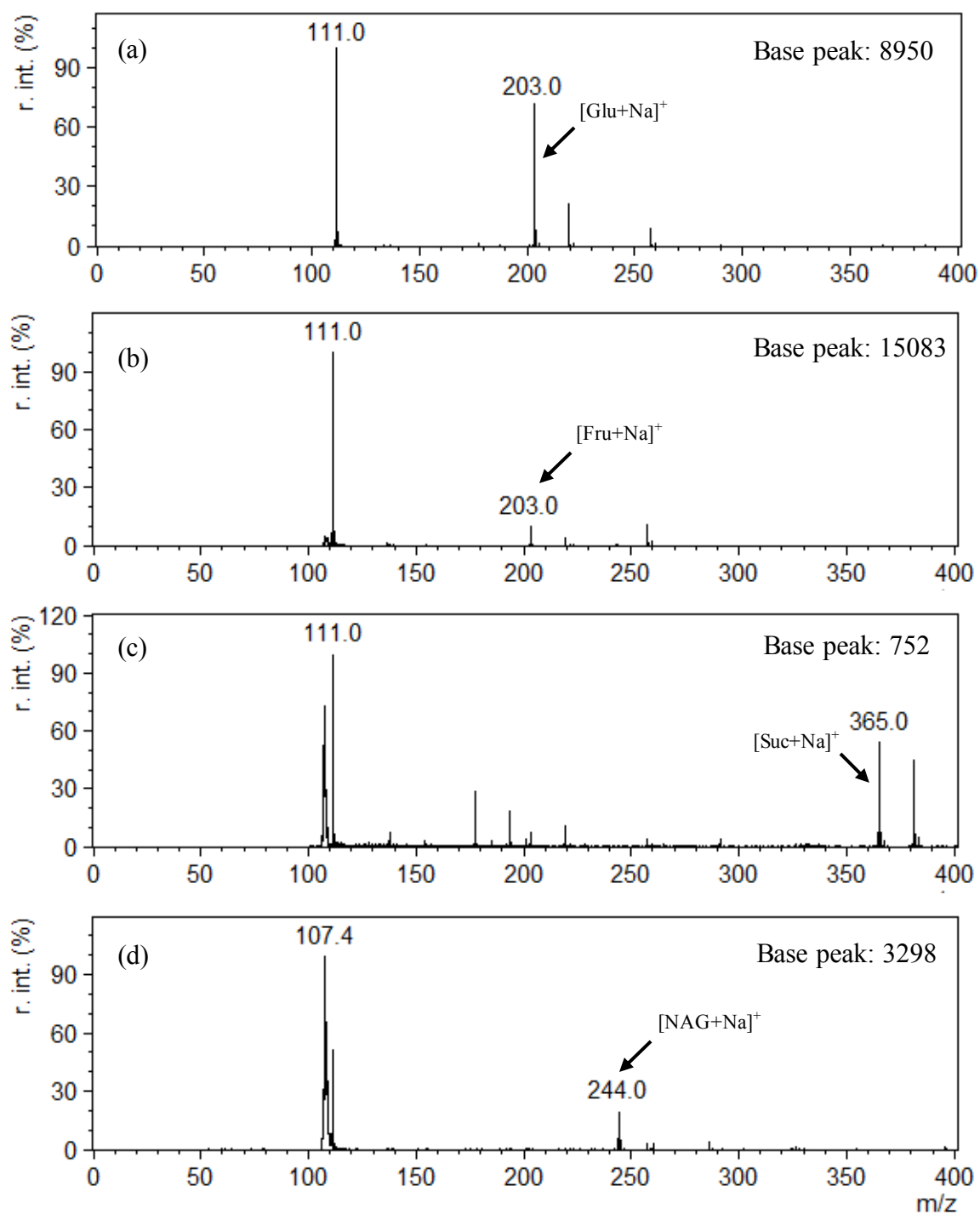


Figure 3-8: Analysis of Sugar Analytes with [EMIM]Cl-DHB Matrix (1:1 M:A + NaCl cationization agent): (a) Glucose, (b) Fructose, (c) Sucrose, (d) NAG

Similar experiments were carried out using the [EMIM]Cl-DHB matrix (Figure 3-8). There are many similarities between the spectra obtained using [BMIM]Cl-DHB and [EMIM]Cl-DHB. Again, the base peak is most often the [EMIM]⁺ cation, with very few observable DHB ions. Each analyte is observed as the sodium adduct, at appreciable (but variable) intensities. One anomaly was noted, however. When analyzed using [EMIM]Cl-DHB, NAG was easily detected, but the base peak was identified at m/z 107.5 rather than m/z 111 which is expected for the [EMIM]⁺ ion. However, the peak at m/z 111 was observed at lower intensity than in the spectra of the other test analytes. In other cases, this ion is apparent at lower relative intensities, as well as [BMIM]⁺ minus 3.5 amu for analysis using [BMIM]Cl-DHB. It is speculated that these peaks correspond to the IL cation, but suffer from loss of mass accuracy from ion detection (the instrument was calibrated using high mass standards), or may be resultant fragments due to the high laser energy employed. Either way, the sodiated analyte adducts of glucose, fructose, sucrose and NAG are easily seen with both chloride-containing ILs tested in this study. This was expected, as these matrices contain DHB (in parent form) and differ only by the cation of the IL employed.

Finally, the analytes were tested using the true ILM formed from the reaction of [EMIM]OAc and DHB (Figure 3-9). Analysis of the same analytes using [EMIM][DHB] yielded significantly different results from what was observed using DHB with either [BMIM]Cl or [EMIM]Cl. Although this matrix did allow the cationization of each analyte with the added sodium, there were significantly more matrix interferences observed than with either of the chloride-containing IL-matrix mixtures. In fact, analysis using

[EMIM][DHB] resulted in more ions in the spectra than analyses using DHB alone. The formation of these unknown ions was also noted in preliminary matrix screening of the ILM [EMIM][CHCA] (Figure 3-2(d)), and to a lesser extent with [EMIM][DHB]. As mentioned previously, these ions do not appear to be adducts of DHB, and were not identified. The abundance of matrix interference may be due to the presence of acetic acid in this matrix, or may be explained by changes in the electronic structure from the parent acid. In order for a compound to be suitable as a MALDI matrix, it must absorb UV radiation at the wavelength of the instrument laser. In this case, a 355 nm Nd:YAG laser was employed for all analysis. Referring to Figures 2-6 and 2-7, it is interesting to note that the true ILMs that formed (both [EMIM][DHB] and [EMIM][CHCA]) exhibited characteristic blue shifts, that result in the relative absorbance at 355 nm being much lower than their parent matrices. The IL-mixtures however, do not exhibit a loss in absorbance at the wavelength of the laser. Therefore, it is speculated that the mixtures containing the protonated acid can absorb more of the incoming energy, and subsequently ionize the analyte more efficiently. The unidentified ions that are formed during the ionization process of analyte and [EMIM][DHB] matrix may be a result of higher laser intensity required to promote analyte ionization, and therefore increased ionization of matrix components, or ions generated from the stainless steel substrate.

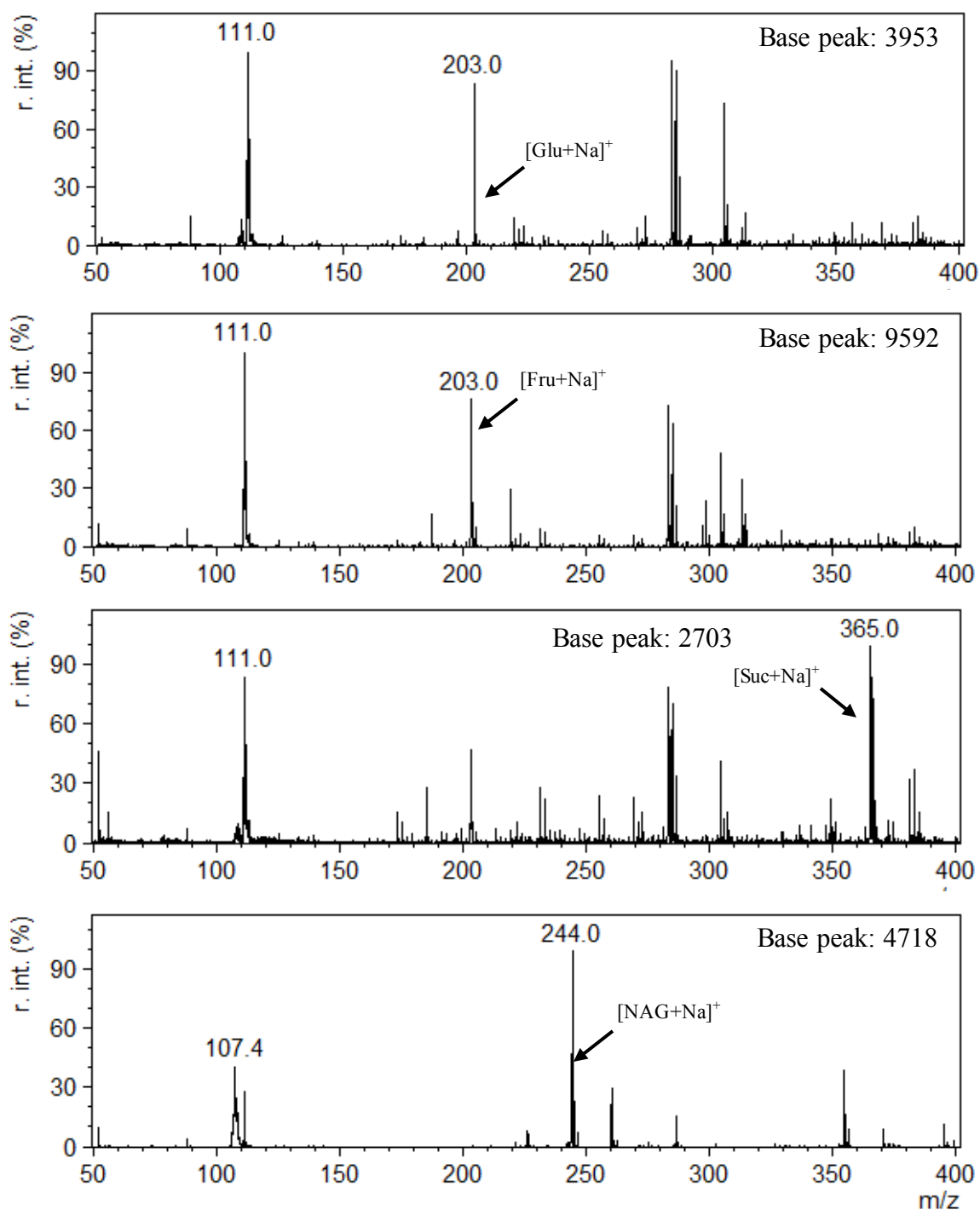


Figure 3-9: Analysis of Sugar Analytes with [EMIM][DHB] Matrix (1:1 M:A + NaCl cationization agent): (a) Glucose, (b) Fructose, (c) Sucrose, (d) NAG

Overall, each of the (sodiated) sugar analytes could be readily detected using each of IL-DHB matrices employed in this study, despite the notable differences between the IL-matrix mixtures (whereby DHB is present in parent acid form) and the true ILM. For the mixtures of the chloride-containing ILs and DHB, there was significantly less matrix interference observed than with DHB alone. It appears that these systems could prove to be useful alternatives for the qualitative analysis of these analytes in various applications, as well as for the analysis of IL-solvated systems.

3.6.2 Matrix Interference

Although direct matrix interference with analyte ions is not readily apparent (despite the formation of new ions), a peak at m/z 203 in the matrix was sometimes identified during analysis with [EMIM]Cl-DHB and [EMIM][DHB] matrices. Upon closer inspection, it appears that at high laser intensities and by hitting the same spot multiple times (depth profiling), a peak does appear at m/z 203 in these DHB containing matrices in the absence of analyte. Furthermore, the isotopic distribution immediately surrounding this peak does not match that of glucose/fructose (Figure 3-10). The abundance of this peak at m/z 203 increases as laser intensity increases and when repetitively analyzing a single spot within a sample spot. Furthermore, it is not observed in DHB (alone) or [BMIM]Cl-DHB, which suggests that this peak is an adduct/contaminant of [EMIM]⁺.

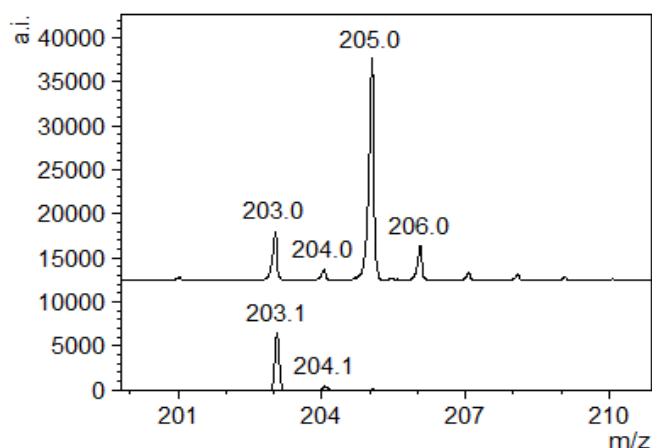


Figure 3-10: Isotopic Distribution Patterns of Glucose (lower) and Interfering [EMIM]⁺ Ion/Adduct (upper)

The identity of this peak has not been determined however, as the isotope pattern does not match well with logical adducts (i.e. adducts of [EMIM]⁺ and common contaminants, adducts of metals that occur in stainless steel, etc.). Careful control of the laser intensity, as well as isotopic distribution patterns, however, can limit the interference caused by this peak when analyzing glucose and/or fructose.

Overall, the DHB-based ILMs were suitable matrices for qualitative analysis of the studied sugars. Although it is apparent that the isomeric relationship between glucose and fructose will not allow differentiation between the two in MALDI-MS analysis, both analytes were separately detected, indicating that the presence of a peak in a sample analysis could refer to either sugar or a combination of both sugars. It appears that unreacted mixtures of IL and acid matrix out-perform both DHB and the ILM [EMIM][DHB]. There are potential advantages associated with this finding. For analytes in chloride-containing ionic liquid media, the direct addition of DHB may afford better

quality MALDI-MS spectra than if samples were extracted and analyzed by DHB alone. In other words, the addition of an IL medium seems to enhance the DHB performance with respect to sugar analysis. Further investigation of these matrices is required to broaden the class of applicable analytes.

3.6.3 Sugar Analysis using CHCA-Based Ionic Liquid Matrices

As previously mentioned, it was observed that the sugar analytes glucose, fructose and sucrose were not easily identifiable when analyzed using CHCA, regardless of the cationization agent employed. The $[\text{Glu}+\text{Na}]^+$ peak at m/z 203 was rarely detected and when observed, suffered from very low intensity (< 0.1 % relative intensity). Increasing the laser power did afford a larger $[\text{Glu}+\text{Na}]^+$ peak, however, at a cost of much more matrix interference (spectrum not shown). Similar observations were made with the analysis of fructose and NAG. Although these peaks can be seen without the interference from the matrix, they suffer from extremely low intensities when analyzed with CHCA (Figure 3-11 (a)). Sucrose analysis using CHCA, however, was much more straightforward. The sodiated sugar was easily identifiable at m/z 365, with fewer surrounding ion peaks (Figure 3-11 (b)).

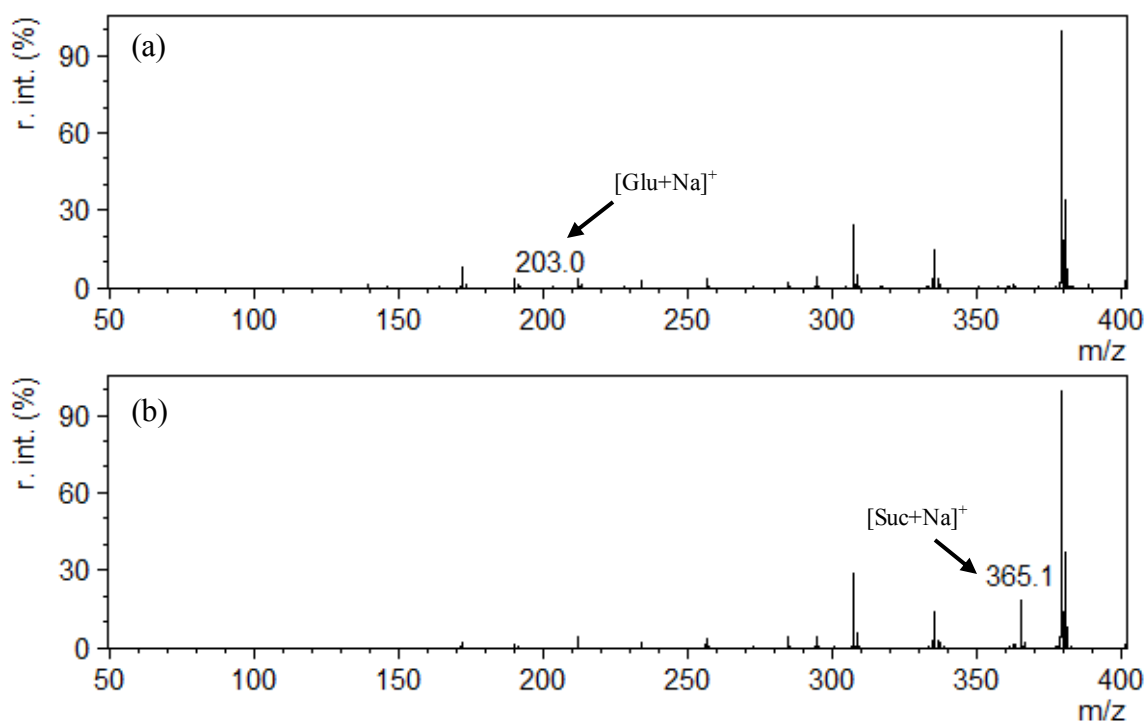


Figure 3-11: MALDI-MS Spectra of (a) CHCA + Glucose; (b) CHCA + Sucrose (1:1 M:A, + NaCl Dopant)

[BMIM]Cl-CHCA and [EMIM]Cl-CHCA showed similar analyte responses to that of CHCA for both glucose, fructose and NAG (data not shown). Although the addition of IL had considerably less matrix peak interference, $[Glu+Na]^+$ and $[Fru+Na]^+$ (m/z 203) and $[NAG+Na]^+$ (m/z 244) were only seldom identified and at extremely low intensities. Both [BMIM]Cl-CHCA and [EMIM]Cl-CHCA also showed distinguishable peaks at m/z 365 corresponding to $[Suc+Na]^+$, however at lower overall intensities than were achieved using CHCA alone.

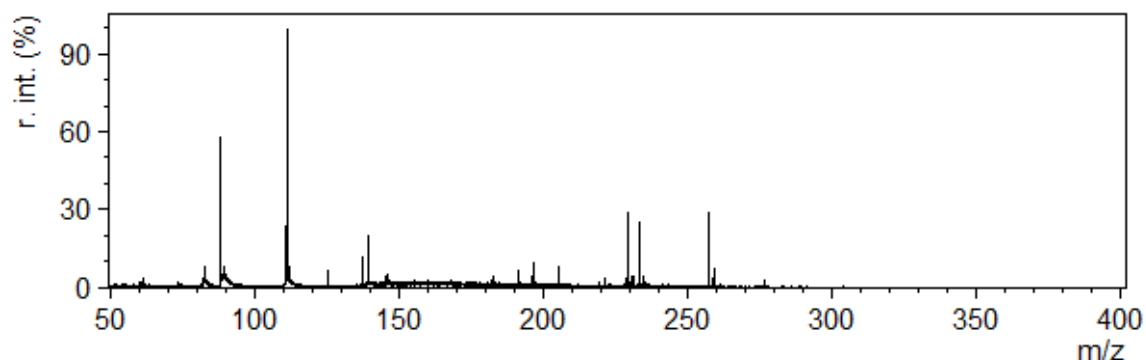


Figure 3-12: MALDI-MS Spectrum of [EMIM][CHCA]

Of the synthesized ILMs, [EMIM][CHCA] exhibited the largest amount of matrix peaks. This matrix also has a very noisy baseline between m/z 125 – 225 (Figure 3-12), which is where sodiated glucose and fructose peaks are expected. Analysis of these analytes did not afford any of the expected sodium adducts. Furthermore, analysis of sucrose also did not show analyte peaks (spectra not shown). Similar to the DHB series IL matrices, neither HMF or levulinic acid were detected using either of the CHCA matrices.

Of the CHCA-based matrices studied, CHCA (without IL) provided better analyte signals for all of the tested analytes. Signals corresponding to glucose, fructose and NAG adducts, however, were of very low intensity. [BMIM]Cl-CHCA and [EMIM]Cl-CHCA appear to suppress the sucrose analyte signal when compared to CHCA alone. To conclude, the synthesized CHCA-based ILMs were not suitable matrices for the analysis of either of the sugar analytes, and were therefore not used for any subsequent analysis.

Interestingly, one of the first ILMs that was developed was very similar to the aforementioned CHCA-IL systems. Armstrong et al. designed the ILM [BMIM][CHCA]

using CHCA and [BMIM]⁺. Similarly, test analytes bradykinin and polyethylene glycol (PEG) were not detected using this matrix. Armstrong concluded that imidazolium-based ILMs were not feasible for MALDI analysis due to poor laser absorption and lack of proton transfer from the imidazolium cation (as compared to quaternary amine salts).^{18,24} Although similar matrices in this study ([EMIM][CHCA] and both IL-CHCA mixtures) also failed to produce analyte signal, the DHB matrices were successful in producing cationized analyte signals. Of course, in this study the protonated analyte is not of interest, but this could signify the usefulness of imidazolium-based ILMs for cationization studies, whereby proton transfer is not required, and the absence of proton transfer may be desirable.

3.6.4 Sample Spot Homogeneity

One of the desired properties of ILMs (and liquid matrices, in general) is that there is a potential to increase spot homogeneity which may lead to better reproducibility in analysis. Solid matrices such as DHB and CHCA limit quantitative MALDI analyses, as both matrices crystallize non-uniformly across the sample well, leading to poor shot-to-shot and spot-to-spot homogeneity. In fact, Armstrong et al. first introduced ILMs as a means of increasing spot homogeneity, as liquids are inherently more uniform.¹⁸

To demonstrate this, images of DHB and DHB-containing ILMs in this study were obtained by scanning electron microscopy (SEM). Upon solvent evaporation, DHB crystallizes forming irregular “needles” along the edge of the spot. The samples containing ILs, however, appear as uniform glassy liquids (refer to Figure 3-3). However, MALDI analyses of these samples exhibited noticeable hot spots. From spot to spot there

was a strong variation in the intensity of the analyte peak. Additionally, multiple analyses of a single sample spot did not always afford analyte peaks.

To determine whether the analyte was evenly distributed within the spot, a simple test was performed. In manual laser firing mode, a series of spectra were acquired at different locations within a single spot. Starting at the far left edge, a spectrum was acquired, before moving across the center of the spot and ending at the right edge of the spot. It was apparent that the analyte was much more easily detected along the edge of the sample spot rather than the center. To confirm this, a series of spectra were acquired to directly compare the analyte peak intensity of shots along the edge of the sample well with shots throughout the center of the spot.

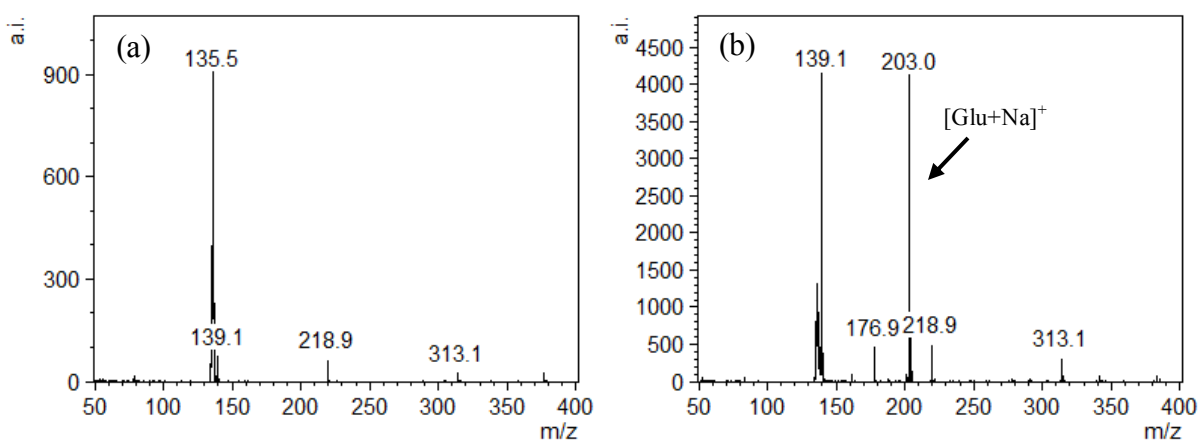


Figure 3-13: Comparison of Spectra Acquired from the (a) Center and (b) Edge of MALDI Spot Containing 1:1:1 DHB:[BMIM]Cl:Glucose

It appears that the analyte was most concentrated at the edges of the sample well, and analyses of the center of the spot seldom yielded appreciable analyte signal (Figure 3-13). Analyses of the center of the spot, however, did often result in IL cation peaks of low

intensity, which suggests that small amounts of matrix acid is present at the center that absorb the laser intensity, or that the IL is simply desorbed from the surface upon irradiation by the laser. Interestingly, these peaks (noted for [EMIM]⁺ ions as well), suffer from poor resolution, lower intensity, as well as poor mass accuracy. Changes in solvent composition and spotting technique were attempted, however, there did not seem to be any improvement. Such phenomena have been previously described, wherein the presence of salts causes separation of the analyte from the bulk matrix to the outer edge of the well, while salts were concentrated within the center.^{21,22} Since a significant component of these samples are ionic in nature, it is not surprising that the crystallization behavior of these samples was affected, causing separation of neutral molecules and ionic compounds due to differences in polarity. Other parameters including the matrix and solvent composition (and hence rate of evaporation) can also effect the segregation of analyte from the matrix and may also play a role in these findings.

This analyte separation was not readily apparent with CHCA or the CHCA-IL matrices (for identifiable analytes such as sucrose). It is well-established that CHCA crystallizes much more homogeneously than DHB, forming crystals over the entire sample spot.²⁵ This suggests that the matrix (even in the presence of IL) may be crystallizing in a similar manner. In the case of DHB, if most of the matrix crystallizes along the edge of the sample spot in the presence of IL (as it does in its absence), there would be minimal matrix throughout the center of the spot. This could explain why few matrix/analyte ions are detected in the center of the spot, as there is insufficient matrix to promote ionization/cationization of the components. Furthermore, the presence of IL likely

suffocates the small amount of matrix that might be present in the center. The low intensity IL ions that are detected, however, can be explained by desorption of the preformed ions (which do not necessarily require the matrix for ionization). Therefore, for all subsequent analysis using DHB (or the IL-containing DHB matrices), a laser pattern (Figure 3-14) was programmed to introduce an edge-biased data acquisition pattern.

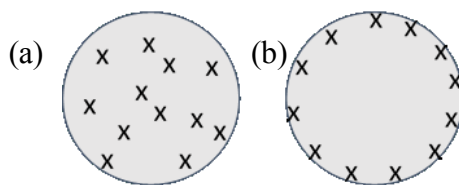


Figure 3-14: Acquisition Patterns Employed in MALDI-MS Analysis: (a) Random and (b) Edge-Biased

By introducing such an acquisition pattern, collecting information from the center of the spot (where analytes are rarely detected) can be avoided, and overall higher average analyte signal intensities can be obtained.

3.6.5 Matrix:IL:Analyte Ratio

All of the previous analyses were conducted at high analyte loadings using a matrix-to-ionic liquid-to-analyte ratio (M:IL:A) of 1:1:1. To enhance signal intensity, other ratios were also employed, by varying the concentration of one or more the components.

Decreasing the analyte concentration (keeping matrix and IL concentrations constant) to yield an overall M:IL:A of 100:100:1 and 10:10:1 were employed, however analysis of these systems seldom yielded analyte signal. It appears that the analyte was

only detectable at very high analyte loading (which is typical for ILM systems).²⁴ Since the IL ions are the most abundant ions in the spectra, it was assumed that the IL caused suppression of the analyte. Therefore, the amount of IL was varied. As previously mentioned, the amount of IL per spot was optimized based on spot integrity. Therefore, a small range of IL concentrations were tested that would not compromise the sample spot. Specifically, IL:M ratios were varied from 1:1 to 2:1 and 1:2 for the chloride-containing ILs. Unfortunately, [BMIM]Cl-DHB did not yield high enough analyte intensities to make a reasonable comparison between each ratio. Therefore, the following data refers to [EMIM]Cl-DHB whereby the ratio of [EMIM]Cl to DHB was varied while the analyte concentration remained constant. Furthermore, [EMIM][DHB] was similarly analyzed to compare the ability of the true ILM and the mixture of IL and matrix. Scatterplots were constructed comparing the signal intensity of the IL cation ($[\text{EMIM}]^+$) and the sodiated analyte signal (Figures 3-15 – 3-18).

For each of the analytes, the highest analyte signal intensity was obtained using a 1:2 ratio of [EMIM]Cl to DHB. It is also notable that this ratio also afforded the largest $[\text{EMIM}]^+$ peak, despite the fact that the 2:1 [EMIM]Cl:DHB matrix contained an excess of IL. This suggests that the presence of excess matrix more easily allows desorption of the IL from the surface. Generally, the overall signal intensity of each analyte was similar using [EMIM][DHB], 2:1 [EMIM]Cl:DHB, or 1:1 [EMIM]Cl:DHB, with the 1:2 [EMIM]Cl:DHB yielding higher analyte signals most of the time. Furthermore, there is a significant spread of data within each sample set (as data was collected as the absolute intensity, rather than a peak height ratio).

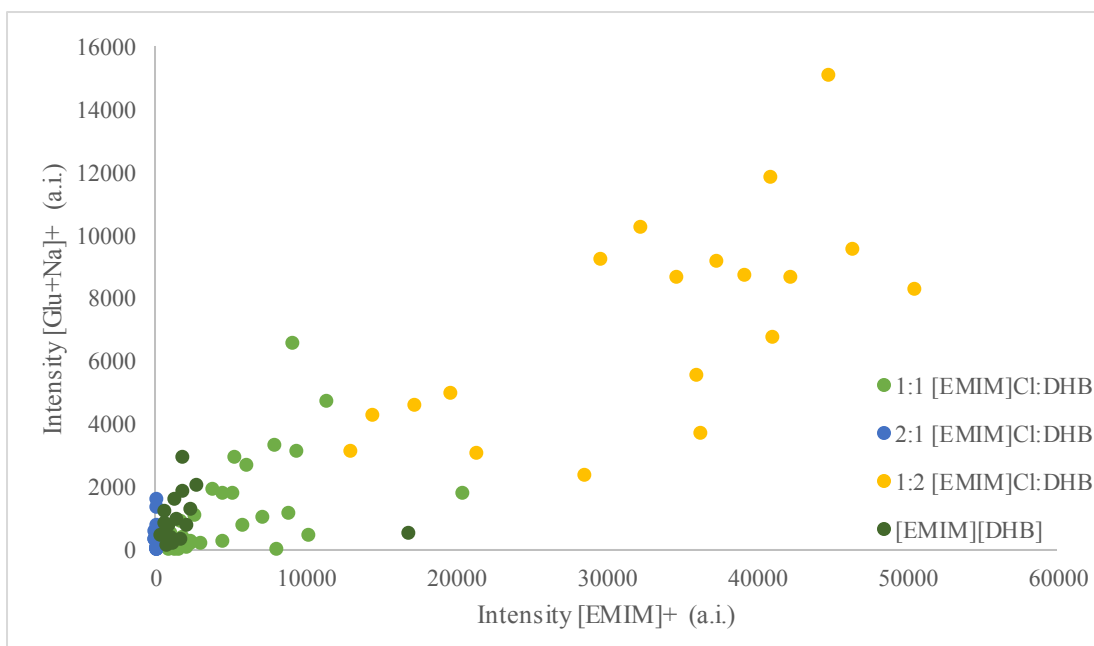


Figure 3-15: Scatterplot of Glucose and [EMIM]⁺ Signals with Varying [EMIM]Cl:DHB Ratio

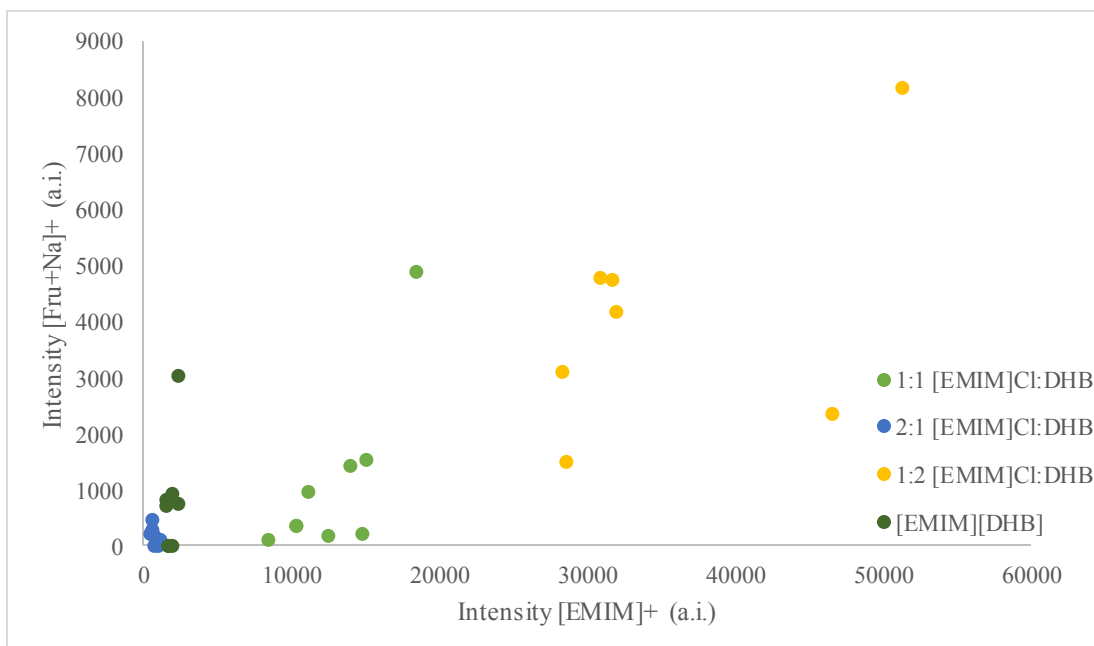


Figure 3-16: Scatterplot of Fructose and [EMIM]⁺ Signals with Varying [EMIM]Cl:DHB Ratio

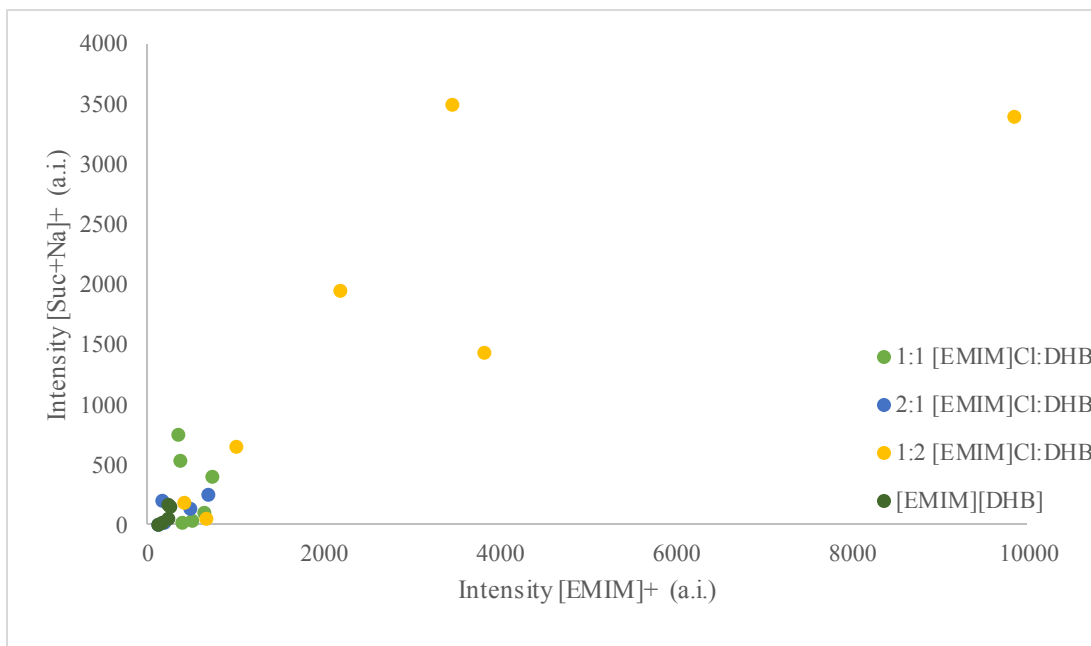


Figure 3-17: Scatterplot of Sucrose and [EMIM]⁺ Signals with Varying [EMIM]Cl:DHB Ratio

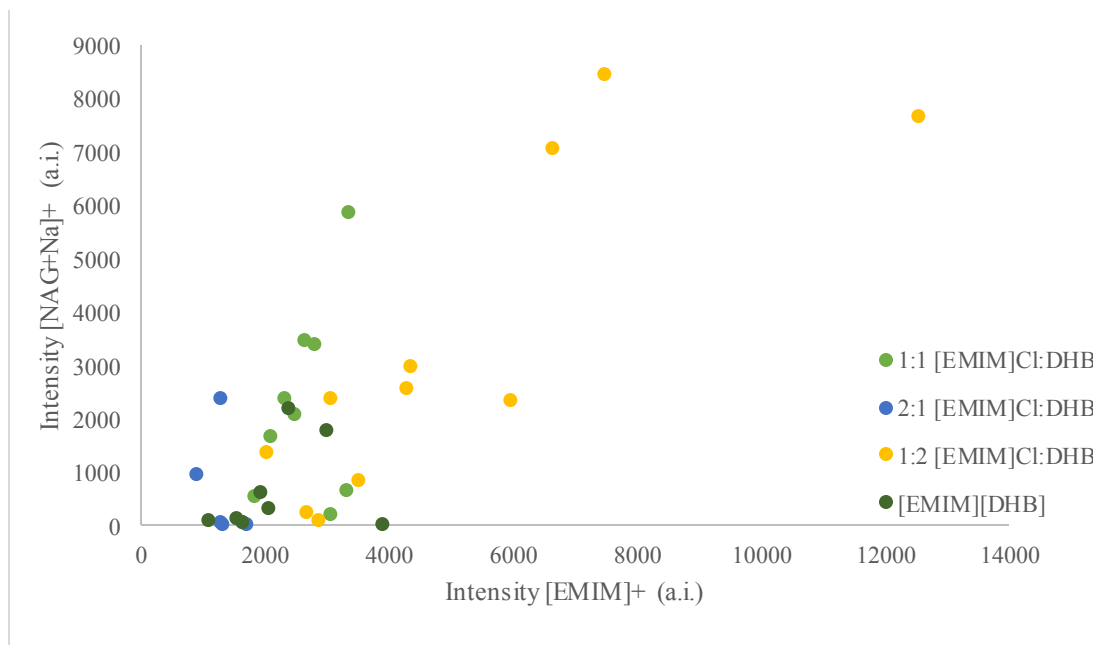


Figure 3-18: Scatterplot of NAG and [EMIM]⁺ Signals with Varying [EMIM]Cl:DHB Ratio

Interestingly, the differing ratios of the tested matrices seems to have a larger effect on the intensity of the $[\text{EMIM}]^+$ cation than on the analyte intensity. As the molar amount of DHB increases, it appears that the amount of IL cation intensity similarly increases. In general, the 1:2 $[\text{EMIM}]\text{Cl}:\text{DHB}$ does yield higher analyte signals than the other tested matrices, but the 1:1 and 2:1 ratios, as well as $[\text{EMIM}][\text{DHB}]$ have similar intensities. It appears that varying the ratio seems to have less of an effect on the analyte signal, and a more pronounced effect on the IL ion signal.

The overall intensity of the $[\text{EMIM}]^+$ peak also appears to be affected by the analyte that is present. Lower overall intensity signals were observed when each matrix was analyzed in the presence of sucrose and NAG, than either glucose or fructose. This was also noted throughout preliminary analyte screening, whereby the overall spectrum intensity was less when analyzing sucrose and NAG.

3.6.6 Matrix/Analyte Suppression

To further investigate the previous findings, studies on matrix and analyte suppression by each of the ILs was studied, using glucose as the test analyte. All of these analyses used a 1:1 ratio of DHB:glucose (containing 50 mM of each matrix and analyte) and the concentration of IL in the spot was varied. For consistency, the laser intensity was held constant, and the resulting absolute intensities of $[\text{DHB}+\text{Na}]^+$, $[\text{Glu}+\text{Na}]^+$ and $[\text{BMIM}]^+ / [\text{EMIM}]^+$ ($n = 5$, error bars represent standard deviation of the mean) were plotted (Figures 3-19 – 3-21) against the IL concentration (expressed as an equivalent of the DHB/glucose concentration).

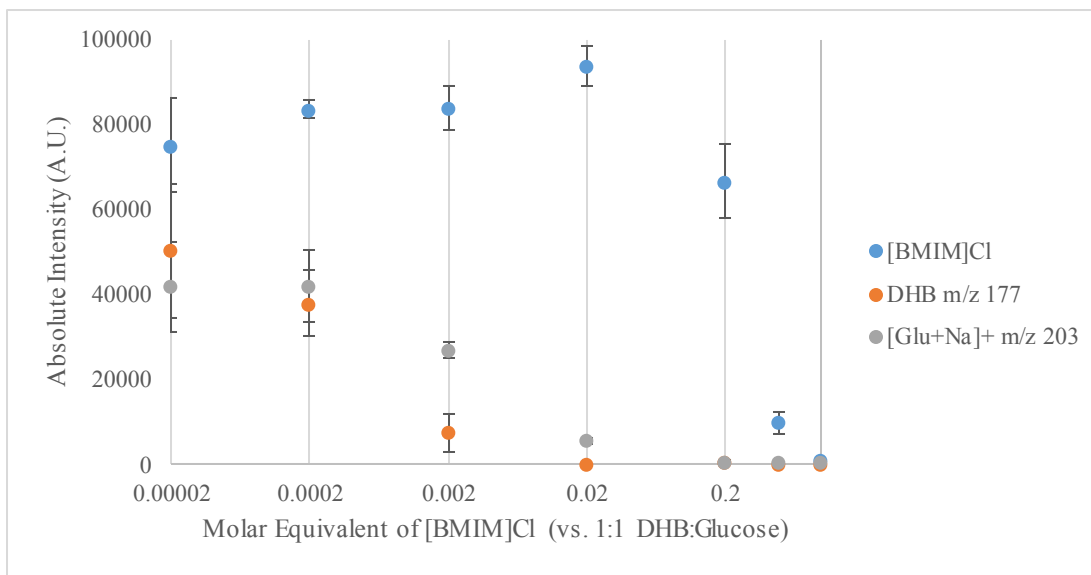


Figure 3-19: Absolute Intensities of DHB, Glucose and [BMIM]⁺ Ions with Increasing [BMIM]Cl Concentration

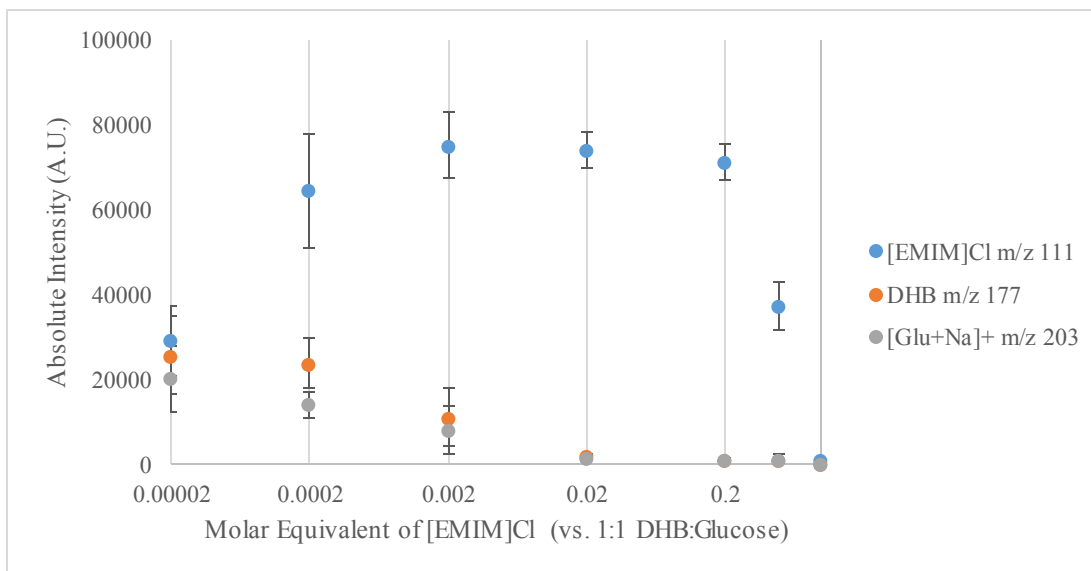


Figure 3-20: Absolute Intensities of DHB, Glucose and [EMIM]⁺ Ions with Increasing [EMIM]Cl Concentration

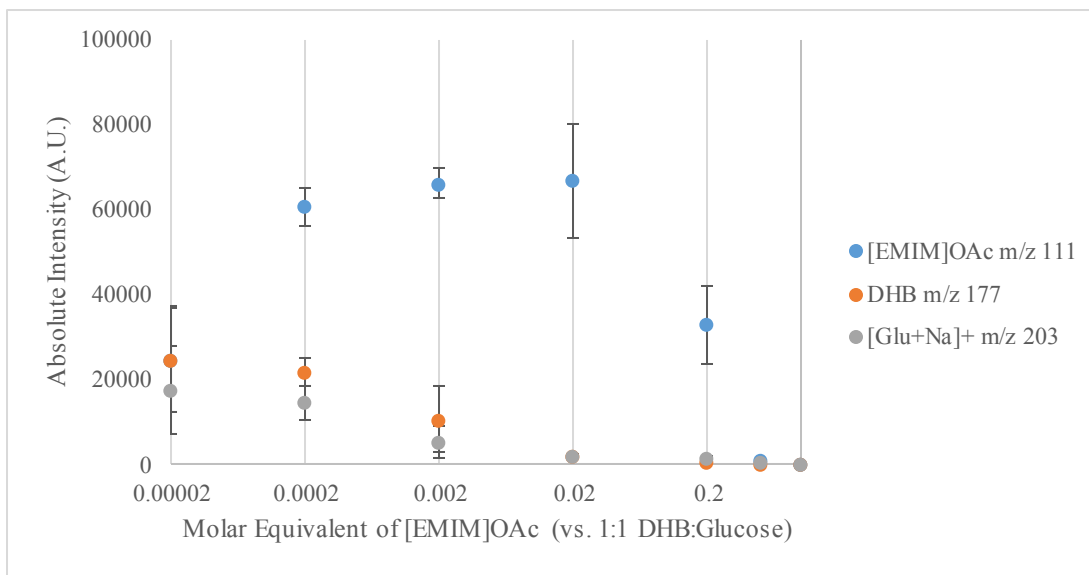


Figure 3-21: Absolute Intensities of DHB, Glucose and [EMIM]⁺ Ions with Increasing [EMIM]Cl Concentration

At even extremely low amounts of IL relative to the matrix and analyte, (i.e. 50000 times lower), the IL cation is still the base peak in all acquired spectra, but matrix peaks, as well as sodiated glucose peaks are readily identifiable. As the amount of IL increases, the IL cation peak eventually levels out indicating saturation of the detector. Meanwhile, the sodiated peaks of glucose and DHB steadily decrease in all cases. When the IL reaches saturation, both matrix and analyte peaks are minute in comparison. Upon reaching the previously optimized concentration of IL per sample spot (50 mM, 1 molar equivalent), all peaks, including the IL peak suffer from very low ion intensities.

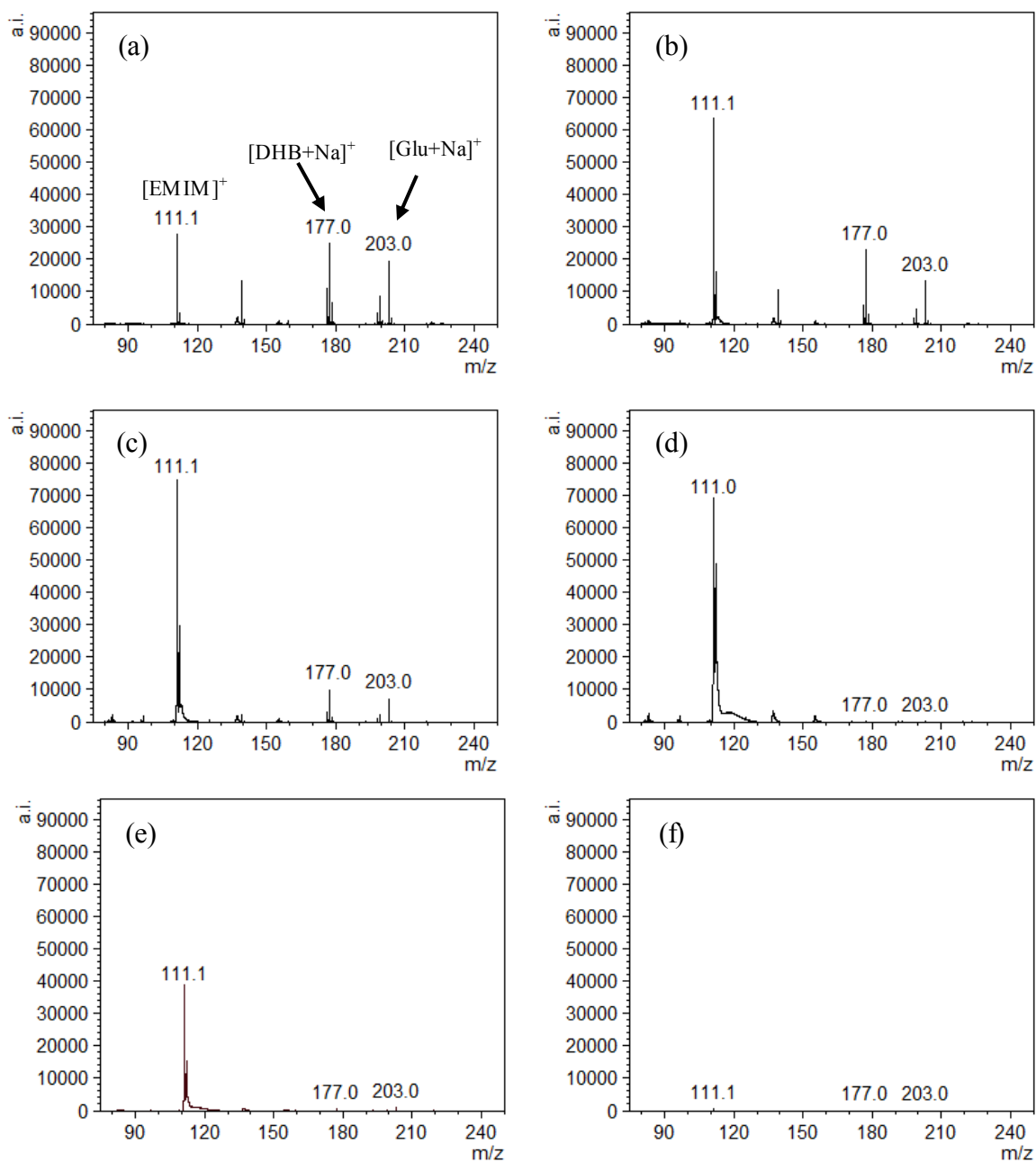


Figure 3-22: MALDI-MS Spectra of Varying DHB:Glucose:[EMIM]Cl Ratios (based on 50 mM DHB and 50 mM Glucose + NaCl Dopant): (a) 50,000:50,000:1; (b) 5000:5000:1; (c) 500:500:1; (d) 5:5:1; (e) 2:2:1; (f) 1:1:1

Matrix and analyte suppression effects (MSE and ASE, respectively) are commonly observed in the analysis of small molecule classes. This leads to less matrix interference peaks, but also to low abundances of analyte signal. Suppression of a particular type of compound due to the presence of another can be explained by secondary gas-phase reactions (i.e. proton, electron or cation transfer). For example, matrix ions can be suppressed by an analyte (if enough analyte is present) if secondary reactions of the matrix with the analyte are favorable (i.e. the charge is placed on the more favored species).²⁶ Similarly, ASE are observed when the presence of one analyte suppresses another, due to differences in ionization efficiency (i.e. analytes which are more easily ionized will suppress those that are less easily ionized). In this study, however, the IL component is a pre-charged species in the sample, and therefore is not formed by secondary gas-phase reactions, and cannot be explained using the previous model. Similar MSE and ASE observations have been made, however, when employing quaternary ammonium salts (QASs).²⁶ Much like ILs, QASs are pre-formed ions which simply require desorption from the substrate to be detected via MALDI-MS. In a previous study by Lou et al., such MSE were observed even at matrix:QAS ratios of 1000:1. The apparent suppression by QASs were explained using the cluster ionization model.²⁷ This model suggests that the final ions observed in a MALDI experiment are the result of desolvation of a cluster of ions (containing matrix, analyte, residues). There are a limited number of charges in a particular cluster, and those species that have the greatest stability (with respect to the MALDI instrumentation and process) upon obtaining charge are those that prevail. A similar model can be used to explain the MSE and ASE of DHB and glucose that are observed in the presence of ILs. It is important to note that the ions

observed in a particular spectrum are the result of a combination of ionization models, and all ions cannot often be explained using one model.¹⁴

Similar to findings of Lou et al., even small amounts of IL have a significant deleterious effect on matrix and analyte ions (Figure 3-22). It is interesting to note that at extremely low IL loading (i.e. Figure 3-22 (a)) the sodiated DHB and glucose peaks are readily apparent, yet all other matrix adducts are suppressed. This suggests that the IL has a much stronger MSE effect on protonated peaks than the sodiated peaks. In this case, a small amount of IL added to the sample is advantageous, as matrix interferences are effectively removed.

It was previously mentioned that low ion intensities of IL resulted when spectra were acquired at the center of the sample spot (with or without matrix). It was speculated that little of the DHB crystallizes in the center, and the sample in the center of the well is mainly IL. This would also suggest that a selective desorption process is occurring, whereby the pre-ionized IL cation is simply desorbed from the surface by a thermal process. The similarities of the spectra obtained in this study, suggest that the IL may effectively be smothering the matrix, and again, a desorption mechanism is mainly responsible for the resulting ion signal. Either way, it is clear through these findings, that even at high analyte loading, the presence of IL is a major limiting factor in the ion abundance. It is apparent that quantitation of these analytes will be difficult.

Also notable, is that the $[\text{Glu}+\text{Na}]^+$ signal is higher than the $[\text{DHB}+\text{Na}]^+$ signal as the concentration of IL increases for $[\text{BMIM}]\text{Cl}$, and not for either of the $[\text{EMIM}]^+$ -containing ILs. The overall intensity of the analyte peak (at constant laser intensity) is

also higher at comparable concentrations in the presence of [BMIM]Cl than [EMIM]Cl and [EMIM]OAc. This may suggest more significant analyte suppression by the [EMIM]⁺ cation than the [BMIM]⁺. Finally, the overall quality of the spectrum is compromised at high IL concentrations. Peak broadening and poor resolution result at high IL loading, along with suppressed analyte peaks. This becomes problematic for potential quantitative analyses under these conditions.

3.7 Conclusions

To conclude, mixtures of imidazolium ILs with the traditional MALDI matrix DHB were very useful for the qualitative detection of small sugars glucose, fructose, sucrose, and NAG. The formation of a true ILM (new ion-pair) does not appear to be necessary for analyte ionization, and in fact suffers from increased matrix suppression as compared to chloride-containing ionic liquid-matrix mixtures. Analogous matrices containing CHCA did not result in appreciable analyte signals under similar conditions. Through trial and error, several parameters including the solvent system, cationization agent, IL concentration and M:IL:A ratios were tested and optimized. Unfortunately, these systems were not useful for the detection of HMF and levulinic acid, likely due to their relative volatilities. As is typical with ILM systems, high analyte loadings were required to yield appreciable analyte signals in the presence of the pre-ionized IL cation. It appears that this is due to matrix and analyte suppression by the IL. Although the suppression of matrix components is desirable for qualitative analyte screening, analyte suppression limits the proposed methods to high analyte concentrations. This restricts

quantitative analyses, as lower concentrations of analyte could not be reliably detected in the presence of the ILs.

Overall, the addition of ILs such as [BMIM]Cl, [EMIM]Cl and [EMIM]OAc can be employed to lessen matrix peaks for qualitative analysis of small sugar analytes. For the purposes of reaction monitoring, however, this method will likely suffer from poor limits of detection and reproducibility. Further investigation into the uses of these IL-matrix systems will be presented in the following chapters.

References

1. Lee, S.; Speight, J. G.; Loyalka, S. K., Eds. *Handbook of Alternative Fuel Technologies*. CRC: Boca Raton, FL, 2007.
2. Bochek, A. M.; Murav'ev, A. A.; Novoselov, N. P.; Zaborski, M.; Zabivalova, N. M.; Petrova, V. A.; Vlasova, E. N.; Volchek, B. Z.; Lavrent'ev, V. K. *Russ. J. Appl. Chem.* **2012**, *85*, 1718-1725.
3. Swatloski, R. P.; Spear, S. K.; Holbrey, J. D.; Rogers, R. D. *J. Am. Chem. Soc.* **2002**, *124*, 4974-4975.
4. Kerton, F. M.; Marriott, R. *Alternative Solvents for Green Chemistry*, 2nd ed. RSC Publishing: Cambridge, UK, 2013.
5. Welton, T. *Chem. Rev.* **1999**, *99*, 2071-2083.
6. Zhang, Z. C. *WIREs Energy Environ.* **2013**, doi: 10.1002/wene.67
7. Wang, H.; Gurau, G.; Rogers, R. D. *Chem. Soc. Rev.* **2012**, *41*, 1519-1537.
8. Zakrzewska, M. E.; Bogel-Lukasik, E.; Bogel-Lukasik, R. *Chem. Rev.* **2011**, *111*, 397-417.
9. Li, C.; Zhang, Z.; Zhao, Z. K. *Tetrahedron Lett.* **2009**, *50*, 5403-5405.
10. Zhao, H.; Holladay, J. E.; Brown, H.; Zhang, Z. C. *Science* **2007**, *316*, 1597-1600.
11. Murzin, D.; Holmbom, E. Analytical Approaches in Biomass Catalysis. In *Catalysis for the Conversion of Biomass and its Derivatives*; Behrens, M., Datye, A. K., Eds.; epubli: Germany, 2013, pp 183-212.
12. Tanaka, K.; Waki, H.; Ido, Y.; Akita, S.; Yoshida, Y.; Yoshida, T. *Rapid Commun. Mass Spectrom.* **1988**, *2*, 151-153.
13. Karas, M.; Bachmann, D.; Hillenkamp, F. *Anal. Chem.* **1985**, *57*, 2935-2939.
14. Zenobi, R.; Knochenmuss, R. *Mass Spectrom. Rev.* **1998**, *17*, 337-366.

15. Tholey, A.; Heinzle, E. *Anal. Bioanal. Chem.* **2006**, 386, 24-37.
16. Cohen, L.; Go, E. P.; Siuzdak, G. Small Molecule Desorption/Ionization Mass Analysis. In *MALDI MS: A Practical Guide to Instrumentation, Methods and Applications*; Hillencamp, F., Peter-Katalinic, J., Eds.; Wiley-VCH Verlag GmbH: Weinheim, 2007; pp 299-337.
17. Harvey, D. J. *Mass Spectrom. Rev.* **1999**, 18, 349-451.
18. Armstrong, D. W.; Zhang, L.; He, L.; Gross, M. L. *Anal. Chem.* **2001**, 73, 3679-3686.
19. Yang, H.; Lee, A.; Lee, M.; Kim, W.; Kim, J. *Bull. Korean Chem. Soc.* **2010**, 31, 35-40.
20. Wang, B.; Feng, H.; Ezeji, T.; Blaschek, H. *Chem. Eng. Technol.* **2008**, 31, 1869-1874.
21. Li, L., Ed.; In *MALDI Mass Spectrometry for Synthetic Polymers*; John Wiley & Sons: New Jersey, 2009.
22. von Hagen, J. *Proteomics Sample Preparation*; John Wiley & Sons: Weinheim, 2011.
23. Yang, H.; Park, K. H.; Kim, H. S.; Kim, J. *J. Am. Soc. Mass Spectrom.* **2010**, 21, 2000-2004.
24. Zabet-Moghaddam, M.; Heinzle, E.; Tholey, A. *Rapid Communications in Mass Spectrometry* **2004**, 18, 141-148.
25. Laugesen, S.; Roepstorff, P. *J. Am. Soc. Mass Spectrom.* **2003**, 14, 992-1002.
26. Lou, X.; van Dongen, J. L. J.; Vekemans, J. A. J. M.; Meijer, E. W. *Rapid Communications in Mass Spectrometry* **2009**, 23, 3077-3082.
27. Karas, M.; Kruger, R. *Chem. Rev.* **2003**, 103, 427-440.

Chapter 4: Derivatization of Bio-Derived Platform Chemicals in Ionic Liquids for Quantitative MALDI-TOF MS Analysis

4.1 Introduction

ILs are very useful solvents for biomass transformation reactions, as they are non-volatile, have great dissolution ability, and can be modified to exhibit desirable properties.¹ In applications whereby an IL is used as a solvent, the IL is generally in excess of the analytes by a factor of 10 – 1000 times. Despite the many advantages of ILs over traditional volatile organic compounds, unlike VOCs, ILs are often difficult and energy-intensive to remove from chemical systems. This can lead to potential incompatibilities with traditional means of analytical separation and detection. Therefore, it is ideal to develop analytical methods that are capable of *in situ* monitoring. The ability to analyze reaction mixtures without prior separation of the IL leads to significant cost and time savings.

MALDI-MS is an attractive alternative to traditional chromatographic analyses as sample preparation and data acquisition are rapid, and consume very little sample. Unfortunately, as demonstrated in Chapter 3 of this thesis, the presence of ILs leads to significant analyte suppression in MALDI-TOF MS analyses. It is speculated that the ease of desorption of a pre-formed ion (i.e. the IL ion) from the MALDI substrate, along with the poor ionization behavior of sugars are responsible for these observations. Therefore, this chapter investigates the use of chemical modification (i.e. derivatization)

of the analytes of interest by introducing a cationic center into the analyte to compete with the IL for desorption/ionization during the MALDI process. Further work describes quantitative analysis of sugars and small platform chemicals in IL solutions and applications of the proposed methods to real systems.

4.2 Materials

D-(+)-Glucose ($\geq 99.5\%$), D-(-)-fructose ($\geq 99.9\%$), sucrose ($\geq 99.5\%$), 2,5-dihydroxybenzoic acid (DHB) (98 %), α -cyano-4-hydroxycinnamic acid (CHCA) ($\geq 98\%$), glycidyltrimethylammonium chloride (GTMA) ($\geq 90\%$), L-ascorbic acid and 1-ethyl-3-methylimidazolium chloride ([EMIM]Cl) (98 %) were obtained from Sigma-Aldrich (St. Louis, MO). The 1-butyl-3-methylimidazolium chloride ([BMIM]Cl) (96 %) was purchased from Alfa Aesar (Ward Hill, MA), and 1-ethyl-3-methylimidazolium acetate ([EMIM]OAc) ($> 95\%$) was purchased from Io-Li-Tec (Tuscaloosa, AL). 5-hydroxymethylfurfural (HMF) (98 %) and *N*-acetyl-D-glucosamine (NAG) (98 %) were obtained from AK Scientific (Union City, CA). Sodium hydroxide pellets (97 %) were obtained from Caledon Laboratories (Georgetown, ON). Levulinic acid (98 %), (\pm)- β -hydroxy- γ -butyrolactone (96 %), benzyl alcohol (99 %) and chromium (III) chloride hexahydrate (98 %) were purchased from Alfa Aesar (Shore Road, Heysham, Lancs.). Isotopically-labeled glucose- d_7 (97 – 98 %), dimethyl sulfoxide- d_6 (99.9 % + 0.05 % TMS v/v) and deuterated water (99.9 %) were all purchased from Cambridge Isotopes (Andover, MA). Water, methanol and acetonitrile (HPLC grade, 99.9 %) were obtained

from Fisher Scientific (Fair Lawn, NJ). All chemicals were used without further purification.

4.3 Instrumentation

4.3.1 MALDI-TOF MS

Mass spectrometric analyses were carried out using an Applied Biosystems MDS SCIEX 4800 MALDI TOF/TOF mass spectrometer equipped with a 355-nm Nd:YAG laser (200 Hz). Ions were accelerated into the mass analyzer at an accelerating voltage of 1.796 kV. Spectra were acquired in positive reflectron ion mode, resulting from 16 sub-spectra comprised of an average of 25 laser shots or a total of 400 sub-spectra. Laser intensity was varied per sample as appropriate. Data was exported to mMass (open source software) for processing.

Data was collected using a laser acquisition pattern with an edge-bias (as described in Chapter 3). At the beginning of a sample set, practice shots were taken to ensure adequate analyte signal. If the analyte signal was weak, the MALDI plate was re-aligned as necessary. Before samples were spotted onto the plate, the plate was wiped with methanol. This seemed to promote the formation of better quality sample spots (less spreading of spots across the plate). For quantitative analyses, test spots were used to obtain an appropriate S/N ratio of the analyte of interest, and these parameters (specifically, plate alignment) were used to acquire further spectra. For quantitative analyses, acceptance criteria were used to select for appropriate data points for calibration. Normally, 5 replicate analyses were used and the mean response plotted vs.

concentration/mass. During data acquisition, normally > 5 replicates were acquired but only those which generated an internal standard response with a S/N ratio > 10 were used in the construction of calibration curves. In cases where > 5 analyses met this criteria, the first 5 replicates were used to generate the mean response to limit personal bias.

4.3.2 ^1H NMR Spectroscopy

^1H NMR spectra were acquired at room temperature using a Bruker AVANCE III 300 MHz NMR spectrometer. Chemical shifts are reported in parts per million (ppm) from the TMS reference peak. Data was analyzed using MestreNova Version 9.0.1.

4.4 Methods

4.4.1 MALDI-TOF MS Sample Preparation

Aqueous 200 mM stock solutions of each IL and analyte were prepared in 2:1 methanol:water (v:v). Analyte solutions were further diluted to yield working solutions of 100 mM, 75 mM, 50 mM, 25 mM, 10 mM, 5 mM and 1 mM. 100 mM DHB solution and 100 mM NaCl solution were similarly prepared by dissolution in 2:1 methanol:water (v:v). The 100 mM stock solution of NaCl was further diluted to yield a 10 mM solution. Equal volumes of IL and analyte solutions were mixed to yield 100 mM IL containing varying amounts of analyte. Equal volumes (typically 200 μL) of the DHB solution and the IL/analyte solution were mixed to afford a solution containing 50 mM DHB, 50 mM IL and corresponding concentration of analyte. The solutions were thoroughly mixed before 1 μL aliquots were spotted onto a stainless steel MALDI plate and allowed to dry

completely. Finally, 1 μL of 10 mM NaCl solution was spotted on top of each sample and the spots were allowed to dry before inserting into the mass spectrometer.

4.4.2 Standard Preparation for Derivatization Studies

Stock solutions (200 mM) of glucose, fructose, sucrose, *N*-acetyl-D-glucosamine (NAG), 5-hydroxymethylfurfural (HMF) and levulinic acid were prepared in HPLC grade H_2O . Serial dilutions of the stock solution yielded working standards of 100 mM, 75 mM, 50 mM, 25 mM, 10 mM, 5 mM, and 1 mM. Similarly, 420 mM glucose- d_7 solution and 210 mM benzyl alcohol (BnOH) were prepared by dissolution in HPLC grade H_2O . 1 M stock solutions of [BMIM]Cl, [EMIM]Cl, and [EMIM]OAc were prepared in HPLC grade H_2O and further diluted to yield 0.5 M solutions. HPLC grade H_2O was used as the method blank.

4.4.3 Derivatization of Analyte Standards

To 2-mL vials, 250 μL of solvent (H_2O or 0.5 M aqueous IL solution), 250 μL of analyte solution (or blank), 20 μL of glucose- d_7 (420 mM) or 40 μL of BnOH (210 mM), 25 μL of 1 M NaOH, and 3.5 μL glycidyltrimethylammonium chloride (GTMA) solution were added. The vials were capped and inverted before being suspended in a hot water bath at 55 $^{\circ}\text{C}$ for 2 h. Finally, vials were removed from heat, thoroughly mixed, and allowed to cool to room temperature.

4.4.4 Reaction Conditions for Dehydration Reaction of Sugar to HMF

Approximately 500 mg of IL was weighed into a 2-mL vial, followed by approximately 50 mg of starting material (fructose). Where applicable, 6 mol % of $\text{CrCl}_3 \cdot 6\text{H}_2\text{O}$ catalyst was added and the vial heated and stirred using a magnetic stir bar for ~10 min to allow dissolution of all reaction components. Vials were suspended and heated in a hot water bath (80 °C) for the specified time.

4.4.5 Derivatization of Reaction Aliquots

At timed intervals, small amounts (~50 mg) of the reaction mixture were transferred to a pre-weighed 2-mL vial. A known amount of water was added to afford a 0.5 M solution based on the estimated mass fraction of IL in the removed sample. This solution was stored in the refrigerator at 4 °C until all remaining aliquots were collected. A 400 μL aliquot of the prepared 0.5 M IL (reaction aliquot) solution was transferred to a vial containing 20 μL 210 mM BnOH, 40 μL 420 mM glucose- d_7 , 25 μL NaOH, and 3.5 μL GTMA. The resulting solution was inverted and heated in a hot water bath at 55 °C for 2 h (as in Section 4.3.3).

4.4.6 MALDI-MS Sample Preparation of Derivatized Samples

To 2-mL vials, 450 μL of H_2O and 500 μL of 100 mM methanolic DHB solution were added. A 50 μL aliquot of the derivatized standards (Section 4.3.3) or 0.5 M IL reaction aliquot of the derivatized reaction mixture (Section 4.3.5) was added to the above solution. The final solution containing 50 mM DHB, was inverted several times, and 1 μL

volumes were deposited onto a stainless steel MALDI plate. Spots were allowed to dry at room temperature (~20 min) before being introduced into the instrument sample chamber.

4.5 Results and Discussion

4.5.1 Sugar Quantitation by MALDI-TOF MS

In a model dehydration reaction of glucose to HMF in IL, glucose is present at approximately 10 times less than the IL solvent. As the reaction proceeds, the glucose will decrease as it is converted to HMF, while the concentration of HMF increases. Upon reaction completion, the concentration of glucose, for example, may be between 10 – 1000 times less than the IL (i.e. 0 – 99 % conversion). Therefore, it is desirable to design analytical methods with wide dynamic ranges that can detect the target analytes in the presence of an excess of IL. Previous quantitative and semi-quantitative analysis of glucose by MALDI-MS have been reported with varying degrees of sensitivity depending on experimental parameters and matrices.²⁻⁴ However, at the current time, quantitative glucose analysis by MALDI-MS in imidazolium-based IL media has not been reported.

The LODs of target sugar analytes glucose, fructose, sucrose and NAG were determined using DHB as the matrix, in the absence of IL to determine instrument detection limits, assuming these conditions result in optimum ion intensities. In all cases, the sodium adduct of the sugar was selected as the quantitative ion. The analyte response ratios with respect to glucose-d₇ (internal standard) were plotted against the mass of analyte per sample spot to construct calibration curves. Due to the high variability of noise in the blank (and the significant differences in spectra that were obtained when the

analyte was present), the LOD and LOQ were calculated based on the standard error of the curve ($S_{y/x}$) using Equations 4-1 and 4-2.

$$LOD = 3 \times \frac{S_{y/x}}{m} \quad \text{Equation 4-1}$$

$$LOQ = 10 \times \frac{S_{y/x}}{m} \quad \text{Equation 4-2}$$

The resulting LODs and LOQs were compared to the average S/N ratios of the analyte at the nearest corresponding concentrations and all agreed with accepted criteria (i.e. LOD and LOQ correspond to S/N ~ 3 and ~ 10 , respectively). In the absence of IL, each of the target sugars could be detected at the low ng-level with varying sensitivities (Table 4-1) and are similar to previously published MALDI-MS methods.²⁻⁴ As mentioned in Chapter 3, neither HMF nor levulinic acid could be detected, even at relatively high concentrations per spot (i.e. μg -level).

Table 4-1: Calibration Data for Selected Sugar Analytes as Analyzed by MALDI-TOF MS using DHB Matrix

Analyte	LOD (ng analyte/spot)	LOQ (ng analyte/spot)	R ²	Slope (<i>m</i>)
Glucose	0.9	3.1	0.9983	0.0501
Fructose	0.7	2.4	0.9989	0.0992
Sucrose	0.9	2.9	0.9922	0.4540
NAG	0.3	0.9	0.9996	0.3664

As mentioned, in this study, the LODs were calculated by taking into consideration the standard error of the curve. The calculated LODs and LOQs agreed well with experimental values of standards of the same concentration (i.e. S/N ~ 3 and S/N ~ 10). Therefore, despite the apparent higher sensitivity of this method to sucrose, the LOD of sucrose was similar to that of glucose due to the greater error associated with the regression (see Table A5-1 in Appendix V). The smaller sugars exhibited similar errors of the standard curves and the LODs can be more reasonably compared. NAG exhibited the lowest LOD and LOQ, followed by fructose, then glucose.

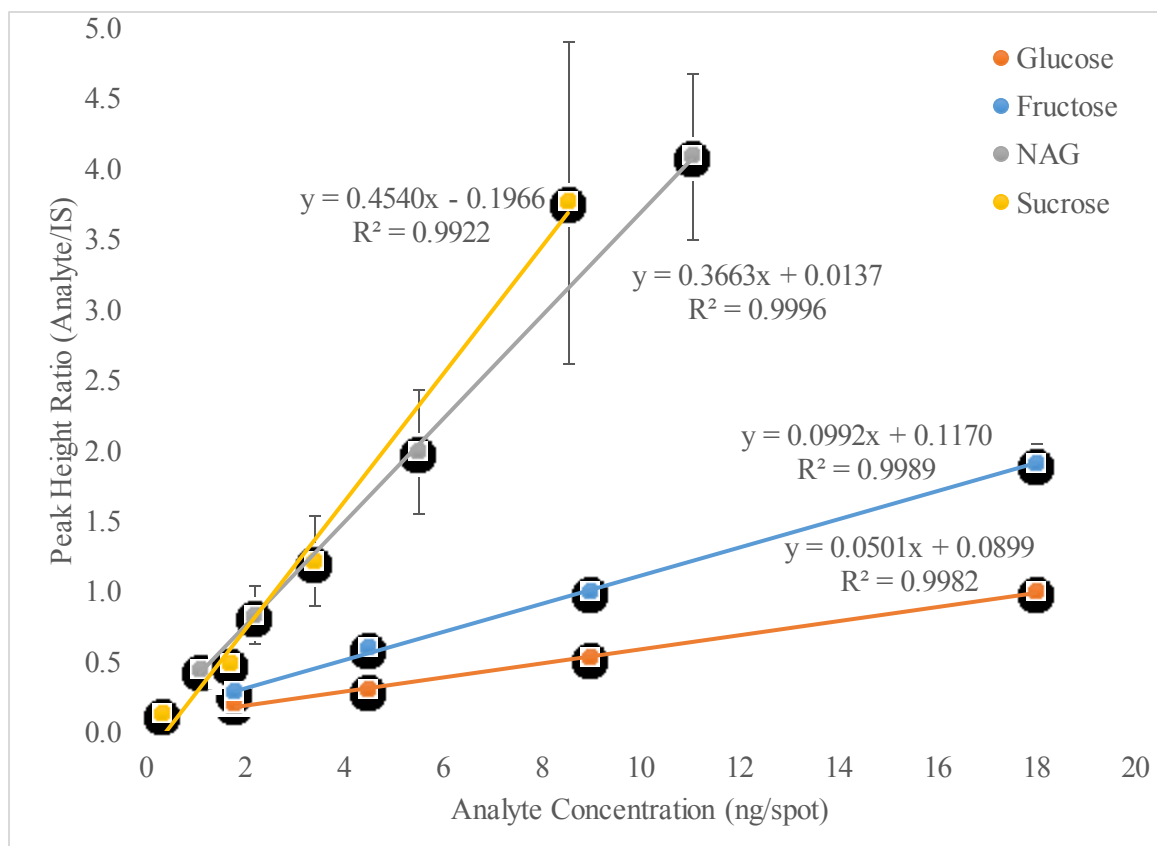


Figure 4-1: Calibration Curve of Selected Sugars Analyzed by MALDI-MS using DHB Matrix (Error bars represent standard deviation of the mean, n = 5)

From the constructed calibration curves, it is apparent that sucrose and NAG are detected at higher sensitivities ($m = 0.4540$ and 0.3664 , respectively) than both glucose and fructose, but also have notably higher standard deviations (as depicted by error bars on corresponding calibration data points). The associated error within the calibration points can be attributed to differences in ionization efficiency of these sugars as compared to glucose-d₇. As expected, the smallest errors are observed with the glucose and fructose calibrations, as these sugars are of nearly equal mass and size, with similar functionality (i.e. they are isomeric). Sucrose exhibits the highest amount of error, possibly due to the fact that it is a disaccharide, and has more available sites for cationization as compared to the smaller monosaccharides tested in this study. The error associated with each analyte is a reflection of the advantage of using isotopically-labeled internal standards for MALDI analyses.

Since the analytes of interest could be detected at ng-level concentrations, it seems plausible that IL-systems containing similar concentration ranges of analytes are feasible candidates for MALDI-MS analyses. The addition of an excess of IL, however has significant effects on the analyte signals. As was seen in Chapter 3, the ILs in this work resulted in significant matrix and analyte suppression. In fact, analytes could only be reliably detected at high analyte loading (M:IL:A 1:1:1).

To enhance analyte sensitivity in the presence of the IL, the analyte must be able to compete with the IL to become ionized in the plume. To demonstrate this, a quaternary ammonium salt (QAS), triethylammonium chloride ($\text{Et}_3\text{N}\cdot\text{HCl}$) was added to the sample in place of the analyte to examine whether the IL would suppress a preformed ion. The

Et₃N•HCl was added at one-fiftieth concentration of both the ionic liquid and matrix (i.e. M:IL:A 50:50:1).

As can be seen in Figure 4-2, the triethylammonium cation (Et₃NH⁺) can be easily identified at *m/z* 130, along with the [EMIM]⁺ cation (*m/z* 111). In this case, the concentration of Et₃NH⁺ is 50 times lower than typical sugar analyte concentrations that were screened in Chapter 3.

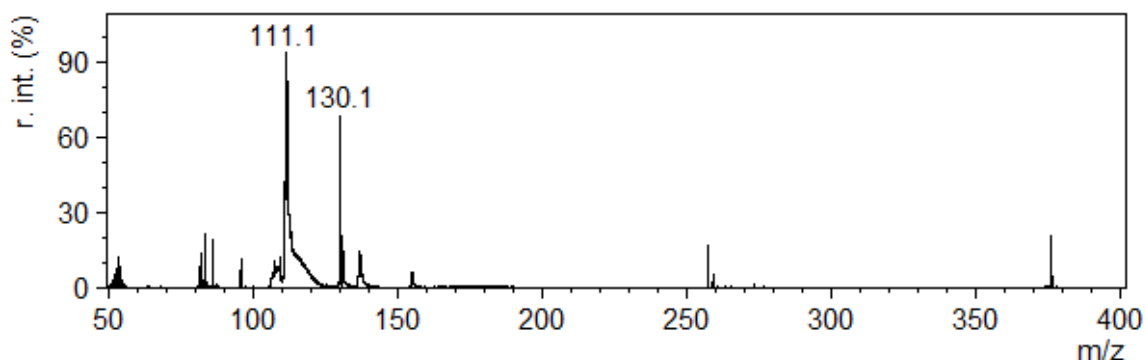


Figure 4-2: MALDI-MS Spectrum of Triethylammonium chloride and [EMIM]Cl with DHB Matrix (M:IL:A = 50:50:1)

The much higher sensitivity observed with Et₃NH⁺ as compared to neutral sugars can be explained by the charge of the species in the sample spot. In the case of the IL cations and QASs such as triethylammonium chloride, the species are already in charged form in solution (as they are a part of an ion pair), and therefore likely require little assistance from the matrix to achieve ionization. The ionization of neutral sugars, specifically glucose, fructose and sucrose, as demonstrated previously, is often difficult to achieve by MALDI-MS. In general, these sugars have low proton affinities, and require the addition of a cationization agent (e.g. NaCl, or KCl).^{3,5} Unfortunately, cationization is

often hard to control and shows relatively low efficiencies. Furthermore, in the presence of ILs, significant analyte suppression is observed in MALDI-MS analysis. However, resulting MALDI-MS spectra of pre-formed ions (i.e. IL cations and Et_3NH^+) are much more straightforward. Therefore, by introducing a pre-ionized species into the analyte via chemical modification, sensitivity of the method can be drastically improved, by allowing competitive ionization with the IL species. Therefore, derivatization was employed to enhance analyte sensitivity in the presence of the ILs.

4.5.2 Derivatization of Sugar Analytes

There are several derivatizing reagents that can be employed for enhancing sensitivity of neutral carbohydrates in analytical applications.^{6,7} Often, suitable derivatives offer advantages such as increased sensitivity and selectivity as compared to the native analyte. Sugars such as glucose can be chemically modified to include chromophores for optical analyses, to disrupt hydrogen-bonding to promote volatility, or to introduce charged centers for improved mass spectrometric analyses. It was demonstrated that charged species (such as Et_3NH^+) could be much more easily detected in the presence of IL by MALDI-MS than the neutral sugar analytes. Therefore, it was speculated that by introducing a charged center into the analyte structure, analyte sensitivity could be increased to allow quantitative analyses in IL-containing reaction systems by MALDI-MS. Fortunately, such derivatizing reagents currently exist and are commercially available.⁸ Examples include glycidyltrimethylammonium chloride (GTMA) and Girard's reagent T ((carboxymethyl)trimethylammonium chloride hydrazide).

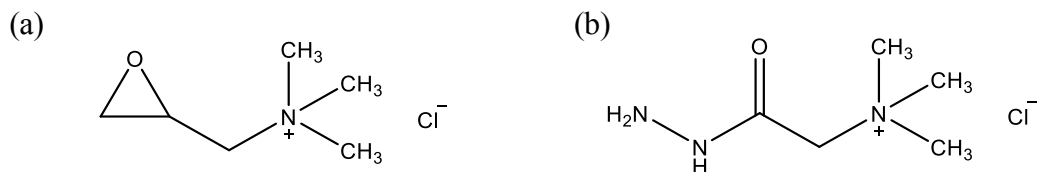


Figure 4-3: Structures of Cationic Derivatizing Reagents for Sugar Modification: (a) GTMA; (b) Girard's reagent T

Such compounds can react with sugars to form larger derivatives containing a cationic center via etherification with GTMA or by hydrazone formation with Girard's reagent T. In fact, both of these compounds have been previously employed specifically for enhancing the sensitivity of carbohydrate analysis by MALDI-MS. The resulting mass spectra can show abundant analyte ions, with increases in sensitivity of up to 2000 times (compared to traditional MALDI-MS of sugars).^{8,9}

Although both of the aforementioned compounds could be employed in this work, GTMA was chosen as the derivatizing reagent due to its reactivity towards hydroxyl groups (as compared to the aldehyde/ketone functional groups). This allows derivatization of both reducing and non-reducing sugars, which is applicable to a variety of biomass transformation studies including sugars, as well as sugar alcohols such as HMF.

The etherification reaction of GTMA with each sugar likely occurs through the primary alcohol group which is less hindered than other hydroxyl groups. Epoxide opening under basic conditions follows an S_N2 -like mechanism, whereby the nucleophile (usually an anion) will attack the less substituted side of the epoxide. Although sugars are very weak acids (with pK_a values close to that of water), the addition of a strong base

such as NaOH can deprotonate the hydroxyl groups to form the corresponding alkoxide. Nucleophilic attack by the deprotonated sugar towards the epoxide results in etherification and introduction of the charged center into the analyte (Figure 4-4).

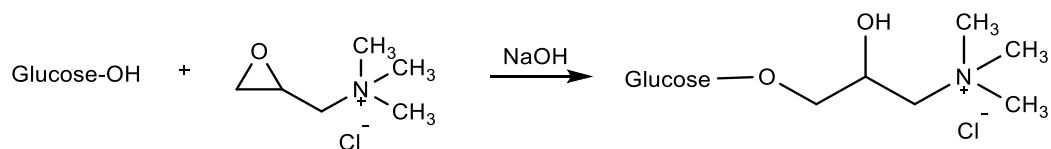


Figure 4-4: Reaction Scheme of Derivatization of Glucose with GTMA

In this work, a similar procedure was carried out for the derivatization as was proposed by Gouw et al.⁸, with some modifications. Firstly, 0.5 M IL (aqueous) solutions containing the analytes of interest were employed, rather than pure aqueous standards. Solutions of ILs were employed, rather than ILs in their natural form, for ease of quantitative transfer. Since IL-analyte mixtures of standards and test samples are generally viscous, solutions of these were prepared based on the amount of IL, and volumetrically transferred.

As previously reported by Gouw et al., the reaction efficiency of this procedure is ~50 % (after 2 h) when carried out in water. The effects of IL on this procedure were studied to determine whether the reaction efficiency is affected. The reactions were monitored by ¹H NMR using D₂O in place of H₂O. The reaction components were added to an NMR tube, and analyzed after the initial addition of GTMA (t = 0) and again upon reaction completion. The glucose conversion after heating at 55 °C for 2 h was determined by the relative integration of selected glucose peaks (marked with * in Figure

4-5) with respect to an IL peak (which is assumed to remain constant throughout the duration of the reaction).

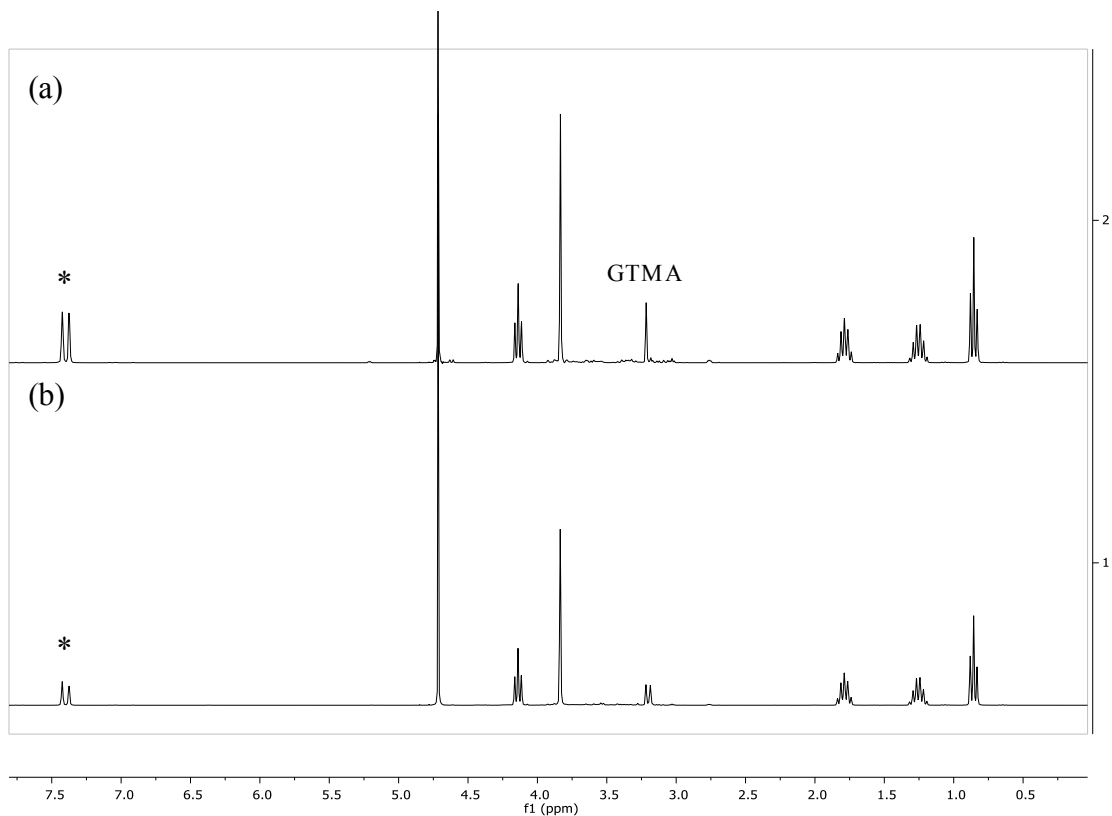


Figure 4-5: ^1H NMR Spectra of Glucose-GTMA Derivatization Reaction in [BMIM]Cl: (a) at $t = 0$, (b) at $t = 2$ h

Although the NMR spectrum of GTMA was not fully characterized (due to abundant, overlapping peaks), specific peaks belonging to GTMA have been identified. The peak at 3.22 ppm which results from GTMA (the *N*-methyl protons) decreases in intensity after the reaction (with respect to the IL peak) and the formation of a new peak at ~ 3.19 ppm was observed. The changes in intensity correspond to $\sim 50\%$ conversion of GTMA, and could represent glucose-GTMA. Note, however, that the glucose conversion was monitored (by observation of glucose peaks labelled *) rather than the yield of

glucose-GTMA. The amount of derivatized sugar was not determined by NMR, as the presence of many overlapping peaks in the relevant region led to difficulties in interpretation. Furthermore, throughout the reaction GTMA can alternatively be attacked by hydroxyl ions in solution leading to the hydrolyzed side-product, which would exhibit similar chemical shifts to glucose-GTMA. The percent conversion of the other analytes was attempted, however, lack of clear peaks for integration rendered this a difficult task. The same reaction was carried out in water, however without an appropriate reference peak, the conversion could not be accurately calculated. The determined percentage of glucose conversion in the ILs is consistent with literature reports of the same reaction in water (~ 50 %).⁸ The seemingly lower conversion of glucose in [EMIM]Cl may be the result of the poor resolution of glucose NMR peaks that were obtained in [EMIM]Cl at t = 0 (data not shown).

Table 4-2: Glucose Conversion by GTMA in Selected Ionic Liquids

Solvent	% Glucose Conversion (n = 1)
0.5 M [BMIM]Cl	48.4
0.5 M [EMIM]Cl	36.9
0.5 M [EMIM]OAc	47.7

4.5.3 Derivatization of Sugar Analytes with GTMA

Although the derivatization of glucose, fructose and sucrose with GTMA has been previously demonstrated,⁸ all test analytes were subjected to the cationization reaction in

the presence of each of the ILs (rather than purely aqueous systems). As expected, each of the sugar analytes react with the GTMA under alkaline conditions, in both water and highly concentrated IL systems. The presence of GTMA-sugar ethers was demonstrated by MALDI-MS, whereby target analytes are present at m/z values of $[M+116]^+$.

Other identified peaks in these mass spectra include unreacted GTMA (m/z 116), and hydrolyzed GTMA (m/z 134). These ions do not directly interfere with analysis, and therefore purification of the reaction solutions was deemed unnecessary. Note that unreacted sugars were not detected in the presence charged IL and GTMA ions.

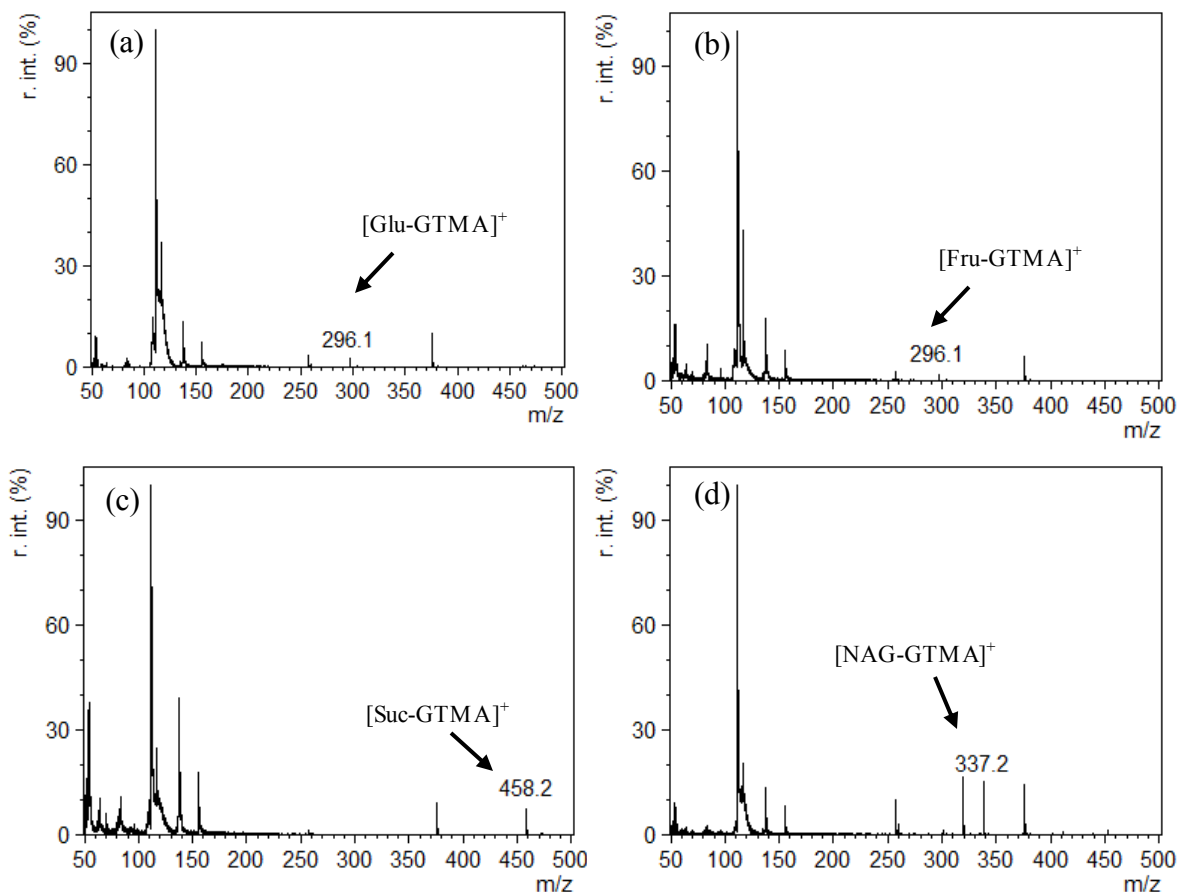


Figure 4-6: MALDI-MS Spectra of Sugar Analytes after Derivatization with GTMA in [EMIM]Cl, M:IL:A = 10:10:1: (a) Glucose-GTMA; (b) Fructose-GTMA; (c) Sucrose-GTMA; (d) NAG-GTMA

Other identified peaks in these mass spectra include unreacted GTMA (m/z 116), and hydrolyzed GTMA (m/z 134). These ions do not directly interfere with analysis, and therefore purification of the reaction solutions was deemed unnecessary. It is notable that unreacted sugars were not detected in the presence of the highly charged IL and GTMA components.

Each of the tested sugar analytes are readily detected in each of the three IL systems studied with no obvious interferences from the matrix components or ILs. In the above spectra, the analyte (as spiked in natural form) is present at 10 times less than the IL. Considering that it is unlikely that all of the sugar has reacted to form sugar-GTMA (as demonstrated with glucose), the presence of these peaks at this IL:A ratio proves to be much more sensitive than without derivatization in IL media. To demonstrate this, a system containing a 10:1 [BMIM]Cl:glucose (molar) ratio was analyzed by MALDI-MS before and after derivatization. As can be seen in Figure 4-7 (a), before derivatization with GTMA, no peak was detected belonging to glucose at m/z 203 (as was previously demonstrated in Chapter 3). However, after derivatization (Figure 4-7 (b)), glucose-GTMA (m/z 296) is readily apparent. This demonstrates that introducing a cation center into the analyte is a feasible means of detecting these analytes at lower concentrations in the presence of IL.

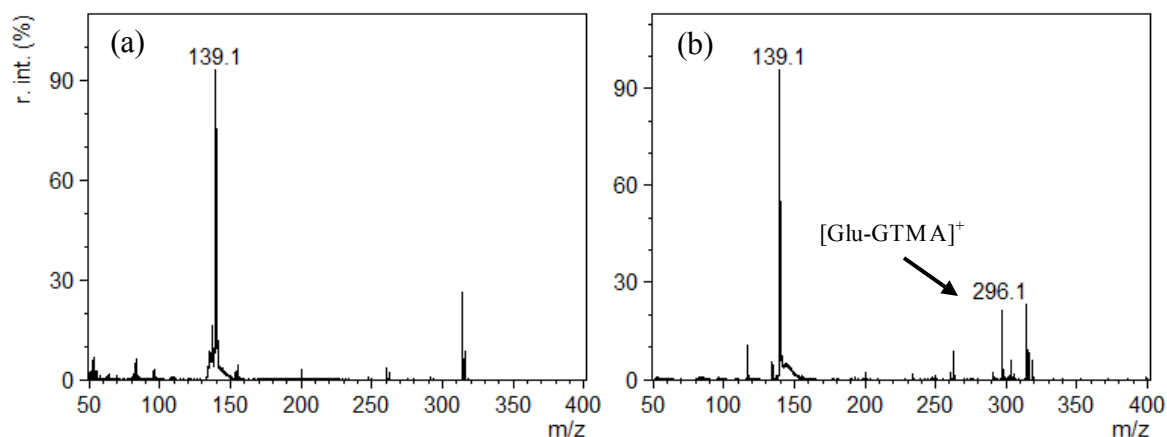


Figure 4-7: MALDI-MS Spectra of 10:1 [BMIM]Cl:Glucose with DHB Matrix (a) Before derivatization with GTMA; (b) After derivatization with GTMA

Further experimentation was conducted using both HMF and levulinic acid analytes. Though these analytes could not be detected by traditional MALDI (with or without IL present), derivatization with GTMA readily affords cationized analyte peaks belonging to each compound (Figure 4-8).

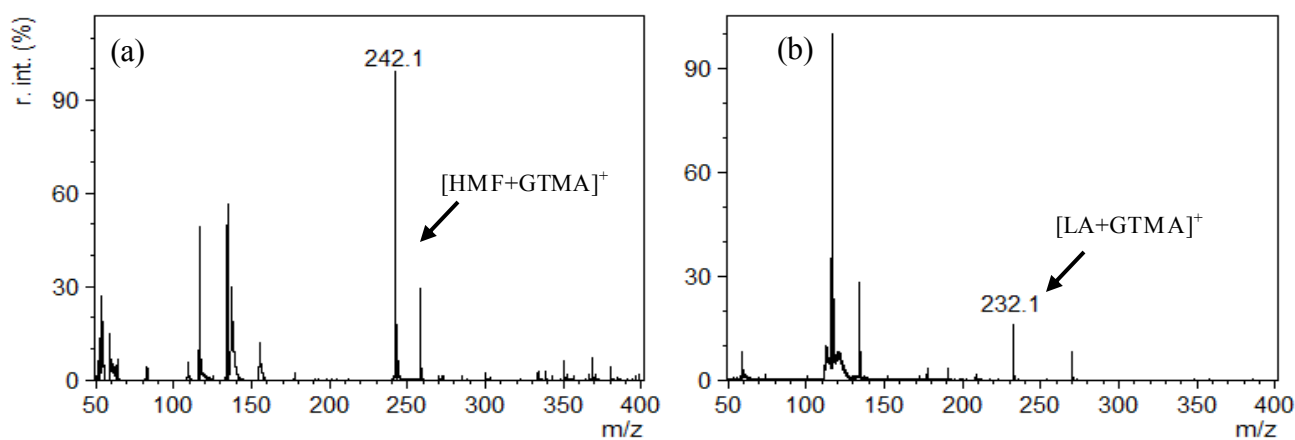


Figure 4-8: MALDI-MS Spectra of (a) HMF-GTMA; (b) Levulinic Acid-GTMA (ester) with DHB Matrix (reaction carried out in H_2O)

Although GTMA is often used specifically with mono- and polysaccharides, it appears that it can also be used to chemically modify the platform chemicals of interest in this study. It is not surprising that HMF reacts with GTMA since it is chemically similar to fructose, and has an available primary alcohol group which can react with GTMA. It was also observed that levulinic acid and GTMA react, hence, it appears that ester formation is another reasonable means of using GTMA to enhance ionization for MALDI-MS analysis. It is speculated that under alkaline conditions, levulinic acid is deprotonated and acts as the nucleophile in the epoxide ring-opening. This reaction may suffer compared to the sugar-ether formation however, due to reversible base-catalyzed hydrolysis which is commonly observed with esters in alkaline conditions. Either way, GTMA was shown to successfully react with each of the target analytes in this study, allowing enhanced detection of biomass transformation reaction components in IL-containing systems by MALDI-MS.

4.5.4 Selection of Appropriate Internal Standards for Quantitation

The ideal internal standard (IS) for quantitative analysis should be as chemically-similar to the analytes of interest as possible, without causing interferences with the analysis. In this case, the ideal IS must not only have similar ionization efficiency to the target analytes, but also react similarly (competitively) to the derivatizing agent.

For the analysis of glucose, fructose, sucrose and NAG, isotopically-labeled glucose (glucose-d₇) was employed as an appropriate internal standard. It is assumed that

the ionization efficiencies of each sugar analyte will be proportional to the ionization of the IS, and therefore quantitative information can be obtained. In fact, the use of this IS seems feasible, given the reasonable error associated with each of these analytes in previously constructed calibration curves. Furthermore, since the reaction yields cationic derivatives with similar mass and charge, it is expected that these ions will interact similarly with incoming laser irradiation.

The analysis of HMF may be limited by use of glucose-d₇ as the IS, however. Due to the much higher sensitivity of the derivatized HMF ion than the derivatized glucose ion, the range of calibration of HMF is affected, as well as the reproducibility. At high concentrations, the calibration curve also begins to plateau, which is observed upon detector saturation. In these cases, dilution could be attempted, but this would simultaneously dilute other, less sensitive compounds in the reaction mixture. The laser intensity could also be adjusted (lowered) to yield less intense ion peaks. However, this would require an IS that would similarly adjust to changes in laser irradiation.

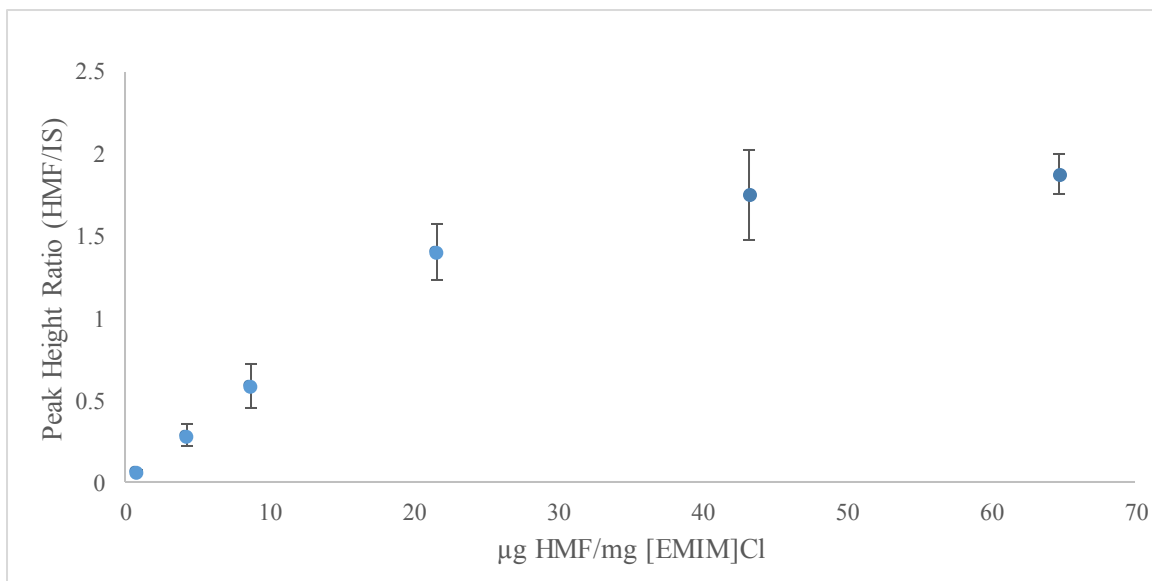


Figure 4-9: Calibration Curve of HMF-GTMA/Glucose-d₇-GTMA in [EMIM]Cl; Error bars represent standard deviation of the mean, n = 5

At first glance, this problem appears to be a matter of ionization efficiency, whereby HMF is more easily ionized, so similar concentrations of sugar (e.g. glucose) and HMF yield much more intense HMF peaks. However, upon derivatization with GTMA, each analyte is pre-ionized in the sample, and the ionization efficiencies should be much more similar to one another than the non-derivatized analogues. Therefore, it is important to consider the reaction efficiency of the derivatization reaction with each analyte. Ideally, the resulting sugar ether would be quantified by NMR to determine the reaction yield, however, poorly resolved peaks, and overlap of reagent peaks make this a difficult task. Therefore, the percent conversion of HMF to HMF-GTMA was not determined.

A more appropriate IS for the quantitation of HMF is an isotopically-labeled HMF standard, which could be prepared from the deuterated glucose standard. This process would require the preparation, separation and external calibration of the isotopically-labeled HMF. Due to costs and time restraints, similar compounds were screened as potential ISs instead. The compounds used as potential ISs were originally chosen based on structural similarity to HMF and availability. The list of compounds was reduced by eliminating compounds that upon derivatization yield interfering ions with reagents and expected reaction products (with respect to m/z ratio) resulting in a shortened list presented in Figure 4-10.

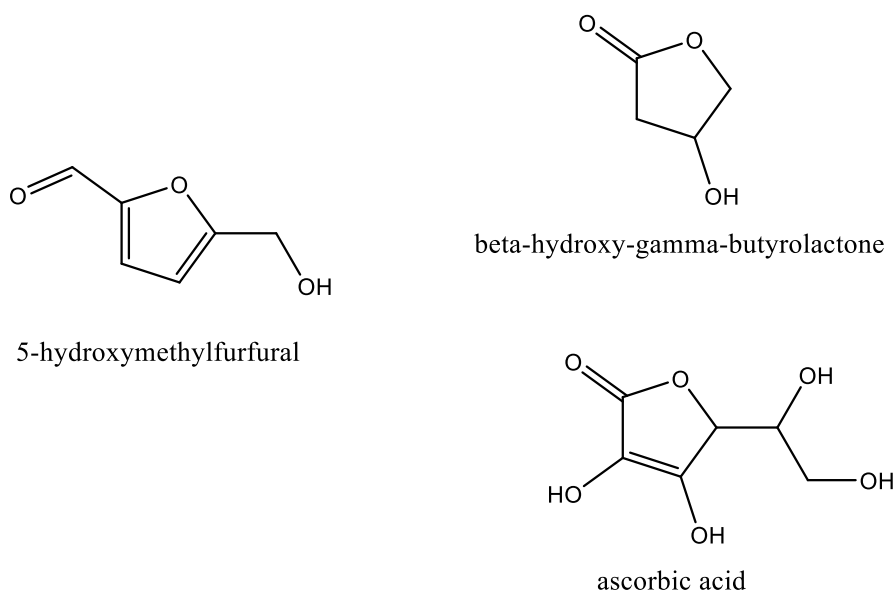


Figure 4-10: Structural Similarity of Potential Internal Standards for the Quantitative Analysis of HMF

The first potential ISs that screened for analysis were furfural, ascorbic acid and β -hydroxy- γ -butyrolactone, due to their structural similarity to HMF. Furfural, however, does not have an available hydroxyl group, through which the GTMA can react. Furfural

is also a dehydration product of HMF and may occur in the reaction systems of interest, and is therefore not useful. Ascorbic acid and β -hydroxy- γ -butyrolactone, however, have hydroxyl substituents. Therefore, these compounds were subjected to the derivatization procedure.

Upon derivatization of each compound with GTMA, the resulting solutions were analyzed by MALDI-MS using DHB as the matrix. Unfortunately, analysis of the β -hydroxy- γ -butyrolactone did not result in any observable GTMA-ether peaks (expected m/z 218). The reaction of ascorbic acid did result in detectable derivatized ions (m/z 292), however, the intensities of similar concentration standards were very low as compared to HMF. The data suggests that the GTMA does not react very efficiently with each of these chosen compounds. Despite containing hydroxyl substituents, β -hydroxy- γ -butyrolactone likely suffers in this reaction, as the hydroxyl group is a secondary alcohol and will be less reactive. Ascorbic acid has a primary alcohol group, however, there is significant steric hindrance that may slow the reaction.

Therefore, it appears that the presence of a primary alcohol group is more representative of the reaction efficiency of HMF with GTMA. Unfortunately, many of the furan alcohols that are available, are bio-derived compounds from similar sugars and may occur in the reaction medium as side products. To avoid this, benzyl alcohol (BnOH) was employed as a potential IS. Much like HMF, BnOH is an aromatic primary alcohol. Therefore, it is speculated that the two compounds will likely react similarly with GTMA.

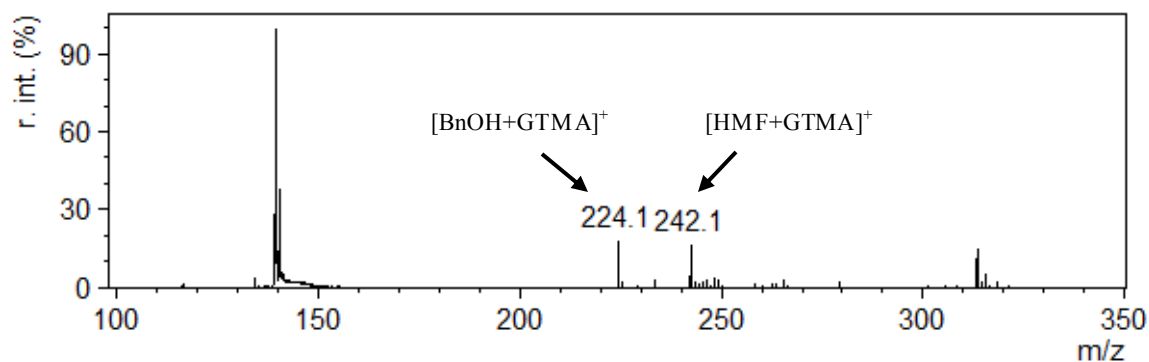


Figure 4-11: MALDI-MS Spectrum of HMF-GTMA and BnOH-GTMA in [BMIM]Cl using DHB Matrix

Preliminary reaction of BnOH with GTMA and subsequent analysis by MALDI yielded significant derivatized ion intensity (m/z 224), which does not appear to cause interference with the analysis of other test analytes. HMF does appear to have a higher response factor than BnOH, but BnOH appears to be more representative of HMF than glucose- d_7 . Therefore, BnOH was employed as an IS for subsequent HMF analysis.

4.5.5 Quantitative Analysis of GTMA-Derivatized Analytes in ILs

For quantitative purposes, calibration curves of derivatized glucose (glucose-GTMA) were constructed (Figure 4-12). Glucose was derivatized in water, as well as in each of the ILs in this study ([BMIM]Cl, [EMIM]Cl and [EMIM]OAc). As expected, the sensitivity of glucose was similar regardless of the solvent system (as isotopically-labeled glucose was used as the IS without the presence of significant interferences of either m/z ratio). In all cases, the calibration curves exhibited linear behavior over a wide dynamic range (LOD – 400 ng) which is appropriate for quantitation of analytes in IL systems (Table 4-3).

Table 4-3: Calculated LODs and LOQs of Glucose-GTMA in Various Solvent Systems by MALDI-MS

System	LOD (ng/spot)	LOQ (ng/spot)	% RSDs*
Glucose-GTMA in Water	14.0	46.6	4.2 – 8.7 %
Glucose-GTMA in [BMIM]Cl	8.3	27.6	2.0 – 5.8 %
Glucose-GTMA in [EMIM]Cl	3.1	10.3	1.2 – 6.4 %
Glucose-GTMA in [EMIM]OAc	7.4	24.7	2.8 – 7.2 %

*of standards in working range of the curve

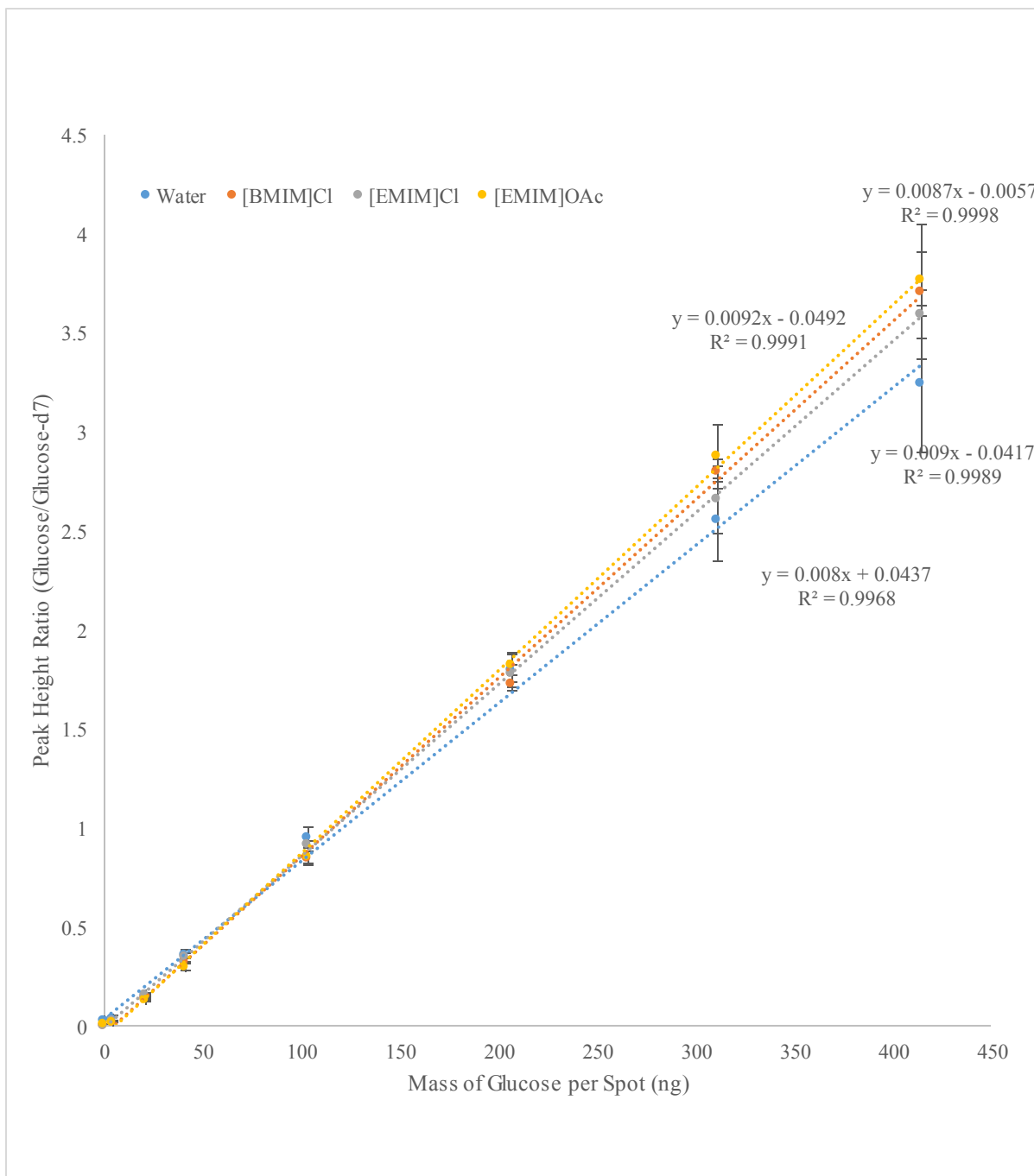


Figure 4-12: Glucose-GTMA/Glucose-d₇-GTMA Response by MALDI-MS using DHB Matrix in the Presence of ILs

LODs of derivatized analytes vary depending on the solvent (H₂O or IL), but in all cases are comparable to the LODs of the native analytes determined in the absence of IL (refer to Table 4-1). In the presence of IL (prior to derivatization), the analyte could only be reproducibly identified at relatively high analyte loading (μg/spot), whereas upon derivatization, ng-level concentrations were observed with minimal matrix interference or suppression. Interestingly, the LODs of glucose-GTMA were lower when analyzed in each IL than in water. Since the LOD is based on the standard error of the regression, it appears that more error is associated with the calibration standards in water than the ILs. Furthermore, lower % RSDs were obtained when glucose was analyzed in the ILs. This may be a result of the glassy liquid sample spots which are more homogeneous than the crystalline sample spots which were observed upon spotting derivatized reaction mixtures in purely aqueous systems.

Since the IS in this case is isotopically-labeled glucose, it is difficult to make comparisons between the calibration curves constructed in the different IL systems, since the IS will theoretically react and ionize by the same means as glucose. This leads to very small differences in the analyte/IS response ratio. The absolute analyte intensity within each system should give more information, however the large error associated with external calibration make this a difficult task. The absolute intensities of the IS (constant concentration in all standards/solvent systems) can, however, give an indication of overall analyte sensitivity.

Table 4-4: Absolute Intensity of Glucose-d₇ in Water and IL Solvent Systems

Solvent	Average Absolute Intensity Glucose-d ₇ (IS) (all standards, n = 40)*	% RSD
Water	4367.0	52.3 %
[BMIM]Cl	6513.2	57.0 %
[EMIM]Cl	7505.0	47.4 %
[EMIM]OAc	2639.6	52.2 %

*values for individual standards can be seen in Table A5-2

The high % RSDs represent the variation in the absolute intensities of IS from spot-to-spot as well as variation arising from different analyte concentrations, reiterating the difficulty in achieving quantitative information by MALDI-MS in the absence of a reference peak. Although the average absolute intensities of the IS in both [BMIM]Cl and [EMIM]Cl are not statistically different, these values are statistically greater than those intensities in water and [EMIM]OAc. This indicates that the chloride-containing ILs afford higher sensitivity of glucose-d₇ and hence, is a good indication of the overall intensities expected for similar sugar analytes. The apparent decrease in overall IS intensity in [EMIM]OAc solvent may be a result of matrix deprotonation which impacts the electronic behavior of the matrix and effects the ability of the matrix to absorb laser radiation and promote desorption/ionization (as discussed in Chapter 2).

Overall, each solvent allows a linear response with increasing glucose concentration from 4 to 414 ng glucose/spot standards (as calculated after dilution). This dynamic range allows for the detection and quantification of a range of analyte

concentrations that would be expected in a typical biotransformation reaction system (i.e. 1 – 100 % consumption).

4.5.6 Application of MALDI-MS for the Analysis of GTMA-Sugar Ethers in IL Systems

Upon constructing appropriate calibration curves, the proposed MALDI-MS method of derivatizing analytes prior to analysis was used to monitor a model biomass transformation reaction. Specifically, the CrCl_3 -catalyzed dehydration of fructose to HMF in $[\text{BMIM}]\text{Cl}$ was monitored.

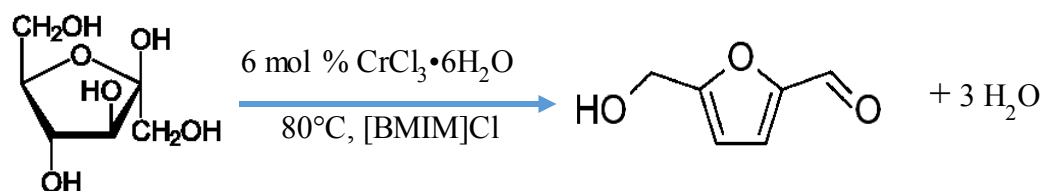


Figure 4-13: Reaction Scheme of $\text{CrCl}_3 \cdot 6\text{H}_2\text{O}$ -catalyzed Dehydration of Fructose to HMF in $[\text{BMIM}]\text{Cl}$

At timed intervals, (after allowing ~ 10 minutes for mixing and complete dissolution of reaction components), ~ 50 mg aliquots of the reaction mixture (containing IL, analyte, products, and catalyst) were removed, diluted, and subsequently derivatized according to the procedure as listed in the Methods section of this chapter. Finally, a portion of the derivatized reaction mixture was mixed with DHB for MALDI-MS analysis. Single-component standards were prepared to represent the reaction systems. Equal volumes of 1 M aqueous IL solution and solutions of varying analyte concentration (100, 75, 50, 25, 10, 5, 1 mM) were prepared to yield 0.5 M IL solutions containing 50, 37.5, 25, 12.5, 5, 2.5, and 0.5 mM analyte. Further dilution upon derivatization, and

subsequent MALDI analysis afforded calibration curves with a range of approximately 1 – 100 ng fructose/ μ g [BMIM]Cl and 1 – 75 ng HMF/ μ g [BMIM]Cl.

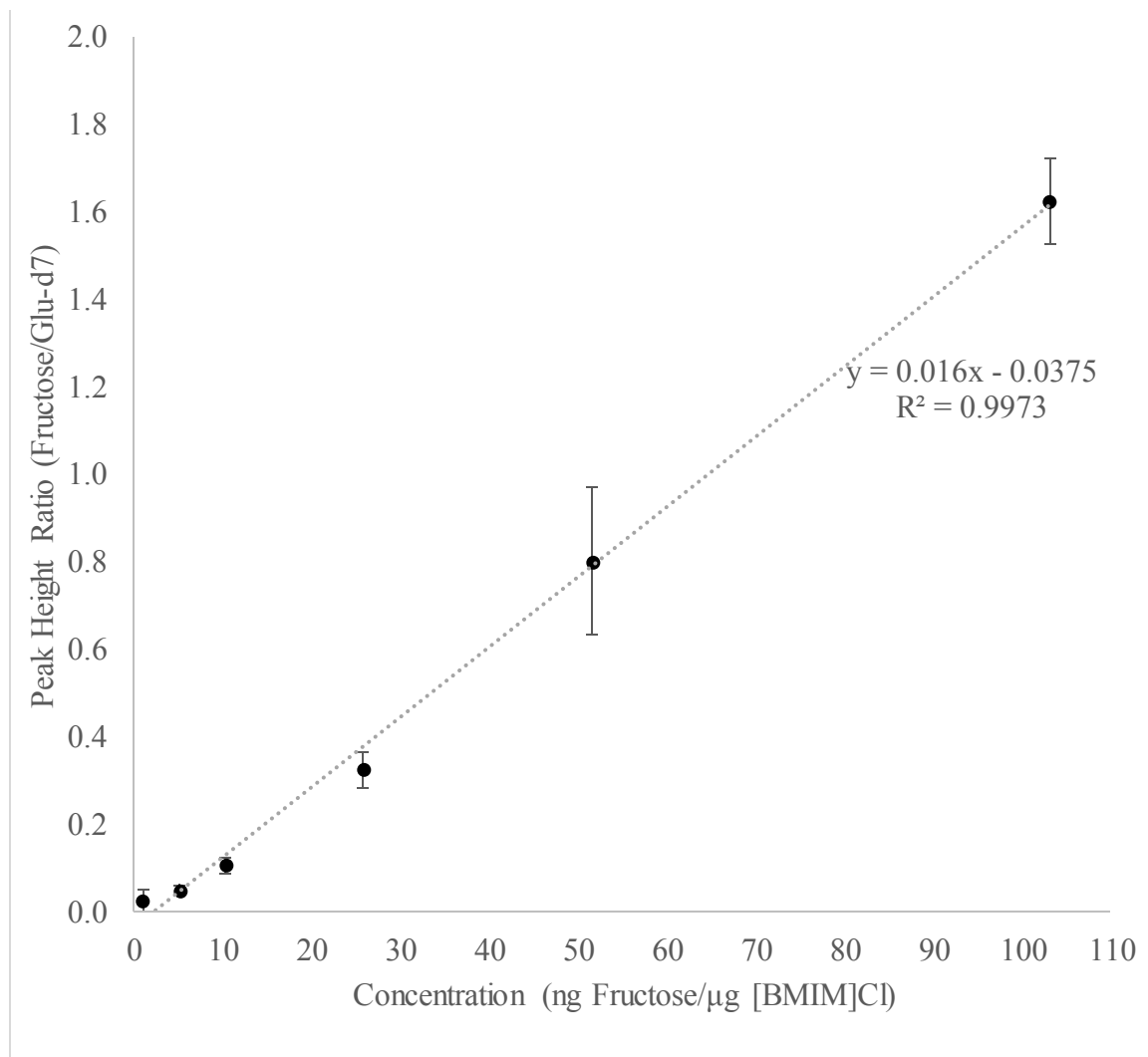


Figure 4-14: Calibration Curve of Fructose-GTMA/Glucose-d₇-GTMA vs. Concentration; Error bars represent standard deviations of the mean response, n = 5

Fructose was calibrated using glucose-d₇ as the IS. The calibration curve exhibits good linearity ($R^2 = 0.9973$) over the range of concentrations used. Note that the standard at ~ 75 ng/ μ g [BMIM]Cl was excluded from the curve, as it was deemed an outlier. The

LOD and LOQ were calculated using the standard error of the curve, and were determined to be 7.2 and 23.9 ng fructose/ μg [BMIM]Cl, respectively. In the case of fructose calibration, the % RSDs ranged from 6.0-24.6 % in the working range of the curve (i.e. above the LOD).

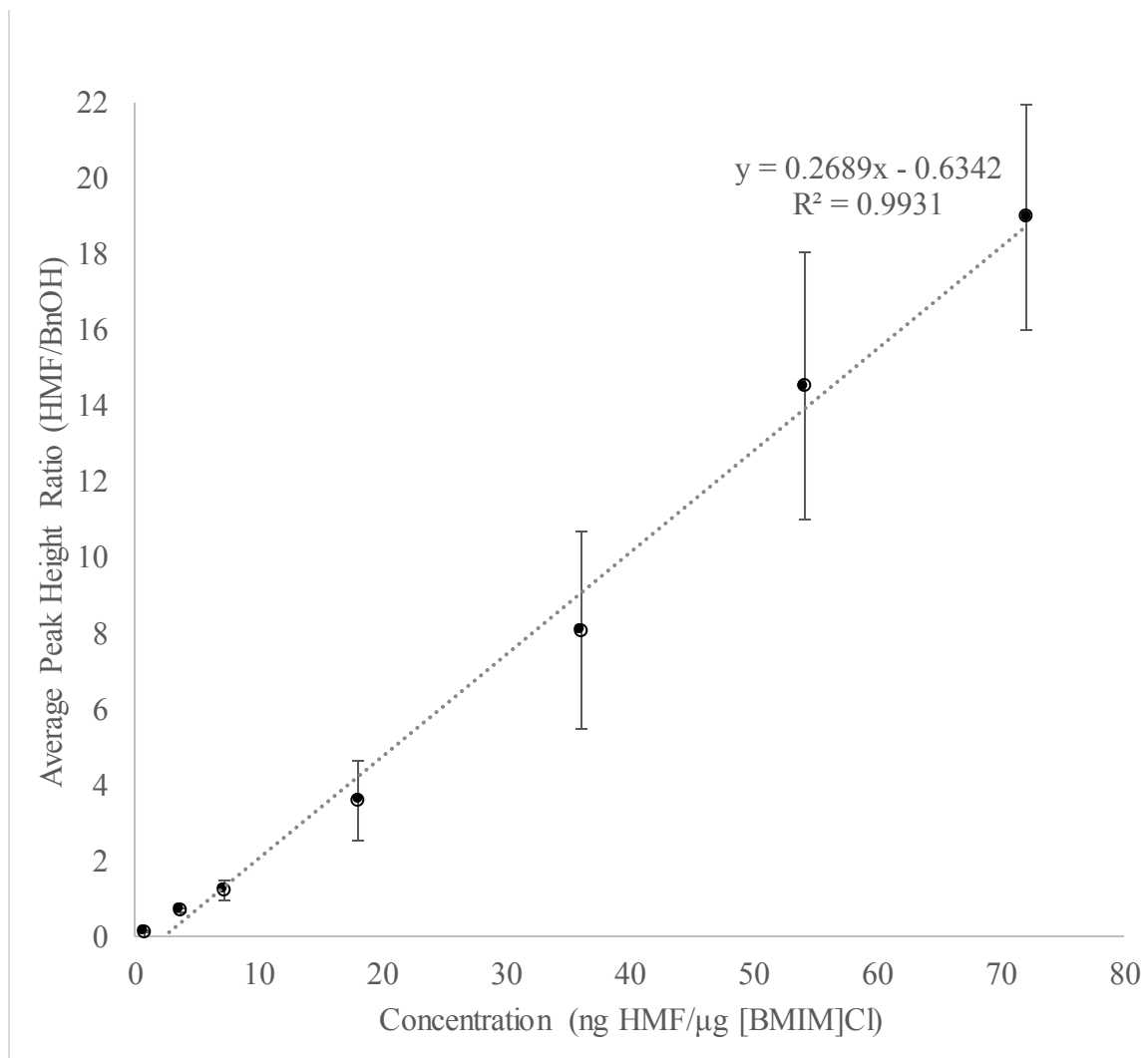


Figure 4-15: Calibration Curve of HMF-GTMA/BnOH-GTMA vs. Concentration; Error bars represent standard deviations of the mean response, $n = 5$

HMF was calibrated using BnOH as the IS rather than glucose-d₇ (as described previously). Again, the calibration (Figure 4-15) exhibits good linearity ($R^2 = 0.9931$) over the range of calibration standards. The HMF/BnOH response is relatively high, as HMF appears to be much more sensitive to the derivatization/ionization process. The limits of detection and quantitation were determined to be 7.5 and 25.2 ng HMF/ μ g [BMIM]Cl, respectively. The % RSDs of calibration standards in the working range were between 15.1 – 30.1 %. Though the error associated with the HMF calibration is larger than that of fructose, these % RSDs are reasonable for MALDI-MS quantitation.

It is important to note that the LOD and LOQ in each case was calculated based on the standard error of the regression line. In these cases, whereby the analyte and IS are not as closely related as glucose and deuterated glucose, for example, the standard error of the curve increases significantly. Therefore, the resulting LODs and LOQs are over-estimated, and do not reflect analyte concentrations with approximate S/N ratios of 3 and 10, respectively. For example, the lowest HMF standard (~ 0.7 ng HMF/ μ g [BMIM]Cl), has a mean S/N ratio of 56, which is much higher than the criteria set by the LOQ (i.e. S/N ~ 10). Furthermore, all fructose standards > 5 ng fructose/ μ g [BMIM]Cl (i.e. all except the lowest standard) have a mean S/N > 10 . Therefore, it seems that this method is not ideal for calculating LOD and LOQ. Furthermore, the S/N ratio is dependent on all components in the sample spot. In the case of reaction mixture samples, the presence of catalyst, by-products, etc., as well as the overall intensity of the mass spectrum can adversely affect the S/N ratio. This means that the prepared standards are not necessarily representative for the purposes of calculating LOD and LOQ. Therefore, for all reported

data, the mean S/N ratio was determined to ensure that the peak was quantifiable (i.e. S/N > 10). This finding reinforces the need of isotopically-labeled ISs in MALDI-MS analyses.

In this experiment, two reactions were monitored; one without catalyst and the other with 6 mol % CrCl_3 catalyst. At 60 min intervals from the time of dissolution until the reaction was ceased, aliquots were removed and quenched with water (to yield 0.5 M IL solutions based on the mass fraction of reaction mixture) and stored in the refrigerator at 4 °C to effectively halt the reaction. All aliquots were derivatized simultaneously to account for potential changes in temperature and time of reaction. It is assumed that through reaction quenching with water, the dehydration reaction of glucose is stopped and that throughout the derivatization procedure no further HMF is formed from glucose (as no sign of HMF formed from glucose- d_7 is evident). The catalyst is effectively diluted and the amount of water present should act to disrupt the dehydration procedure. The resulting peak height ratios of fructose/glucose- d_7 and HMF/BnOH were compared to the constructed calibration curves and tabulated (Tables 4-5 and 4-6).

The % RSDs of the calculated fructose and HMF concentrations are all < 30 %, with the majority of errors between 10 – 15 %. These % RSDs are reasonable considering that each analyte was quantified based on a chemically different compound (IS). This can be attributed to the differences in either the ionization efficiencies of each analyte, or the degree of derivatization with GTMA.

Table 4-5: Concentration of Fructose and HMF as a Function of Reaction Time in the Non-Catalyzed Dehydration Reaction in [BMIM]Cl at 80 °C

Vial	Time (min)	[Fructose] ($\mu\text{g}/\text{mg}$ [BMIM]Cl)	%RSD	[HMF] ($\mu\text{g}/\text{mg}$ [BMIM]Cl)	% RSD
	0	96.4 [†]	---	---	---
1-1	10*	91.3 \pm 10.5	11.5 %	4.43 \pm 0.65	14.6 %
1-2	70	42.3 \pm 2.2	5.2 %	3.44 \pm 0.06	1.7 %
1-3	130	19.2 \pm 0.9	4.5 %	9.16 \pm 1.07	11.7 %
1-4	190	8.28 \pm 0.57	6.9 %	13.9 \pm 1.2	8.6 %

Table 4-6: Concentration of Fructose and HMF as a Function of Reaction Time in the CrCl₃-Catalyzed Dehydration Reaction in [BMIM]Cl at 80 °C

Vial	Time (min)	[Fructose] ($\mu\text{g}/\text{mg}$ [BMIM]Cl)	%RSD	[HMF] ($\mu\text{g}/\text{mg}$ [BMIM]Cl)	% RSD
	0	96.0 [†]	---	---	---
2-1	10*	57.4 \pm 8.8	15.4 %	12.1 \pm 2.7	22.1 %
2-2	70	32.9 \pm 5.3	16.2 %	47.1 \pm 7.5	16.0 %
2-3	130	8.27 \pm 2.30	27.8 %	41.7 \pm 5.5	13.3 %
2-4	190	6.00 \pm 0.77	12.8 %	31.8 \pm 3.7	11.6 %

[†] As weighed directly into reaction vial; * First aliquot taken after ~10 min to allow melting and dissolution of reaction components

Note that the mean S/N ratio for each peak was calculated to ensure that the peak was above the LOQ. In all cases, the HMF peaks were well above S/N ~ 10. The aliquots taken at 130 and 190 min from the catalyzed reaction (vials 2-3 and 2-4), however, each

had fructose peaks with S/N ratios of ~ 5 . Therefore, these peaks are below the LOQ criteria (but above the LOD criteria). These peaks were included in the following figures for informational purposes only. Interestingly, vials 1-4 and 2-3 had similar calculated concentrations. The mean S/N ratio of the peaks in the mass spectra belonging to vial 1-4, however, is 18. This shows that the limits of detection can vary greatly depending on the reaction matrix, and should be carefully examined before data is reported.

Comparison of the initial reaction mixtures (after dissolution of analyte, in the presence of catalyst) in Figure 4-16 (a), shows easily identifiable peaks for fructose-GTMA (m/z 296) and glucose-d₇-GTMA (m/z 303), as well as peaks corresponding to HMF-GTMA (m/z 242) and BnOH-GTMA (m/z 224). After 190 min when the reaction was ceased (Figure 4-16 (b)), the fructose-GTMA peak has decreased with respect to the glucose-d₇ IS peak, while the HMF-GTMA peak has significantly increased (relative to BnOH-GTMA). It is important to note that due to the differences in the relative sensitivities of each of the analytes to this method, the peak heights for fructose and HMF will not necessarily change proportionally (i.e. the HMF-GTMA peak will not increase by the same amount as the fructose-GTMA peak decreases). It can also be noted that there is minimal interference from other ion peaks.

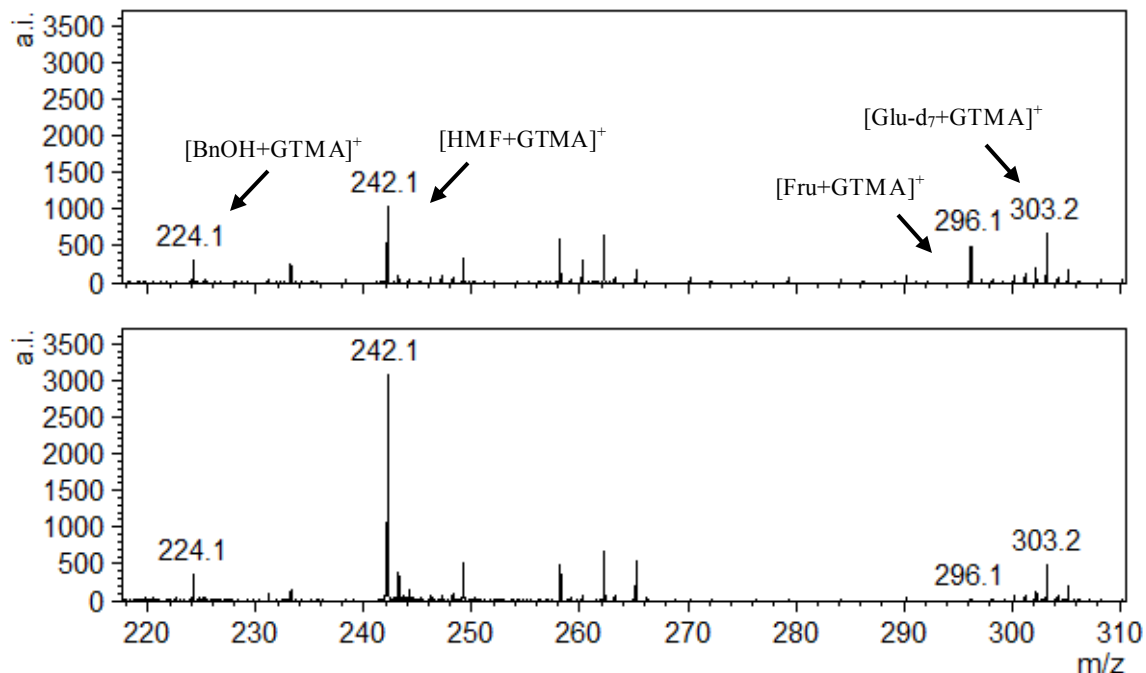


Figure 4-16: MALDI-TOF MS Spectra of the Catalyzed Dehydration Reaction of Fructose to HMF in [BMIM]Cl: (a) at $t = 10$ min, (b) at $t = 190$ min

Graphically, this reactions can be monitored by the steady decrease in fructose concentration, accompanied by an increase in the HMF concentration. Comparison of the non-catalyzed (Figure 4-17) and catalyzed reactions (Figure 4-18) show much faster fructose conversion with the catalyst, as well as higher overall yield of HMF. Alternatively, this data can be used to monitor the fructose conversion rate, or the percent yield of HMF as a function of time (as shown in Figure 4-19). Corresponding data can be seen in Table A5-4.

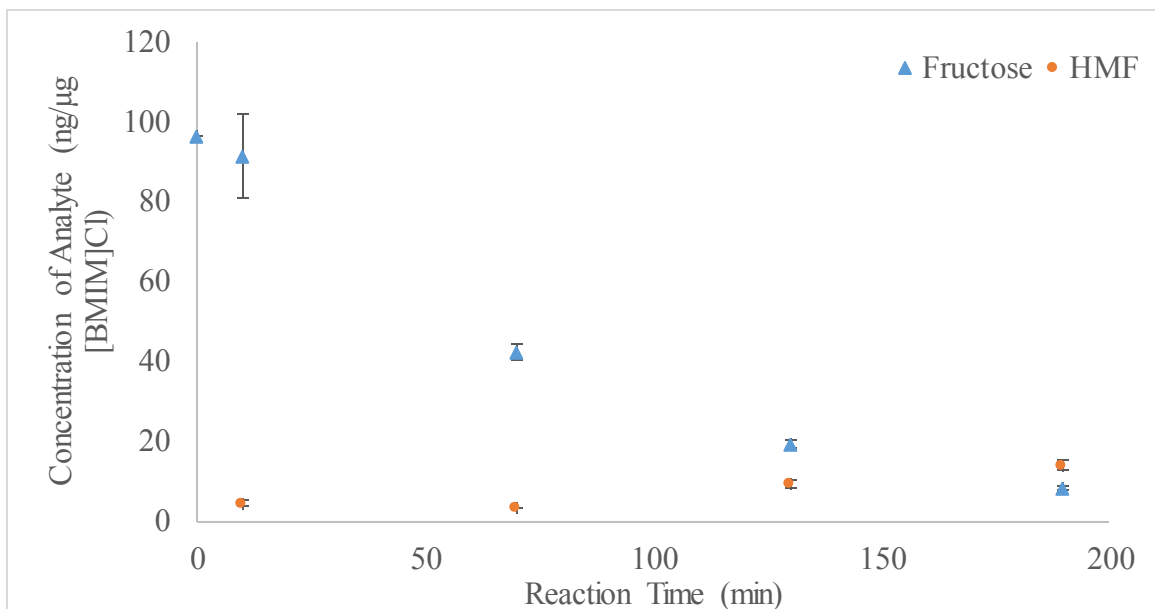


Figure 4-17: Reaction Monitoring of the Dehydration of Fructose to HMF (without catalyst) in [BMIM]Cl as a Function of Reaction Time by MALDI-MS

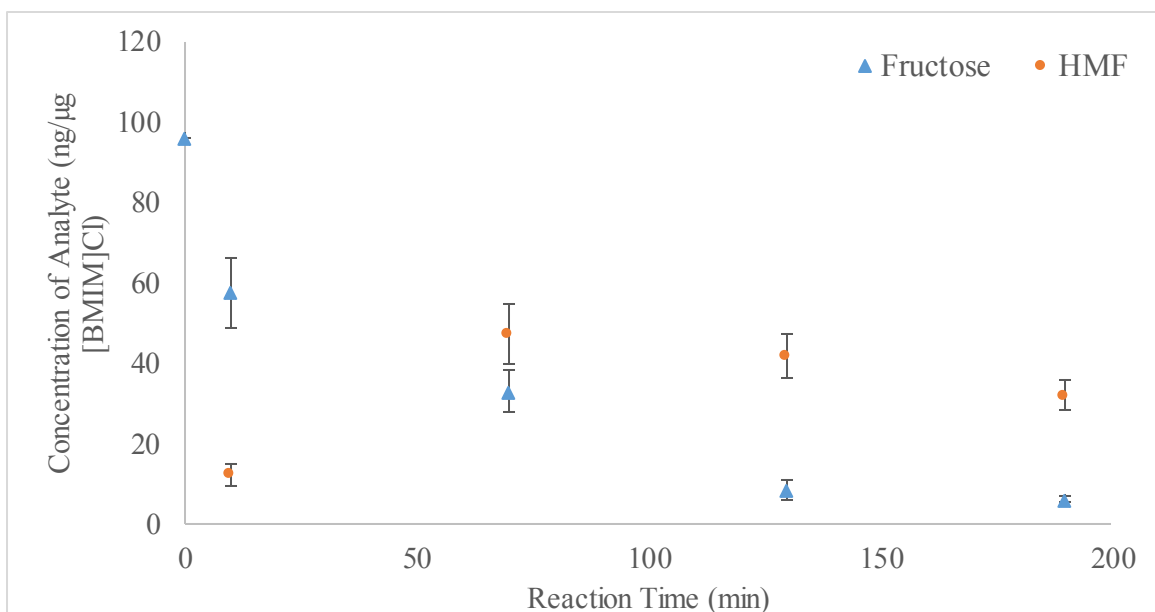


Figure 4-18: Reaction Monitoring of the Dehydration of Fructose to HMF (catalyzed by CrCl₃) in [BMIM]Cl as a Function of Reaction Time by MALDI-MS

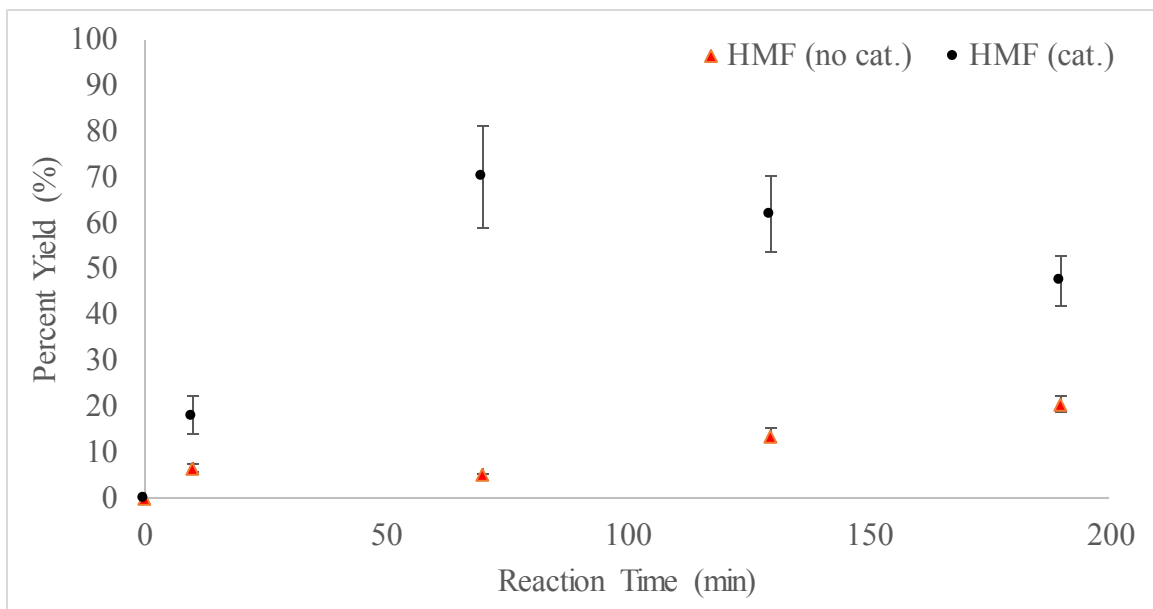


Figure 4-19: Comparison of HMF Yield as a Function of Reaction Time with and without Catalyst

This experiment is consistent with literature reports of the dehydration of fructose, whereby the addition of a catalyst promotes faster fructose conversion.^{10,11} By monitoring the reaction by MALDI-MS as a function of time, it can be noted that the yield of HMF in the catalyzed reaction actually decreases after reaching a maximum at 70 min. This may indicate the formation of side products in the reaction. Typical side products in the dehydration of fructose to HMF include levulinic acid, formic acid and the formation of insoluble polymeric humins. Specifically, levulinic acid and formic acid can react with GTMA (m/z 232 and 162, respectively), however, neither of these products were identified in either of the resulting spectra (possibly below analyte detection limits which were not determined in this study). By removing additional aliquots in a future experiment, the yield can be more accurately demonstrated to give a better understanding of the reaction kinetics.

The ability of this method to monitor reactions at various points during the experiment allows for the accumulation of many data points (depending on the intervals at which aliquots are removed). Aliquots can then be simultaneously derivatized and analyzed by MALDI-MS. The effect of a catalyst, for example, on a reaction system (whereby temperature and reaction time are equal) can be effectively monitored using the proposed method.

4.5.7 Conclusions and Future Work

In conclusion, the proposed method allows for the quantitation of biomass components such as sugars and platform chemicals (containing accessible hydroxyl functional groups) in ILs by MALDI-TOF MS. This is accomplished by introducing a charged functional group into compounds which allows sugars to be pre-ionized and allow for analyte suppression by IL ions to be overcome. LODs of derivatized glucose and fructose are comparable to typical MALDI analyses in the absence of ILs. This procedure also allows for the simultaneous detection of more volatile compounds such as HMF and levulinic acid, which were not detected by traditional MALDI methods. With the use of an appropriate IS to account for ionization efficiency, these analytes can readily be quantified by comparing to representative standards, and do not require prior separation from the IL solvent.

Further experimentation is required to validate the proposed method with existing methods for the analysis of sugars and platform chemicals (i.e. by GC-MS, LC-MS). Other cationic derivatizing agents could be screened for the potential to react with other functional groups, to allow more rapid conversion or for the analysis of dehydration

products that do not contain hydroxyl groups. Calibration curves for the other analytes could be constructed and similarly applied to reaction systems containing NAG, sucrose and levulinic acid, as well as biopolymers such as cellulose and chitin, to monitor depolymerization of raw feedstocks into sugars, followed by further transformation into platform chemicals. Finally, the reaction efficiency of the derivatization could be more accurately determined to determine the reproducibility of the derivatization, as well as to enhance the reaction and thereby increase overall method sensitivity.

References

1. Kerton, F. M.; Marriott, R. *Alternative Solvents for Green Chemistry*, 2nd ed. RSC Publishing: Cambridge, UK, 2013.
2. Lee, S. *Mass Spectrom. Lett.* **2010**, *1*, 33-36.
3. Yang, H.; Lee, A.; Lee, M.; Kim, W.; Kim, J. *Bull. Korean Chem. Soc.* **2010**, *31*, 35-40.
4. Ren, S. F.; Zhang, L.; Cheng, Z. H.; Guo, Y. L. *J. Am. Soc. Mass Spectrom.* **2005**, *16*, 333-339.
5. Harvey, D. J. *Mass Spectrom. Rev.* **1999**, *18*, 349-451.
6. Harvey, D. J. *J. Chromatogr. B* **2010**, *879*, 1196-1225.
7. Lamari, F. N.; Kuhn, R.; Karamanos, N. K. *J. Chromatogr. B* **2003**, *793*, 15-36.
8. Gouw, J. W.; Burgers, P. C.; Trikoupi, M. A.; Terlouw, J. K. *Rapid Commun. Mass Spectrom.* **2002**, *16*, 905-912.
9. Naven, T. J. P.; Harvey, D. J. *Rapid Commun. Mass Spectrom.* **1996**, *10*, 829-834.
10. Zhang, Z. C. *WIREs Energy Environ.* **2013**, doi: 10.1002/wene.67
11. Zhao, H.; Holladay, J. E.; Brown, H.; Zhang, Z. C. *Science* **2007**, *316*, 1597-1600.

Chapter 5: Qualitative Analysis of Small Molecule Platform Chemicals in Ionic Liquids by Desorption Electrospray Ionization Mass Spectrometry

5.1 Introduction

Desorption electrospray ionization mass spectrometry (DESI-MS) is a novel means of achieving ionization under ambient conditions. This allows for the acquisition of chemical information from samples in their native state. By combining surface desorption ionization with traditional electrospray, DESI-MS can be tailored to a huge range of applications from surface analysis, imaging, biological and forensic analyses, and many more.

DESI-MS has grown significantly in popularity due to rapid data acquisition and minimal sample preparation. The ability of the source to ionize analytes of interest from their native state allows a more accurate depiction of complex chemical systems.¹ Previous studies have employed DESI-MS for the analysis of carbohydrates and a variety of small compounds.^{2,3} Until now, however, DESI-MS has not been used to analyze such analytes in ionic liquid media.

In this chapter, DESI-MS is employed for the qualitative screening of target platform chemicals glucose, 5-hydroxymethylfurfural (HMF) and levulinic acid in ILs, as an alternative means of monitoring biomass transformation processes without the need of derivatization. Unlike MALDI-MS, where analytes are ionized in a low pressure atmosphere, DESI-MS can be used to promote ionization at ambient pressure. Since HMF

and levulinic acid were not detected by traditional MALDI-MS experiments, it was proposed that DESI-MS could provide a means of detection of the analytes without the need for chemical modification.

5.2 Materials

D-(+)-Glucose ($\geq 99.5\%$) and 1-ethyl-3-methylimidazolium chloride ([EMIM]Cl) (98 %) were obtained from Sigma-Aldrich (St. Louis, MO). The 1-butyl-3-methylimidazolium chloride ([BMIM]Cl) (96 %) was purchased from Alfa Aesar (Ward Hill, MA), and 1-ethyl-3-methylimidazolium acetate ([EMIM]OAc) ($> 95\%$) was purchased from Io-Li-Tec (Tuscaloosa, AL). 5-Hydroxymethylfurfural (HMF) (98 %) was obtained from AK Scientific (Union City, CA) and levulinic acid (98 %), (\pm)- β -hydroxy- γ -butyrolactone (96 %), and chromium (III) chloride hexahydrate (98 %) were purchased from Alfa Aesar (Shore Road, Heysham, Lancs.). Water, methanol and acetonitrile (HPLC grade, 99.9 %) were obtained from Fisher Scientific (Fair Lawn, NJ). All chemicals were used without further purification.

5.3 Instrumentation

5.3.1 DESI-MS

All mass spectrometric analyses were carried out using a Xevo T-QS mass spectrometer (Waters) equipped with a 2-D DESI ion source (Prosolia). The spray solvent (1:1 methanol:water or 1:1 methanol:water + 0.1 % formic acid) was delivered using a syringe pump at a flow rate of 2 μ L/min, with a N₂ gas nebulizer pressure of 100 psi. The source temperature was set as 100 °C. For analyses in positive ion mode, the capillary

voltage was set to + 3 kV, while in negative ion mode the capillary voltage was set to - 4 kV.

The spray tip was positioned at an incident angle of 55 °, the distance between the spray tip and the Omni-slide surface was 2 mm, and the distance between the ion transfer line and the surface was ~ 0.5 mm (refer to Figure 1-13 for schematic).

Data was acquired as the total ion current (TIC) over 0.5 min of sampling (manual dwell oscillating over the sample spot surface to avoid analyte depletion). All reported mass spectra are the combined total of the TIC over the entire sampling time. Data was exported to mMass for processing.

5.4 Methods

5.4.1 Standard Preparation

Stock solutions of HMF and levulinic acid were prepared in 2:1 acetonitrile/water at a concentration of 20 mM. These stock solutions were used to prepare working standards containing 20 μ M, 200 μ M and 2 mM of each analyte. Stock solutions of 100 mM [BMIM]Cl, [EMIM]Cl and [EMIM]OAc were similarly prepared in 2:1 ACN:H₂O (v:v). These solutions were then used to prepare 20 mM working solutions. Equal volumes (500 μ L) of each analyte and each IL were separately mixed in 2-mL vials to yield solutions containing 10 mM IL and 100 μ M or 1 mM analyte. The method blank was composed of 10 mM IL in 2:1 ACN:H₂O.

5.4.2 Sample Deposition

Sample volumes of 1 μL of each solution were spotted onto a 66-well Teflon-coated Omni slide DESI substrate (via dried droplet method). The solvent was allowed to evaporate at room temperature (~ 15 min) before the slide was manually loaded into the sample chamber at atmospheric pressure.

5.5 Results and Discussion

5.5.1 Sample Preparation

The spray solvent serves to provide an electrically charged mist directed at the sample, as well as a solvation and extraction medium upon sample wetting.⁴ Typical spray solvents for a particular analysis are based on compatibility with instrumentation and ability to dissolve (often, selectively) the analyte of interest. Additives are often employed to promote protonation or cationization as required by the analyte class.⁵ In this study, the spray solvent was chosen as 1:1 methanol:water, in which each of the analytes are readily soluble. For the analysis of glucose, NaCl (10 μM) was added to the spray solvent to promote cationization, while for HMF analysis, 0.1 % formic acid was added to promote protonation.

Similar to MALDI analyses, the sample spotting technique can be tailored to promote homogeneous sample spots. In this case, the dried droplet method was used, whereby standards containing the analyte of interest in solutions of IL were spotted onto a Teflon-coated Omni slide and allowed to dry. Initially, 1:1 methanol:water solution was employed for this purpose, as the solution provided dissolution of both IL and analyte

with relatively quick drying times. For the analysis of HMF, however, the presence of methanol resulted in an abundant ion with m/z 141. MS/MS studies indicate that this ion is likely the methyl ester of HMF (formed through acid-catalyzed esterification). Interestingly, this ion was not identified in resulting mass spectra when methanol was employed as the spray solvent. The spotting solvent was therefore changed to 2:1 ACN:H₂O, which did not result in appreciable amounts of these ions.

5.5.2 Instrument Parameters

The capillary voltage was optimized by increasing the voltage while monitoring the peak intensity of the molecular ion of the highest concentration standard. The capillary voltage was set to avoid detector saturation and to minimize unwanted interference from other ions. Increasing the voltage generally resulted in increased analyte signal, however, at the cost of increased noise and interfering ions. Through trial and error, the near optimum capillary voltage was found to be + 3 kV for analysis of HMF in positive mode and - 4 kV for analysis of levulinic acid in negative mode.

The DESI spray and collection process is highly dependent on the geometric parameters of the spray tip and ion transfer line.³ The angle and distance from which the spray contacts the sample affect the ionization process, whereas the angle and distance of the ion transfer line from the sample affect the ion collection efficiency. By manually changing these parameters, generally an optimized ion signal can be obtained for a particular set of analytes. These parameters have been arbitrarily set by previous experimentation for the analyses of carbohydrates (i.e. glucose).³ Although glucose was not detected in this work, the geometric parameters were set to mimic previous analyses

of sugars. Therefore, the methodology could be tailored to suit an abundance of bio-derived compounds, specifically those of poorer ionizability and volatility.

5.5.3 Initial Analyte Screening by DESI-MS

In previous work by Khemchyan et al., IL reaction systems of biomass components have been analyzed using a modified ESI-MS method.⁶ As pre-ionized species, the IL ions overwhelmed and saturated resulting spectra. To combat this, Khemchyan et al. employed MS gating, to allow only analyte ions to be detected, which resulted in improved sensitivity. In this work, a similar experiment was carried out, however, IL ions could be detected after the sample was depleted. This carry-over can be harmful to the instrument and result in contamination. Since DESI-MS ionizes analytes by a similar mechanism, it was speculated that DESI could be tailored to ionize analytes of interest while avoiding detector saturation by less volatile IL ions.

Glucose and other small carbohydrates have been successfully ionized via DESI-MS in previous work.^{2,3,7-9} Using similar operating parameters, however, resulted in no detectable ions for glucose using the available instrumentation. The capillary voltage, spray solvent (and additives), source temperature, as well as geometric parameters were systematically altered to enhance ion signal, but these attempts were unsuccessful. At relatively high concentrations of analyte ($\mu\text{g}/\text{spot}$), parameters were adjusted and the resulting mass spectrum monitored in real-time. The solvent spray, in particular, was also tailored to include varying concentrations of cationization agents (NaCl , NH_4Cl and KCl in aqueous methanol or acetonitrile). Unfortunately, despite many efforts, glucose was not detected by DESI-MS. Therefore, the focus of this work was shifted to the analysis of

volatile platform chemicals HMF and levulinic acid which could not be directly analyzed by MALDI-MS (in vacuum).

The other test analytes HMF and levulinic acid are much more easily ionized by DESI, and also have appreciable volatilities at room temperature. Initial screening of aqueous standards of HMF and levulinic acid generated abundant $[\text{HMF}+\text{H}]^+$ and $[\text{LA}-\text{H}]^-$ ions (in positive and negative ion modes, respectively). Therefore, these analytes were analyzed in IL solvents to determine the applicability of DESI-MS for reaction monitoring. Operating parameters were adjusted in real-time to yield appreciable ion signal without causing spectrum saturation by the IL ions. In each case, parameters were not fully optimized, rather set to achieve reproducible spectra and validate the potential of DESI-MS for such applications.

5.5.4 DESI-MS of IL Media

Analysis of ILs using MALDI-MS generates high intensity ion peaks leading to detector saturation and analyte ion suppression. Unlike MALDI, however, DESI can be tailored to selectively ionize a particular compound based on its chemical properties and adjustment of operating parameters. The spray solvent acts an extractive medium, and secondary ions are formed due to sample “jetting” and are projected towards the MS.⁵ During initial IL screening by DESI, it was noted that to achieve ion signal (for the IL cation), operating parameters often needed to be adjusted, which could be advantageous in the analysis of more volatile compounds.

To determine the applicability of ILs in DESI-MS analyses, three ILs of interest ([BMIM]Cl, [EMIM]Cl, and [EMIM]OAc) were screened as matrix blanks. A spectrum of 2:1 ACN:H₂O on the Omni-slide was collected as the background (Figure 5-1 (a)), and compared to the resulting positive ion spectra of ILs (Figure 5-1 (b)-(d)).

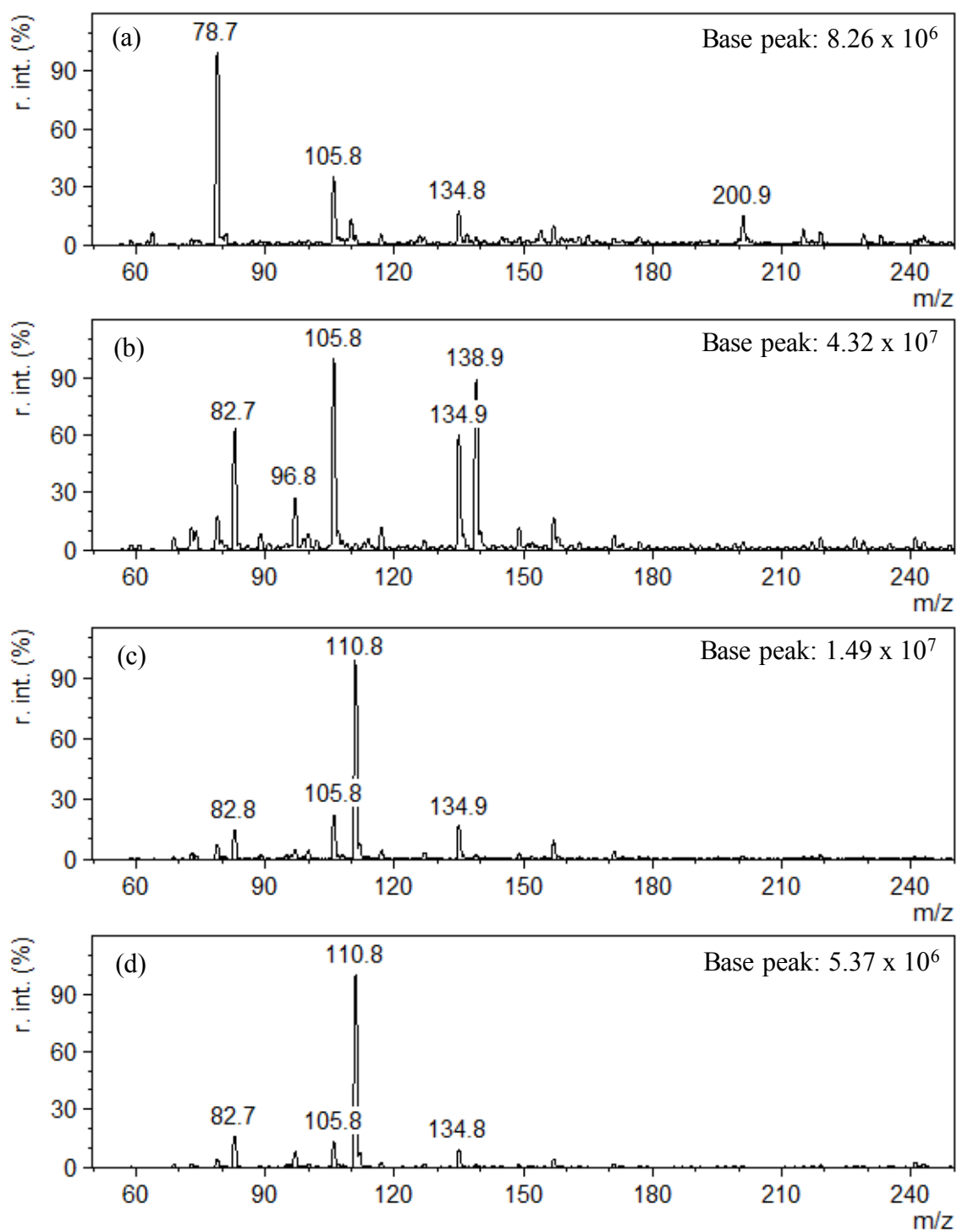


Figure 5-1: DESI-MS Spectra of Method Blanks in Positive Ion Mode: (a) 2:1 ACN:H₂O, (b) 10 nmol [BMIM]Cl, (c) 10 nmol [EMIM]Cl, (d) 10 nmol [EMIM]OAc

As can be seen in Figure 5-1 (a), the Omni-slide blank has few ions present, despite the high sensitivity of the DESI source and the TQ-S mass analyzer. The most abundant ions present are those that appear at m/z values of 79, 106, 135, and 201 (unidentified). Upon addition of IL (Figure 5-1 (b), (c), (d)), the IL cation is readily apparent ($[BMIM]^+$ at m/z 139, and $[EMIM]^+$ at m/z 111). The ions in the blank can also be observed, with the addition of ions with m/z 83, which likely belong to protonated 1-methylimidazole, a decomposition product of 1,3-dialkylimidazolium ILs. In general, the spectra are relatively clean (as compared to MALDI-MS, for example) as there is no need for added matrices to promote ionization. There is ample opportunity for small molecule analysis with minimal interference, such as for the analysis of small platform chemicals.

In negative mode, spectra were acquired of the same spots to determine potential interferences for the analysis of levulinic acid. Unlike the acquired spectra in positive mode, there are very few differences between each of the IL substrates in negative ion mode (Figure 5-2). Many of the ions that appear in the ILs, also appear in the method blank (2:1 ACN:H₂O). In fact, none of the resultant ions in the spectra of the ILs could be identified as 1,3-dialkylimidazolium ions. Since the ILs of interest are composed of large, bulky cations and small anions, it is not surprising to see few negatively charged species in the low mass region. This is potentially beneficial for the analysis of low mass negatively charged ions.

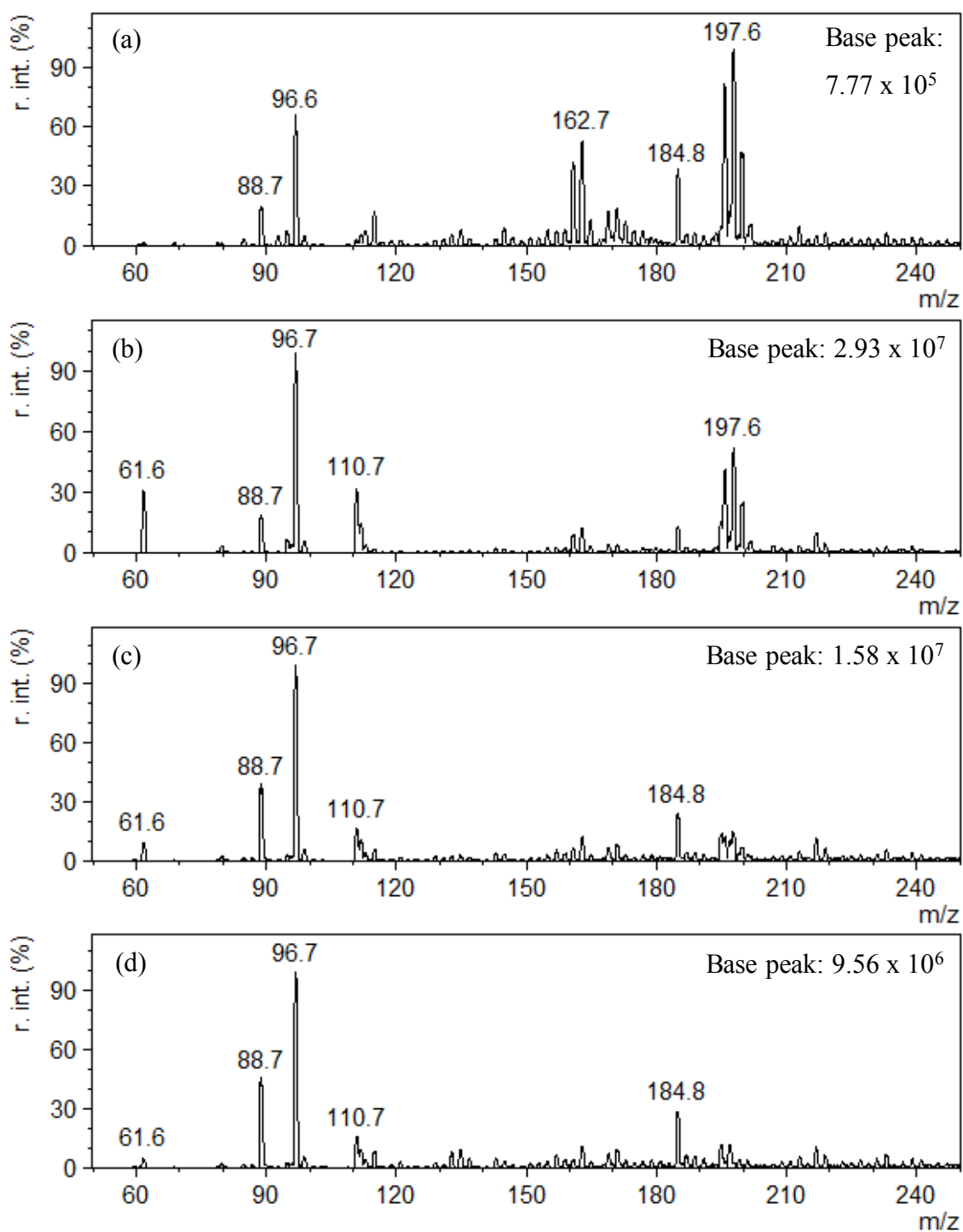


Figure 5-2: DESI-MS Spectra of Method Blanks in Negative Ion Mode: (a) 2:1 ACN:H₂O, (b) 10 nmol [BMIM]Cl, (c) 10 nmol [EMIM]Cl, (d) 10 nmol [EMIM]OAc

5.5.5 Qualitative DESI-MS Analysis of HMF in IL Media

Through preliminary screening, HMF could easily be detected by DESI-MS as the protonated molecular ion $[M+H]^+$ at m/z 126.8. Other fragment ions at m/z 108.8 corresponding to dehydrated HMF (i.e. $[HMF-H_2O+H]^+$) are also observed (refer to Figure 5-3). In this study, HMF was analyzed by DESI-MS in the presence of an excess of IL (10 – 100-fold) to determine whether DESI-MS is a viable analytical technique for the analysis of small volatile compounds in ILs.

Standards were prepared as per the Methods section in this chapter. The resulting sample spots contain 10 nmol of IL and either 1 nmol HMF (10:1 IL:A ratio) or 100 pmol HMF (100:1 IL:A ratio). At the 10:1 ratio, HMF ions (m/z 126.8 and 108.8) can be easily identified along with the corresponding IL cation (Figure 5-3). In all cases, the protonated molecular ion (m/z 126.8) was detected with a S/N ratio of ~ 10 . Furthermore, at lower concentrations (i.e. 100:1 IL:A), $[HMF+H]^+$ can still be easily detected in the presence of each IL with a S/N ratio of ~ 3 (data not shown). Further optimization of operating parameters could allow enhanced sensitivity and a viable means of quantitation.

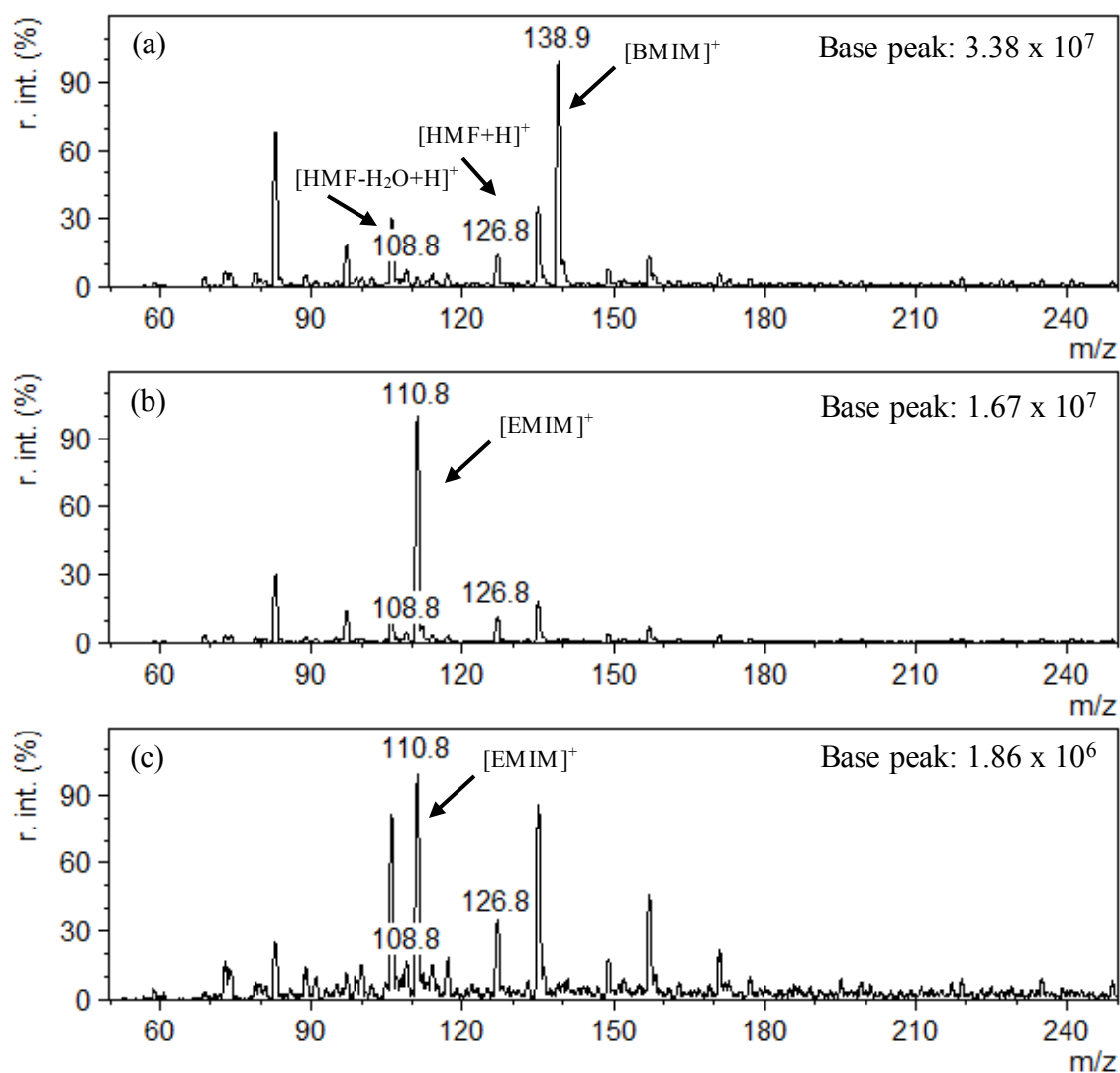


Figure 5-3: DESI-MS Spectra of 10:1 IL:HMF in Positive Ion Mode: (a) [BMIM]Cl, (b) [EMIM]Cl, (c) [EMIM]OAc

5.5.6 Qualitative DESI-MS Analysis of Levulinic Acid in IL Media

Similarly, levulinic acid could be readily detected using DESI-MS during preliminary studies. In negative mode, the deprotonated ion at m/z 114.8 is easily distinguishable from background ions (see Figure 5-4). In the presence of ILs, similar results were obtained. As shown previously, in negative mode, the IL causes very few interfering ions, and the analyte is a prominent ion in the resulting mass spectra. At an IL:A ratio of 10:1, levulinic acid can be detected at S/N ratios > 23 , showing a higher sensitivity than HMF in positive mode. At 100:1 IL:A, the analyte can be detected at S/N ratios > 7 (data not shown). With very little noise (as compared to HMF analyses in positive mode), there is ample opportunity to develop methodology for the analysis of levulinic acid in IL media.

Although not specifically studied, it appears that the presence of IL does not have a significant suppression effect on the analytes. One of the issues that was observed during initial analyte screening was that the analyte ion signal (especially for HMF) would decrease substantially over time during spectra acquisition. This is likely due to the high volatility of the target analytes. When spotted with IL, however, this finding was less pronounced. The IL may serve as a medium in which the analyte can partition, and effectively minimizing analyte depletion and uncontrolled volatilization. Further studies are required to confirm these observations.

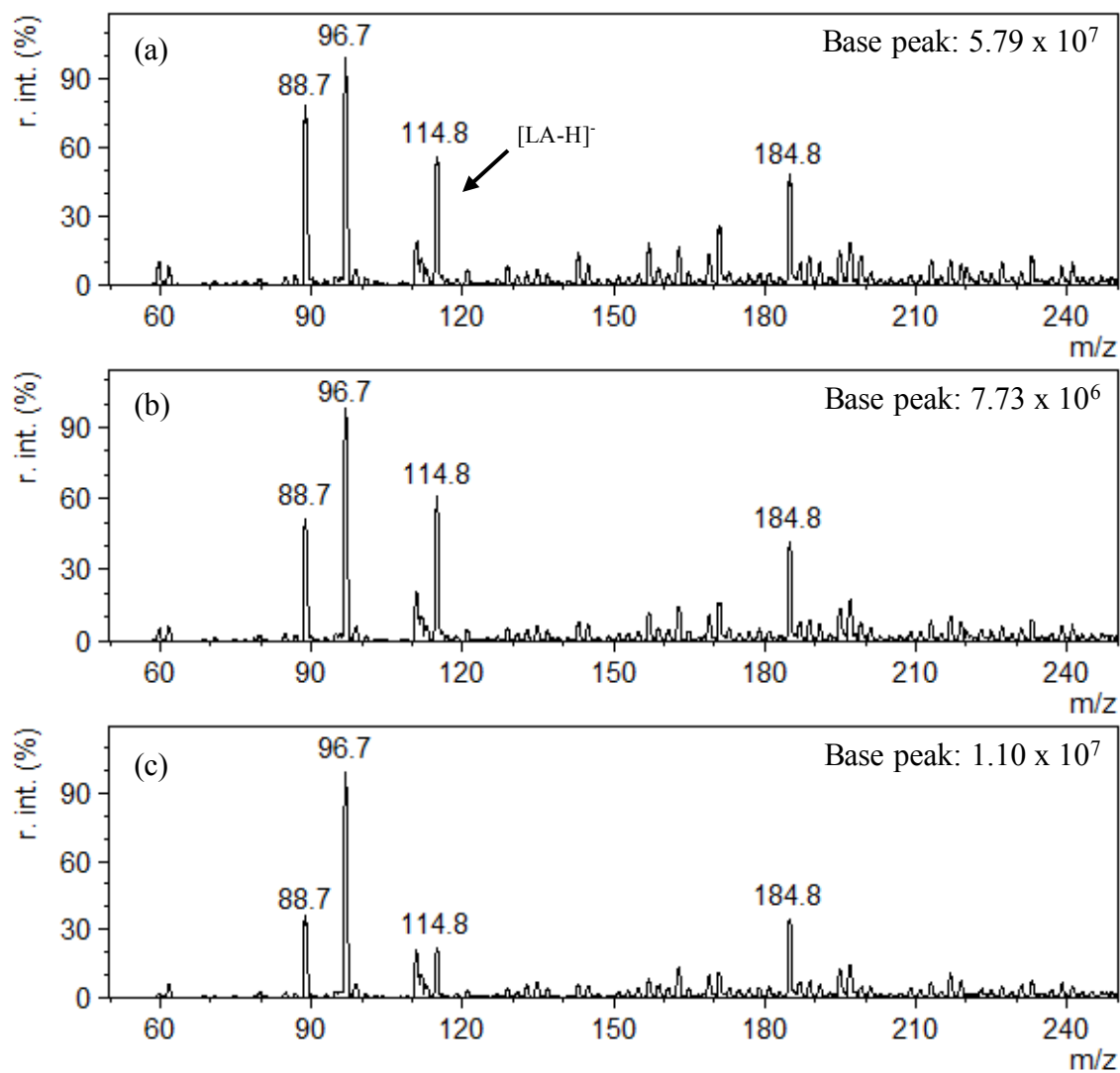


Figure 5-4: DESI-MS Spectra of 10:1 IL:LA in Negative Ion Mode: (a) [BMIM]Cl, (b) [EMIM]Cl, (c) [EMIM]OAc

5.6 Conclusions

DESI-MS was employed for the qualitative screening of HMF and levulinic acid, two versatile platform chemicals produced from biomass feedstocks, in IL solvents. This novel technique shows good potential for the rapid quantitative analyses of these chemicals in IL media, without the need of chemical modification. Analytes of interest can be detected without interferences from IL solvents within seconds. Although glucose was not detected in this study, there is potential to further optimize and develop DESI-MS methods to include a wide variety of biomass-relevant analytes, to provide an alternative means of reaction monitoring compared to traditional chromatographic methods.

References

1. Takats, Z.; Wiseman, J. M.; Gologan, B.; Cooks, R. G. *Science* **2004**, *306*, 471-473.
2. Kauppila, T. J.; Talaty, N.; Jackson, A. U.; Kotiaho, T.; Kostianinen, R.; Cooks, R. G. *Chem. Commun.* **2008**, 2674-2676.
3. Takats, Z.; Wiseman, J. M.; Cooks, R. G. *J. Mass Spectrom.* **2005**, *40*, 1261-1275.
4. Venter, A.; Nefliu, M.; Cooks, R. G. *Trends Anal. Chem.* **2008**, *27*, 284-290.
5. Cooks, R. G.; Ouyang, Z.; Takats, Z.; Wiseman, J. M. *Science* **2006**, *311*, 1566-1570.
6. Khemchyan, L. L.; Khokhlova, E. A.; Seitkalieva, M. M.; Ananikov, V. P. *ChemistryOpen* **2013**, *2*, 208-214.
7. Stephens, C. H.; Shrestha, B.; Morris, H. R.; Bier, M. E.; Whitmore, P. M.; Vertes, A. *Analyst* **2010**, *135*, 2434-2444.
8. Chen, H.; Cotte-Rodriguez, I.; Cooks, R. G. *Chem. Commun.* **2006**, 597-599.
9. Zhang, Y.; Chen, H. *Int. J. Mass Spectrom.* **2010**, *289*, 98-107.

Chapter 6: Conclusions and Future Work

In this work, MALDI-TOF MS and DESI-MS were employed as alternative analytical methods to traditional chromatographic methods for the analysis of platform chemicals in IL solvents. Specifically, this work focused on the analysis of small sugars, glucose, fructose, sucrose and NAG, as well as two versatile value-added chemicals HMF and levulinic acid. Currently, analysis of these compounds in IL-mediated reaction systems require energy-intensive extraction and separation before chromatographic analyses. By developing methods that allow rapid analysis with minimal to no sample preparation, the overall cost of biomass transformation reactions in green solvents such as ILs can be minimized, and results from experimental reactions can be obtained much more quickly.

In Chapter 2 of this thesis, ionic liquid matrices (ILMs) were designed using common MALDI-MS matrices and 1,3-dialkylimidazolium ILs that have been previously used as solvents for biomass transformation of carbohydrates into value-added platform chemicals. By incorporating a UV-active matrix, it was speculated that a portion of an IL-reaction mixture containing analytes could be removed and mixed with an appropriate matrix to form an ILM *in situ* for MALDI-MS analysis. Six ILMs were designed, using matrices 2,5-dihydroxybenzoic acid (DHB) and α -cyano-4-hydroxycinnamic acid (CHCA) with 1-butyl-3-methylimidazolium chloride ([BMIM]Cl), 1-ethyl-3-methylimidazolium chloride ([EMIM]Cl) and 1-ethyl-3-methylimidazolium acetate ([EMIM]OAc). Through NMR, UV-Vis and IR studies, it was determined that only two

of the six designed matrices resulted in true ILMs, where the matrix component was incorporated into a new IL as the anion counterpart (i.e. matrix and [EMIM]OAc). Interestingly, it appears that the mixture of IL and matrix out-performed the true ILMs, and that the formation of a new ion pair is not necessary for analyte detection.

In Chapter 3, the ILMs were screened as MALDI matrices for the analysis of the target analytes (sugars and platform chemicals). Sample preparation was optimized with respect to solvent systems, cationization agents, matrix:analyte ratios and sample deposition. Each of the sugar analytes were readily detected using each DHB-based matrix, but were not detected at appreciable quantities using the analogous CHCA-based ILMs. Unfortunately, neither matrix employed in this study allowed for the detection of HMF or levulinic acid using MALDI-TOF MS. Throughout this research it was observed that MALDI analysis of DHB-based ILMs resulted in significant analyte and matrix suppression by the IL cation in each matrix. Analytes could only be reliably detected at high analyte loading (M:IL:A = 1:1:1). It was determined that quantitative analysis of these systems using the aforementioned MALDI-MS method would be difficult.

To achieve quantitative analysis, further studies were designed to promote analyte competition in the presence of excess IL. To compete with pre-charged IL ions in sample spots, the target analytes were chemically modified by introducing a cationic center through etherification with commercially available glycidyltrimethylammonium chloride (GTMA). LODs of derivatized analytes were similar to those that were determined in the absence of IL (ng-level). Quantitative analyses were carried out by constructing appropriate calibration curves, and the methods applied to model dehydration reactions of

fructose to HMF in ILs. Calibration curves exhibited excellent linearity, with reasonable standard deviations within calibration points.

Finally, DESI-MS was employed in Chapter 5 as an alternative means of analyte ionization without the need for derivatization. Although the method did not allow for the analysis of sugars despite previously reported examples in scientific literature, it has shown potential for the analysis of small volatile platform chemicals. HMF and levulinic acid were easily detected in the presence of each IL by DESI-MS at ratios of 10:1 and 100:1 IL:A.

There is considerable opportunity to continue this work in future studies. ILMs could be fully characterized to determine optimized sample preparation techniques, and screened for their potential with various other analytes. The homogeneity of sample spots could be accurately determined and compared to traditional solid matrices. The formation of colored complexes of [EMIM]Cl in the presence of DHB and CHCA could also be further investigated for potential uses in optical and electronic applications.

In Chapter 4, the derivatization procedure employed could be optimized to reduce the reaction time thus decreasing the overall analysis time. The reaction efficiencies of each analyte could be accurately determined and optimized to enhance the overall method sensitivity. MS/MS studies could also be incorporated to analyze complex reaction systems of several analytes.

From the preliminary work done in Chapter 5, it can be concluded that there is substantial opportunity to develop DESI-MS methods for the analysis of semi-volatile

compounds in IL media. Operating parameters could be optimized by experimental design to enhance analyte signal while avoiding detector saturation by IL ions (i.e. selective analyses). For analytes such as glucose which were not easily detected using DESI-MS in this study, investigation of reaction mechanisms by DESI-MS could offer insight into analyte sensitivity. Similar derivatization as was employed in Chapter 4 could also be employed to simultaneously analyze a variety of biomass transformation intermediates prior to analysis. Use of an appropriate internal standard in this method would also be beneficial, to allow rapid quantitation of reaction systems.

Although the proposed methods offer a significant reduction in analysis time as compared to chromatographic methods, there are several other figures of merit that can be assessed. Each of these desorption/ionization methods require validation against existing chromatographic methods such as GC- and LC-MS for sensitivity, selectivity, and cost effectiveness. The finalized methods could then be applied to a variety of complementary IL-mediated biomass transformation reactions.

Development of novel analytical techniques such as those proposed in this work for green applications represents an emergent field in analytical chemistry. It is believed that mass spectrometric methods, in particular, can provide cost-friendly alternatives to traditional means of analytical separation and detection while providing compatible techniques for analysis in alternative solvents. This work represents a step towards achieving this goal, however future research is required to fully develop sustainable analytical methods that are complementary to rapidly-growing green technologies.

Appendix I: Preparation of Ionic Liquid Matrices

(1) 1-butyl-3-methylimidazolium chloride/2,5-dihydroxybenzoic acid ([BMIM]Cl-DHB): 1.4965 g (8.57 mmol) of [BMIM]Cl (white crystalline solid) was weighed into a round-bottom flask. 1.3791 g (8.95 mmol) of DHB (pale beige solid) was weighed into a vial, and dissolved in minimal acetonitrile (~40 mL). The DHB solution was quantitatively transferred to the RBF resulting in a clear, pale yellow solution. The solution was heated to 80 - 85 °C in a hot water bath for 30 min. The solvent was removed by rotary evaporation (226 mbar, 40 °C) followed by drying under N₂ gas for 30 min. 2.9877 g of thick, brown solution was recovered (104 % yield based on mass balance).

(2) 1-ethyl-3-methylimidazolium chloride/2,5-dihydroxybenzoic acid ([EMIM]Cl-DHB): 1.6935 g (11.55 mmol) of [EMIM]Cl (bright, green solid) was weighed into a round-bottom flask containing a magnetic stir bar. 1.8448 g (11.97 mmol) of DHB was weighed into a vial and dissolved in minimal acetonitrile (~40 mL) and quantitatively transferred to the flask. The mixture was heated in a hot water bath at 85 °C for 30 min. The resulting solution was clear, light green. The bulk of the solvent was evaporated by rotary evaporation (220 mbar, 45 °C), followed by further drying under a gentle stream of N₂ gas for 30 min. 3.7506 g of pale yellow solid was recovered (106 % yield based on mass balance).

(3) 1-ethyl-3-methylimidazolium 2,5-dihydroxybenzoate ([EMIM][DHB]): 1.6378 g (9.62 mmol) [EMIM]OAc (viscous, brown liquid) was transferred to a round-bottom flask with a magnetic stir bar. 1.4672 g (9.52 mmol) DHB was dissolved in ~ 40 mL

acetonitrile and transferred to the round bottom flask. The mixture was heated for 30 min in a hot water bath (80 – 85 °C) resulting in a clear, brown solution. The solvent was evaporated by rotary evaporation, leaving 3.0403 g brown, viscous solution (121 % yield). To this product, 10 mL of toluene was added. The resulting mixture was heated in an oil bath (175 °C) and the toluene and acetic acid (azeotrope) distilled at 110 °C by simple distillation. This procedure was repeated seven times until 91 % of the acetic acid was removed (as determined by ^1H NMR). The resulting product was a brown, waxy solid obtained in 101 % yield.

(4) 1-butyl-3-methylimidazolium chloride/ α -cyano-4-hydroxycinnamic acid

([BMIM]Cl-CHCA): 1.3363 g (7.65 mmol) [BMIM]Cl was added to a round-bottom flask. 1.4691 g (7.77 mmol) CHCA was dissolved in ~ 40 mL acetonitrile and transferred to the flask with a magnetic stir bar. The resulting mixture was heated in a hot water bath for 30 min forming a clear, light yellow solution (some undissolved material). Upon removal of the solvent (via rotary evaporation and drying under N_2), 2.7899 g of yellow block crystals were obtained (106 % yield based on mass balance).

(5) 1-ethyl-3-methylimidazolium chloride/ α -cyano-4-hydroxycinnamic acid

([EMIM]Cl-CHCA): 0.4399 g (3.00 mmol) of [EMIM]Cl was transferred to a round-bottom flask along with a magnetic stir bar. 0.5680 g (3.00 mmol) of CHCA was weighed into a vial and transferred to the flask with ~ 20 mL of acetonitrile. The resulting solution was clear yellow. The solvent was removed by rotary evaporation and dried under a gentle stream of N_2 . 1.0381 g of the final yellow solid was obtained in 103 % yield (based on the mass balance).

(6) 1-ethyl-3-methylimidazolium α -cyano-4-hydroxycinnamate ([EMIM][CHCA]):

1.4276 g (8.36 mmol) [EMIM]OAc was added to round-bottom flask with a magnetic stir bar. 1.5807 g (8.35 mmol) CHCA was dissolved in 40 mL acetonitrile and transferred to the flask. The mixture was heated in a hot water bath at 80 °C for 30 min resulting in a clear yellow solution. Rotary evaporation was employed to remove the bulk of the solvent, followed by drying under a gentle stream of N₂ gas. 2.9096 g of viscous, yellow solution was obtained in 116 % yield (as per the mass balance).

(7) Sodium 2,5-Dihydroxybenzoate (NaDHB): NaHCO₃ (0.4989 g, 5.9 mmol) was dissolved in ~20 mL of water to form a clear, colourless solution. An equimolar amount of DHB (0.8910 g, 5.78 mmol) was weighed into a round bottom flask. Aqueous NaHCO₃ was added in small increments with swirling which liberated CO₂ gas, and formed a clear, light brown solution (pH 7 by universal pH indicator). The solution was gently refluxed in an oil bath at ~130 °C for 30 min, followed by the removal of bulk water by simple distillation. The product was dried under a gentle stream of N₂ for 30 min, yielding a beige solid. The solid was suspended in 10 mL of ethyl acetate, sonicated, and suction filtered to remove excess starting material. Upon drying, NaDHB was a pale off-white powder obtained in quantitative yield (1.1408 g).

(8) Sodium α -cyano-4-hydroxycinnamate (NaCHCA): A 20 mL aqueous solution of NaHCO₃ (0.3987 g, 4.74 mmol) was prepared forming a clear, colourless solution. A molar equivalent of CHCA (0.8973 g, 4.74 mmol) was weighed into a round bottom flask. The aqueous NaHCO₃ solution was slowly added with swirling, liberating CO₂ gas and forming a clear, yellow solution (pH 7 by universal pH paper). This solution was

gently refluxed in an oil bath at $\sim 140\text{ }^{\circ}\text{C}$, and the bulk solvent was removed by simple distillation. The remaining thick yellow solution was dried for 30 min under N_2 gas resulting in a yellow powder. The powder was washed with small amounts of ethyl acetate and allowed to dry yielding 1.2633 g of NaCHCA.

Appendix II: ^1H NMR Spectra

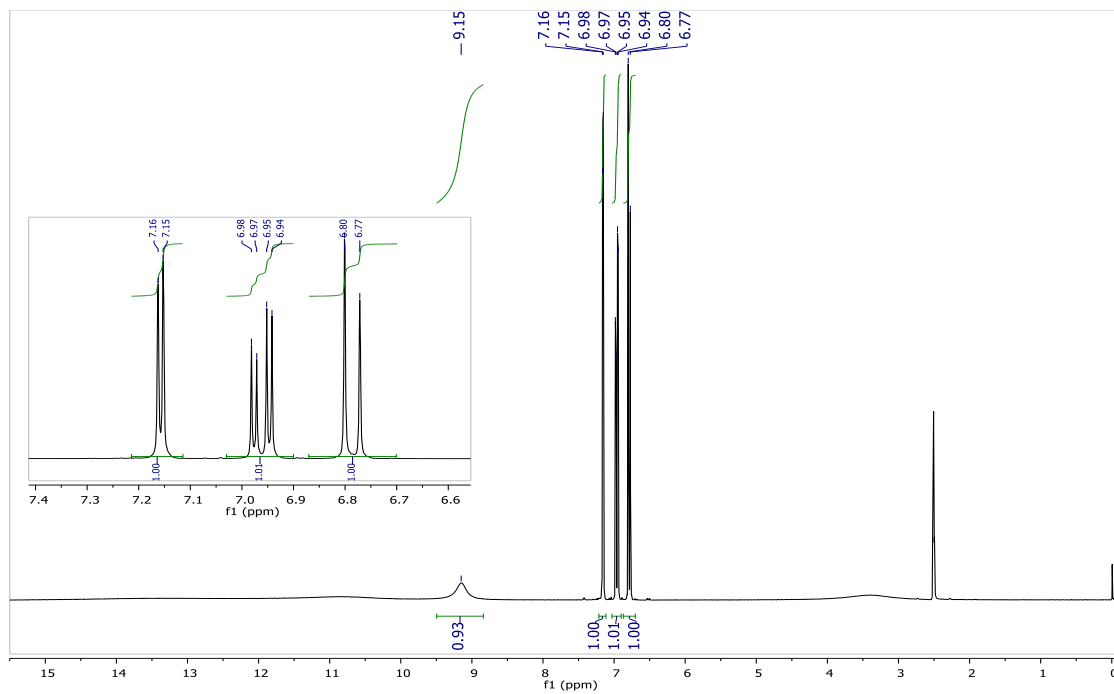


Figure A2-1: ^1H NMR Spectrum of 2,5-dihydroxybenzoic acid (DHB)

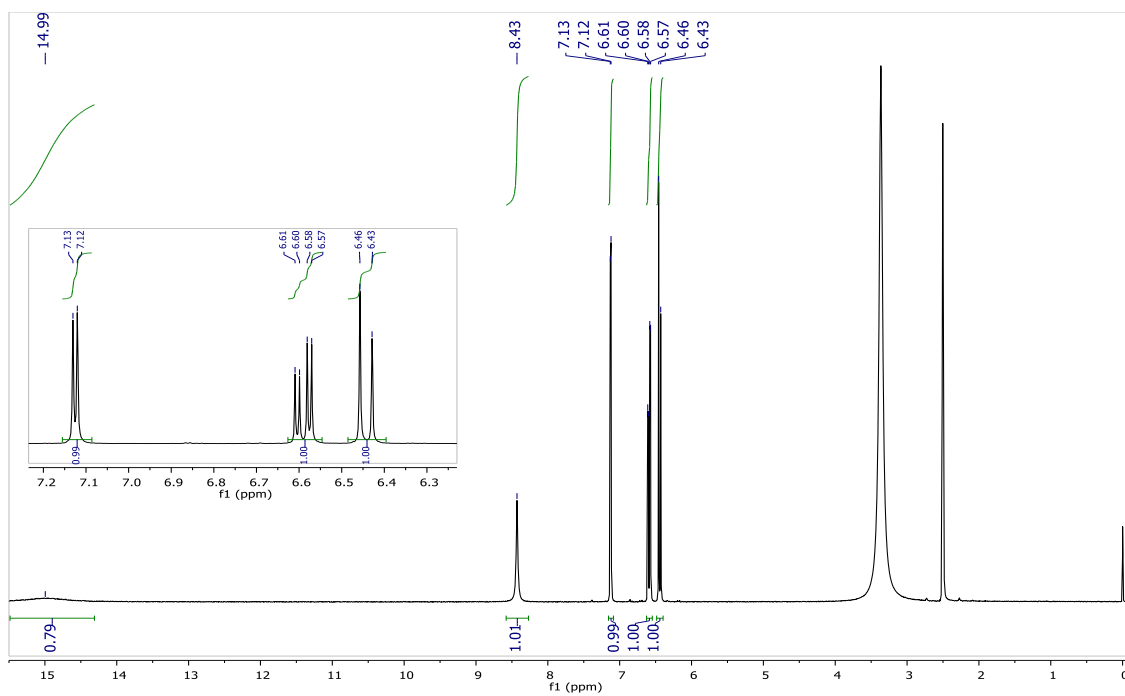


Figure A2-2: ^1H NMR Spectrum of Sodium 2,5-dihydroxybenzoate

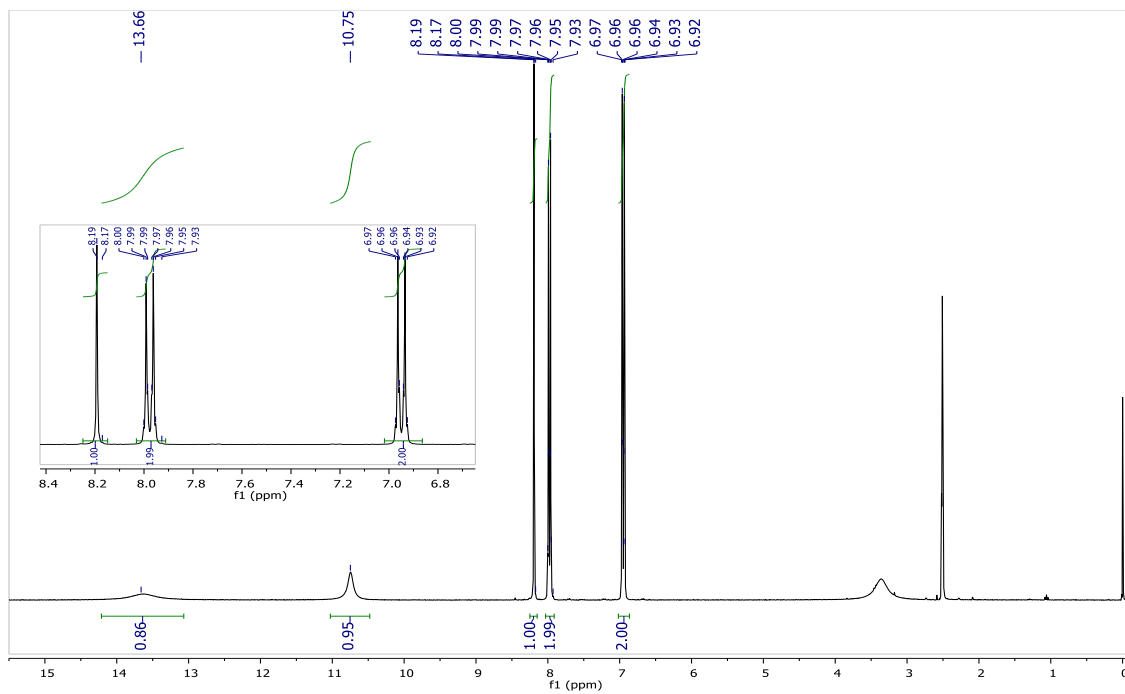


Figure A2-3: ¹H NMR Spectrum of α-cyano-4-hydroxycinnamic acid (CHCA)

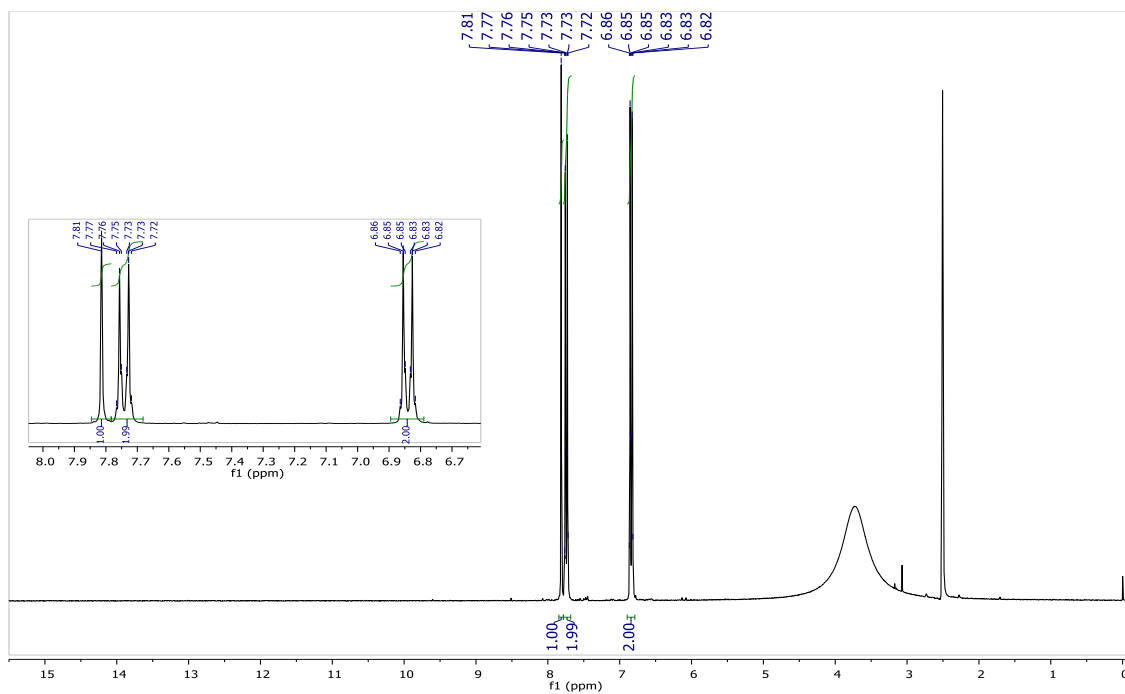


Figure A2-4: ¹H NMR Spectrum of Sodium α-cyano-4-hydroxycinnamate (NaCHCA)

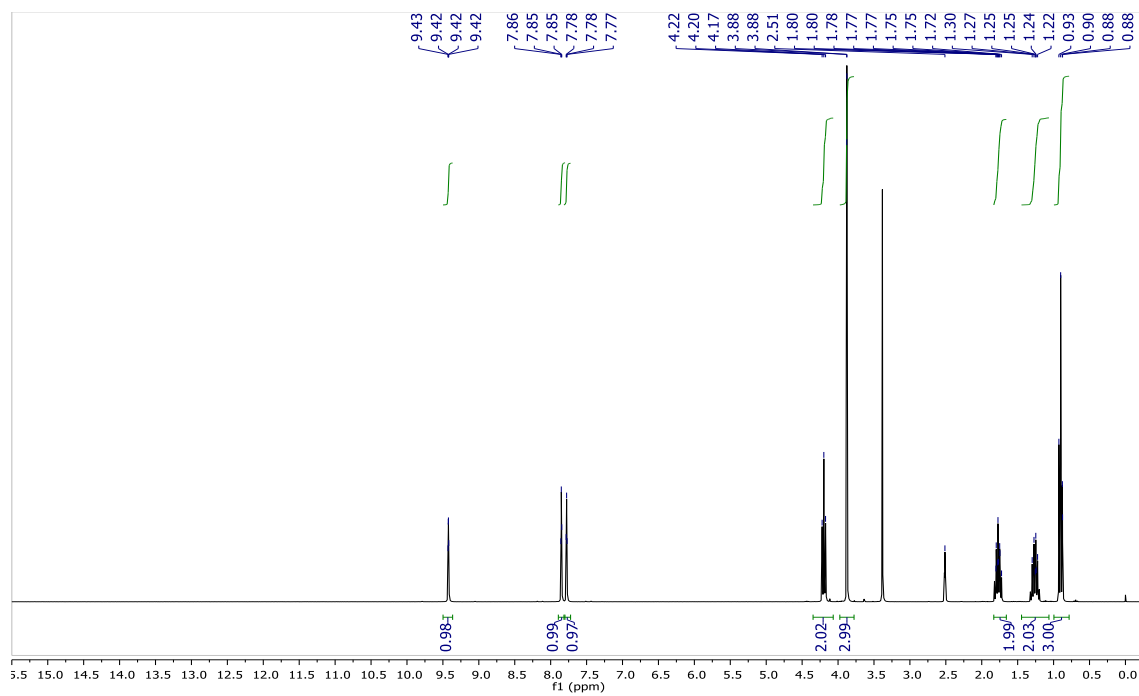


Figure A2-5: ^1H NMR Spectrum of 1-butyl-3-methylimidazolium chloride ([BMIM]Cl)

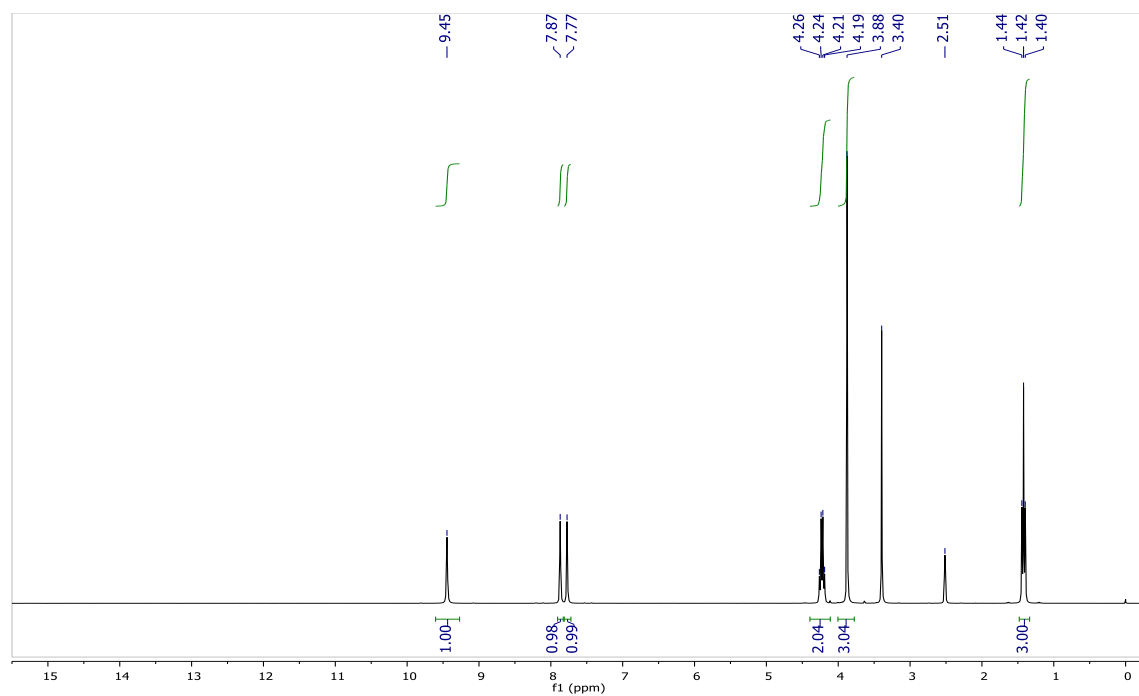


Figure A2-6: ^1H NMR Spectrum of 1-ethyl-3-methylimidazolium chloride ([EMIM]Cl)

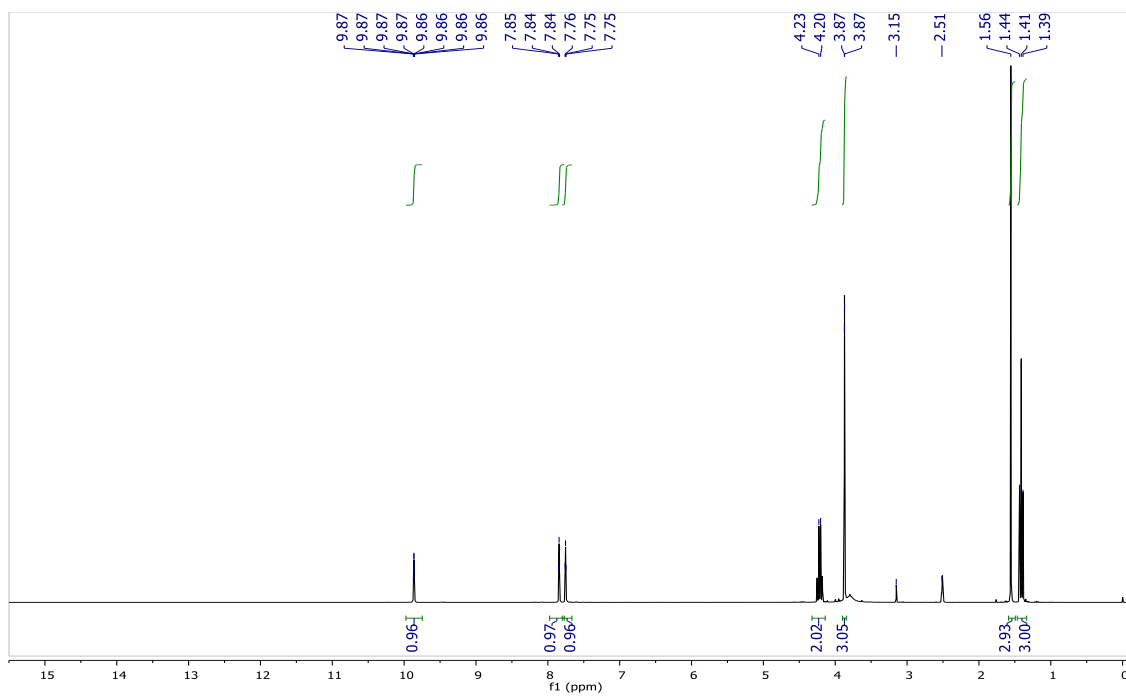


Figure A2-7: ^1H NMR Spectrum of 1-ethyl-3-methylimidazolium acetate ([EMIM]OAc)

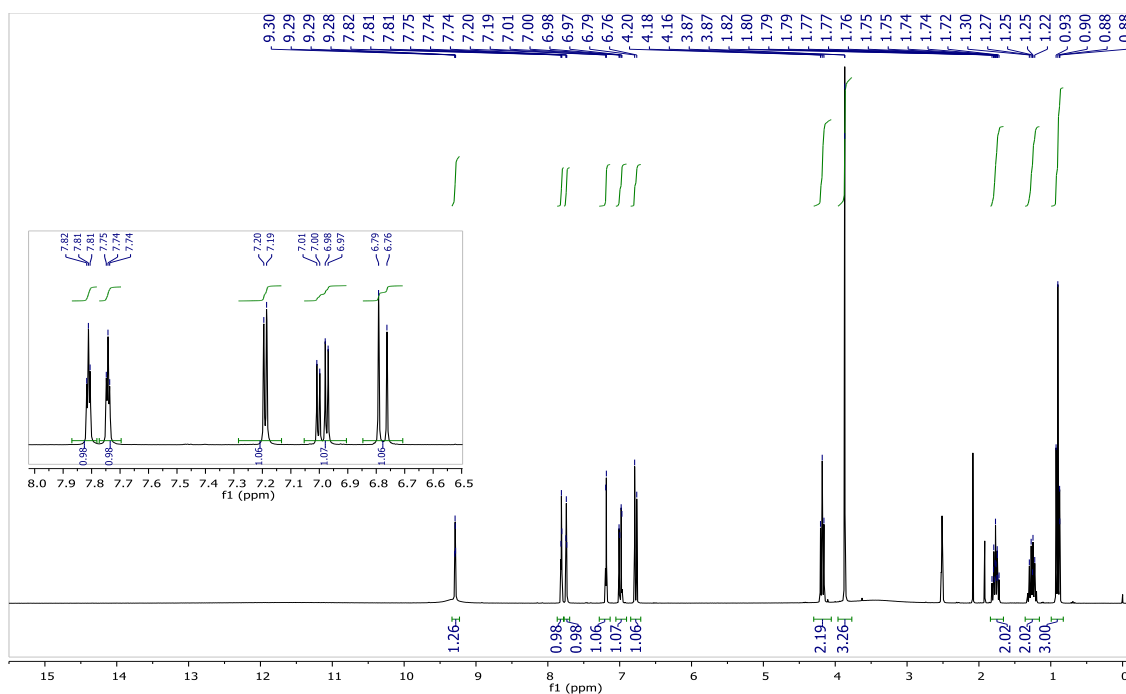


Figure A2-8: ^1H NMR Spectrum of 1-butyl-3-methylimidazolium chloride/2,5-dihydroxybenzoic acid ([BMIM]Cl-DHB)

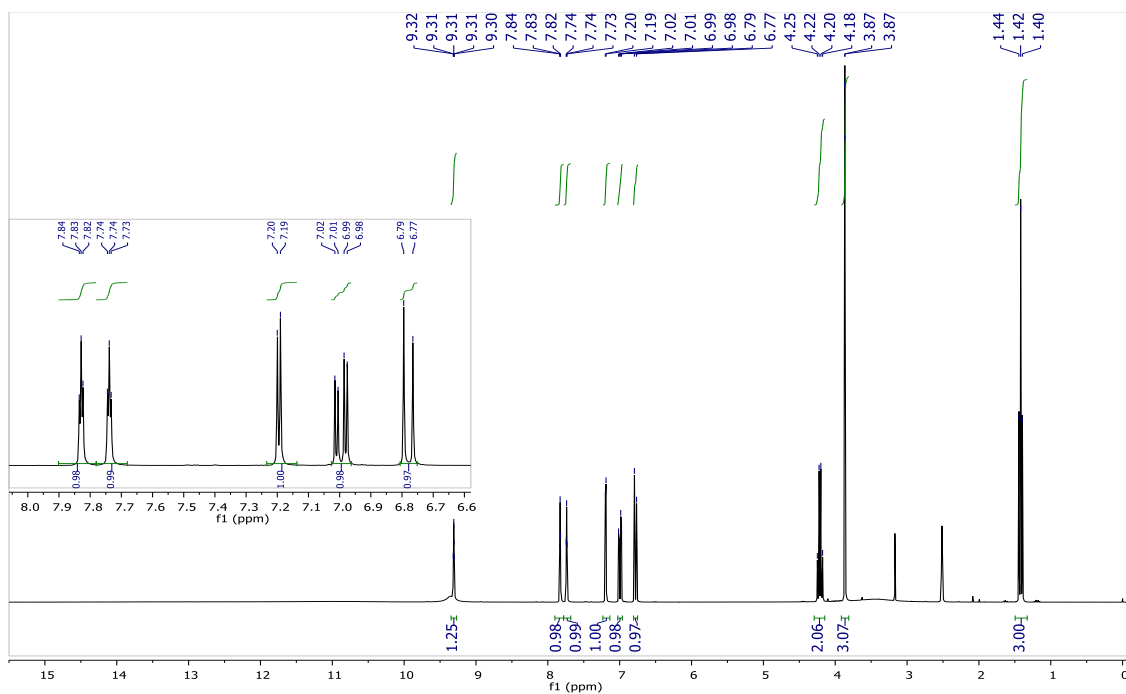


Figure A2-9: ^1H NMR Spectrum of 1-ethyl-3-methylimidazolium chloride/2,5-dihydroxybenzoic acid ([EMIM]Cl-DHB)

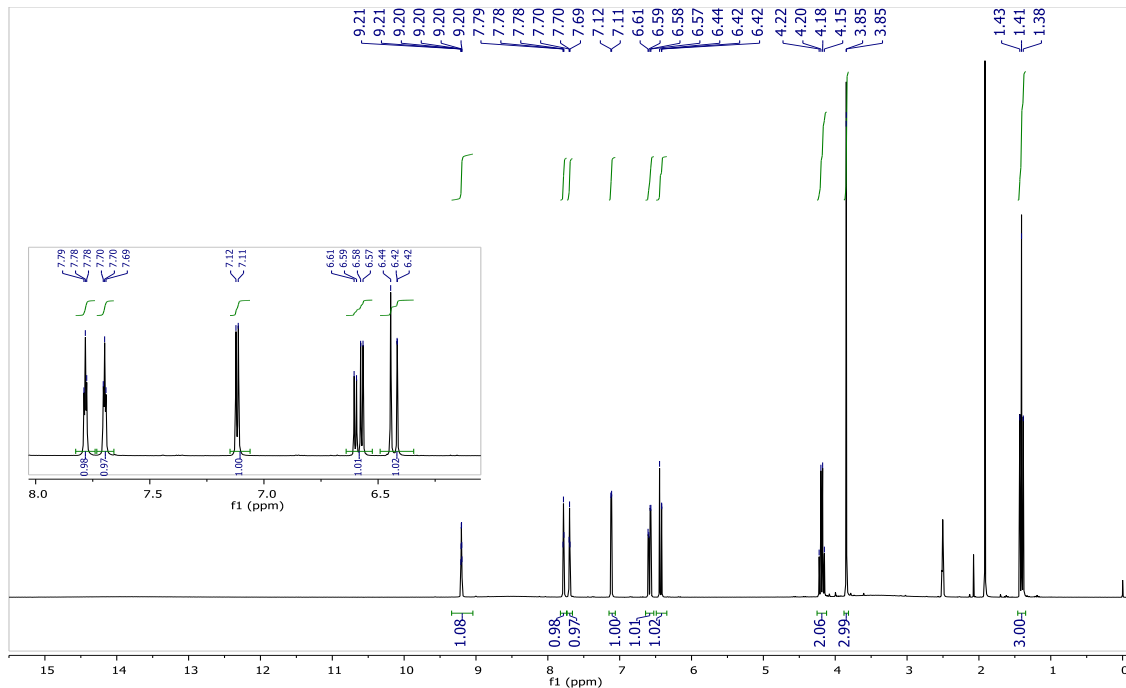


Figure A2-10: ^1H NMR Spectrum of 1-ethyl-3-methylimidazolium 2,5-dihydroxybenzoate ([EMIM][DHB])

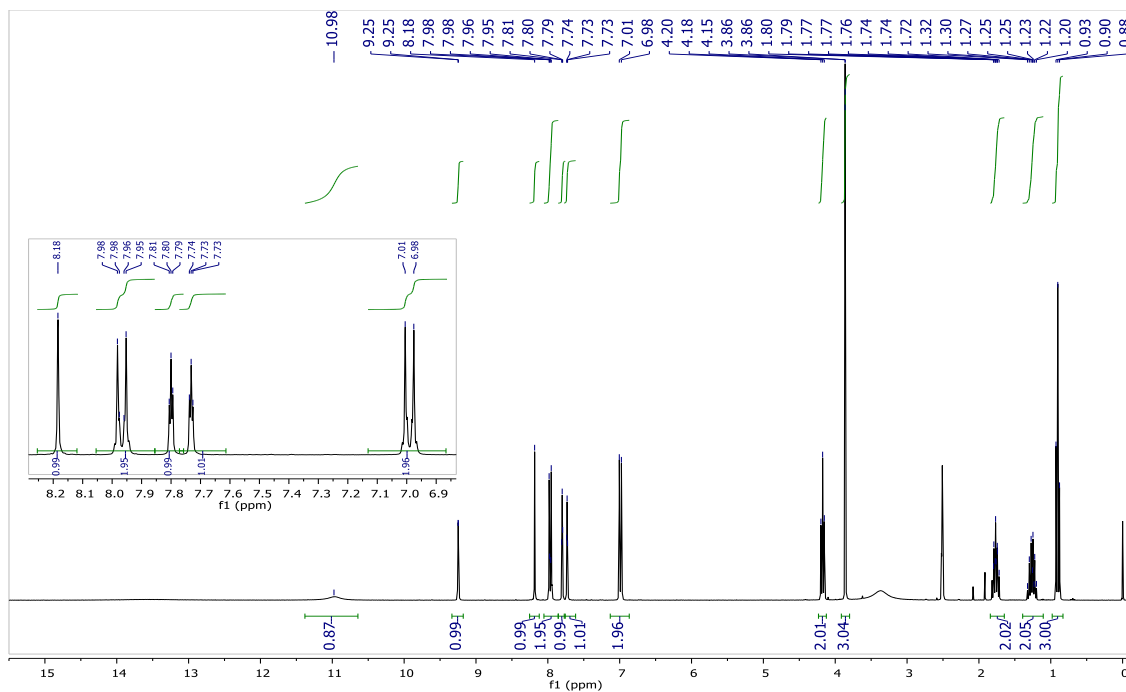


Figure A2-11: ^1H NMR Spectrum of 1-butyl-3-methylimidazolium chloride/ α -cyano-4-hydroxycinnamic acid ([BMIM]Cl-CHCA)

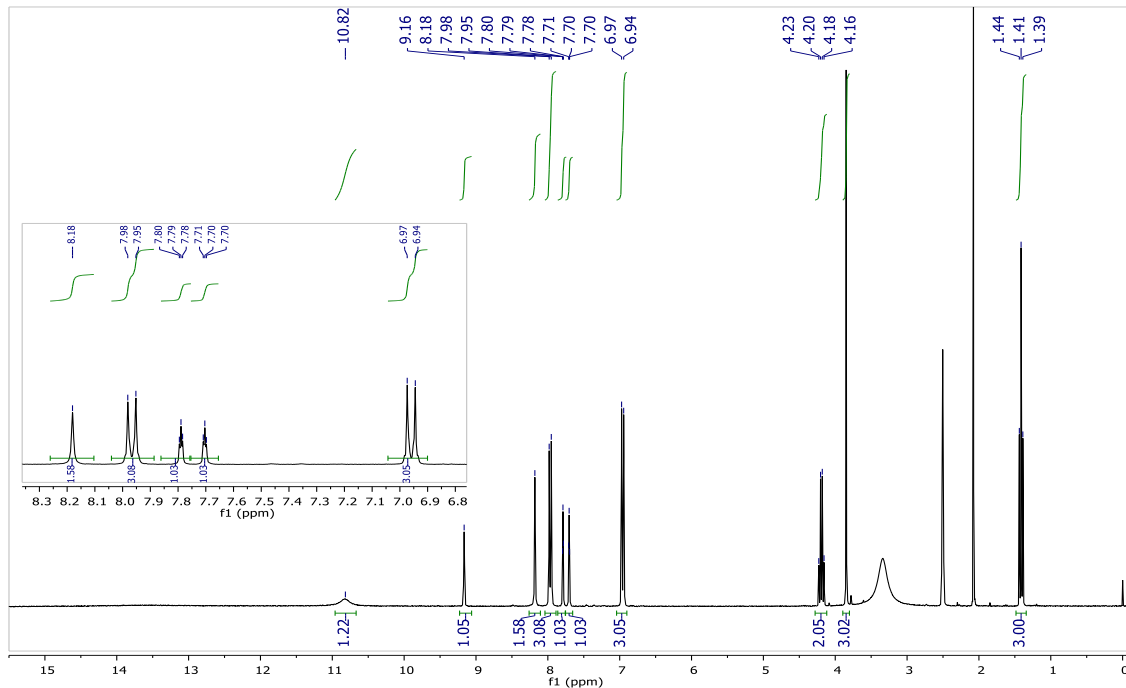


Figure A2-12: ^1H NMR Spectrum of 1-ethyl-3-methylimidazolium chloride/ α -cyano-4-hydroxycinnamic acid ([EMIM]Cl-CHCA)

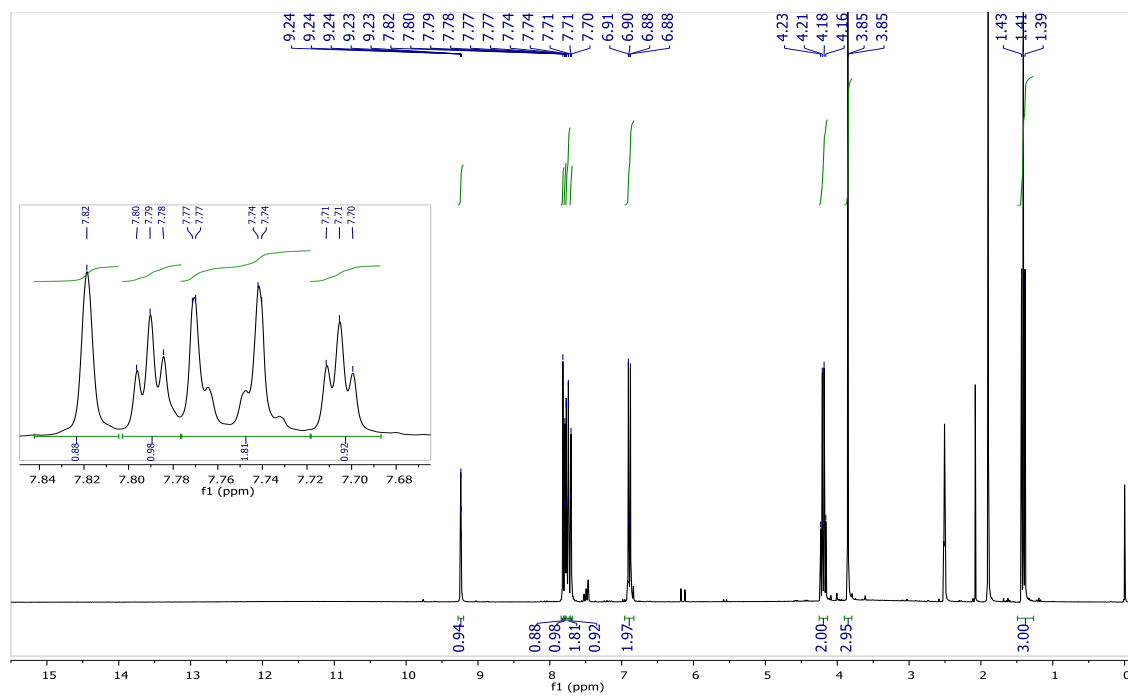


Figure A2-13: ¹H NMR Spectrum of 1-ethyl-3-methylimidazolium α-cyano-4-hydroxycinnamate ([EMIM][CHCA])

Appendix III: ^{13}C NMR Spectra

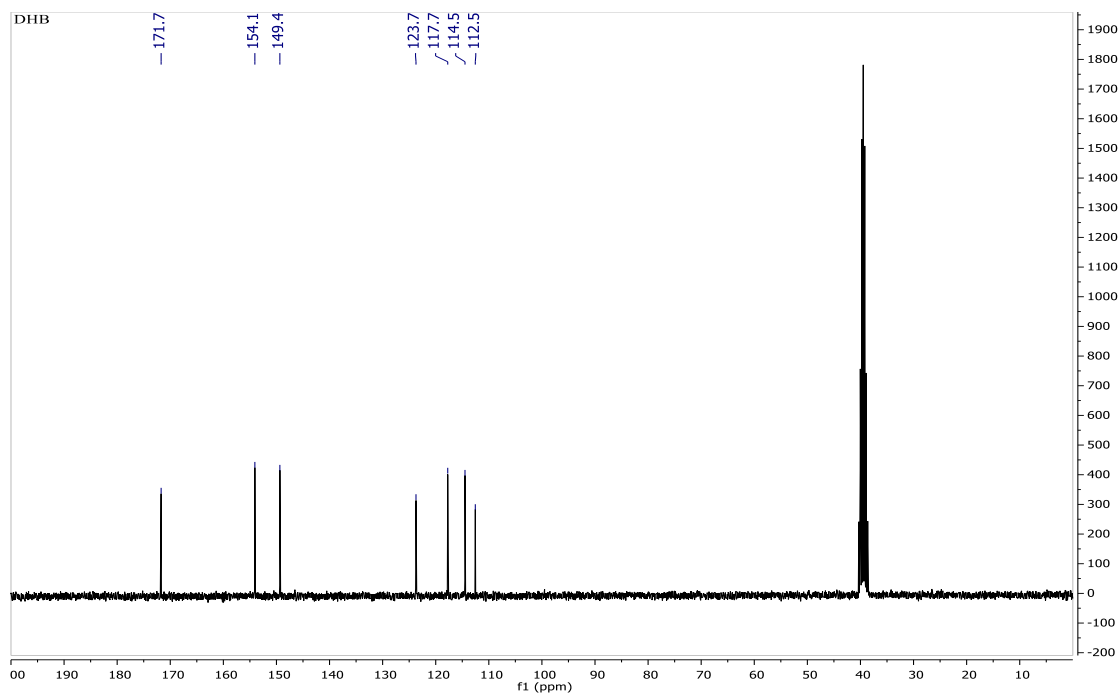


Figure A3-1: ¹³C NMR Spectrum of 2,5-dihydroxybenzoic acid (DHB)

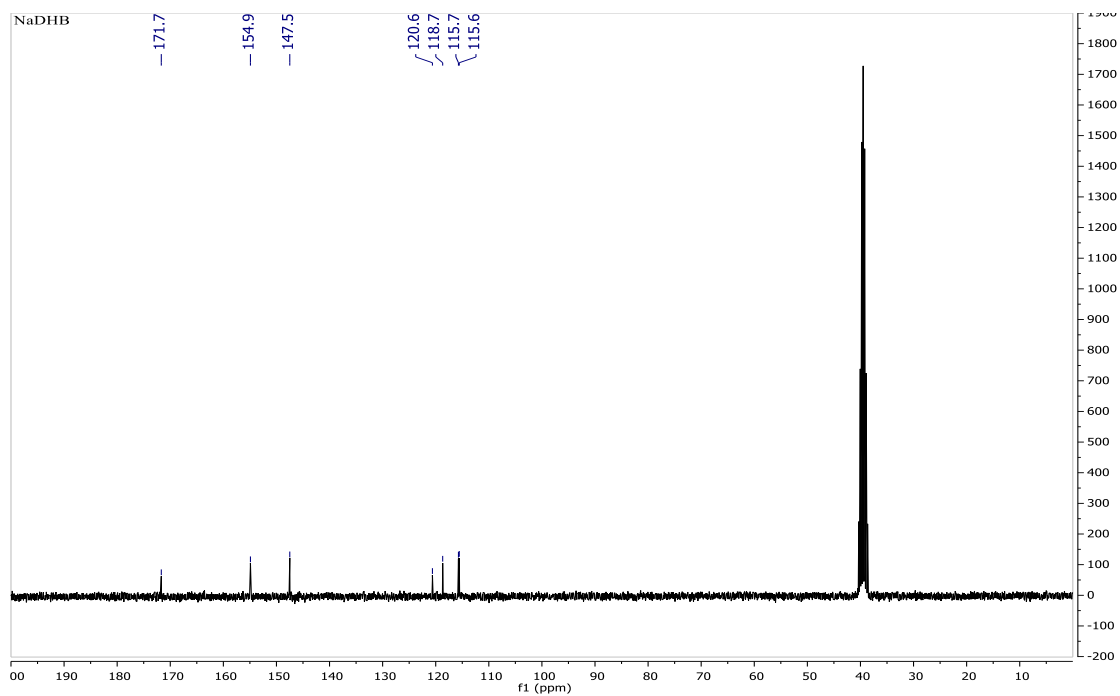


Figure A3-2: ¹³C NMR Spectrum of Sodium 2,5-dihydroxybenzoate (NaDHB)

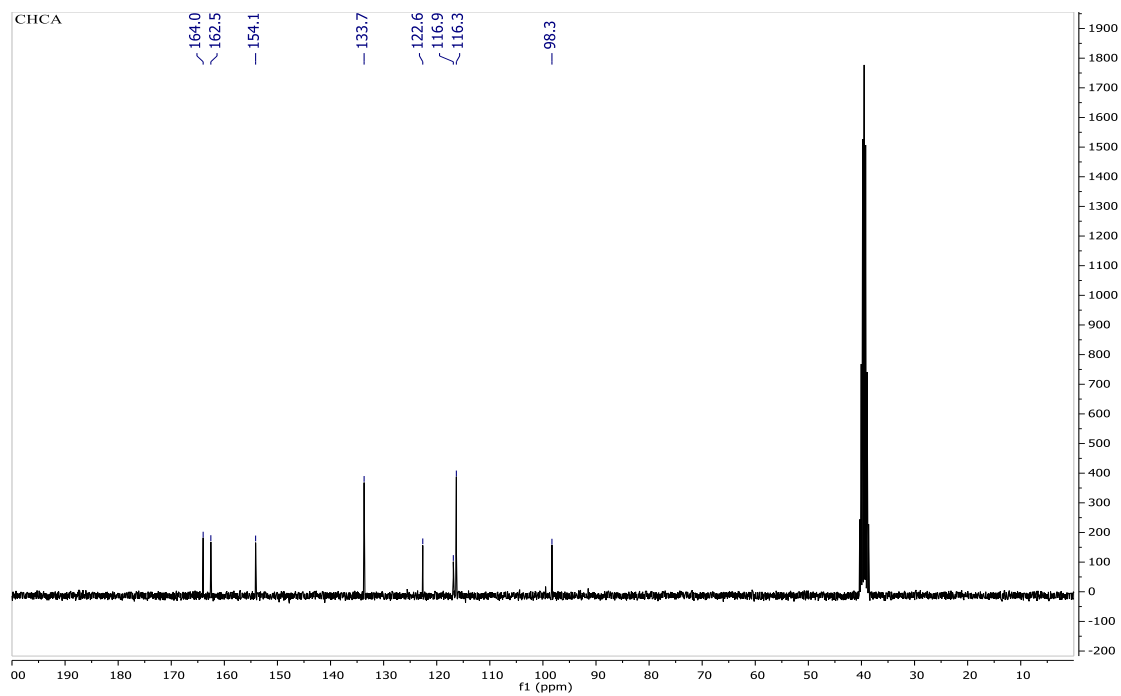


Figure A3-3: ^{13}C NMR Spectrum of α -cyano-4-hydroxycinnamic acid (CHCA)

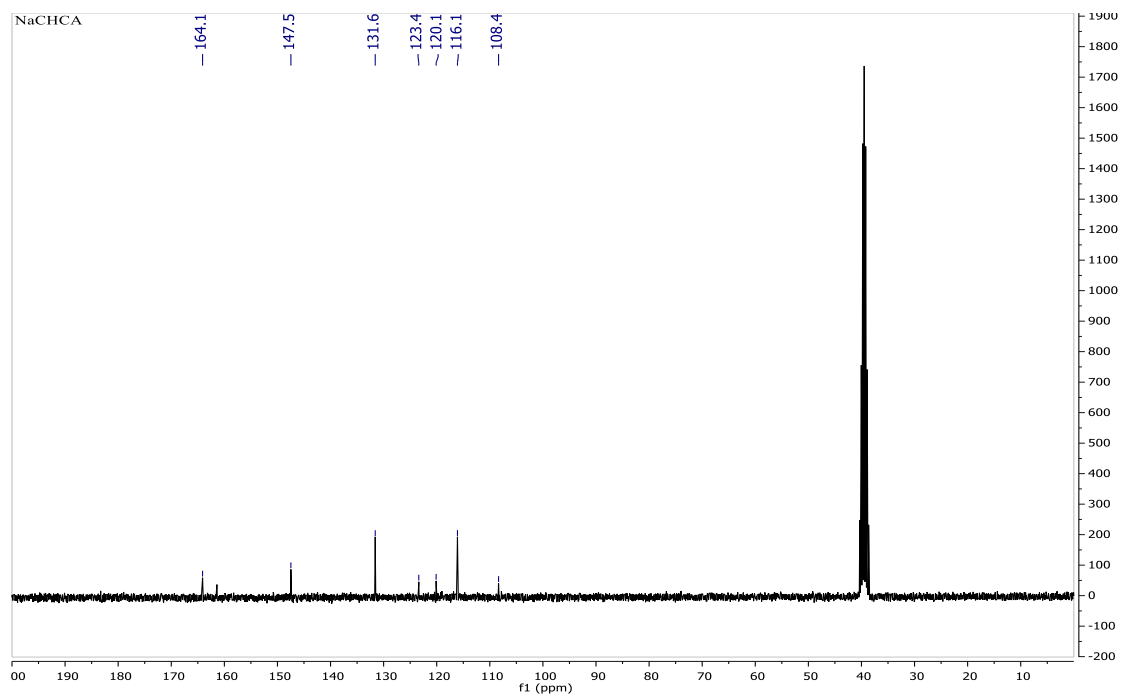


Figure A3-4: ^{13}C NMR Spectrum of Sodium α -cyano-4-hydroxycinnamate (NaCHCA)

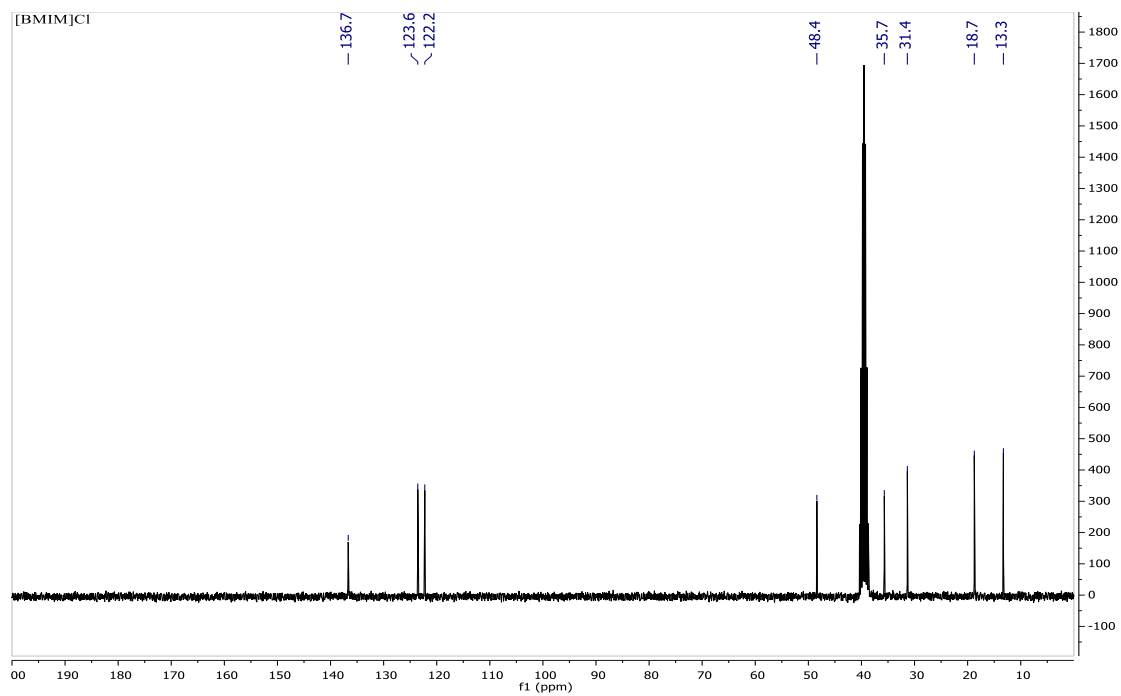


Figure A3-5: ¹³C NMR Spectrum of 1-butyl-3-methylimidazolium chloride ([BMIM]Cl)

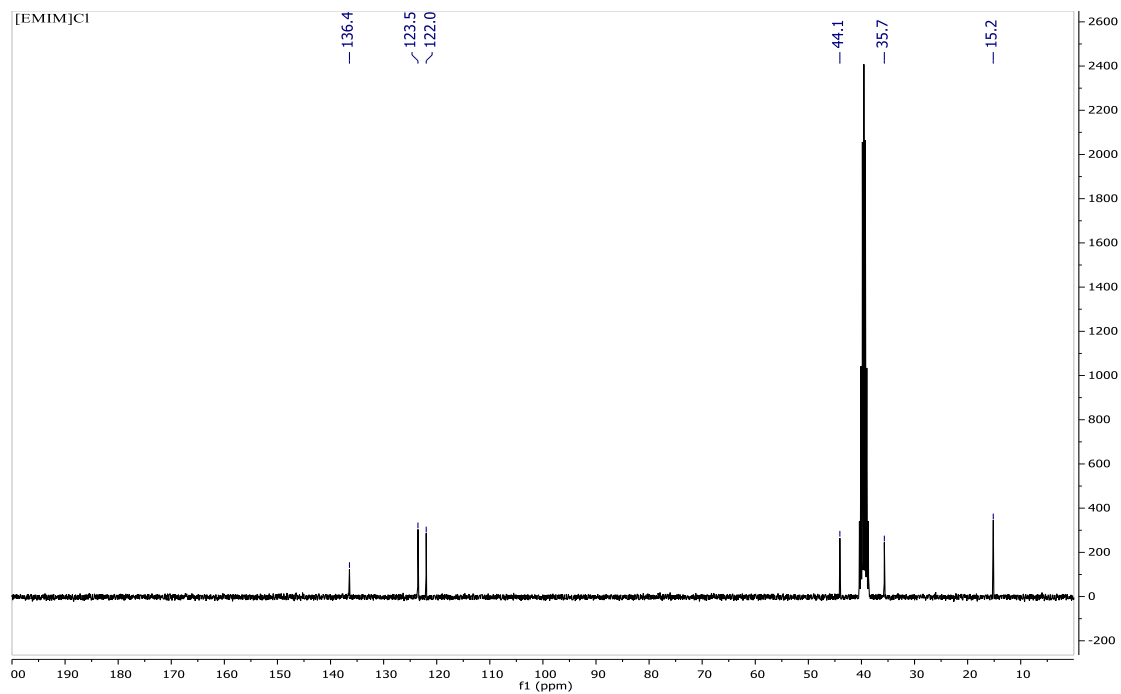


Figure A3-6: ¹³C NMR Spectrum of 1-ethyl-3-methylimidazolium chloride ([EMIM]Cl)

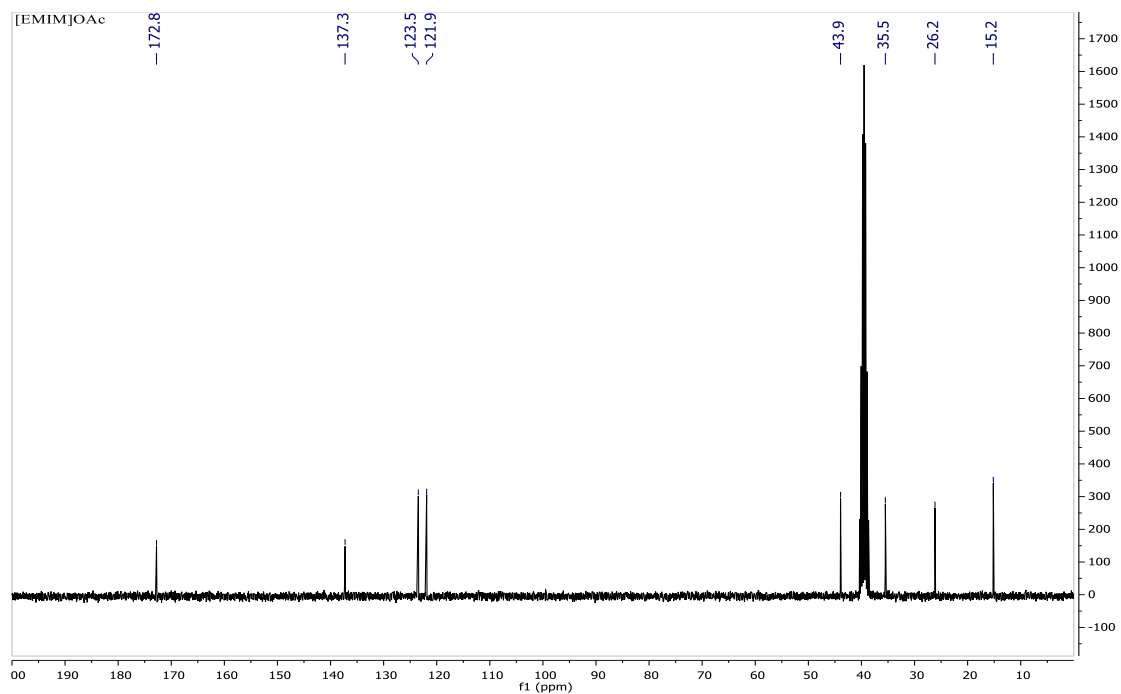


Figure A3-7: ^{13}C NMR Spectrum of 1-ethyl-3-methylimidazolium acetate ([EMIM]OAc)

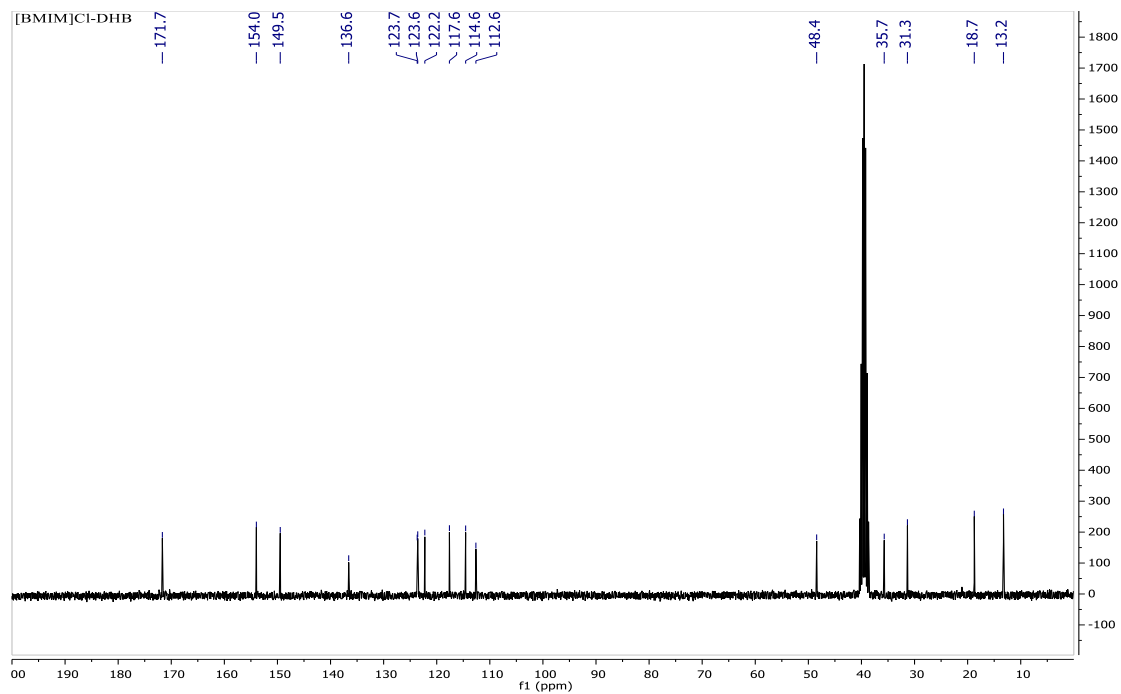


Figure A3-8: ^{13}C NMR Spectrum of 1-butyl-3-methylimidazolium chloride/2,5-dihydroxybenzoic acid ([BMIM]Cl-DHB)

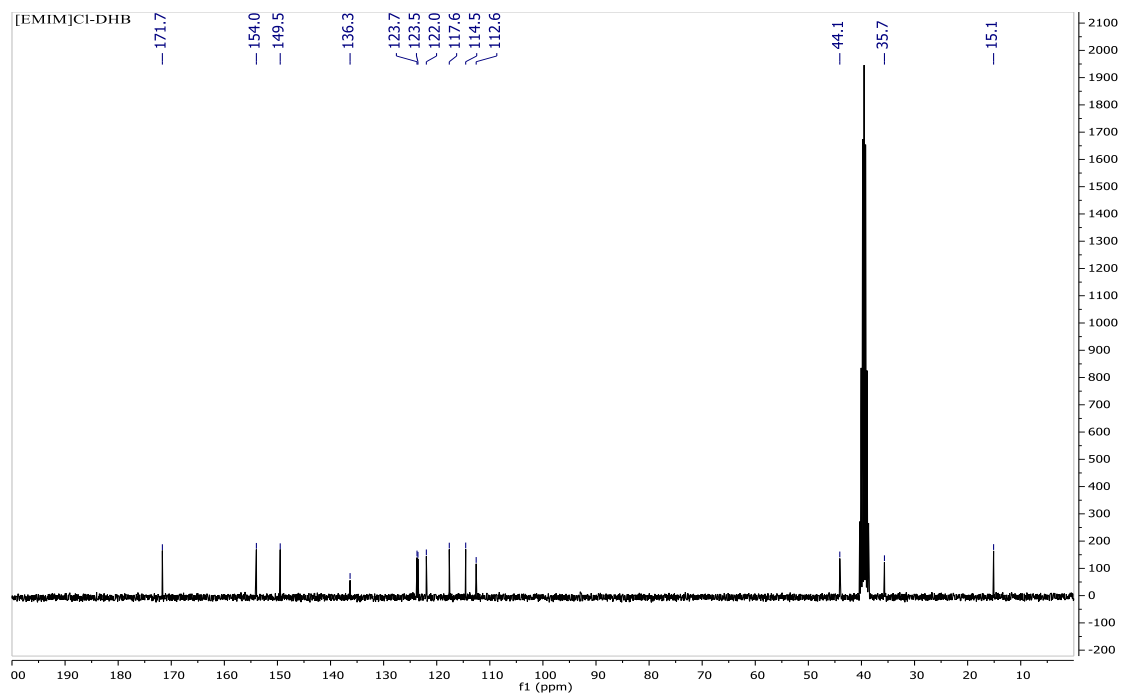


Figure A3-9: ^{13}C NMR Spectrum of 1-ethyl-3-methylimidazolium chloride/2,5-dihydroxybenzoic acid ([EMIM]Cl-DHB)

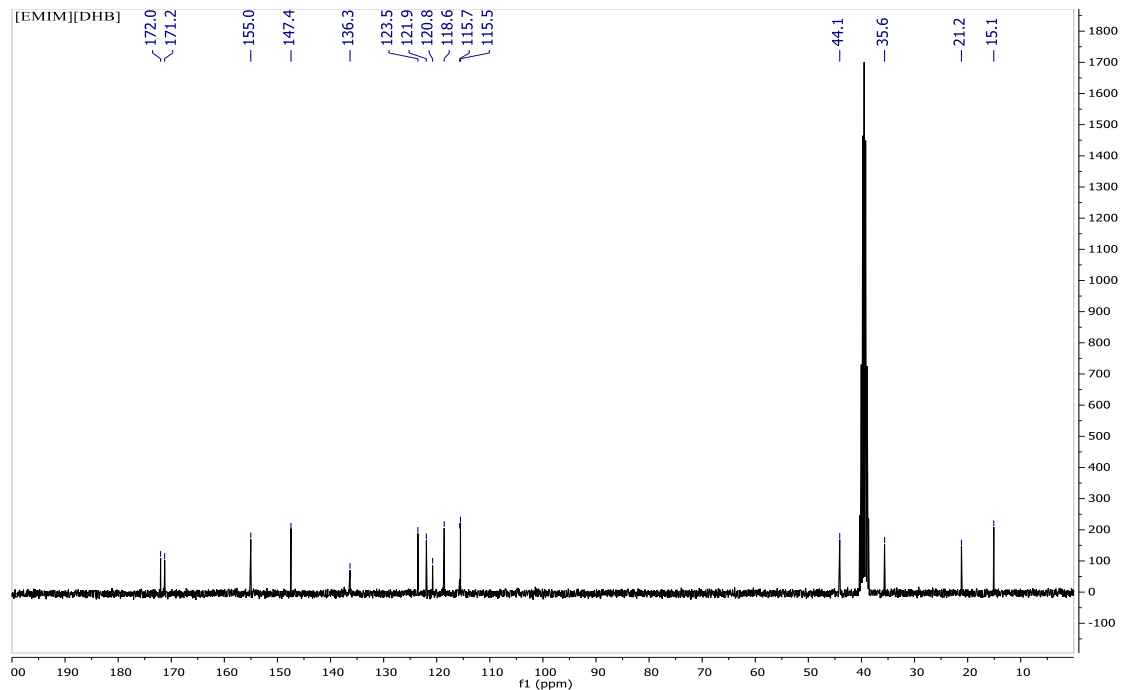


Figure A3-10: ^{13}C NMR Spectrum of 1-ethyl-3-methylimidazolium 2,5-dihydroxybenzoate ([EMIM][DHB])

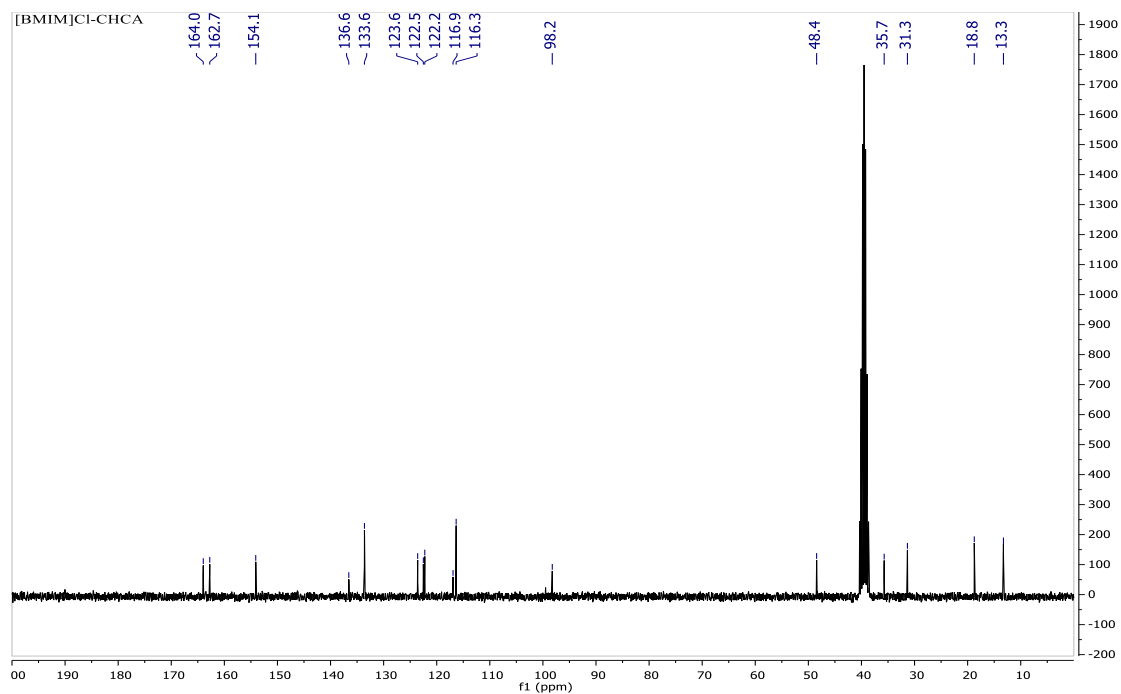


Figure A3-11: ^{13}C NMR Spectrum of 1-butyl-3-methylimidazolium chloride/ α -cyano-4-hydroxycinnamic acid ([BMIM]Cl-CHCA)

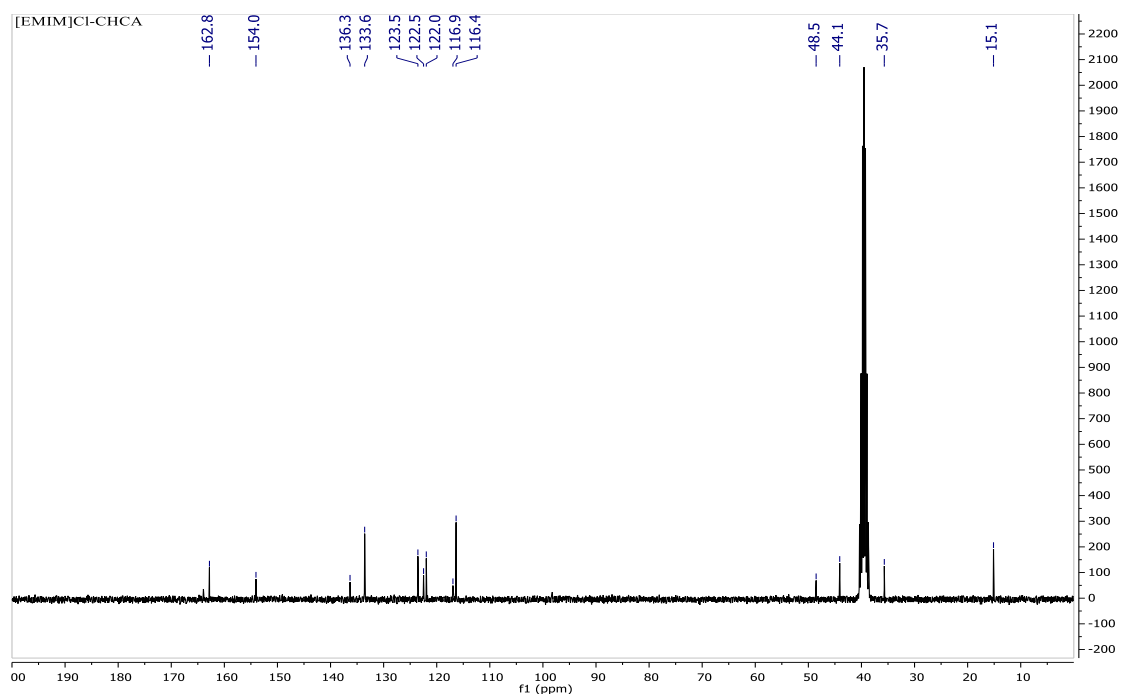


Figure A3-12: ^{13}C NMR Spectrum of 1-ethyl-3-methylimidazolium chloride/ α -cyano-4-hydroxycinnamic acid ([EMIM]Cl-CHCA)

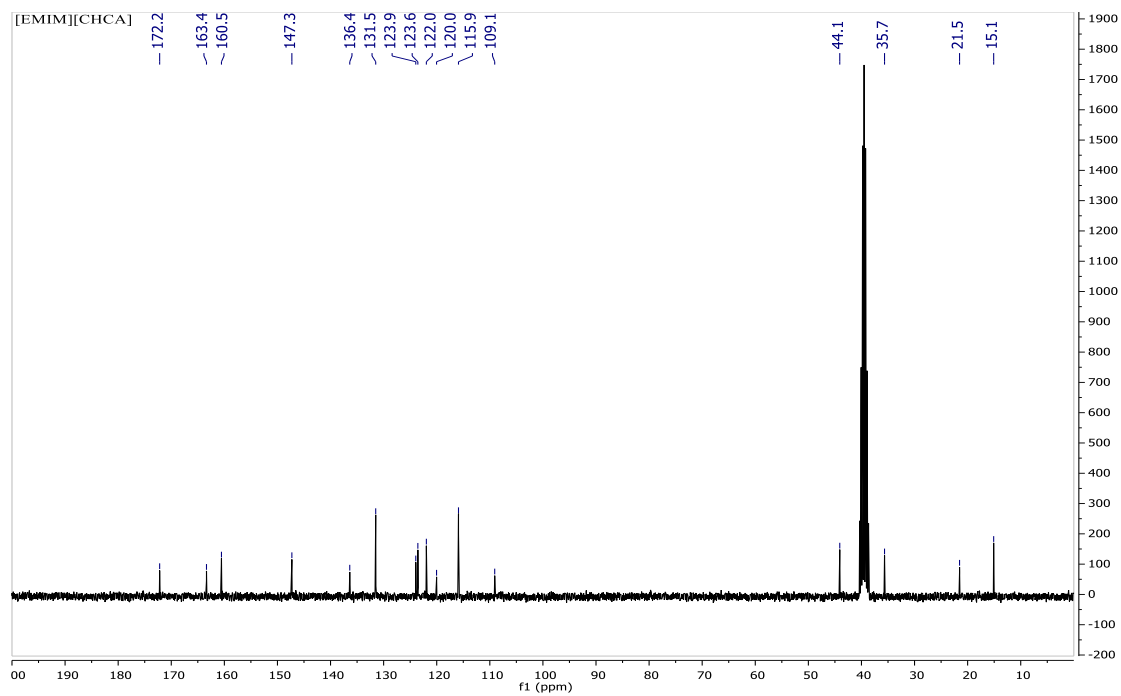


Figure A3-13: ^{13}C NMR Spectrum of 1-ethyl-3-methylimidazolium α -cyano-4-hydroxycinnamate ([EMIM][CHCA])

Appendix IV: FT-IR Spectra

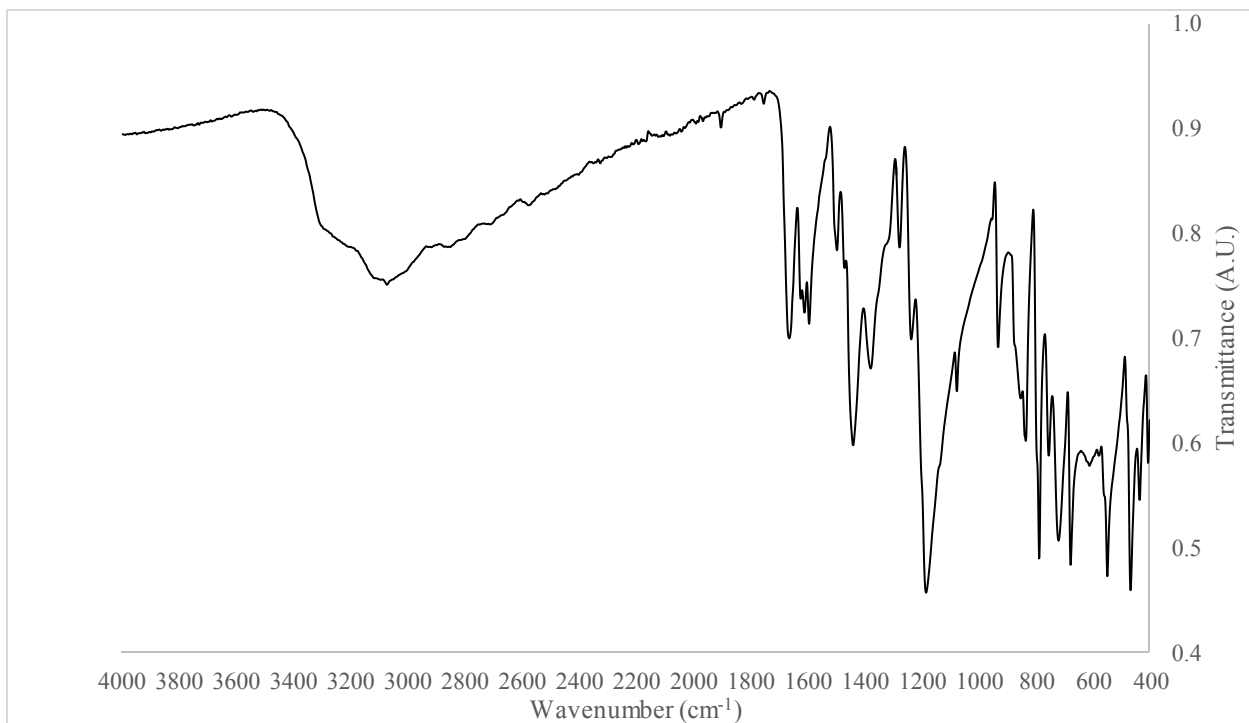


Figure A4-1: FT-IR Spectrum of Sodium 2,5-dihydroxybenzoic acid (DHB)

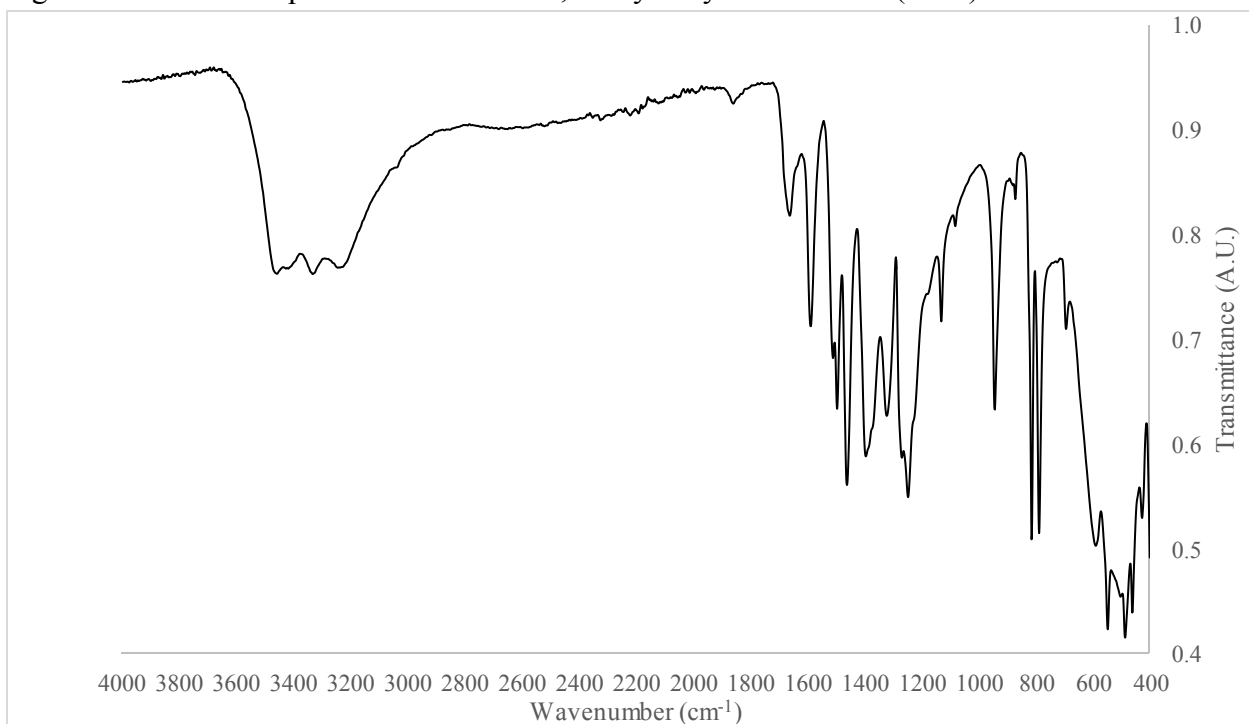


Figure A4-2: FT-IR Spectrum Sodium of 2,5-dihydroxybenzoate (NaDHB)

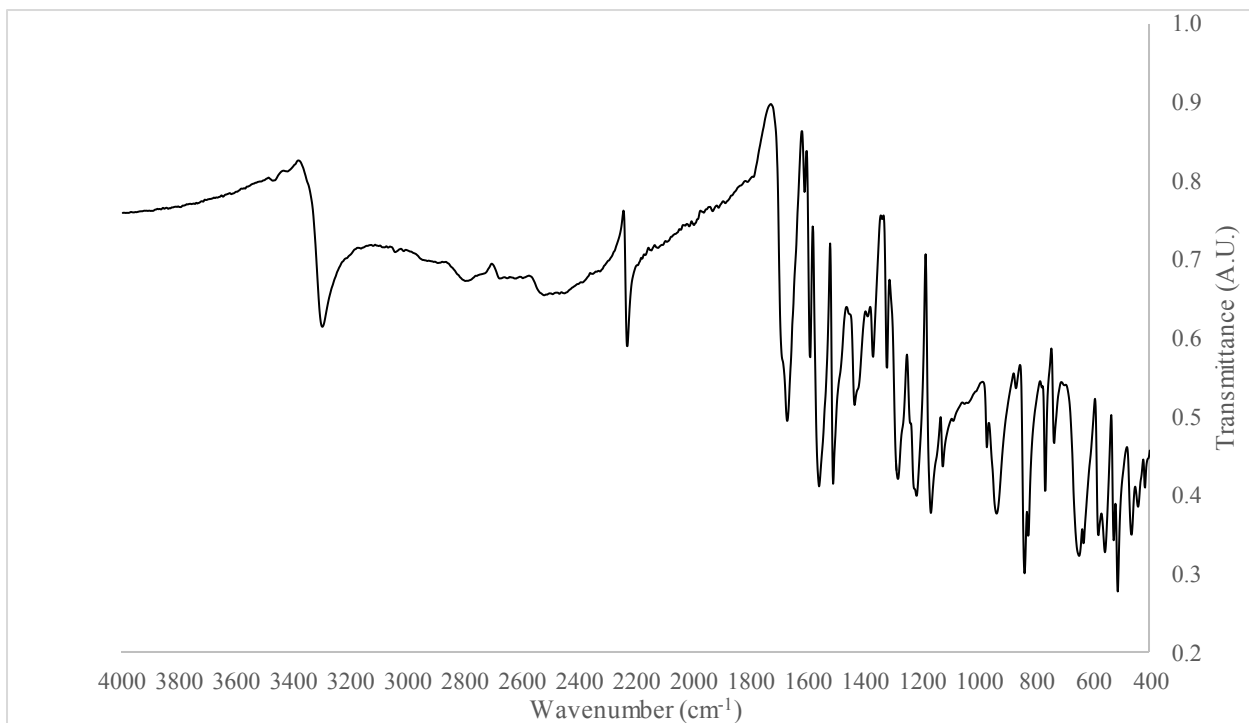


Figure A4-3: FT-IR Spectrum of α -cyano-4-hydroxycinnamic acid (CHCA)

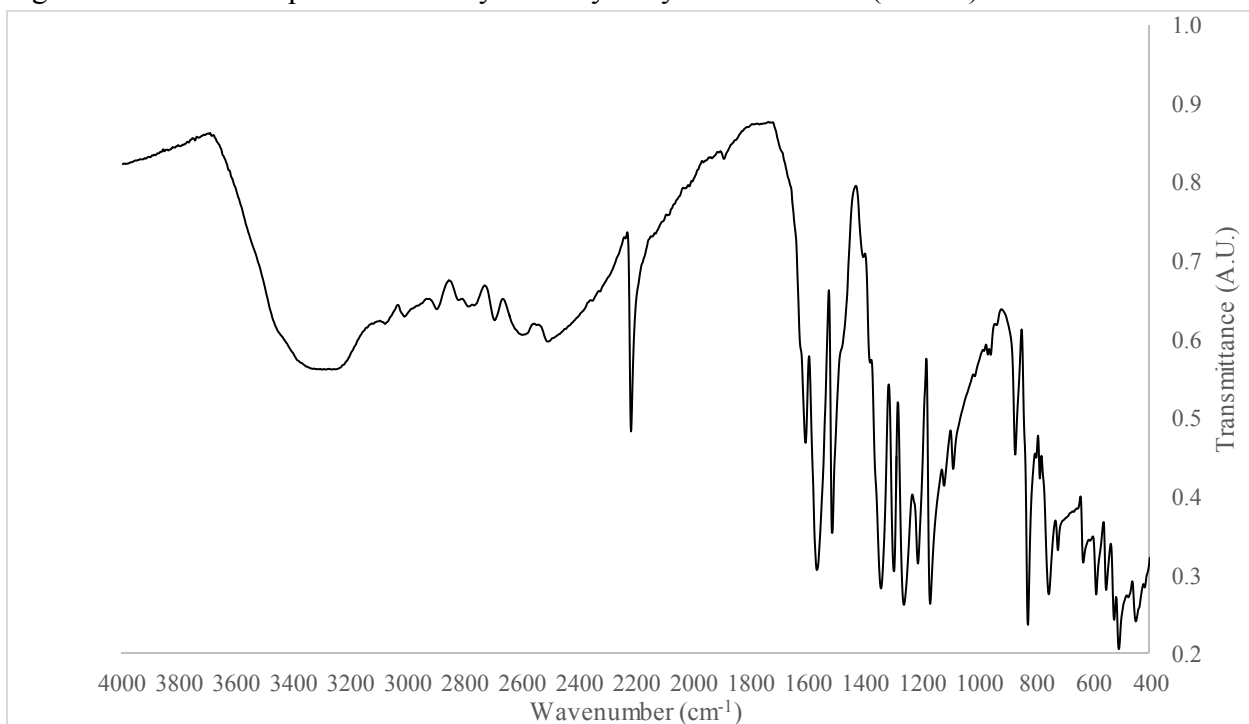


Figure A4-4: FT-IR Spectrum of Sodium α -cyano-4-hydroxycinnamate (NaCHCA)

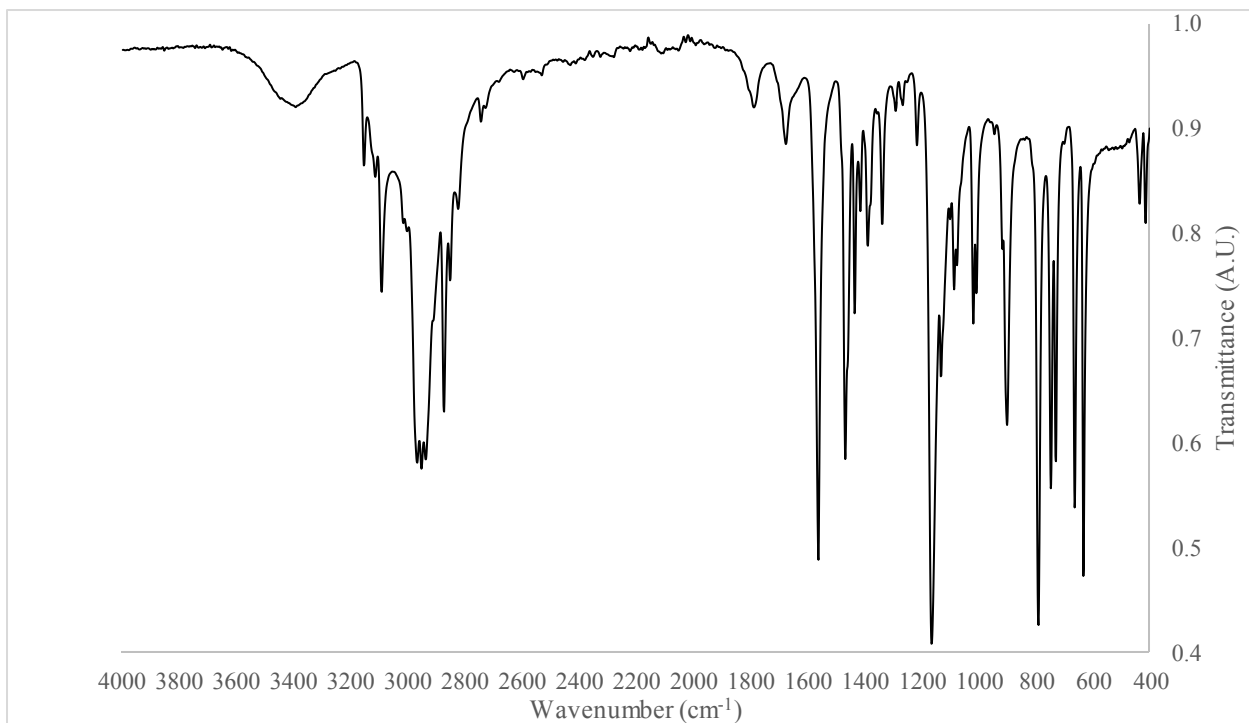


Figure A4-5: FT-IR Spectrum of 1-butyl-3-methylimidazolium chloride ([BMIM]Cl)

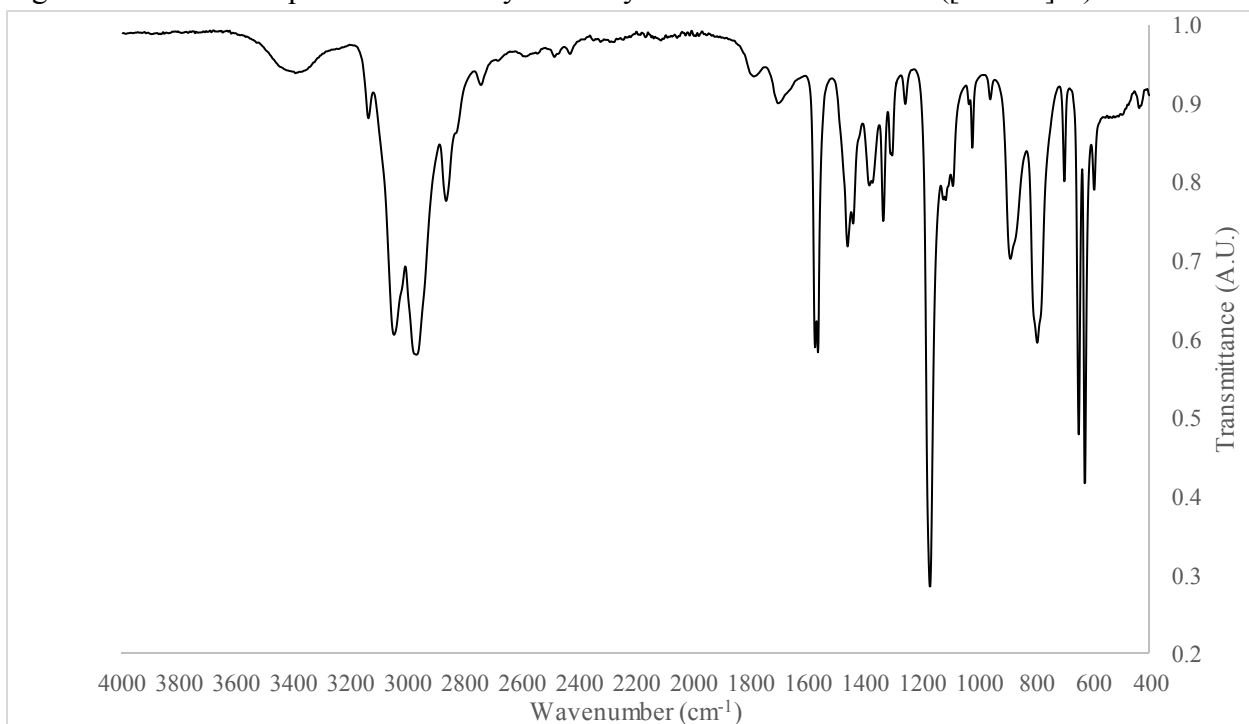


Figure A4-6: FT-IR Spectrum of 1-ethyl-3-methylimidazolium chloride ([EMIM]Cl)

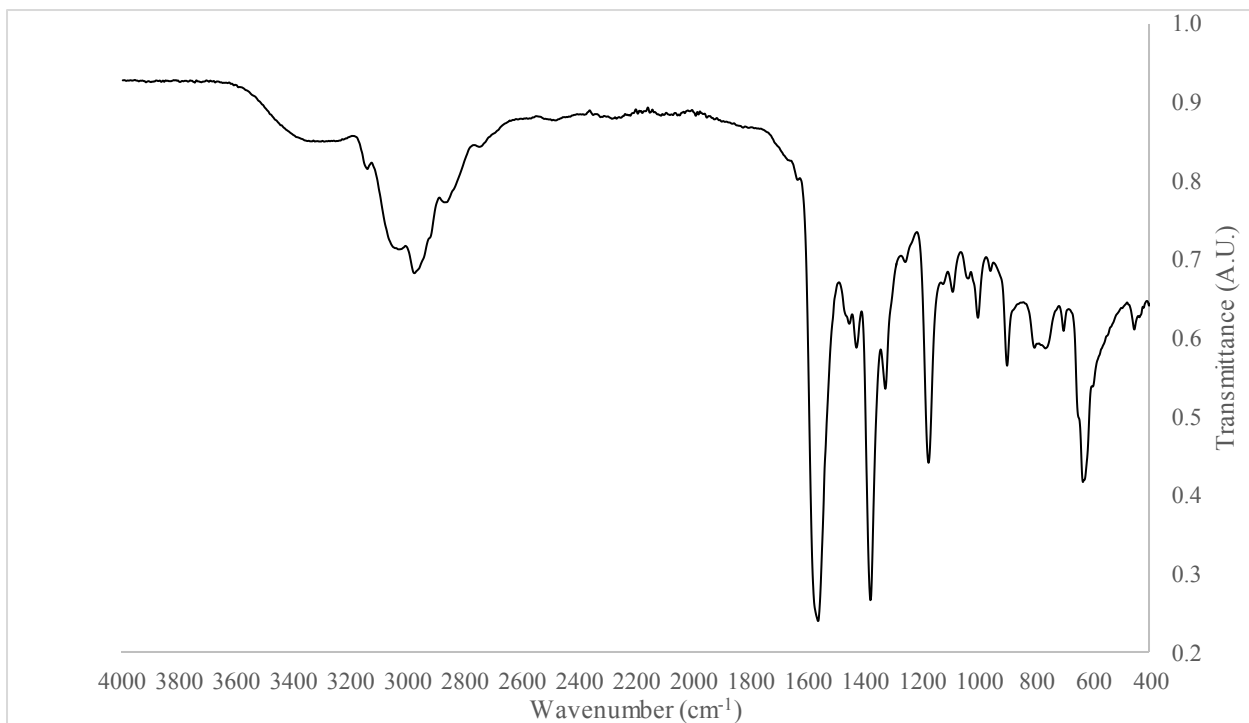


Figure A4-7: FT-IR Spectrum of 1-ethyl-3-methylimidazolium acetate ([EMIM]OAc)

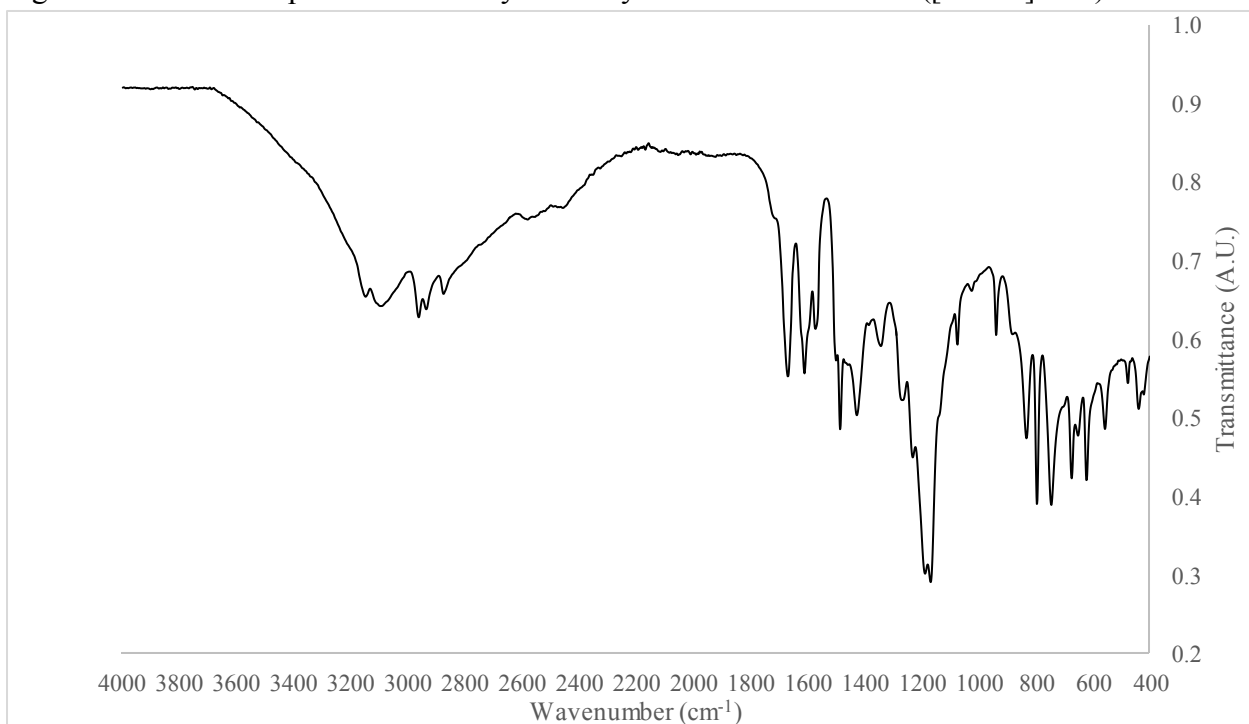


Figure A4-8: FT-IR Spectrum of 1-butyl-3-methylimidazolium chloride/2,5-dihydroxybenzoic acid ([BMIM]Cl-DHB)

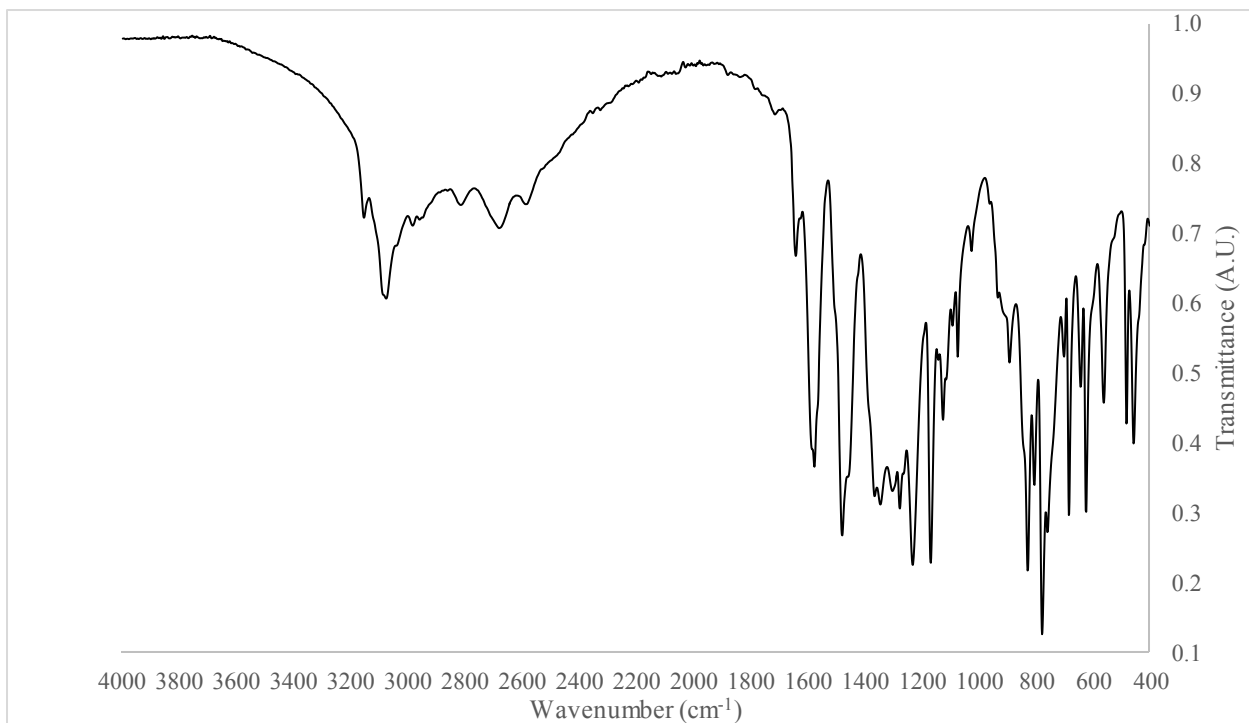


Figure A4-9: FT-IR Spectrum of 1-ethyl-3-methylimidazolium chloride/2,5-dihydroxybenzoic acid ([EMIM][Cl-DHB])

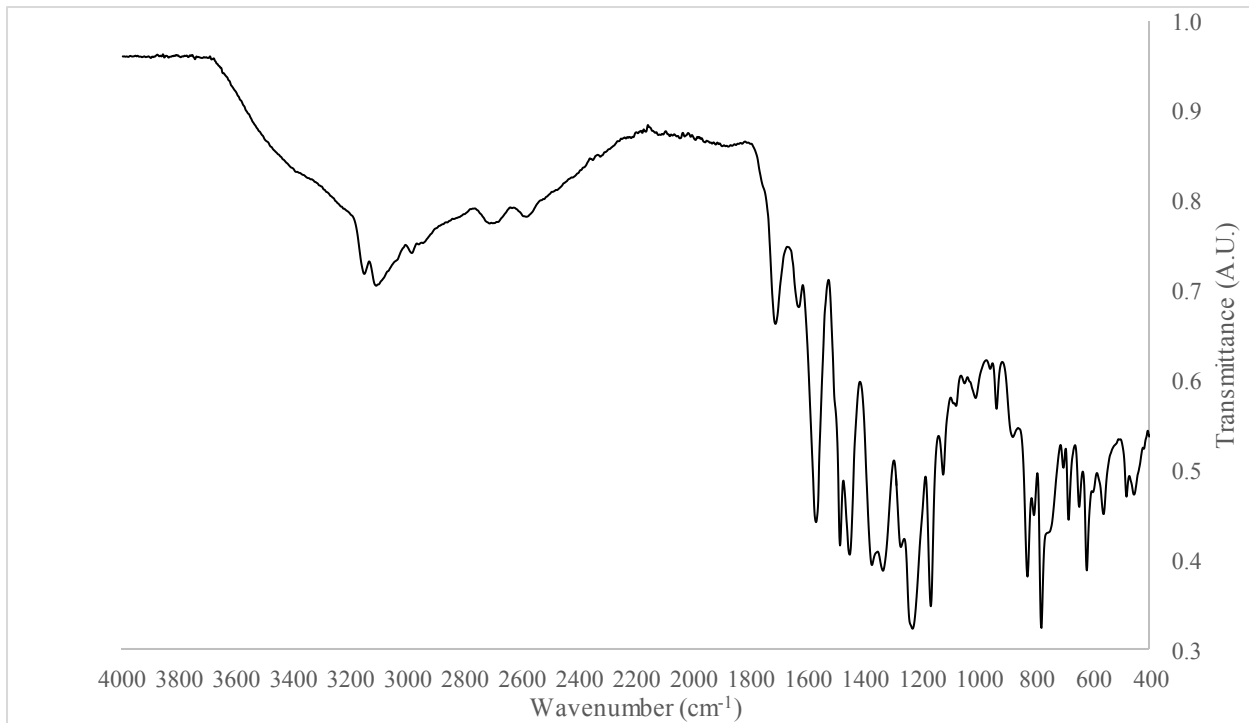


Figure A4-10: FT-IR Spectrum of 1-ethyl-3-methylimidazolium 2,5-dihydroxybenzoate ([EMIM][DHB])

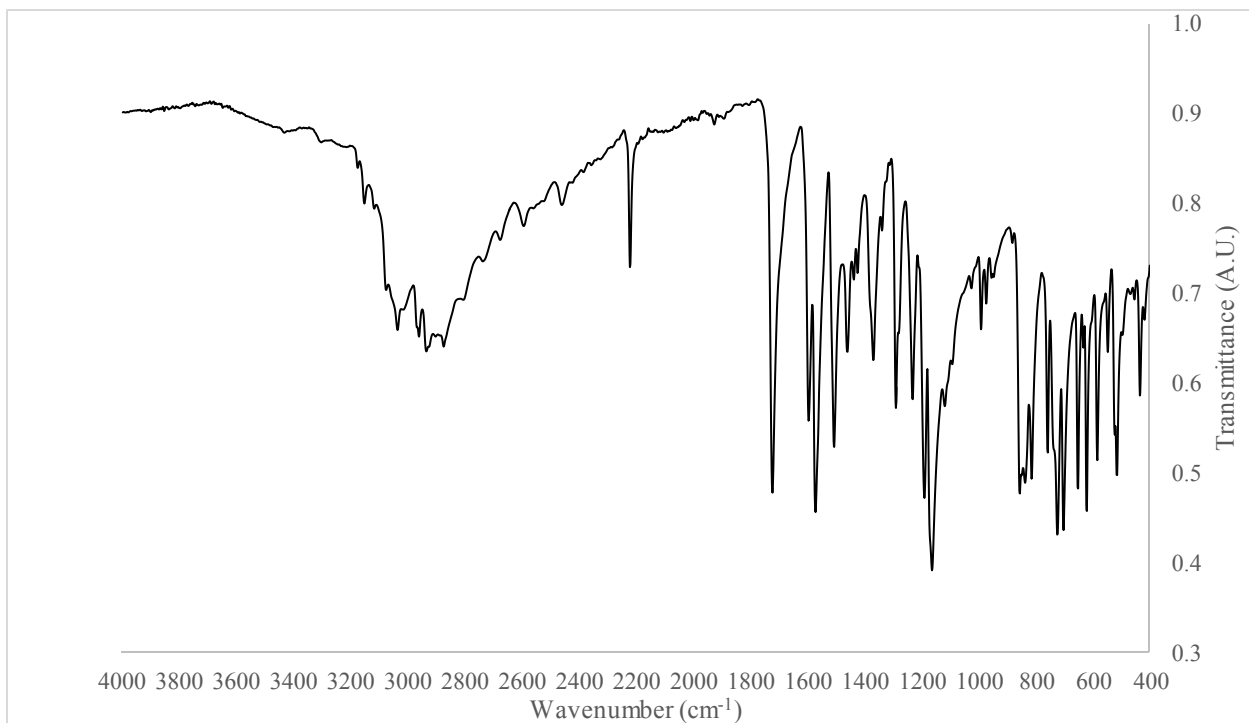


Figure A4-11: FT-IR Spectrum of 1-butyl-3-methylimidazolium chloride/ α -cyano-4-hydroxycinnamic acid ([BMIM]Cl-CHCA)

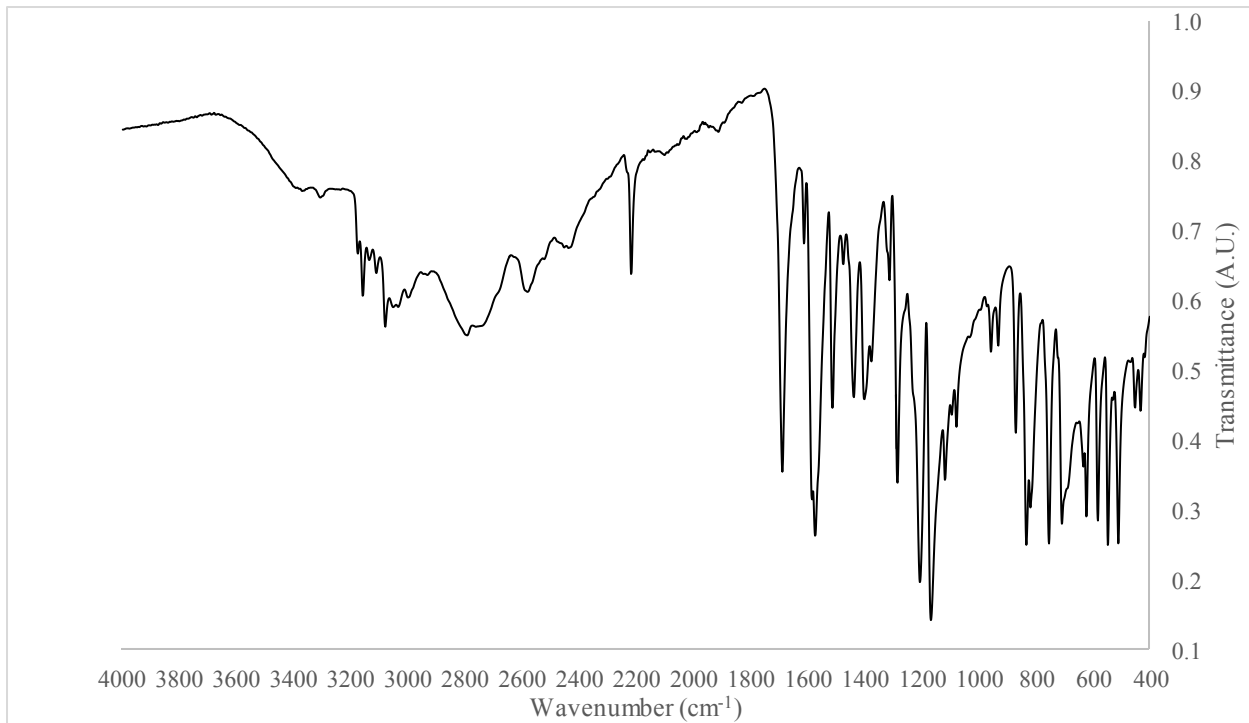


Figure A4-12: FT-IR Spectrum of 1-ethyl-3-methylimidazolium chloride/ α -cyano-4-hydroxycinnamic acid ([EMIM]Cl-CHCA)

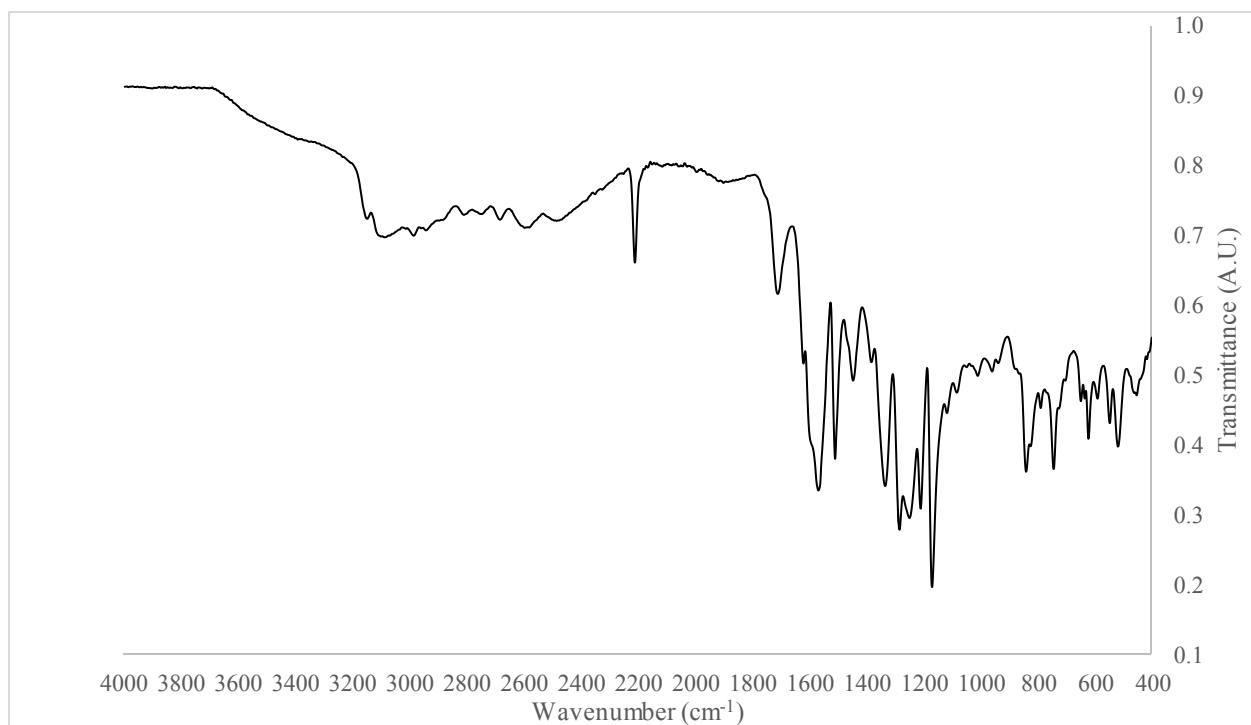


Figure A4-13: FT-IR Spectrum of 1-ethyl-3-methylimidazolium α -cyano-4-hydroxycinnamate ([EMIM][CHCA])

Appendix V: Chapter 4 Supplementary Material

Table A5-1: Regression Statistics for Sugar Calibration Curves Constructed using MALDI-TOF MS (DHB Matrix); n = 5; 4-point calibration

	m	S_m	b	S_b	$S_{y/x}$	R^2
Glucose	0.0501	0.0015	0.0899	0.0154	0.0183	0.9983
Fructose	0.0992	0.0023	0.1170	0.0239	0.0284	0.9989
Sucrose	0.4540	0.0284	-0.1966	0.1333	0.1770	0.9922
NAG	0.3664	0.0053	0.0137	0.0337	0.0413	0.9996

Table A5-2: Average Absolute Peak Heights for Glucose

Standard (initial concentration of stock solution)	Glucose Average Absolute Peak Heights \pm SD (% RSD)			
	H ₂ O	[BMIM]Cl	[EMIM]Cl	[EMIM]OAc
1 mM	73.9 \pm 27.9 (37.8 %)	247.4 \pm 89.8 (36.3 %)	259.0 \pm 149.0 (57.5 %)	70.8 \pm 34.6 (48.9 %)
5 mM	549.9 \pm 305.8 (55.6 %)	1256.4 \pm 671.8 (53.5 %)	1590.1 \pm 593.9 (37.4 %)	412.2 \pm 110.7 (26.9 %)
10 mM	1409.8 \pm 407.3 (28.9 %)	2461.0 \pm 334.3 (13.6 %)	3527.4 \pm 593.2 (16.8 %)	1142.2 \pm 481.3 (42.1 %)
25 mM	3238.9 \pm 1300.4 (40.2 %)	4135.0 \pm 1111.4 (26.9 %)	5972.5 \pm 3425.3 (57.4 %)	2194.1 \pm 859.2 (39.2 %)
50 mM	9274.7 \pm 1719.1 (18.5 %)	8999.2 \pm 1833.3 (20.4 %)	9937.4 \pm 3866.8 (38.9 %)	4739.5 \pm 1214.4 (25.6 %)
75 mM	16549.0 \pm 5245.5 (31.7 %)	7776.4 \pm 2803.0 (36.0 %)	15895.5 \pm 4823.3 (30.3 %)	3910.6 \pm 1854.4 (47.4 %)
100 mM	21866.1 \pm 10117.1 (46.3 %)	10888.5 \pm 3337.2 (30.6 %)	23275.8 \pm 8346.4 (35.9 %)	6030.9 \pm 2197.1 (36.4 %)

Table A5-3: Average Peak Height Ratios of Glucose/Glucose-d₇ used for Calibration

Standard (initial concentration of stock solution)	Glucose/Glucose-d ₇ Average Peak Height Ratio \pm SD (% RSD)			
	H ₂ O	[BMIM]Cl	[EMIM]Cl	[EMIM]OAc
1 mM	0.038 \pm 0.016 (40.6 %)	0.021 \pm 0.003 (15.7 %)	0.026 \pm 0.002 (8.80 %)	0.022 \pm 0.005 (24.3 %)
5 mM	0.154 \pm 0.006 (4.19 %)	0.140 \pm 0.008 (5.80 %)	0.159 \pm 0.007 (4.43 %)	0.130 \pm 0.009 (7.19 %)
10 mM	0.355 \pm 0.031 (8.67 %)	0.328 \pm 0.010 (3.04 %)	0.351 \pm 0.013 (3.67 %)	0.298 \pm 0.019 (6.48 %)
25 mM	0.950 \pm 0.053 (5.55 %)	0.848 \pm 0.032 (3.82 %)	0.920 \pm 0.011 (1.20 %)	0.856 \pm 0.031 (3.60 %)
50 mM	1.800 \pm 0.088 (4.89 %)	1.732 \pm 0.038 (2.22 %)	1.779 \pm 0.041 (2.33 %)	1.822 \pm 0.051 (2.81 %)
75 mM	2.558 \pm 0.209 (8.17 %)	2.804 \pm 0.057 (2.04 %)	2.660 \pm 0.169 (6.36 %)	2.878 \pm 0.160 (5.57 %)
100 mM	3.242 \pm 0.346 (10.7 %)	3.707 \pm 0.342 (9.23 %)	3.596 \pm 0.119 (3.32 %)	3.774 \pm 0.137 (3.63 %)

Table A5-4: Calculated Fructose Conversion and HMF Yield as a Function of Reaction Time

Time	Mean Fructose Conversion (%)		Mean HMF Yield (%)	
	No catalyst	Catalyst	No catalyst	Catalyst
10	5.3	40.2	6.6	18.0
70	56.1	65.7	5.1	70.1
130	80.1	91.4	13.6	62.0
190	91.4	93.7	20.6	47.3

Appendix VI: Statistical Analysis

Statistical analysis was performed using Microsoft Excel's LINEST function.

The calculated x-values (in ng) of analyte were used to construct an array of x-values and average y-values. Using Excel, the LINEST function was used to generate the corresponding values: slope (m), intercept (b), standard error of the slope (S_m), standard error of the intercept (S_b), correlation coefficient (R^2), and standard error of the regression ($S_{y/x}$) as pertaining to the slope of the regression line: $y = mx + b$.

Equations

Standard Error of Regression:

$$S_{y/x} = \sqrt{\frac{\sum (y_i - \hat{y}_i)^2}{n-2}} \quad \text{Equation A6-1}$$

Standard Error of the Slope:

$$S_m = \frac{S_{y/x}}{\sqrt{\sum (x_i - \bar{x})^2}} \quad \text{Equation A6-2}$$

Standard Error of the Intercept:

$$S_b = S_{y/x} \sqrt{\frac{\sum x_i^2}{n \sum (x_i - \bar{x})^2}} \quad \text{Equation A6-3}$$

Definitions:

$S_{y/x}$ = standard error of the regression

y_i = measure y value

\bar{y}_o = mean of measured y values

\hat{y}_i = predicted y value from regression

$n - 2$ = degrees of freedom

x_i = measured x value

\bar{x} = mean x of calibration points (centroid)

\bar{y} = mean y of calibration points (centroid)

S_m = standard error of the slope

S_b = standard error of the intercept

n = number of replicate measurements

N = number of calibration points

For quantitative analyses, to determine the concentration of an unknown sample, the individual y values were interpolated from the regression line.

$$x = \frac{y-b}{m} \quad \text{Equation A6-4}$$

The standard deviation in x was determined from the mean x value from individual y values.